DYNAMIC RESPONSE OF A HYDROELASTIC MODEL OF A TYPICAL SEMI-SUBMERSIBLE TO WAVES AND BERGY-BIT IMPACT

HUSSEIN WAHBA MOHAMMED EL-TAHAN

DYNAMIC RESPONSE OF A HYDROELASTIC MODEL OF A TYPICAL SEMI-SUBMERSIBLE TO WAVES AND BERGY-BIT IMPACT

By

Hussein Wahba Mohammed El-Tahan, B.Sc. (Hon.), M.Eng.

A Thesis Submitted to the School of Graduate Studies in Partial Fulfillment of the Requirements for the degree of Doctor of Philosophy

Faculty of Engineering and Applied Science
Memorial University of Newfoundland
May, 1985

St. John's Newfoundland Canada

ABSTRACT

This study addresses the problems of semi-submersible platforms operating year-round under harsh environmental conditions. The main objective of this study is to develop techniques for modelling, construction, handling, and testing a model that is dynamically and structurally similar (as close as possible) to a typical semi-submersible and use it to study its motion and global structural response to wave forces and bergy bit impact.

Extensive review of the available numerical, experimental and full-scale studies is presented. The review identified the need for developing techniques to overcome the problems associated with modelling, construction, handling and testing of a structurally and dynamically similar (hydroelastic) semi-submersible model.

The review also identified the lack of data on the impact strength of iceberg ice and the need for experimental and analytical studies to investigate the problem of semi-submersible/bergy-bit impact.

A hydroelastic model of a typical semi-submersible was developed. In addition to simulating hydrodynamic

forces, a hydroelastic model achieves structural similarity (i.e. mode shapes, natural frequencies and stresses). The model, believed to be the first of its kind, was fabricated with 0.8 mm (0.03 in.) thick high impact polystyrene sheets. Cellulose acetate butyrate tubes, 1.58 mm thick, were used as bracings. The model was extensively instrumented with strain gauges to measure strains in critical sections of all the semi-submersible members.

The response of the model to regular and irregular waves under operating/survival conditions and impacts of modelled bergy-bits is presented.

The experimental response in waves is compared with the available numerical and full-scale values. The measured forces, stresses and motion due to simulated impact are presented and compared with numerical results of impact models.

There is very good agreement between the experimental and analytical results of this study and other published results.

The effect of varying local stiffness of the structure/ice on the impact force has been studied using a two-degrees-of-freedom model and introducing a local stiffness element. The impact strength and load-deformation characteristics of iceberg ice were obtained from a comprehensive ice testing program carried out as part of this study.

The maximum bergy-bit mass and impact velocity conditions that a column can withstand, without local damage, have been estimated using the results of the impact tests on the semi-submersible models and blocks of iceberg ice.

It was found that semi-submersibles designed for wave forces only may not be able to withstand impact of small bergy-bits without suffering local damage.

The study demonstrated the viability and reliability of hydroelastic modelling, and the usefulness of hydroelastic models in studying the response to impact.

Based on the findings of the study, areas for further research have been identified and recommendations made for further work on the bergy-bit/semi-submersible impact.

ACKNOWLEDGEMENT

The author wishes to express his sincere gratitude to his supervisor, Professor M. Arockiasamy, for his guidance, encouragement, financial support and indispensable help in the completion of this thesis. Grateful acknowledgements are due to Professor D. V. Reddy, who initiated the project during his stay at Memorial University, and to Dr. M. Booton and Dr. A. J. Christian, members of the Supervisory Committee, for their help and constructive suggestions.

The author would also like to gratefully acknowledge the following persons and organizations for their help and contribution:

- Dean F. A. Aldrich, School of Graduate Studies for his encouragement, understanding and for the award of Memorial University Fellowship.

- Dean Ross Peters, Faculty of Engineering and Applied Science, for his interest and encouragement in the completion of the thesis.

- Dr. T. R. Chari, Associate Dean, Faculty of

Engineering and Applied Science, for his encouragement and interest.

- The Centre for Cold Ocean Resources and Engineering for the award of the C-CORE Fellowship, and organizing a field trip to collect iceberg ice.

- Dr. A. S. J. Swamidas, Associate Professor, for his encouragement, useful discussion and assistance in the numerical computations.

- Professor D. B. Muggeridge, Chairman of the Ocean Engineering Group, for his interest and suggestions.

- Fenco Newfoundland Limited for providing some of the ice testing equipment and its President, Mr. Eric Gray, for his permission to have the thesis typed on the company's word processor.

- Nordco Ltd. for lending us the strain gauge conditioner and amplifier units for the testing program.

- Mr. Greg Warbanski, Environmental Co-ordinator, Husky/Bow Valley for making the motion response of the SEDCO-706 Semi-Submersible available for this study.

- Mr. Mark Weishaupt, Staff Engineer, SEDPEX Inc., for providing the model test results for the SEDCO-700 and SEDCO-707.

- The Technical Services Department for manufacturing the tesing equipment, and in particular, Mr. Stephen Foster who built the hydroelastic model.

- Work term students Mr. Todd Osmond, Mr. William Wells, Mr. Ying Liaw, and Mr, Ivi Hermanto, for their help during the ice testing program; and Mr. Randy Doyle for his help during the hydroelastic model testing.

- Mr. G. Guy, Mr. A. Bursey, Mr. T. Lanning and Mr. D. Tilley, laboratory staff, for their help in the set up and testing.

- Mrs. Cynthia Lovell for typing the manuscript on very short notice with considerable care and patience, and Miss Mary Evans for helping Mrs. Lovell.

- Mr. Paul Paschke for proof reading the manuscript with patience and care.

- Mr. Razek Abdelnour, President, Arctec Newfoundland Limited for his continuous encouragement to complete the thesis.

I would like to express my sincere thanks to Mona, Tahmir, Yassir and my Mother, to whom this work is dedicated, for their patience and support.

Before all and after all thanks to God for everything.

LIST OF RELATED PUBLICATIONS

Arockiasamy, M., El-Tahan, H., Swamidas, A.S.J., Russell, W., and Reddy, D.V., "Semi-submersible Response to Bergy Bit Impact", Proc. of RINA Offshore Engineering Group International Symposium on 'Semi-Submersible, The New Generations', London, March 17-18, 1983.

El-Tahan, H., Swamidas, A.S.J., Arockiasamy, M. and Reddy, D.V., "Strength of Iceberg and Artificial Snow Ice Under High Strain Rates and Impact Loads", Proc. of the 3rd International Symposium on Offshore Mechanics and Arctic Engineering, New Orleans, La., 12-16, 1984.

Arockiasamy, M., El-Tahan, H., Swamidas, A.S.J., Russell, W., and Reddy, D.V., "Semi-submersible Response to Transient Ice Forces", J. of Ocean Engineering, Vol. 11, No. 5, 1984, pp. 463-490.

Swamidas, A.S.J., Arockiasamy, M., Reddy, D.V. and El-Tahan, H., "Dynamic Response of Moored Semi-Submersibles to Ice-Floes and Bergy-Bits", Preprint 84-021, Spring Meeting, ASCE, Georgia, May 1984, 18p.

El-Tahan, H., Arockiasamy, M. and Swamidas, A.S.J., "Motion and Structural Response of a Hydroelastic Semi-Submersible Model to Waves and Ice Impact", Proc. of the 4th Int. Symposium on Offshore Mechanics and Arctic Engineering, Dallas, Texas, February 17-22, 1985.

El-Tahan, H., Arockiasamy, M. and Swamidas, A.S.J., "Model Studies on the Response of a Semi-submersible to Bergy Bit Impact", to be presented at the CANCAM 85, London, Ontario, June 2-7, 1985.

Arockiasamy, M., Swamidas, A.S.J. and El-Tahan, H., "Response of Offshore Structures to Bergy-Bit and Iceberg Impacts", to be presented at the 4th International Conference on Behaviour of Offshore Structures, BOSS'85, Delft, The Netherlands, July 1-5, 1985.

El-Tahan, H., Swamidas, A.S.J., and Arockiasamy, M., "Impact Strength of Iceberg and Artificial Snow Ice", to be presented at Canadian Coastal Conference, St. John's, Newfoundland, August 13-16, 1985.

El-Tahan, H., Swamidas, A.S.J., and Arockiasamy, M., "Response of a Semi-Submersible Model to Bergy-Bit Impact", to be presented at POAC'85, Narssarssanq, Greenland, Sept. 7-14, 1985.

El-Tahan, H., Arockiasamy, M., and Swamidas, A.S.J., "Impact Tests on Icebergs and Artificial Snow Ice", to be presented at POAC'85, Narssarssanq, Greenland, Sept. 7-14, 1985.

CONTENTS

Contents (cont'd)

Contents (cont'd)

LIST OF TABLES

LIST OF ILLUSTRATIONS

LIST OF ILLUSTRATIONS (cont'd)

LIST OF ILLUSTRATIONS (cont'd)

LIST OF ILLUSTRATIONS (cont'd)

LIST OF ILLUSTRATIONS (cont'd)

LIST OF ILLUSTRATIONS (cont'd)

LIST OF ILLUSTRATIONS (cont'd)

LIST OF ILLUSTRATIONS (cont'd)

LIST OF ILLUSTRATIONS (cont'd)

LIST OF ILLUSTRATIONS (cont'd)

NOMENCLATURE

$[A]$	Added mass matrix
A	Cross-sectional area
A_s	Cross-sectional area for shear
a_{ij}	Inertial coefficient
$[B]$	Damping matrix
b_{ij}	Damping coefficient
$[C]$	Restoring matrix
c_{ij}	Restoring coefficient
c^c_{ij}	Mooring stiffness
c_1, c_2	Damping coefficients in the 2-D.O.F. Model
D	$\frac{\partial}{\partial t}$
E	Young's, Modulus
$\{F\}$	Force vector
F_I	Froude-Kriloff force
F_D	Wave difraction force
G	Shear Modulus
$\overline{GM}$	Metacentric height
h	Thickness of the cross-section wall
I	Moment of inertia
i	$\sqrt{-1}$
J	Polar moment of inertia
k	Spring stiffness
k_1, k_2	Local and global stiffnesses for the 2-D.O.F. Model

L	Structural member length
M	Bending moment
$[M]$	Mass matrix
m_1, m_2	Masses of the 2-D.O.F. Model
P_j	Total wave force on a structural element
R	Radius of gyration (gyradius)
S	Structural stiffness
S_a	Axial stiffness
S_b	Bending stiffness
S_s	Shear stiffness
S_t	Torsional stiffness
s	Length of the cross-section wall
t	Time
$\{U\}$	Motion component vector
$V(0)$	Impact velocity - semi-submersible model
v_1, v_2	Local and global displacement in the 2-D.O.F. Model
W	Model weight
x_1, y_1, z_1	Co-ordinates of the point of impact with respect to the semi-submersible centre of gravity
δ	Local deformation
δ_1, δ_2	Defined in Figure.6.1
$\dot{\delta}(0)$	Impact velocity
ε	Strain
ε_k	Phase angle

ζ	Heave
$\{\eta\}$	The motion amplitude vector
η	Sway
θ	Pitch, heel angle
λ	Linear scale factor (model/prototype)
μ	Poisson's ratio
ξ	Surge
ρ	Density
σ	Stress
ϕ	Roll
χ	Component of rigid-body motion of the semi-submersible at point of impact
ψ	Yaw
ω	Circular frequency of waves

CHAPTER I

INTRODUCTION

1.1 General

Increasing demands for offshore oil and minerals necessitate exploration in the hazardous and hostile environments of the North Sea and the east coast of Canada. It is believed that the Canadian East Coast has more potential hydrocarbon reserves than any other known oil and gas areas in the world outside the Middle East. The oil and gas reserves offshore Newfoundland are estimated to represent about 30% of the total inland and offshore oil and gas resources in Canada.

In 1979 over one billion barrels of recoverable oil were discovered in the Hibernia fields northeast of the Grand Banks of Newfoundland. Another major discovery was recently reported in the Terra Nova field, southeast of the Hibernia Field.

On the Grand Banks of Newfoundland there are various factors which make drilling operations and the development of the discovered oil fields particularly difficult, viz. pack ice, icebergs, weather and sea state (Table 1.1). In

addition to the presence of sea ice and icebergs, the environmental conditions of the Grand Banks are even harsher than the severe conditions of the North Sea (Figure 1.1). In such environmental conditions semi-submersible platforms provide an ideal solution due to their stability, mobility and good motion characteristics. Moored semi-submersible platforms have successfully been used for year-round operations on the Grand Banks for the past few years; up to seven semi-submersibles have been simultaneously drilling in the area.

The presence of icebergs and their fragments (Figure 1.2) poses a great threat to these offshore structures. The severity of iceberg threat varies widely from year to year. For example, 1,587 icebergs crossed latitude 48°N in 1972 (the record year) while in 1966 no icebergs were sighted south of this latitude. Because of a sophisticated and effective iceberg management system, developed over the past 14 years, the downtime due to weather conditions and iceberg threat has become insignificantly small and is now less than 2%. Icebergs that may pose a threat to a platform are deflected away by towing, bow-pushing or propeller-washing, while the ones that cannot be deflected are avoided by moving the platform off location. However, 'small' fragments of icebergs (growler and bergy bits) of masses up to 2,000 tonnes may escape radar and visual detection, especially in heavy seas. Such ice masses,

oscillating in waves with velocities up to 4-5 m/sec., pose a great hazard to the structural components of the semi-submersible. Therefore semi-submersibles operating in iceberg infested waters must be designed to withstand collision with ice masses as large as bergy-bits.

This study addresses the problem of semi-submersible platforms operating year-round under harsh environmental conditions by investigating the structural and motion responses of a typical semi-submersible to wave forces and bergy-bit impact.

1.2 Scope

Semi-submersibles are subjected to various types of environmental loads due to winds, waves, currents, ice floes, bergy bits and ice accretion. The most important loadings from the point of view of motion characteristics and structural integrity are those due to wave action and impact of small pieces of ice (ice floes and bergy bits).

The second-order wave forces, which are almost steady for regular waves and vary very slowly in irregular waves at frequencies which may be close to the natural frequencies of semi-submersible platforms, lead to resonant excitations and increasing mooring forces. Loads due to wind, currents

and ice accretion are of more importance to platform stability.

Since this study is mainly concerned with semi-submersible motion and its structural integrity, only forces due to waves and transient ice forces will be considered.

Several analytical methods have been developed, over the past two decades, to determine the wave-induced motion and structural responses of semi-submersibles. Computed motion responses were generally in good agreement with model test results and full-scale measurements. However, computed structural response values have not agreed very well with those obtained from various field measurements and model tests.

Only very limited studies are available on the motion and structural responses of semi-submersible platforms to bergy bit impact based on theoretical models. In these studies the impact force was found to vary by at least an order of magnitude depending on the assumptions of type of impact (plastic or elastic) and the characteristics of impact zones in the structure and ice. In addition, simplified assumptions were made for the transient hydrodynamic loadings on the semi-submersible and the bergy bit.

Therefore field studies or model tests are necessary to check the validity of computational methods, structural modelling and theoretical assumptions for both types of loadings (wave action and bergy bit impact). However, published reports on field measurements and experimental studies on the structural response of semi-submersibles in waves using structural models are very limited. No field or experimental studies on the motion and structural responses of semi-submersibles to bergy bit impact are available. Also there is a considerable lack of information on the strength and failure characteristics of iceberg ice under high strain rate and impact conditions.

Measurements on full-scale platforms are very useful since they are made under natural environmental conditions and free from scaling effects or theoretical assumptions. However, they are expensive, and time consuming. Besides, the investigators have no control over the type or range of the environmental conditions encountered during the observation period. In the case of a study on bergy-bit impact the risk of structural damage to the platform members is too great to undertake. Large-scale models are faced with the same problems as full-scale studies.

In small-scale models it is possible and relatively easy to handle load conditions but some difficulties are involved in achieving hydrodynamic and structural similarities.

The model represents the real structure on a small scale and the hydrodynamic forces (except drag forces) are scaled properly. Water drag has negligible effect on the motion and is only important at resonance (only heave natural period of semi-submersibles is close to the long periods of the waves). However, it is much more difficult to achieve structural similarity than hydrodynamic similarity. In addition to other modelling difficulties, very thin material with a low elastic modulus and high density is needed to secure dynamic structural similarites. Therefore, exactly similar structural modelling is extremely difficult and this is one reason why few experimental studies using structural models have been reported. In the available structural response models, attempts are made to simulate the stiffness of bracing members and deck girders only. The stiffness of the columns and pontoons are distorted (much higher than required) and therefore no measurements are made in these structural components. The reason being that a structurally similar model will be very delicate and therefore construction, handling and testing of the model are thought to pose very difficult problems and challenges.

The main purpose of this study is to develop techniques for modelling, construction and testing of a dynamically

and structurally similar model (as close as possible) to a typical semi-submersible platform and use it to study its motion and global structural responses to wave forces and bergy bit impact.

1.3 Thesis Outline

Chapter II presents a comprehensive review of available theoretical, experimental and field studies on the structural and motion responses of semi-submersible platforms to wave forces and transient ice impact.

Chapter III presents the results of a testing program to determine the strength and behaviour of iceberg and snow ice under high strain rates and impact conditions. These results are needed for the study on bergy-bit impact presented in Chapter VI.

Chapter IV presents hydroelastic modelling principles; description of the model and the prototype; the static and dynamic properties of the model; construction, handling and testing techniques; and an outline of the testing program.

Chapter V presents the motion and structural responses of the model in regular and irregular waves; a study to check the validity of model results; and a parametric study to

investigate the effect of varying mooring system stiffness and to check the linearity of the response.

Chapter VI presents a study to investigate the response of the semi-submersible to bergy-bit impact. The study presents variations of impact forces, stresses and motions with bergy-bit mass, impact velocity and mooring system stiffness. The chapter contains one section on verification of numerical impact model and another section on the effect of local stiffness on the response using a two-degree-of-freedom model. The last section presents examples showing how to use the experimental results to estimate the extent of local damage due to ice impact.

Chapter VII presents concluding remarks including contribution and recommendations for further studies.

The list of references is provided after Chapter VII followed by the Tables and Figures.

Appendix A presents details of data processing and analyses.

CHAPTER II

STATE-OF-THE-ART

2.1 Semi-submersible Platforms

Offshore drilling has, over the past five decades, moved from shallow water platforms to deep water floating structures. The first offshore wells were drilled in the lakes and swamps of the American Continent in the 1920's using piled structures (Rodnight, 1983). The first mobile drilling units were based on bottom supported barges in water depths up to 30 feet in the late 1940's. The submersible and jack-up drilling units were introduced in the early 1950's, and the drill ships in the mid-1950's. The drillship has a large deck load capacity but its poor motion characteristics limit its use in hostile seas.

The semi-submersible drilling unit (SSM) evolved from the submersible design in the early 1960's. The first semi-submersible was the BLUEWATER-I which was converted from a submersible, sit-on-bottom type vessel and was used in an operation during late 1962. The semi-submersible has since improved and evolved to be self propelled, dynamically positioned, ice strengthened, and structurally redundant.

The first dynamically positioned semi-submersible drill rig, the SEDCO 709 was built and commissioned into service in 1977. Today there are about 170 semi-submersible units in service.

It is estimated that the petroleum industry has more than 1600 rig-years experience in using semi-submersible drilling units. The semi-submersible unit is considered to be the workhorse of the petroleum industry for rough, deepwater exploration. In spite of the ALEXANDER KIELLAND and the OCEAN RANGER disasters, the safety record of semi-submersible platforms is far better than other offshore drilling units and conventional vessels, considering the rough environments in which the semi-submersible must operate (Hammett, 1983).

The semi-submersible (Figures 2.1 and 2.2) is a floating column-stabilized platform consisting structurally of a large deck structure supported by columns attached to large displacement hulls, all joined together by truss members (bracings). The purpose of this design is to reduce the effects of wave action and improve motion characteristics and stability. This is achieved by spreading the water plane area, the transparency to waves, and by locating the major buoyant members (hulls) below the level of the most severe wave action. The smallest natural period of the six semi-submersible motions is in heave and is usually greater than 20 seconds, which is far above the every day wave

period (6-12 sec.) experienced during drilling (Hammett, 1983). The natural periods of semi-submersible motion are much longer than those of the drill ships, thus allowing the SSM to drill and survive severe ocean storms while other marine vessels must either go to sheltered water or stay away from the storm.

The semi-submersibles are designed to drill in up to 15 m waves, structurally withstand waves up to 23 m, and survive 35 m waves combined with 100 knots (50 m/sec) of wind and a 1.5 m/sec current. They have been used for drilling under severe environmental conditions. In 1968, the SEDCO 135-F, operating in the North Pacific off western Canada stayed on location in 30 m waves without damage (Hammett, 1981). Moored semi-submersibles can operate in water depths up to 600 m, and the dynamically positioned ones in water depths up to 3,000 m (Ocean Industry, 1983b).

The semi-submersible was originally envisaged as a drilling tool, and this function has always dominated its use. Other uses of the semi-submersible however have emerged in the latter part of the 1970's such as: heavy lift crane platforms, dredging, and accommodation platforms, and multi-function support vessels with diving, fire fighting and crane facilities.

Semi-submersibles have been improved substantially during the last few years and now have structural redundancy, ice-

strengthened hulls and columns, columns with water tight subdivisions (compartments), water tight decks for reserve buoyancy, a strong double deck structure to replace the usual complicated configuration of bracing, and large displacements of up to 60,000 tonnes to allow for a variable deck load of up to 7,000 tonnes.

One of the major problems for semi-submersible platforms is their vulnerability to ice impact (pack ice or bergy bit). A great deal of research has been done leading to the design of ice-class semi-submersible drilling platforms featuring ice strengthened hulls and columns with a simple bracing configuration (Corona and Yashima, 1983 and Ocean Industry, 1982 and 1983).

These semi-submersibles are designed to withstand some sea ice forces but, to the best of the author's knowledge, no semi-submersible has been built to resist bergy bit impact. The problem of semi-submersible/bergy bit impact, while not fully understood yet is studied in the present investigation.

2.2. Semi-Submersible Response in Waves

2.2.1 Equations of Motion

In general, response analysis methods for a floating offshore structure can be broadly divided into two groups

(Satake and Katayama, 1977):

a) The motion response analysis in waves is first carried out on the overall structure taken as a rigid body. Then using these results, the structural analysis is carried out on the entire structure taken as an elastic body by a space frame analysis or a plate and shell approach in order to obtain the member forces.

b) The overall structure is treated as an elastic body from the first stage. The flexibility of structural members is included in the equation of motion and the structural response is calculated simultaneously with the motion response (Yoshida and Ishikawa, 1980).

For various types of semi-submersible platforms, which are generally of higher overall rigidity, the former method is commonly used. However, it may be necessary to account for structural deformation of semi-submersible platforms in some special cases. For example, a large-scale platform such as an offshore terminal or a floating airport cannot be regarded as a rigid structure. Also, a platform that may be considered rigid in intact conditions, may have to be regarded as a flexible structure under certain structural damage conditions (Yoshida, et al, 1984). It should be noted that some of the current classification

society rules require structural analysis in the damaged condition.

The calculation of wave-induced loads on semi-submersibles using the rigid body approach can basically be considered to consist of three steps:

i) Determination of the coefficients of motion for the semi-submersible considered as a rigid body.

ii) Solution of the equations of motion for six degrees of freedom.

iii) Calculation of distributed loads on all the structural elements of the semi-submersible.

The linearized equations of motion of a semi-submersible platform in regular waves can be expressed in the following matrix form:

$$([M]+[A])\{\eta\} + [B]\{\dot{\eta}\} + [C]\{\eta\} = \{Fe^{-i\omega t}\} \quad \ldots 2.1$$

where

[M] = generalized mass matrix,

[A] = added mass matrix,

[B] = damping matrix, including linearized viscous damping and potential damping (energy taken away by radiation of waves)

$[C]$ = restoring matrix, including hydrostatic and linear mooring force coefficients,

$\{n\}$ = the motion vector with six components,

$i = \sqrt{-1}$,

ω = wave frequency,

t = time,

and

$\{Fe^{-i\omega t}\}$ = the exciting force vector.

The components of the matrices $[A]$, $[B]$ and $\{F\}$ are generally frequency dependent. The assumption of small amplitude waves and motion allows all the other coefficients to be considered as constants. The mooring line reactions depend on their shape, configuration, weight, material and hydrodynamic loading. The load-deformation characteristics of the lines are often non-linear. It is, however, permissible sometimes to approximate the load-displacement curve by a straight line within the range of its application (Chakrabarti, 1980).

The equations of motion actually imply the linear superposition of three regular wave trains with the same frequency, viz., incident waves, diffracted waves on a fixed structure, and radiated waves due to the structure oscillating in still water.

The wave exciting force, F, may be considered as the hydrodynamic force acting on a fixed body in waves. It is divided into two parts (Salvenson et al, 1970).

$$F = F_I + F_D \qquad \text{.....2.2}$$

the force F_I due to the pressure distribution of the undisturbed incident wave is referred to as the Froude-Kriloff force. The diffraction force F_D, corresponds to the scattering of the incident waves by the structure. It is the force required to generate the scattered waves. Both F_I and F_D are calculated without considering motion of the structure.

The hydrodynamic effects of the structure motion can be divided into two parts. The first is the added mass inertia force in phase with acceleration, caused by local disturbance due to the structure motion in calm water. The second part is the damping force in phase with velocity due to the energy dissipation of wave radiation caused by the structure motion in calm water (as inviscid fluid), or is attributed to the energy dissipation of viscous effect.

Although the effect of viscous damping is not large for the motion in general, in resonance and some particular frequency range, such as zero potential exciting force range, the effect of viscous damping and viscous exciting

forces will become important on the motion characteristics (Bain, 1964, Sun, 1982 and Chakrabarty and Cotter, 1984).

Wave exciting forces and hydrodynamic coefficients can be computed using methods based on the 2-dimensional strip theory, or a 3-dimensional source-sink technique. Wave exciting forces can also be computed using the Morison's equation of approach. A review of each of these methods is presented in Section 2.2.3.

Having determined all the coefficients in the equations of motion, a psuedo-dynamic solution may be sought for the set of dynamic equation given by Equation 2.1.

Substituting $\eta_k = \eta_{ok}\, e^{-i(\omega t + \varepsilon_k)}$ 2.3

where η_{ok} is the amplitude of steady motion and ε_k its phase angle, equation 2.1 becomes:

$$[-\omega^2([M]+[A]) + i\omega[B] + [C]]\{\eta_o\, e^{-i\varepsilon}\} = \{F\} \quad .....2.4$$

which may be solved for η_o and ε vectors by a matrix inversion for a series of frequencies ω and heading angles. Then the 'response amplitude operators' (RAO's) of the semi-submersible motion which represent the ratios of η_o to wave amplitude can be determined. Using the RAO's and a given wave spectrum, the spectral motion characteristics of

the semi-submersibles in irregular waves can be determined.

2.2.2 Structural Loadings

Having determined the motion of the centroid of the semi-submersible, the motion of any other point can be easily obtained using rigid body mechanics. Therefore the added mass and damping forces on an individual structural element can be obtained and added to the wave exciting forces on the element to obtain the amplitude of the total force P_j acting on that element.

$$P_j e^{-i\omega t} = F_j e^{-i\omega t} - (A_j + M_j)\,\ddot{n}_j - B_j \dot{n}_j - C_j n_j \quad \ldots\ldots\ldots 2.5$$

Matrices A_j, B_j, C_j and M_j are the contributions of the element to the corresponding coefficient matrices for the whole semi-submersible.

These element forces can be used as exciting forces in a structural analysis program to obtain the six components of section forces and moments. The semi-submersible is generally idealized for structural analysis using space frame elements, shell elements, plate elements or a combination of these elements. Several integrated programs have been developed to determine the structural and motion responses

of semi-submersible platforms to wave excitations. A review of these programs is presented later.

2.2.3 Calculations of Hydrodynamic Loadings

Methods used to compute the hydrodynamic loadings on semi-submersible platforms are based on Morison's equation, two dimensional strip theory or three dimensional singularity distribution methods. Mathisen and Carlsen (1980) presented a brief review of the available methods for calculation of wave-induced motions and loads on twin pontoon semi-submersibles and discussed the problems associated with the evaluation of wave load components due to diffraction. In spite of the considerable progress made in the development of these methods during the last decade, general agreement has not been reached on the most suitable method.

Sluijs and Minkenberg (1977) described the developments of wave induced hydrodynamic calculation methods based on the strip theory and commented on the limitations of Morison's equation as applied to semi-submersible platforms.

Chung (1977) reviewed the methods developed to compute hydrodynamic forces on semi-submersibles based on Morison's equation and the strip theory approaches. The limitations of each method were pointed out in terms of accounting for

the free surface effects and water depths in computing the hydrodynamic coefficients (added mass and wave damping).

The methods based on two-dimensional and three-dimensional singularity distribution methods were critically examined by Hsiung (1984) who indicated that the three-dimensional method yield, in general, better results than the two-dimensional approach. However, it was pointed out that the three-dimensional technique requires much more numerical work and computer time.

A brief review of the methods used to calculate hydrodynamic loads on the most common type, twin-hull semi-submersible is presented below. Emphasis is placed on the physical meaning rather than mathematical expressions.

2.2.3.1 Morison's Equation

Morison's equation is a semi-empirical relationship widely used to calculate wave forces on small-diameter cylindrical members of offshore structures. The total hydrodynamic force is the sum of a drag term and an inertia term. The drag term is proportional to the square of the particle velocity and is therefore non-linear. This term is usually linearized for use in linear equations of motion (e.g., Equation 2.1) or for computations of irregular wave forces on fixed structures (El-Tahan, 1979). The inertia term

is proportional to particle acceleration and is linear.

When relative fluid motions are small, the drag term becomes negligible with respect to the inertia term. The drag term becomes significant only in long waves (long period). Applying the Morison formula to Eqation 2.1, part of the drag term contributes to the damping matrix [B] and part of the inertia term contributes to the added mass matrix [A]. The rest of the drag and inertia terms represent the wave exciting force [F]. In Morison's formula the wave diffraction force component in phase with particle velocity is ignored (Chung, 1976). This component is significant for structural members fairly close to the water surface for wave lengths less than five times the member diameter. Therefore, Morison's equation is valid only when the structure diameter is less than one fifth of the wave length. It should also be noted that Morison's equation is not suitable when interaction effects between neighbouring elements are significant.

Sluijs and Minkenberg (1977) pointed out that the greatest uncertainty in using Morison's equation lies in the selection of the values of the drag and inertia coefficients. If frequency-independent values were used, this may lead to inaccurate results. Frequency dependent coefficients were used by Chung (1976) who reported good agreement between the computed and measured motions of two semi-submersibles.

Selection of the inertia coefficient is generally based on values calculated from potential flow theory while the drag coefficient is based on model test results. Comprehensive reviews of published data on the drag and inertia coefficients have been presented by Hogben et al (1977) and Chakrabarti (1980).

Based on an experimental and numerical study on the motion of the GVA-4000 semi-submersible, Mathisen, Borresen and Lindberg (1982) indicated that the Morison's equation approach has been very successful for survival and operational draft, when hydrodynamic interaction effects between different parts of the structure can be neglected with respect to the motions and overall loads.

2.2.3.2 Two-Dimensional Strip Theory

This method, widely used for calculating wave-induced motions and loads for ordinary ships, is based on the so-called "slender-body theory" which assumes that the transverse dimensions are small compared to the body length and that the cross-section should change gradually in the longitudinal direction (Salvesen et al, 1970). This method simplifies the forced oscillation problem by reducing the three-dimensional problem into a two-dimensional one for structures satisfying the slenderness assumption.

To apply the strip theory, the hull is first sub-divided into a finite number of sections (strips). Each strip has approximately constant cross-sections so that the two-dimensional potential theory can be applied to determine the added-mass, damping and excitation forces on the individual strips (Salvesen et al, 1970). Use of potential theory implies that the fluid is considered inviscid, incompressible and irrotational. Integrating the sectional coefficients over the length of the hull gives the total hydrodynamic coefficients. The hydrodynamic interactions between the neighbouring structural members and the three-dimensional effects are generally neglected. Strip theory has been extended to catamarans and twin pontoon semi-submersibles by making each strip include opposite sections of both hulls (e.g., Nordenstrom et al, 1971 and Kim, 1976).

Kim (1980) indicated that most of the methods based on strip theory assume that sectional dimensions of the structural members are small relative to wave length. With this assumption the following simplification is made: i) added mass is independent of frequency, ii) wave making damping is negligible, and iii) the diffraction of waves is negligible. Examples of the methods following these assumptions are Tasai et al (1970), Burke (1969), Hooft (1971) and Sun (1980).

However, for platforms with relatively large members compared to wave length, the above simplifications are not permissible. Therefore Kim (1973; 1980) and Chung (1976) developed methods based on the assumption that the sectional dimensions are not necessarily small compared with the wave length and water depth.

Hsiung (1984) and Mathisen and Carlsen (1980) discussed the limitations of strip theory. They pointed out that (i) the diffraction potential is not computed in some of the strip theories (ii) the strip method is well known for its deficiency in the low frequency region and (iii) it has limited applications to bodies with blunt ends or high width/length ratios.

The diffraction effect is determined by the incident wave and motion radiated wave potentials using an integral theorem known as Green's second identity. This method provides the total diffraction force over the whole wetted surface of the structure, but it cannot provide diffraction forces on parts of the structure. This creates a problem when determining element loading for structural anlysis. Attempts to ignore this 'local' diffraction component when computing structural response have been shown to produce erroneous sectional forces (Carlsen and Mathisen, 1980).

To overcome this problem Mathisen et al (1982) used an alternative radiation potential known as "Opposed Motion Potentials" whose boundary conditions are chosen in such a way that integration over the whole structure will provide the contribution of the diffraction force to the sectional forces. The results (sectional forces) obtained using the "improved strip theory" were in much better agreement with those obtained by the three dimensional singularity distribution method than by the usual strip theory.

The problem associated with the low frequency region is based on the high frequency assumption which implies that the radiated wave length should be of the order of pontoon width rather than length. Hsiung (1984) pointed out that this is a critical assumption, since the maximum motion responses are in the low-frequency (long wave) range, but stated that the effect on the final results would be relatively minor. Computations of motion response in waves based on the two-dimensional strip theory usually provide good and fast results.

2.2.3.3 Three Dimensional Singularity Distribution Method

This method - also known as the method of distributed sources, or boundary integral method - is based on the Green's function approach and was primarily developed for application to large structures when Morison's equation no

longer applies. In this method the incident wave potential is given as in the strip theory, but the motion-radiated and diffraction potentials can be determined by three dimensional source techniques (Hsiung, 1984). Since the diffraction potential itself is computed, the problem of the distribution of diffraction forces (found in the strip method) is overcome. To apply this method, the wetted surface of the structure is represented by a number of source panels. The accuracy of the computed results depends on the fineness of the panel meshes on the body surface. Because of the geometric complexity of semi-submersible structures, the number of source panels required to properly represent the immersed surface is very large. Besides, Garrison (1984) indicated that the vertical dimensions of the panels must be kept small for short wave computations. Therefore the computer time required can be prohibitively high unless care is taken in the numerical approach to improve the computational efficiency. Tse (1984) developed a modified numerical scheme and reported considerable savings in computer time.

Aside from the computer cost problem, there is no difficulty in applying this method to semi-submersible platforms. It does not require particular restrictions on the shape of the body considered and can in principle provide an exact solution (Nojiri, 1981). Although this method was applied to diffraction problems for large

offshore structures during the past decade, it was applied to semi-submersible problems only in recent years. This method proved very successful and provided better results than the strip theory (Carlsen and Mathisen, 1980; Mathisen et al, 1982; Price and Wu, 1983 and Chakrabarti and Cotter, 1984). Descriptions of the theory are provided by Garrison (1984), Hsiung (1984), Klosner and Chen (1980) and Price and Wu (1983).

2.2.3.4 Slender Body Diffraction Theory

To overcome the problem of diffraction forces in strip theory and the large computation time of the three dimensional source distribution method, Mathisen and Carlsen (1980) suggested that the slender body diffraction theory be applied to semi-submersible platforms. This theory employs the same frequency and body geometry assumptions as in the strip theory but the diffraction forces are determined directly from two dimensional diffraction potentials. It also requires less numerical work than the three dimensional source distribution theory. This theory had first been applied to ships and later to a catamaran, indicating that this method can be applied to twin-pontoon semi-submersibles.

2.2.4 Non-Linear Effects

The equations of motion presented above assumes a linear system, and the evaluation of wave forces is based on small wave amplitude. However, for an actual SSM in a real sea non-linearities may be caused by several factors including high wave, viscous effects, mooring forces and certain list and draft conditions.

Sun (1982) indicated that the motion responses of a semi-submersible are of low amplitude and have a nearly linear relationship with waves. However, the effects of viscous damping and viscous exciting forces become important at certain frequency regions near resonance and at zero potential exciting forces (when the exciting forces due to wave pressure and wave accelerations cancel each other). For a typical semi-submersible, the natural periods of all motions fall outside the range of wave periods that have significant energy in any wave spectrum, and the zero potential exciting force region has a very narrow frequency band. Therefore, it can be concluded that the overall effect of non-linearity is of minor importance.

Hence, it is common practice to assume that conventional semi-submersibles behave in a linear manner at operating drafts. Based on a series of model tests on a typical two pontoon semi-submersible at operating and

survival drafts, Kistler and Nash (1975) indicated that non-linear behaviour was observed in heave response only, for wave periods greater than 20 sec. Similar results were obtained by Katayama et al (1978) and Satake and Katayama (1977) from model tests and theoretical analyses based on linear and non-linear formulations. They concluded that linear analysis based on the small amplitude and linearized theory can produce motion characteristics with sufficient accuracy even in very high waves. However, based on section force measurements, they point out that the structural response analysis in very high waves should be carried out assuming non-linearity.

Natvig and Pendered (1977, 1980) carried out linear and non-linear analyses on a moored twin-pontoon semi-submersible and indicated that the motion response obtained by the linear method agreed well with that obtained from the non-linear method.

Field measurements of the heave response of two semi-submersibles reported by Forristal et al (1979) showed high coherence between the measured waves and heave motion indicating actual linear behaviour. The measured motion and structural responses of a full-scale semi-submersible reported by Langfeldt et al (1975) and Olsen and Verlo (1976) confirmed the linearity of the motion and structural responses.

Non-linear effects, however, may become significant for the transit and heavy list conditions when the water plane area becomes variable during one wave cycle (Mathisen et al, 1982). Studies on the motion response of semi-submersible models in transit condition indicate that near the resonance region, the measured pitch and roll motion were considerably lower than the values obtained from linear analysis (Suhara et al 1974 and Mathisen and Carlsen, 1980). However, this discrepancy was not observed for the heave motion. Model studies carried out by Huang et al (1982) on a heavily listed semi-submersible indicate that linear methods completely fail to predict the observed behaviour under such conditions. Therefore, a non-linear time domain solution technique described by Huang and Naess (1983) and Naess and Hoff (1984) was developed which provided fairly good agreement with the experimental results.

2.2.5 Review of Related Work

This section presents a review of available literature on the field, experimental and theoretical investigations carried out to study the motion and structural responses of the semi-submersible platforms in waves.

2.2.5.1 Motion Response Analysis

Burke (1969 and 1970) developed one of the early mathematical methods to compute the motions of semi-submersibles in waves based on the Morison's approach. The semi-submersible was assumed to be a rigid space frame made up of cylindrical members with arbitrary diameters, lengths and orientations. Non-cylindrical members were simulated by one or more "equivalent" cylindrical members. The effect of the free surface on the hydrodynamic coefficients was neglected in the study. The theoretical motions of three different SSM's were compared with model test results. The results indicated that the mathematical values were accurate within a range of 10-20% and it was pointed out that the accuracy could be improved with more complete data on the hydrodynamic coefficients for large diameter cylinders and non-cylindrical members.

Chung (1975, 1976) used the potential flow theory for computing the hydrodynamic forces and the six-degrees-of-freedom motion for a SSM of general configuration at an arbitrary heading in waves. The derived hydrodynamic force equation was shown to be identical to the Morison formula under certain assumptions. The general equation was reduced to an approximate equation which is more complete than the Morison formula by accounting for diffraction and motion-dependent forces with effects of wave damping, and

free surface effects. The computed motions showed good agreement with experimental data for two semi-submersibles and were in better agreement than those obtained by Burke (1969) for the same SSM based on the Morison's approach. It was pointed out that although the added mass and damping coefficients used in this study produced good motion results, it was found necessary to use more accurate values of these coefficients for structural analysis.

Hooft (1971) developed one of the early mathematical methods to determine the motion response of semi-submersibles in waves based on the strip theory approach. The method was based on Morison type formula and on the assumptions that the submerged part of the structure could be subdivided into elements such as spheres, cylinders, etc., whose added mass and viscous damping are known (Bain, 1964). The hydrodynamic forces were assumed linearly dependent on the motion and independent of the frequency of oscillation. The validity of the method was verified using experimental data on two semi-submersible models.

Nojiri and Inoue (1981) followed the basic ideas set forth by Hooft (1971) and developed a more generalized formulation of the strip theory to compute the motion response of semi-submersible platforms. The method was used to compute the motion of a twin-pontoon and a column-footing type

semi-submersible in regular waves. The computed motion of each semi-submersible was compared with model test results. They indicated that, except for the region close to resonance, calculations based on the Froude-Kriloff assumptions would yield estimations of motion without serious error.

Pauling et al (1977) developed a method to estimate SSM motions in waves based on strip theory and a modified Frank close-fit technique. The interaction effects between the pontoons and the effects of the free surface were accounted for along with the viscous damping and damping of radiated waves. The exciting forces considered included the Froude-Kriloff Force, diffraction force and drag force. Alternative methods were introduced to represent the columns, viz., hulls and columns were represented together by stripwise segmentation, columns separated from hull and represented by the sparse slender method; or columns not represented but with their water plane areas included in the restoring force matrix. A comparison of the heave response obtained using the above column representations showed diverse results in the case of large cross-section, closely-spaced columns. For a typical large SSM having slender columns which were widely spaced, the method produced motion values in good agreement with experimental results.

Sun (1980 and 1982) developed a practical method for the estimation of motion characteristics of semi-submersibles in waves using strip theory and assuming that the section dimensions were small compared to wave length. The method accounts for the effect of viscous damping and viscous exciting forces. The principle of minimum energy difference was applied to linearize the damping and drag terms. He introduced the concept of "equivalent wave height" for calculating the transfer functions with which both the short-term and long-term distributions and statistical characteristics of the motion of a semi-submersible could be estimated. The computed motions were in fair agreement with the experimental values of a 1:50 model of a twin-pontoon semi-submersible. Some discrepancies were observed between the computed and experimental values at wave periods less than 8 sec. It was pointed out that this discrepancy was probably due to interaction effects between elements which were observed during the model tests but not accounted for in the theory. It was therefore indicated that these interaction effects and the free surface effects on the added mass and damping coefficients should be further investigated to improve the accuracy of motion estimations.

Kim (1980) developed a method for estimating motions of multi-member semi-submersible platforms in head and beam sea waves using the strip theory and considering wave

diffraction and frequency-dependent added mass and damping coefficients. The computed added mass varied slightly with wave period but the damping due to radiated waves fluctuated significantly in the low period range (up to 16 sec). Viscous damping effects were not considered. Comparison of heave motions when including and excluding radiated wave damping revealed that the effect of damping was negligible outside the resonance region. The effect of damping in the resonance region (20-26 sec.) was found to be significant. The theoretical motion compared very well with the limited model test data, available for periods of 8-16 sec.

Nojiri (1981) compared the motion response of a semi-submersible derrick barge model with the computed values obtained using i) a two-dimensional strip method and ii) a three-dimensional singularity distribution method. The study indicated the validity of the three-dimensional analysis which showed better agreement with the experimental values. The results also showed non-linear behaviour in the resonance region of roll, indicating the need to account for viscous damping in roll in the numerical analysis.

Price and Wu (1983) modified and improved the three-dimensional source distribution theory used for ships to account for multi-body structures and used it to compute

the motion characteristics of a four- and an eight-column semi-submersible platform in regular waves. Comparing their results with experimental values reported by Lundgren and Berg (1982) and Tasai et al (1970), they found their numerical method to be efficient in determining the response of moored or freely-floating semi-submersibles in regular waves. A parametric study was carried out to investigate the sensitivity of the computed heave motion to variations in the mooring line angle in the vertical plane. The study revealed that the computed heave was insensitive to variations in the mooring line angle at wave periods less than 20 sec, but above this value the form of the response was found to change sharply with the angle. This led to the conclusion that a more refined numerical approach was required.

Lundgren and Berg (1982) carried out tests on a 1:65 model of the twin-pontoon, four-column GVA 4000 semi-submersible. The motion of the model was measured in regular and irregular waves. The effect on the motion due to variation of metacentric height (GM) of the rig and pretension of the eight catenary mooring lines was investigated. The results showed the motion response spectra in irregular waves contained motion components at lower frequencies than those contained in the wave spectra. These low frequency-motions had peaks which coincided with the natural frequency of the motion indicating second order effects. They indicated

that due to second order effects, the motion in irregular waves obtained using RAO's for regular waves, would be underestimated. It was also pointed out that the values of RAO's obtained from model tests in regular or irregular waves depended on the wave heights used during the tests. The results indicated that the motions due to first order wave effects were generally insensitive to variations of GM or mooring pretensions. However the effects of GM and pretension on the slow motion in the low frequency ranges of the second order wave was found to be significant.

Kallstrom (1983) developed a mathematical model for the motion of the GVA-4000 drilling rig by applying a system identification technique to motion data obtained from model tests in irregular waves by Lundgren and Berg (1982). The mathematical model included both mooring and dynamic positioning systems. Comparisons of the two systems were carried out in winds, waves and currents. The study illustrated the usefulness of mathematical simulation techniques in investigating the performance of floating structures in winds, waves and currents. It should be pointed out that some basic model tests are usually required as a basis for a mathematical model of this type.

Chakrabarti and Cotter (1984) analyzed the first and second order motions of a moored semi-submersible pipelaying barge in regular waves, wave groups and irregular waves using

numerical methods and an experimental scale model. The motion and mooring cable forces were computed using a three-dimensional source-sink method which accounted for the appropriate first and second order terms. A non-linear damping term based on a drag coefficient was included in the analysis. The analytical results were presented including and excluding the non-linear damping term. The first order solution correlated well with the experimental data except near the natural period. The correlation near the natural period significantly improved by the introduction of the non-linear viscous term. The slowly oscillating mooring line forces in surge (or sway) were obtained by solving a second order non-linear differential equation for the semi-submersible surge (or sway) motion near the natural period of the system. The results indicated that the computed mooring forces compared reasonably well with the measured values in irregular waves and wave groups.

Watts and Faulkner (1968) reported on full scale measurements of heave and wave characteristics made from the SEDCO 135-F semi-submersible while drilling offshore British Columbia in 1967 and 1968. A waverider buoy was used to measure wave profile and an accelerometer was used to measure the SSM heave. Close agreement was found between the measured heave response and the results obtained from model tests.

Full scale measurements of heave response of the Pentagone 81 semi-submersible obtained using an accelerometer and wave height and period obtained by a waverider buoy were reported by Rey-Grange (1971). The measured heave response was in general smaller than that obtained from a model test. Similar results were also reported by Kobus et al (1977) for the Zapata Ugland semi-submersible.

Vugts (1971) reported heave and wave measurements made from two semi-submersible drilling rigs in the North Sea. In the case of the Staflo SSM, both the motion and waves were measured using waverider buoys. A resistance wire wave staff mounted on a column of the other SSM, the Sedneth I, was used to measure the waves, while the heave motion was measured by a taut wire connected to the marine riser. The wave measurements obtained by the wave staff were corrected using the heave measurements. The correlation between the measured heave response and the calculated values was found to be satisfactory.

Forristal et al (1979) reported on wave and heave measurements made from the SEDCO 706 semi-submersible in the Gulf of Alaska and from the Ocean Prospector SSM, offshore Southern California. The heave motion and waves were measured using accelerometers and wave staff, respectively. Again, wave measurements were corrected by adding heave. The simultaneous wave profile and heave measurements were

analyzed by cross-spectral methods to obtain the amplitude and phase of the heave transfer function and the coherence between the two signals. The coherences were found to be very high in the energetic part of the spectrum, demonstrating the linearity of the heave response. Close agreement was observed between the measured transfer function, model test results, and the computed values using the MOSAS computer program (Opstal et al, 1974).

2.2.5.2 Structural Response Analysis

Bell and Walker (1971) presented the first published field measurements of stresses experienced by a semi-submersible through its operating life under normal and extreme storm conditions. The Sea Quest semi-submersible had three columns, each supported by a separate footing. Stresses were measured at a number of critical sections of the horizontal bracing members. Stresses were computed using space frame analysis with the hydrodynamic forces evaluated by Morison's formula and a 5th order wave theory; both drag and inertia terms were taken into account. The measured stresses were found to be, on average, about 80 percent of the calculated values.

Later on, Bell (1974) reported on motion responses and stress measurements of the Sea Quest SSM during 700 days of drilling in the North Sea. Waves were measured using

waverider buoys, heave motion by an accelerometer and the roll and pitch angles were derived from wire wound potentiometers attached to a gyroscope. Transfer functions of measured stresses, roll, heave and pitch were determined using spectral analysis. The transfer functions of the calculated stresses, obtained using the method outlined by Bell and Walker (1971), had a series of humps and hollows. This feature was not observed on the transfer function of the measured stresses. The correlation between the measured and calculated transfer function was presented for stresses only. It was found that the structural response to short waves was appreciably less than the calculated value but over a wide range of periods the agreement between measured and computed stresses was "encouraging".

Langfeldt et al (1975) and Olsen and Verl[illegible]1976) reported on full-scale measurements of structural and motion responses of the twin-pontoon, eight column Aker H-3 semi-submersible. The six degrees of freedom motion of the SSM were measured using a gyro-stablized platform while a wave-rider buoy was used to measure the wave profile. The strains were measured at 30 selected points located on a corner column, a secondary column, a transverse deck girder and bracing elements. Mooring cable forces were also measured using pressure cells at the anchor winches. Motion and structural responses were computed using a space frame analysis and an integrated program with determin-

istic, quasi-static, and stochastic dynamic capabilities. The computed motion and structural responses were compared with the corresponding measurements made over a period of one year. The study indicated that the measured motion characteristics and stress levels were consistently lower than those predicted by computation. The over estimation was higher for stress values than for the motion response. Better agreement was observed between the measured and calculated stresses in the bracing members than in the columns and girders. The results also confirmed the linearity of the structural and motion responses with respect to wave heights.

Opstal et al (1974) described an integrated motion and strength analysis system for semi-submersibles. The wave hydrodynamic forces were computed using strip theory. They also took into account viscous damping and the non-linearity of the mooring forces. Added mass coefficients were assumed independent on frequency and the wave damping considered negligible. The viscous damping coefficients were obtained from experimental data for units of comparable geometry. The non-linear equations of motion were solved by iteration. The structural response was carried out assuming space frame idealization of the SSM and using the ICES STRUDL structural analysis system. Computed added mass, exciting forces and motion of a typical semi-submersible were compared to corresponding

model test results. Fairly good agreement was observed between the computed and experimental values except at long periods. Sample computations were presented for the motion response and section forces in a horizontal bracing, secondary column, girder and a pontoon of a SEDCO-700 series SSM.

A similar integrated motion and structural analysis program was developed by Pincemin, et al (1974). The hydrodynamic force computations were based on Morison's equation considering inertial forces but neglecting drag and diffraction forces, and the hydrodynamic interaction between the different platform members. The computed motion response of a large catamaran type semi-submersible and the SEDCO 135 semi-submersible agreed reasonably well with the corresponding model test results. Complete stress analysis of SEDCO 135 was carried out using space frame idealization of the platform. The computed stresses in one of the horizontal braces seemed to be in reasonably good agreement with the corresponding measured stresses from the full scale platform operating in the North Sea, reported by Bell and Walker (1971).

Pauling et al (1978) developed a computation system for the determination of the wave induced structural loads on a twin-pontoon SSM using the method for hydrodynamic force computations described in a 1977 paper (Pauling et al,

1977). The inertia loads due to the platform mas assumed to be distributed along the length of each hull in proportion to sectional area and then added to the hydrodynamic forces (hydrodynamic loadings on the braces were neglected). The results of the computation could be expressed in one of the following three forms depending on the purpose and the degree of sophistication required in structural analysis. The three alternatives were i) a detailed distribution of loads over a modal mesh for input to a finite element structural analysis program, ii) forces and moments in the cross-structure connecting the two pontoons, or iii) vertical and horizontal shear and bending moment distribution along the length of the platform. Sample computations were presented for different sectional forces and moments. However, no experimental values were used to verify the computations.

Katayama et al, (1978) and Satake and Katayama (1977) reported on the motion and structural response analysis of a twin-pontoon semi-submersible using model tests and numerical methods. They presented an approximate response analysis method based on strip theory and Morison's formula considering linear/non-linear effects and neglecting hydrodynamic interaction between members and the variations of the hydrodynamic coefficients with frequency. The linear analysis was based on the small amplitude linearized theory

while the non-linear analysis was based on the finite amplitude and non-linearized theory. In the non-linear analysis wave forces were computed for the displaced and rotated structure position up to the wave surface, incorporating the non-linearities of drag force and mooring force. A space frame analysis was used to obtain the structural response. Tests were carried out on a 1:50 model of a twin-pontoon eight column semi-submersible. The model was split at the centre except for the fore and aft horizontal braces. Member force gauges were used to measure the horizontal force in these braces and the horizontal and vertical forces at the top of the corner columns. The results indicated that accurate prediction of semi-submersible motion characteristics was possible, even in very high waves, using linear analysis. However, it was pointed out that non-linear effects were important for the structural response analysis in high waves.

A comprehensive computer program was developed by Mitsui Engineering (1979) for the calculation of hydrostatic characteristics, motion response and structural analysis of semi-submersible platforms. The method of computing the hydrodynamic forces was based on the strip theory for the pontoons and Morison's equation for the columns, which neglected the hydrodynamic interaction among hull elements. The wave exciting force on the hull included Froude-Kriloff, inertial, drag and diffraction components. The

method accounted for wave damping, viscous damping and the frequency dependency of the hydrodynamic coefficients. The structural response was determined based on space frame analysis. The computed motion response was verified using model tests reported by Yoshida et al (1974). The computed stresses in 40 points in the bracings and in a corner column were compared with full scale measurements of the Aker-H3 semi-submersible in still water. The loads imposed on the structure was adjusted by controlling the amount of ballast water in the pontoons of the SSM. Relatively good agreement was observed between the measured and calculated stresses.

Bainbridge (1981) described an integrated structural analysis system for semi-submersible platforms. Forces considered were due to waves, currents, winds, weight, buoyancy, mooring and ice floes. The wave forces were based on Morison's equation and the diffraction forces were also accounted for. Finite element analysis was carried out using the NASTRAN computer program with beam, truss, plate, shell and shear elements for accurate idealization of the structure, in particular the junction between the main components.

Dao and Baily (1982) carried out a redundancy analysis of the SEDCO 710 semi-submersibe (similar to the one in Figure

2.1) to determine its ability to survive a catastrophic structural failure. Different assumptions were made for failures ranging from the loss of a single bracing member to the loss of a joint connecting several bracing members. Realistic modes of failure were assumed including supply vessel collision, dropped objects, blow-outs, or fatigue. For each case a dynamic structural analysis was performed using space frame idealization of the structure. The hydrodynamic forces were obtained using Morison's equation and neglecting the drag forces. It was pointed out that the mooring cables were found to have little effect on the motion of the SSM. The structural analysis indicated that all the resulting stresses due to combined static and dynamic loadings were less than the material yield strength. It was, therefore, concluded that the semi-submersible would not suffer any structural failure for the assumed loss conditions.

Incecik (1981) presented calculation procedures to determine the structural response values of floating structures. Space frame analysis was used for determinate structures, while a series of two-dimensional frame analyses was employed for indeterminate structures. The analysis which was carried out assuming restrained and free floating semi-submersibles indicated that the difference in the magnitude of structural response between the two cases was a maximum of ±20% in the operational region. It was pointed out that

a restrained structural model was found to lead to more accurate calculations and gave a factor of safety in design. The maximum structural response was found to occur in beam seas. The effect of non-linear free surface and the second-order forces were found to induce a maximum increase of 10% in the bending moment values on the transverse deck beam. A simplified model of a semi-submersible instrumented to measure the axial strains in a bracing member and bending strains in a transverse deck girder was used to check the validity of the calculated procedures. The measured bending moments of the flexible deck girder were found to agree better with the predicted values of the dynamic analysis than with the quasi-static analysis.

Carlsen and Mathisen (1980) used the two-dimensional strip theory, accounting for hydrodynamic interaction between the pontoon, and the three-dimensional source distribution method to study the motion and section forces of two semi-submersibles, one with widely spaced pontoons and the other with narrow spacing between the pontoons. The results showed good agreement between the motion responses obtained from both methods. For the section forces, however, considerable deviations occurred indicating large differences in the hydrodynamic loadings obtained by the two methods. It was pointed out that these differences were primarily due to the method used to compute the diffraction component

of the wave exciting forces in the strip theory (see Section 2.4.2). The improved strip theory presented by Mathisen et al (1982) provided much better agreement.

Mathisen et al (1982) presented an improved strip theory (Section 2.4.2) and studied the motion and structural responses of the GVA 4000 semi-submersible. The results were compared with theoretical results obtained using Morison's equation for the operating draft and the three-dimensional source distribution for the transit draft. The numerical results were compared with a 1:65 scale (glass) FRP-81 model data, for the operating draft only. The model was moored by eight chains, but the cables were not accounted for in the numerical models. The forces and moments at the centreline of the deck were measured by splitting the model into two halves and using specially designed sensors. The results indicated fair agreement between the calculated and measured motion at the operating draft. As for the section forces, reasonable agreement was obtained between the measured and computed shear forces and bending moment about the vertical axis. However, poor agreement was observed for the torsional moment and there were large differences for the normal force and the moment about the horizontal axis. The study illustrated the validity of the Morison equation approach for survival and operating conditions. The section forces obtained for the transit draft using the improved strip theory provided much

better agreement with the three-dimensional results than with the usual strip theory.

Chao (1978) investigated the structural response of a semi-submersible platform in regular and irregular waves using the strip theory for hydrodynamic loading computations and employing space frame idealization of the structure. The results of the structural analysis indicated that the bracing members were in general the most stressed members in the platform. It was pointed out that occurrence of maximum stresses depended on the separation distance between the major structural members in comparison with the wave lengths. The stresses in irregular waves were found to increase only moderately in high sea states, since the peak stresses for most of the structural members in a regular sea occur in waves with periods less than 10 seconds. A model test program was conducted to verify the theoretical stress calculations. A simplified aluminum model was built to a scale of 1:40. The model consisted of two cylindrical pontoons, four cylindrical columns, two tubes representing horizontal bracing members and two tubes representing deck girders. Each of the four transverse tubes were fitted with strain gauges to measure axial forces and bending moments about the horizontal/vertical axes. The transfer functions of the stresses measured in irregular waves were found to be in good agreement with the measured regular wave response amplitude operators

indicating the linearity of the structural response. Linearity of the response was also substantiated by regular wave measurements with varied wave steepness ratio. The measured stresses were found to compare well with theoretical calculations for both regular and irregular waves.

Yoneya (1984) presented the only published study on the structural response of semi-submersibles to regular waves using an extensively instrumented model of an actual twin-pontoon, eight-column semi-submersible. The structural members were made of acrylic pipes and plates, while steel and brass bars were used to simulate the mass distribution. Due to the difficulties in making and carrying the 1:50 scale model, complete structural similarity was not achieved. The ratio of axial rigidity between the braces and the deck transverse member was adjusted to be almost the same as that of a full-scale platform. However, the absolute values of axial rigidity of these members were two or three times the required model stiffness. Furthermore, the structural rigidities of all the other members (columns, pontoons and longitudinal deck members) were about ten times the required model values. Therefore, strains were measured in all the bracing members and two transverse deck girders only. The motion response was determined using three accelerometers attached to the decks. The measured motion and structural responses were

compared with theoretical results obtained from space frame analysis and strip theory. Wave diffractions and the interaction between members were neglected. Fairly good agreement was observed between the measured and computed motion response values, except at lower frequencies. However, the agreement between the measured and computed structural response was in general less than that of the motion response, especially at high wave frequencies. The study indicated that the mooring forces hardly influenced either the motion or structural responses and that the motion and structural responses were mostly linear. The structural response in most of the members reached a maximum for waves with lengths slightly longer than twice the transverse distance between the centres of columns or pontoons (full-scale period of 9-10.5 seconds).

The analytical methods to determine the motion and structural responses presented above are based on the rigid body assumption where the hydrodynamic forces and platform motion are first determined considering the platform as a rigid body and then the internal forces are analyzed using elastic structural analysis. Taylor (1974) investigated the motion response of general floating structures and indicated that for a structure of high rigidity, it would be sufficient to carry out elastic response analysis using the forces associated with rigid body motion, whereas member forces of a flexible floating structure should be

estimated using an analysis based on the motion involving elastic deformation. Very large semi-submersibles or a common semi-submersible under certain structural damage conditions may behave as an elastic structure. The elastic deformations of the structural members might affect the mode of motion of the whole structure; resonance of elastic deformations may occur within the range of wave frequencies (Yoshida and Ishikawa, 1980).

To account for structure flexibility, Yoshida et al (1974), and Yoshida and Ishikawa (1975, 1980) developed an analytical method, based on potential theory, to determine structural and motion responses of moored semi-submersibles. The flexibility of structural members was included in the equation of motion so that the internal stresses can be calculated simultaneously with the motion. A linearized drag term was added to the hydrodynamic forces while the hydrodynamic interactions due to multi-members were neglected. The semi-submersible was discretised into a finite number of elements. The elements were classified into two types according to their function, a hull element (for estimating external hydrodynamic and inertial forces) connected to a beam element (representing the structural stiffness). The analytical results were checked using simplified semi-submersible models with flexible bracing and deck girders. The measured motion and structural responses were in good agreement with the computed values.

The results indicated that in the case of flexible structures a frequency range existed where the elastic deformation of members affected the motion. For rigid structures, the frequency characteristics of internal forces was found to be a function of the ratio between wave length and the length of the structure.

Yoshida et al (1984) applied the above analytical method to tension leg platforms and reported better agreement between the experimental and analytical values when the structural flexibility was taken into account in the numerical computations.

2.3 Semi-Submersible/Bergy Bit Impact

Very detailed design methods have been developed based on analytical, experimental and field investigations of the behaviour of offshore platforms under various types of environmental and operational loadings. However, not much work has yet been done in the area of protection of offshore platforms against collision with ships, supply boats or icebergs and their fragments. Most of the work in this area is mainly in the research and development stage.

Most of the available studies deal with ship/supply boat collision with fixed/floating platforms. The actual interest in the problem of iceberg collision with gravity

platforms, and bergy bit impact on semi-submersibles started after the discovery of oil in the iceberg frequented waters of the Grand Banks of Newfoundland.

Extensive surveys of the existing literature indicated that detailed studies on the impact response of offshore structures have been reported by Fenco et al (1971), Fenco (1972), Sorensen (1976), Carlsen (1977), Larsen and Engseth (1978), Brakel et al (1979), Furness and Amdahl (1980), Oliveira (1981), Caldwell and Billington (1981), Davies and Mavrides (1981), Peterson and Pedersen (1981), Petterson and Johnson (1981), Cammaert and Tsinker (1981), Mavrikios and Oliveira (1983), Soreide and Amdahl (1983), Arockiasamy et al (1983 a, b), Croteau et al (1984), Swamidas and Arockiasamy (1984), Swamidas et al (1984), and El-Tahan et al (1985). These studies indicate that three analytical approaches have been utilized in dealing with the impact mechanics, one based on statical principles and the other two on dynamical principles.

In the statical approach the detailed non-linear behaviour of structural elements resisting impact have been considered using classical (elastic/elasto-plastic behaviour of isotropic cylindrical tubes) and numerical (finite element) approaches. These studies consider only the behaviour of the structural member at and around the point of impact. The impacting body is assumed to be a

rigid indentor (which is not the case) while the impacted structural member is assumed to absorb all of the impact energy by local deformation. The possibility of energy absorbtion by the deformations of the other members, motion of the impacted structure, deformation of impacting body, and inelastic rebound are not accounted for. The transient nature of the impact load, and its dynamic effects are neglected. Examples of the studies that adopt this approach are: Sorenson (1976), Carlsen (1977), Oliveira (1981), Furness and and Amdahl (1980), and Soreide and Amdahl (1983).

In another statical approach, the impacting body (namely, iceberg) is assumed to deform plastically (crush) while the impacted structure assumes the role of the rigid indentor (Cammaert and Tsinker, 1981).

Two different approaches have been used in the dynamical formulation of the impact on offshore structures: the plastic impact and the inelastic impact. In the plastic impact approach, the two bodies are assumed to stick together upon impact and then move as one body. The common initial velocity is obtained using a momentum equation. This type of impact is possible only when the interfacial stiffness of the colliding bodies is very small and the energy absorbed by elastic deformation in the contact area is negligible. The main drawback of this approach is that

the actual stiffness characteristics of the impact area are neglected and the possibility of separation (rebound) is not accounted for. Studies adopting this approach have been reported by Fenco et al, 1971, Fenco (1972), Reddy et al (1982), Arockiasamy et al (1983 a, b) and Mavrikios and Oliveira (1983). The impacting forces obtained assuming plastic impact are usually very small being up to 10% of the weight of the impacting body for a collision speed of 1 m/sec. These values present the lower bound of the impact forces since the impacting surface is assumed to deform (or crush) considerably during the initial impact period so that both the bodies can move together during the remaining impact period.

In the inelastic impact approach the local load-deformation characteristics of the colliding bodies are simulated using either linear springs (Swamidas et al, 1984) or non-linear springs with elasto-plastic impact (Petterson and Johnson, 1981). This approach is more realistic than the plastic impact assumption since it permits a better simulation of the interaction process during impact. It also allows the impacting body to separate from the structure and rebound. This type of impact is more likely to take place under certain conditions when the energy absorbed by local elastic deformation is released back into the system. The possibility of rebound has been considered in some recent studies by Swamidas and Arockiasamy (1984), Swamidas et al

(1984), and El-Tahan et al (1985). The analytical results indicated that rebound will occur. This finding was verified by the results of the impact tests on the hydro-elastic model reported in the present study. The impact forces obtained using the inelastic impact approach are at least one order of magnitude higher than those obtained assuming plastic impact.

A brief reviw of the available studies on the impact of bergy bits and ice floes on semi-submersible platforms is presented below.

Fenco (1972) carried out a study to evaluate the ability of semi-submersible platforms to withstand impacts caused by ice floes and growlers of various sizes and speeds, without structural damage. Four types of load application were considered: i) gradually applied loads; ii) transition between gradual and sudden; iii) short duration; and iv) very high velocity impact. Two approaches were used in the analysis, a momentum and energy approach, and the solution of the exact differential equation for the transition range. The results were presented in the form of curves for the forces in various members of the semi-submersible as a function of the mass and drift velocity of the ice masses. The main conclusion of the report is that the semi-submersible platform, "...does not seem suitable for ice-infested regions of the North Atlantic". Since large

ice masses are capable of moving with velocities in the order of 6 m/sec, the study indicated that the required structural strengthening should cover the complete range of wave action.

Reddy et al (1982) and Arockiasamy and Reddy (1982) presented the impact force and surge and pitch responses of a typical semi-submersible to a 50,000 tonne iceberg impacting the pontoons. The analytical model was based on a two degrees-of-freedom spring-mass system and the plastic impact approach. They pointed out that the impact forces and responses depended mainly on the stiffness of the mooring cables, and that the pontoons need extra strengthening to withstand the impact loads.

Swamidas et al (1983) investigated the global response of a moored eight-column semi-submersible and the local indentation of an adequately reinforced column due to bergy bit impact. Two numerical models were presented. The first is based on the principle of conservation of total energy of the system and the other on the plastic impact approach. Numerical solutions were presented only for the plastic impact assumption and used a five-degrees-of-freedom system to represent the rigid body motion of the platform (heave was excluded). The results were presented for the collision of 5,000 and 10,000 tonne bergy bits moving at speeds of 1 and 1.5 m/sec with a corner column at

an angle of 60° to the direction of surge. The results indicated that the maximum impact load was about 3.7 MN (3.7% of weight of the 10,000 tonne bergy bit) and that the local denting of the column will take place when the impact load reaches 0.25 MN.

Arockiasamy et al (1983 a, b) presented the transient response of a semi-submersible to sea ice and bergy bit impact. The analysis was carried out using the numerical model outlined by Swamidas et al (1983) for a 5,000 tonne bergy bit colliding with a corner column of an eight-column semi-submersible, at impact speeds of 1 and 1.5 m/sec. In the case of ice sheets, the ice sheet was assumed to move at an angle of 45° to the direction of the surge and to exert forces on the three iceward corner columns. The results indicated that the response to ice forces was mainly due to the constant part of the ice forces while the contribution from the varying part of the ice forces was almost negligible. The impact force due to bergy bit impact was found to be about 1.2% of the bergy bit's weight for an impact speed of 1 m/sec, and 1.8% for a speed of 1.5 m/sec. The local denting of the column was determined using an energy approach and assuming perfectly rigid plastic behaviour and yield conditions for the dented area. It was found that the column will suffer only local denting without undergoing overall failure.

The five degrees-of-freedom rigid body model developed by Swamidas et al (1983) was extended to incorporate two local degrees-of-freedom in order to represent the local characteristics of the ice and the structure at the impact zone. The load-deformation relationship for the ice and the structure was assumed to be linear and was simulated using linear springs with tension cut-off. Hence the model can account for the inelastic impact assumption and be used to investigate the possibility of bergy bit rebound during impact. The model was then used to study the response of a semi-submersible to bergy bit and ice floe impact (Swamidas et al, 1984). The results were presented for bergy bits with masses of 2,000 to 10,000 tonnes impacting a corner column at speeds of 1 to 4.5 m/sec. The study indicated that the impact forces were highly dependent on the characteristics of the impact zone in the ice and the structural member. The peak impact force was found to be about 4 times higher than the weight of a 2,000 tonne iceberg at an impact speed of 4.5 m/sec. The impact forces were linearly proportional to the impact velocity. The analytical model also predicted rebound of the bergy bit after impact.

Curtis et al (1984) used a numerical model having three global (surge, sway and yaw) and two local degrees-of-freedom (for ice and structure) to investigate the impact of bergy bits and small icebergs on the braces and pontoons

of a semi-submersible. The local deformation was simulated using four non-linear springs. Three iceberg masses were considered, 5,000, 20,000 and 50,000 tonnes and the initial iceberg velocities varied from 1 to 4.5 m/sec. The results indicated that the deformation energy absorbed by the semi-submersible was strongly dependent on the force-penetration relationship, especially at low energy impacts. The impact forces produced yielding in the horizontal braces and the pontoon for iceberg velocities of 2.5 m/sec and greater (with the exception of the 5,000 tonne bergy bit moving at 2.5 m/sec). The study also indicated that the semi-submersible experienced significant structural damage and that the minimum anchor pullout capacity is exceeded for almost all of the impacts. The global response of the semi-submersible was almost independent of the local characteristics of the impact zone.

Kitami et al (1984) investigated the structural safety of a semi-submersible due to the collision of a bergy bit with one of its four columns. The numerical model used in the study considers three-degrees-of-freedom for the rigid body motions (surge, sway and yaw) and a non-linear load deformation relationship for the structure and the ice. The masses of the bergy bits varied from 500 to 10,000 tonnes and the impact speeds from 0.5 to 2.5 m/sec. Ice thickness was assumed to vary from 1 to 13 m. For a 2,000 tonne bergy bit moving at a speed of 1 m/sec, the impact

force was about 75% of the bergy bit's weight. It was found that the semi-submersible could sustain the impact of a 2,000 tonne bergy bit moving at 1.5 m/sec. without permanent deformation to the column.

Noble and Singh (1982) carried out a series of tests to determine the total load exerted by ice floes on four, six and eight-column semi-submersibles. Rigid models of the columns, representing one half of the SSM, were towed at a speed corresponding to 1 m/sec in full scale into a synthetic ice floe field. The results indicated that the measured ice loads at 70-80% ice field concentration were about 10-20% of the maximum loads which occurred at 100% concentration. The maximum ice loads (at 100% concentrations) for the full scale four, six and eight-column semi-submersibles were 28 MN, 53 MN and 46 MN respectively, indicating favourable performance of the four-column SSM.

2.4 Impact Strength of Iceberg Ice

Icebergs have been of interest to various groups for many years. In the beginning iceberg concentrations, types and movements near the shipping routes were of interest. With increasing drilling activities in the North Atlantic, more attention has been paid to iceberg characteristics, (e.g., mass, draft, above water dimensions, drift speed, etc.).

Not until very recently have the mechanical properties of iceberg ice become of interest.

The strength and load-deformation characteristics of iceberg ice during impact are needed to estimate impact forces on offshore structures and to determine the extent of local damage to the impacted member (Section 2.3).

Extensive review of the literature has revealed that while there is a considerable amount of information available on the physical and mechanical properties of Arctic and Antarctic glacier ice, there is very limited information available on the mechanical properties of ice obtained from icebergs. In fact, the first published data on the strength of iceberg ice was the one reported by Arockiasamy et al (1983a), based on preliminary findings of the testing program reported in the present-study. This was followed by a paper by Gammon et al (1983) who reported on uniaxial compressive strength of iceberg ice. The only published in-situ measurements of iceberg strength (flaking pit tests and borehole jack tests) were obtained by Fenco (1975, 1976) for two icebergs while conducting in-situ measurements on sea ice.

Apart from the above-mentioned studies, there is no data available in open literature on iceberg strength. However,

several studies have been carried out on glacier and snow ice.

The United States Army SIPRE (now CRREL) have carried out extensive deep core drilling research programs on the glacier ice of Greenland and the Antarctic. Physical, structural and mechanical properties of glacier ice were determined from those tests. Uniaxial, ring tensile, flexural and shear strength of Greenland ice were reported by Butkovich (1956, 1959) and Kovacs et al (1969). The dynamic modulus of elasticity of Greenland ice was determined by Nakaya (1959) and Smith (1969). The uniaxial compressive strength and the dynamic modulus of elasticity for Greenland and Antarctic glacier ice were reported by Ramseier (1966). Kovacs (1978) presented the results of axial double point-load tests on Antarctic glacier ice.

Another deep core drilling program in the Antarctic has been carried out by the Japanese Antarctic Research Expedition (JARE). Very limited information on the mechanical properties of ice obtained from these cores has been reported by Maeno et al (1978) and Shoji (1978).

There are also considerable amounts of data on the strength of natural snow ice (found on rivers or lakes) and artificial snow ice. Some of these tests are reported by Butkovich (1955), Frankenstein (1959), Weeks and Assur

(1969), Carter (1970), Hawkes and Mellor (1972), Haynes (1978) and Mellor and Cole (1983).

Almost all of the above studies present the uniaxial strength of glacier and snow ice under strain rates up to 10^{-3}/sec. Very limited information is available on the strength of glacier and snow ice at high strain rates (greater than 10^{-3}/sec) and multiaxial stress conditions.

2.5 Summary

A review of the available theoretical, experimental and field studies on the structural and motion responses of semi-submersible platforms to wave forces and transient ice impact has been presented. The review revealed that there are a significant number of experimental and analytical studies on the motion response of semi-submersibles in waves. Several integrated motion and structural analysis computer program systems have been developed over the past two decades. There are a limited number of available experimental studies on the structural responses of the SSM's in waves. Only the forces in bracing members and/or deck girders have been measured in simplified models. Available full scale measurements of the motion of SSM's are limited, while those of stresses are rare.

The computed motion response values of SSM's in waves were generally in good agreement with those obtained from model tests or field measurements. However, the computed structural response values (forces and stresses) using space frame analysis were consistently higher than those obtained from field measurements. Better agreement was observed between the computed and measured stresses in the bracing members than in columns and girders. One possible explanation for this is that the bracing member is a slender one and can be represented by a beam element in space frame analysis. But the columns, for example, are more likely to behave like a shell rather than a beam. The agreeement between the computed and experimental structural response values (measured in bracing and girders only) was in general less than that of the motion response.

All the available studies on bergy-bits impacting structural members of a SSM are based on theoretical models. The impact force and duration obtained from these models were found to vary by at least an order of magnitude depending on the assumption of plastic or inelastic impact and the characteristics of the impact zones in the structure and ice. The impacting bodies were treated as rigid bodies and all the deformations assumed to take place in a zone around the collision point only. The energy absorbed by the global structural deformations or by the rigid body rotation of the impacting body was neglected.

In addition, simplified assumptions were made for the transient hydrodynamic loadings on the SSM and the bergy-bit. The actual load deformation characteristics of the bergy-bit contact zone were not properly simulated in most of the studies due to the lack of needed information about iceberg ice. The values used by Curtis et al (1984) were based on uniaxial compressive strength values at a strain rate of 10^{-3} while those used by Kitami et al (1984) were based on sea ice strength values.

The above discussion indicates the need for model tests to check the validity of computational methods, structural modelling (i.e., space frame analysis etc.) and theoretical assumptions for both types of loadings (wave action and bergy-bit impact) on a semi-submersible. In addition, it also indicates the need for experimental studies on the impact strength of iceberg ice under multi-axial state of stress to obtain its load-deformation characteristics.

CHAPTER III

IMPACT STRENGTH OF ICEBERG ICE

3.1 General

In order to design offshore structures to withstand ice impacts, it is necessary to know the force and stresses caused by ice during impact. Therefore, the mechanical properties of ice under multi-dimensional stress state and high strain rate conditions are needed. Although a significant amount of knowledge on the mechanical properties of ice has been gained during the last two decades, the behaviour of ice during impact is not fully understood yet.

Very few studies have been reported on the impact strength of sea ice (Likhomanov and Kheisin, 1971; Kheisin and Likhomanov, 1973; Kheisin et al, 1975; and Glen and Comfort, 1983). Impact strength tests on river ice have been reported by Timco and Martin (1979). No similar studies are available for iceberg ice, glacier ice or snow ice.

The strength and load-deformation characteristics of iceberg ice during impact are needed to estimate impact forces

on offshore structures and to determine the extent of local damage to the impacted members (see Chapter VI).

Since ice samples from an iceberg are hard to come by and expensive to acquire, it would be advantageous to make an analogous ice, viz., snow ice, possessing similar physical and mechanical properties so that studies could be made in the laboratory. The objective of the study presented in this chapter is to investigate the strength of iceberg ice and artificial snow ice under impact conditions (multiaxial stress state and high strain rates).

3.2 Ice Testing Program

Although the structure of iceberg ice will be the same as that of the parent glacier ice, mechanical properties may not be the same. Cracks develop in icebergs due to stresses caused by balancing gravitational and buoyant forces and thermal stresses due to the fluctuation in the ambient temperatures during drifting and overturning. Therefore, the standard uniaxial compression tests were carried out to correlate the ice strength to that of glacier and other types of ice. The uniaxial compression tests were carried out on cylindrical specimens. The snow ice specimens were 2 inches (50.8 mm) in diameter and 5 inches (127 mm) long. For the iceberg ice specimens the

dimensions were 3 inches (76.2 mm) and 8.25 inches (209.6 mm), respectively.

Because of the three dimensionality of the stress state during impact, the pressure on the structure can be much higher than the unconfined (uniaxial) compressive strength. In situ measurements carried out by Fenco (1975, 1976) indicated that the confined compressive strength of iceberg ice (from the bore hole jack test) can be as much as five times the unconfined compressive strength (from the flaking pit test). Studies on the impact of ice sheets on a fixed structure indicate that the effective pressure could be as high as five or six times the uniaxial strength of ice (Lipsett and Gerard, 1980). Therefore, indentation and impact tests were carried out to correlate the contact pressure during impact to the uniaxial strength of ice.

The indentation tests were used to simulate the sudden load application over a small portion of the ice surface. In these tests, load was applied at the centre of the top face of a 16 x 16 x 10 cm ice block through cylindrical or flat circular indentor. The maximum dimension of the indentor was about 1/4 of the width of the block. Tests were carried out on both confined and unconfined ice blocks. The confined tests were carried out by confining the ice blocks within rigid aluminum boxes open at the top (wall

thickness of 12.5 mm). The unconfined ice blocks were supported at the bottom over the entire base area.

The impact tests were carried out by dropping a heavy cylindrical indentor, instrumented with an accelerometer and a force transducer, onto confined ice blocks measuring 27 x 20 x 15 cm. The velocity of the impact of the falling weight was 2 m/sec. The falling body was heavy enough to cause failure of the impacted surface. The accelerometer measured the deceleration of the indentor, while the force transducer measured the instantaneous pressure produced in the ice at the centre of the indentor.

All the above tests were carried out on both iceberg and artificial snow ice.

3.3 Preparation of Test Specimens

The iceberg ice was collected during three field trips from 'small' pieces of ice broken off a grounded iceberg near St. John's, Newfoundland, in the period June-July, 1982. The ice, after being cut into about 80 smaller blocks, was stored in sealed plastic bags in deep freezers at -18°C. The snow used in making snow ice was produced by scraping fresh water ice using a metal disc containing four grinding blades and a drill bit (Figure 3.1) at a temperature of -20°C. As presented in Figure 3.2, the artificial snow had

grain size distribution (Figure 3.2) similar to that of the natural snow reported by Halvorsen (1959).

The snow ice was produced as follows: the aluminum mould, 18 x 16 x 75 cm for uniaxial and indentation test samples (Figure 3.3) and 30 x 30 x 20 cm for impact test samples, was placed on a vibrator and the artificial snow was sieved into the mould using #16 sieve (1.1 mm). The snow was compacted in layers by placing a 12 mm thick steel plate on the top of each layer and turning the vibrator on. This took place at a temperature of -20°C. The snow was then left for approximately 2 hours at a temperature of about -3 to -5°C. The snow was then saturated by allowing de-aired water at 0°C to enter through holes at the bottom of the mould forcing the air out. After the snow was saturated the mould was insulated from the top and sides to allow the freezing to take place from the bottom. The temperature was lowered to -20°C for three days. The snow ice blocks were removed and cut to required dimensions and stored in sealed plastic bags at -18°C.

The cylindrical specimens for the uniaxial tests were cut on a metal lathe to within 0.1 mm of the required diameter using a rounded, high rake cutting tool which produced a smooth finish. The sample ends were made parallel to each other and perpendicular to the specimen axis using a special jig and lapping plate. The produced ends were

polished and parallel within 0.05 degrees. The ice blocks for the indentation and impact tests were cut to the required size (within 1 mm) using a band saw. The top and bottom surfaces of the ice block were sanded and polished, using the lapping plate to obtain smooth and parallel faces.

3.4 Physical Properties

The density of the ice was obtained by the hydrostatic weighing method. The density of iceberg ice (12 pieces) ranged from 0.900 to 0.906 with an average of 0.904 Mg/m^3 and a standard deviation of 0.002. The density of snow ice (40 pieces) ranged from 0.845 to 0.885 with an average of 0.861 Mg/m^3 and a standard deviation of 0.008 (Figure 3.4). The density of snow ice was maximum at the bottom of the block with a percentage difference of 2.9% from bottom to top. The average porosity of iceberg and snow ice were 1.4% and 6.1%, respectively.

The density of iceberg ice falls within the reported range of the Greenland glacier ice of 0.900 to 0.916 Mg/m^3 (Butkovich, 1959). The density of the artificially produced snow ice was lower than that of the glacier ice and can be improved to obtain as high a value as 0.917 Mg/m^3 using special techniques similar to those developed at CRREL (Cole, 1979). However, since the strength of the

snow ice was found to be close enough to that of the iceberg ice, no attempt was made to increase the snow ice density.

Crystallographic analysis was carried out on both the snow and iceberg ice following the standards proposed by the working group of the International Association for Hydraulic Research, IAHR, (1980). The results are presented in Figures 3.5 to 3.7.

The analysis of thin sections of the iceberg ice indicated that almost all the crystals consisted of irregular interlocking grains with no preferred c-axis orientation. Some sections showed high crack intensity (2-3/cm) while no cracks were observed in other sections. The cracks generally showed a preferred orientation. Air bubbles were nearly round with typical diameter of about 0.3 mm. Grain size distribution was obtained from seven thin sections containing 431 grains. The grain size ranged from 1 to 25 mm with a mode of 3 mm and an average of 7 mm (Figure 3.5). The snow ice had higher bubble densities than the iceberg ice, but no cracks were observed. The grains of snow ice had regular shapes and grain size had a normal distribution which ranged from 0.1 to 1.8 mm with an average of 0.85 mm and a mode of 0.7 mm (Figure 3.6).

3.5 Test Procedure

The uniaxial compressive strength and indentation tests were carried out using the model 905.99 MTS closed-loop electrohydraulic testing machine in the stroke-control mode under two different stroke time histories. The first is a ramp function which gave a constant strain rate while the second is a step function. Two constant strain rates were chosen: 10^{-3} and 10^{-2} per sec. The machine deformation was taken into account in setting the machinehead speed to produce the required strain rates. For the indentation tests, the relation between the surface indentation and the strain in the failure zone under the indentor was determined using finite element analysis of the ice block.

The tests were carried out in the No. 2 Cold Room at Memorial University of Newfoundland. All the impact and indentation tests and most of the uniaxial compression tests were carried out at a temperature of -5°C. It was assumed that the temperature of ice at the region of impact (in the field) would average about -5°C. This is based on the results of temperature measurements carried out on the drifting glacier ice island "North Pole 19" by Legenkov, et al (1974), and is supported by the results of recent field measurements of the temperature of several icebergs reported by Diemand (1984). This temperature of -5°C also

takes into account the effect of the faster melting of icebergs in warmer waters.

Some uniaxial compression tests were carried out at a temperature of -2°C, to study the behaviour of ice near the freezing point of sea water.

Since the ice samples were stored in a freezer at a temperature of about -18°C and tested at temperatures of -5°C and -2°C, sufficient time had to be allowed for the samples to reach an equilibrium state at the test temperatures. A dummy sample with a thermocouple at its centre was used to determine the minimum conditioning time, which ranged from 3 to 4 hours depending on sample size and type.

The tests were carried out at least one hour after the samples reached the equilibrium temperature. Temperature at the centre of each sample was checked after the testing using a thermometer. The measured temperatures were within less than 0.5°C from the required temperature.

Time histories of test parameters measured by the load cell, LVDT, extensometer, etc., were stored on an 8-channel HP tape recorder, since the fastest test lasted only a few milliseconds. This information was digitized using the HP Fourier analyzer and transferred to the PDP 11 computer for

further processing. The value of maximum load was read directly from the MTS digital memory readout.

In order to ensure the validity of the experimental results, at least five samples were tested for each condition of loading, strain rate, ... etc. Altogether, 136 samples were tested, of which 63 were for uniaxial, 54 were for indentation and 19 for impact tests.

3.5.1 Uniaxial Compression Test

The standards followed for sample shape, size, end conditions, and testing procedure were those recommended by the working group of the IAHR (1980).

Immediately before the testing, the ends of the cylindrical specimen were trimmed on the bandsaw (using a miter guide) to the required length (127 mm for snow ice and 210 mm for iceberg ice). The ends were made parallel to each other and perpendicular to the specimen axis using a special lapping jig. The specimen was introduced into the jig and the ends were rubbed over sandpaper placed over the lapping plate until the ends were truly perpendicular to the axis of the jig. The ends were then polished by rubbing over the lapping plate. The length and diameter of the specimen were measured to the nearest 0.1 mm. To ensure perfect

contact between the specimen ends and the testing machine heads, the specimen was frozen to the platens of the testing machine. First the specimen was frozen to the bottom platen of the machine. Then the machine head was moved manually until the top end of the specimen was within 2 mm of the top machine platen. Cooled water at 0°C was squirted on the top of the specimen and the specimen was brought into contact with the top platen by applying a very small load.

The sample was then left to freeze and attain thermal equilibrium for at least 10 minutes. During this time an MTS model extensometer was installed on the sample using a specially designed holding device to extend the gauge length from 25.4 mm to the required gauge length (102 mm for snow ice and 165 mm for iceberg ice). Figure 3.8 presents the test set up for an iceberg ice sample. After the test, each sample was photographed and a sketch of the failure pattern was made. The temperature at the centre of the specimen and the maximum load were recorded.

3.5.2 Indentation Test

When a vertical compressive load is applied through a limited area on a larger block surface, a confining (horizontal) pressure develops and the strength becomes higher than the uniaxial strength. The magnitude of this

confining pressure depends on the ratio of the loaded area to the total surface area of the block. A parametric study to determine the effect of relative sizes of the block and indentor on the confining pressure and stress distribution through the block was carried out using a plane strain finite element model (Figure 3.9). The study indicated that the confining pressure under the load centre increases rapidly as the ratio of the block width to the indentor width varies from 1 to 3. As the ratio exceeds 4 the confining pressure varies very slightly. At this ratio (of 4) it was found that the confining pressure below the indentor centre increased by only 15% if the sides of the block were assumed to be rigid. This indicated that for a ratio of 4 or more, the strength could vary by a maximum of 15% if the block sides extended to infinity, or the block was confined. It was also found that the confining pressure was affected by the block height variation. The confining pressure does not vary if the block height is more than 1.25 times the indentor width. Based on that the ice block for the indentation test was chosen to be 160 x 160 x 100 mm. Figures 3.9 and 3.10 present the contours of principal shear and normal stress in the block. Confining pressure under the centre of the indentor is about 67% of the vertical applied pressure. Tensile stresses are present in the centre of the block and at its surface.

Two indentors were used in this test. The first one was a flat circular indentor with a diameter of 45.2 mm (area of 1600 mm^2). The second one was a cylindrical indentor (axis parallel to ice surface) with a length of 50 mm and radius of 25 mm.

The indentor was attached to the upper head of the testing machine, while a 160 x 160 x 25 mm steel plate was attached to the lower head. To prepare the samples for tests, the top and bottom surfaces (160 mm x 160 mm) of the ice block were sanded and polished, using the lapping plate, to obtain smooth and parallel faces. For the unconfined tests, the ice block was frozen to the base plate (Figure 3.11). For the confined tests a small amount of water at 0°C was placed immediately into the mould, forcing a thin film of water all around the ice block for perfect contact. After the water was completely frozen (at least 2 hours), the mould was placed onto the base plate of the machine so that the centre of the indentor coincided with that of the specimen (Figure 3.12). To achieve perfect contact between the specimen and the indentor surfaces, a thin film of cold water was frozen between them.

After the test was carried out, the specimen was photographed and a sketch of the failure pattern was made.

3.5.3 Impact Test

Figure 3.13 presents the impact test set-up. The 270 x 200 x 150 mm blocks were confined in a 12.7 mm thick aluminum mould. Only two tests were carried out on unconfined snow ice blocks. Two blocks of S2 type fresh water ice were impacted in a direction perpendicular to the crystal axis, for qualitative comparison with the snow and iceberg ice.

Figure 3.14 presents an outline of the impact device while Figure 3.15 presents the locations of the instrumentation of the indentor. The total mass of the indentor assembly was 59.85 kg. The indentor used had the same dimensions as the cylindrical indentor used in the indentation test. It was equipped with a 12.7 mm dia. impact force transducer and an accelerometer. The indentor was dropped from a height of 204 mm which produced an impact velocity of 2 m/sec. The indentor assembly was guided during the fall to keep it from rotating. The assembly was dropped using a manual mechanical trigger. An electric switch was used to record a triggering signal on the magnetic tape about 25 milliseconds before the indentor impacted the ice surface. This signal was used to trigger the Fourier Analyser for processing the data.

After the test was completed, the sample was photographed and a sketch of the failure pattern was made. The indenta-

tion depth was measured using a dial gauge. Each block was cut into thin sections to study the crack patterns in different planes inside the block.

3.6 Results and Discussion

3.6.1 Uniaxial Compression Tests

All the snow ice specimens tested at strain rates of 10^{-3} and 10^{-4} exhibited ductile failure. After reaching the maximum load, the middle portion of the specimen started to bulge but no cracks could be seen (Figure 3.16). The specimen diameter at the middle increased with increase in displacement. At a strain rate of 10^{-2} and higher, the failure of the snow ice specimen was brittle. Near the maximum load cracks initiated at the middle. Then the specimen collapsed suddenly by bursting into round crystals (about 1 mm) at the middle of the specimen (Figure 3.17).

All the iceberg specimens tested at a temperature of -5°C exhibited brittle failure at strain rates of 10^{-3} and higher. However, at a temperature of -2°C, the failure became more ductile at 10^{-3} per sec, but returned to the brittle type at higher strain rates. The brittle failure in the iceberg ice developed as follows: near the maximum load, vertical cracks initiated at the middle portion of the specimen and spread towards the specimen ends as the

load increased. Then transverse cracks developed causing sudden failure (Figure 3.18). The same crack pattern was also observed for the ductile failure. However, after the maximum load was reached, the load did not drop abruptly but slowly to zero.

Stress-strain curves for snow and iceberg ice are presented in Figure 3.19. These curves represent the average values of strength and strain at failure for each category. Figure 3.20 presents the uniaxial strength of both types of ice versus the actual strain rate. The dotted and solid lines connect the average values at each strain rate for iceberg and snow ice, respectively. The scatter in the strength of iceberg ice is considerably larger than that in the snow ice. This is to be expected, since the snow ice was produced in the laboratory under controlled conditions while the iceberg ice was collected from the iceberg over a period of about six weeks.

Table 3.1 presents a summary of the test results. The properties of the snow ice are comparable to those of the iceberg ice. The strength of the snow ice is slightly lower than that of the iceberg ice at any given strain rate. The reverse is true for elastic modulus (initial tangent) values. As expected the elastic modulus increased as the strain rate increased. The mean strength of the snow ice almost doubled as the strain rate increased from

10^{-4} to 10^{-3} per sec. For strain rates of 10^{-3} and higher, the strength of both types of ice did not vary significantly with strain rate. The snow ice failed at higher strain than the iceberg ice, probably due to the higher porosity of the snow ice which reduced crack formation.

As mentioned earlier, the failure of all specimens initiated at the middle of the specimen, indicating perfect end conditions. To ensure that the technique of freezing the specimen ends to the machine platens did not affect the test results, some snow ice specimens were tested using compliant platens of the type developed by CRREL. The ends of the specimens were prepared as described earlier ensuring extremely smooth ends of the specimens. The specimens failed at the middle with an average strength of 6.81 MPa at a temperature of -5°C and a strain rate of 10^{-3}. This value was very close to the value of 6.98 MPa obtained for specimens frozen to the machine heads at the same temperature and strain rate.

3.6.2 Indentation Tests

The failure of all the unconfined blocks took place suddenly, soon after the maximum load was reached, indicating brittle failure. The same behaviour was observed for the confined blocks at strain rates of 10^{-2} and higher. Only at the strain rate of 10^{-3}, did the confined blocks show

ductile behaviour. Typical failure patterns of confined and unconfined ice blocks are presented in Figures 3.21 to 3.23. The failure of the unconfined blocks took place in two stages: local crushing of the most stressed region under the indentor, and fracture of the whole block. The crushed volume under the circular indentor had a conical shape, its base coincided with the indentor surface and height was about 1 - 1.2 times the indentor diameter. For the cylindrical indentor the crushed volume had a wedge shape.

The block fracture took place when this crushed wedge or cone was sheared off at planes of maximum shear stress (Figure 3.9), and driven into the block causing its sudden fracture by tensile stresses on vertical planes passing through the block centre, mid-sides and corners. Iceberg ice blocks broke into more pieces than the snow ice blocks did, under similar conditions. Again this was probably due to the existence of micro-cracks in the iceberg ice and the higher porosity of snow ice. Only the local crushing failure was observed in the confined blocks.

Figures 3.24 and 3.25 depict representative load-displacement curves for the iceberg ice (cylindrical indentor) and snow ice (circular indentor), respectively. The solid lines represent the unconfined blocks while the

dotted lines represent the confined blocks. Table 3.2 presents a summary of the indentation test results.

The confined blocks had an average strength about 10-20% higher than the unconfined blocks under similar conditions. This was to be expected since the results of the finite element analysis indicated that confining pressures would increase up to 15%, if the ice block was confined.

The indentor shape influenced the strength considerably. For example, cylindrical indentation increased the average strength of snow ice by about 30% of that for flat circular indentation at a temperature of -5°C and a strain rate of 10^{-3} per sec. The corresponding increase for iceberg ice was about 25%. The lower strength for the circular indentor is probably due to the effects of the stress concentration around the edge of the flat circular indentor. For the same indentor shape and strain rate, the indentation strength of snow ice was very close to that of the iceberg ice. The indentation strength of snow ice increased slightly as the strain rate increased. However, for iceberg ice the strength had a peak at a strain rate of 10^{-2} per sec. This peak usually takes place near the transition from ductile to brittle failure. Iceberg ice was more brittle than snow ice and therefore the transition in iceberg ice took place at lower strain rates than in the snow ice.

Figure 3.26 presents the average uniaxial (UNI) and indentation (IND) strengths of the snow (SI) and iceberg ice (II) at different strain rates. The indentation strength was much higher than the uniaxial strength. For example, unconfined snow ice blocks at a strain rate of 10^{-3} per sec and a temperature of -5°C, had an indentation strength, for circular and cylindrical indentors, which was 2.34 and 3.04 times the uniaxial strength, respectively. The corresponding ratios for iceberg ice were 2.28 and 3.14. The strains at failure for indentation tests were higher than those of the uniaxial strength tests at the corresponding strain rates.

3.6.3 Impact Tests

Figures 3.27 to 3.30 present typical failure patterns in the tested ice blocks as obtained from longitudinal, transverse and horizontal slices (1 cm thick). The failure took place as crushing of the area under the indentor accompanied by radial cracking of the ice around the crushed region and vertical fracture planes passing through the whole block. For confined ice blocks, the patterns, extent and intensity of the cracks and the number of the fracture planes varied from one type of ice to another depending on the density of air bubbles. For example, extensive cracks developed around the region of crushed ice in the S2 ice samples (Figure 3.30). The crack density was considerably

lower in iceberg ice (Figure 3.29) and no such cracks were observed in snow ice (Figure 3.27). The failure at ice surface was confined to the area under the indentor in the snow ice blocks. However, for iceberg ice, the surface around the indented area was shattered by impact. This same phenomenon was observed during the indentation tests at strain rates of 10^{-2} and higher (Figures 3.22 and 3.23). A possible explanation for this failure outside the indented area, as the results of the finite element analysis (Figure 3.10) indicate is that tensile stresses are present in this area. The impact also created elastic waves that caused this type of failure when reflecting at the surface.

For the unconfined snow ice (Fugure 3.28), the same local failure took place but the block was broken into several pieces.

Figures 3.31 and 3.32 present sample plots of the time history of the pressure under the indentor centre as measured by the impact force transducer. Figures 3.33 and 3.34 present corresponding plots of the time history of the indentor deceleration as measured by the accelerometer. Figures 3.35 and 3.36 present the time variation of the indentor velocity and indentation depth obtained by integrating the acceleration time history.

The average impact pressure was computed as the impact force (indentor mass x acceleration), divided by the corresponding contact area (computed as a function of indentation depth and the indentor geometry). Sample plots are presented in Figures 3.37 and 3.38. Figure 3.39 presents the variation of the pressure at the centre of the contact area with the indentation depth. Sample plots of the load-indentation relationship are presented in Figures 3.40 and 3.41. The impact process as can be deduced from Figures 3.27 to 3.41 is outlined below.

As the indentor came in contact with the ice surface, the contact pressure built up very quickly till crushing of the ice in a thin layer in contact with the indentor took place. Then the pressure dropped suddenly and subsequent failures took place at a lower value (Figures 3.31 and 3.32). The ice in the layers under the crushed zone became weaker due to radial crack propagation (Figures 3.27 to 3.30). The contact pressure was, in most of the cases, significantly lower than the pressure at the initial failure (Figures 3.31 and 3.32).

In the initial stage of the impact the indentation depth varied almost linearly with time, then it became highly non-linear (Figure 3.36). The indentation rate was almost linear until the maximum indentation was nearly reached (Figure 3.35); then the pressure and impact force dropped

abruptly (Figures 3.39 to 3.41). After that the ice released the elastic deformation and the indentor rebounded slightly. The amount of rebound was dependent on the type of ice; ice with higher air bubble density had a higher rebound velocity (Figure 3.35). The rebound velocity was as high as about 10% of the impact velocity for the confined snow ice blocks.

A summary of the impact test results is presented in Table 3.3. Impact strength of iceberg ice was in general lower than that of the snow ice due to the effect of a higher density of air bubbles in the snow ice, which reduced crack propagation in the snow ice, and due to the cracks that existed in the iceberg ice before the test. The impact period and the indentation depth are larger for iceberg ice. Average impact period for the iceberg and snow ice was 19 and 15 milliseconds, respectively. Fourier analysis of the deceleration and pressure time histories indicated that the records had frequency constants ranging from zero to about 180 Hz with more than 90% of the energy between 0 and 60 Hz. The peak frequency was about 15 Hz. It was found that the energy spent in fracturing and indenting the ice specimens was more than 95% of the input energy.

The average contact pressure in the impact area was slightly lower than the pressure at the centre in the early stage of the impact test. As the indented area increased

the ratio of average pressure to the pressure at the centre became lower. This ratio varied between 0.9 and 0.5.

3.7 Comparison with Published Data

Table 3.4 presents a comparison of the uniaxial test results with those of other investigations of artificial snow ice, iceberg ice and Greenland glacier ice, under similar test conditions (at a strain rate of about 10^{-3} sec^{-1}). The strength of snow ice in the present study is lower than that reported by Haynes (1978) and Mellor and Cole (1983) due to the difference in ice density. Taking into account the difference in testing speed, the uniaxial strength of the iceberg ice compares well with the values reported by Butkovich (1959). The strength of iceberg ice reported by Gammon et al (1984) is lower than in the present study under almost identical conditions due to possible imperfect end conditions as evidenced by the failure initation at the specimen ends for most of their tests.

Although only limited data is available on the uniaxial compressive strength of snow ice at strain rates higher than 10^{-3} sec^{-1}, the observed variation of the uniaxial strength of the snow and iceberg ice with strain rate has the general features reported by other investigators.

It is interesting to note that the average confined strength of iceberg ice obtained from the in-situ borehole jack tests by Fenco (1975, 1976) at a temperture of -3 to -5°C ranged from 26.8 to 30.0 MPa, which compares well with the indentation strength of confined iceberg ice of 28.43 MPa at a strain rate of 10^{-3} sec^{-1}.

As indicated earlier there is no data available on the impact strength of iceberg and snow ice. The results of impact tests on lake ice reported by Likhomanov and Kheisin (1971) indicated that the peak pressure for impact velocity of 2 m/sec at a temperature of -5 to -10°C was about 12 MPa. The contact pressure after the peak was 5 to 6 MPa. These tests were carried out by dropping 300 kg and 156 kg steel hemispheres on a lake ice cover. The impact strength of river ice (Timco and Martin, 1979) obtained by dropping a 0.4 kg ball from a height of 0.5 m (impact speed 3 m/sec) was 13.2 MPa for grey ice and 19.6 MPa for flooded, refrozen ice. The tests were carried out at a temperature of -17 to -26°C.

The values obtained by Likhomanov and Kheisin (1971) are lower than those obtained from the impact tests on S2 ice, snow ice or iceberg ice. The values obtained by Timco and Martin (1979) are close to the results reported herein. Due to the differences in ice type and test conditions a direct comparison between the results is not possible.

3.8 Summary

Results of uniaxial compression, indentation and impact tests for iceberg and snow ice have been presented. The strength values and behaviour of the artificial snow ice are almost the same as those of the iceberg ice; the essential difference between the two was that the iceberg ice was more brittle than the snow ice due to the difference in bubble density.

The results of these tests will be used to determine the impact force on and extent of damage to semi-submersible members as outlined in Chapter VI.

CHAPTER IV

THE HYDROELASTIC MODEL

4.1 General

The review of literature presented in Chapter II identified the need for elastic models, structurally and dynamically similar to the full-scale semi-submersible, in order to check the structural response in waves obtained from numerical models.

As indicated in Chapter II, better agreement was obtained between the measured and computed values of motion response than those of the structural response. There are two possible reasons for this. The first is that the total hydrodynamic forces on the semi-submersible can be more accurately estimated than the detailed local forces on each member. The other reason is that all the structural members in space frame analysis were modelled using beam elements. However, the columns and pontoons may not behave like a slender beam element. A column, for example, is more likely to behave like a shell than a beam.

Hydroelastic models are also needed to study the problem of semi-submersible collision with ice masses or supply boats.

To our knowledge, no numerical model is available to evaluate stresses in the structural members of a semi-submersible due to impact of ice. The same is true for ships where elastic models are needed to study: i) the problem of wave slamming which produces impact loads on the low part of the hull and induces hull vibrations (whipping), ii) wave excited vibrations in large ships (springing), and iii) ship-ice interactions in the process of ramming.

Pawlowski (1983) presented a comprehensive review of the existing studies that use ship models to measure forces and bending moments in the hull. He indicated that almost all of the existing ship models are either rigid-segmented models or elastic-segmented models. There is only one published and one proprietary study where an elastic model of a ship has been tested. Pawlowski (1983) indicated that there are serious reasons of both a theoretical and a practical origin to develop a consistent methodology for model tests with elastic models of ships and semi-submersibles; these models are needed to support corresponding theoretical investigations, design studies and full-scale trials.

Although the need for elastic semi-submersible models has existed for some time, no elastic model of a semi-submersible has been developed. In addition to other

various modelling difficulties, very thin material with low elastic modulus and relatively high density is needed to secure dynamic and structural similarities. Therefore, exactly similar structural modelling is believed to be extremely difficult and this is considered to be one reason why no experimetnal studies using dynamic structural models have been reported. In the available structural response models, attempts are made to simulate the stiffnesses of bracing members and deck girders only.

The best available model was developed by Yoneya (1984). In this model complete structural similarity was not achieved. The ratio of axial rigidity between the braces and the deck transverse member was adjusted to be almost the same as that of a full-scale platform. However, the absolute values of axial rigidity of these members were two or three times higher than the required stiffness. Furthermore, the structural rigidity of all the other members (columns, pontoons and longitudinal deck members) was about ten times the required model values. Therefore, strains were measured in all the bracing members and two transverse deck girders only. Yoneya (1984) indicated that the model thickness needed to achieve structural similarity was about 0.7 millimeter. Therefore, he had to use much thicker material so that the model could be constructed and handled.

The main purpose of the study reported herein was to develop techniques for modelling, constructing and testing a model that was dynamically and structurally similar (as close as possible) to a typical semi-submersible and use it to study its motion and global structural response to wave forces and bergy-bit impacts.

4.2 The Prototype

The Tim-77 semi-submersible platform presented in Figures 4.1 to 4.3 is similar in geometry and weight distribution to the Sedco-700 series semi-submersibles (Figure 2.1 and 2.2). Information on the dimensions and detailed mass distribution of the Sedco-709 semi-submersible reported by Sims et al (1976), as well as the detailed structural drawing of the similar Aker-H3 semi-submersible (Figure 4.4) given by Taylor (1974), form the basis for the design of the Tim-77 semi-submersible.

Figures 4.5 to 4.7 present the structural detailing of the pontoons, columns and deck-girders. Bracing thickness was assumed to be 5 cm (2 in). Table 4.1 presents the total mass of the semi-submersible components at survival draft while Table 4.2 presents the main dimensions and its static and dynamic properties as obtained from the model tests reported later on in this chapter.

This type of semi-submersible was chosen because it is common (15 of the 700 series have been built). It also has the most complicated configuration which makes for a good test of the viability of hydroelastic modelling of semi-submersibles.

4.3 Modelling

4.3.1 Modelling Principles

The model used in this study is termed "hydroelastic" because in addition to modelling the fluid-system, the structural response to that system is also modelled (Sharp, 1981). To achieve hydrodynamic similarity Froude scaling laws (Table 4.3) were used since the motion of a floating body is dominated by inertial and gravitational forces. Three different requirements must be satisfied in hydroelastic models. According to Sharp (1981) these requirements are geometrical similarity, similarity of the mass and mass distributions, and the ratio of elastic forces must be the same as that of gravity and inertial forces.

To achieve mass distribution and inertial and damping force similarities, the density and damping ratio of the model material should be equal to those of the prototype. Plastic has lower density and higher damping than steel (prototype material). Therefore, it is necesary to add

mass to the model in such a way as to give the correct total mass and mass distribution, without affecting the structural rigidity. Structural damping is believed to have little importance in determining response to impact loads and frictional forces may dominate the damping effect (Sharp, 1981). Damping has a significant effect for resonance studies.

To secure the similarity of structural rigidity (elastic forces), the linear and rotational stiffness of the structural members must be scaled down using the same scale for corresponding hydrodynamic restoring forces (according to Froude modelling). Therefore, the scale of the linear and rotational stiffnesses must equal λ^2 and λ^4 (Table 4.3), respectively, where λ is the linear (geometry) scale (length in model/length in prototype).

The axial stiffness S_a, bending stiffness S_b, torsional stiffness S_t, and shear stiffness S_s of a structural element with a uniform cross-section can be written as:

$$S_a = \frac{EA}{L} \qquad \text{4.1}$$

$$S_b = \frac{4EI}{L} \qquad \text{4.2}$$

$$S_t = \frac{GJ}{L} \quad \text{..... 4.3}$$

$$S_s = \frac{GA_s}{L} \quad \text{..... 4.4}$$

where

E = the Young's Modulus of Elasticity

I = the moment of inertia of the cross-section about the principal axis

A = the cross-sectional area

J = the torsional rigidity of the cross-section

A_s = the equivalent cross-sectional area for shear computation

G = the modulus of shear rigidity

L = the length of the member

S_a and S_s must be scaled by a factor of λ^2 while S_b and S_t

by a factor of λ^4. Therefore, the ratio of the stiffness of the model (m) to that of the prototype (p) can be written as:

$$\frac{(S_a)_m}{(S_a)_p} = \lambda^2 \quad \text{.....4.5}$$

$$\frac{(S_b)_m}{(S_b)_p} = \lambda^4 \quad \text{.....4.6}$$

$$\frac{(S_s)_m}{(S_s)_p} = \lambda^2 \quad \text{.....4.7}$$

$$\frac{(S_t)_m}{(S_t)_p} = \lambda^4 \quad \text{.....4.8}$$

Applying Equations 4.1 to 4.4 into 4.5 to 4.8 yields:

$$\frac{E_m A_m L_p}{E_p A_p L_m} = \lambda^2 \quad \text{..... 4.9}$$

$$\frac{E_m I_m L_p}{E_p I_p L_m} = \lambda^4 \quad \text{..... 4.10}$$

$$\frac{G_m A_{sm} L_p}{G_p A_{sp} L_m} = \lambda^2 \quad \text{..... 4.11}$$

$$\frac{G_m}{G_p}\frac{J_m}{J_p}\frac{L_p}{L_m} = \lambda^4 \quad \text{..... 4.12}$$

For a thin walled section with constant thickness t, the sectional properties are (Popov, 1969):

$$A = h\,s \quad \text{..... 4.13}$$

$$A_s = \alpha\,A \quad \text{..... 4.14}$$

$$I = h\int z^2\,ds \quad \text{..... 4.15}$$

$$J = 4hA_o^2/s \quad \text{..... 4.16}$$

where

h = the thickness of the cross-section wall

s = the length of the centre line of the wall cross-section

α = a constant representing the shear shape factor which is dependent on the shape of the cross-section

z = the distance between the principal axis of the cross-section and the centre line of the wall

A_o = the area bounded by the centre line of the wall

Since the model and prototype have similar geometry, to maintain the hydrodynamic force similarity, then:

$$\frac{A_{sm}}{A_{sp}} = \frac{A_m}{A_p} = \frac{h_m}{h_p}\lambda \quad \ldots\ldots\ldots\ldots\ldots\ldots\ldots\ldots\ldots\ldots 4.17$$

$$\frac{I_m}{I_{sp}} = \frac{J_m}{J_p} = \frac{h_m}{h_p}\lambda^3 \quad \ldots\ldots\ldots\ldots\ldots\ldots\ldots\ldots\ldots\ldots 4.18$$

Also E and G are related by:

$$G = E/2(1+\mu) \quad \ldots\ldots\ldots\ldots\ldots\ldots\ldots\ldots\ldots\ldots 4.19$$

where

μ = the Poisson's ratio.

Applying Equations 4.17 to 4.19 into Equations 4.9 to 4.12 yields:

for axial and bending stiffness similarities:

$$\frac{E_m}{E_p}\frac{h_m}{h_p} = \lambda^2 \quad \ldots\ldots\ldots\ldots\ldots\ldots\ldots\ldots\ldots\ldots 4.20$$

for shear and torsional stiffness similarities

$$\frac{E_m}{E_p} \quad \frac{(1+\mu_m)}{(1+\mu_p)} \frac{h_m}{h_p} = \lambda^2 \quad \ldots\ldots\ldots\ldots\ldots\ldots\ldots\ldots \quad 4.21$$

If the Poisson's ratio of the model material is equal to that of steel, then Equation 4.21 will be identical to Equation 4.20. In this case axial, shear, bending and torsional rigidities will be properly simulated.

Since the axial and bending stresses represent the dominating stresses for the design, we will try to satify Equation 4.20.

For a difference in Poisson's ratio between the steel and modelling material of 10%, the shear stiffness will be affected by only 2.2%. Therefore, satisfying Equation 4.20 will be good enough to secure the axial, bending, shear and torsional stiffness in the model and the prototype.

An alternate approach to modelling is to maintain similar elastic line shapes during flexural vibrations. The differential equation of an elastic line is given by:

$$\frac{d^2y}{dx^2} = \frac{M}{EI} \quad \ldots\ldots\ldots\ldots\ldots\ldots\ldots\ldots\ldots\ldots \quad 4.22$$

where x is the longitudinal co-ordinate of any point on the elastic line, y is the deflection at this point and M is the bending moment of the cross-section. To maintain similar elastic line shape during the flexural vibrations of the structural members, the following condition must be satisfied.

$$\left(\frac{d^2y}{dx^2}\right)_m \Big/ \left(\frac{d^2y}{dx^2}\right)_p = 1/\lambda \quad \ldots\ldots\ldots\ldots\ldots\ldots\ldots \quad 4.23$$

Therefore:

$$(M/EI)_m \Big/ (M/EI)_p = 1/\lambda \quad \ldots\ldots\ldots\ldots\ldots\ldots \quad 4.24$$

For Froude scaling, the scale of M is λ^4 (Table 4.3). Substituting for I using Equation 4.14, Equation 4.24 is reduced to

$$\frac{E_m}{E_p}\,\frac{h_m}{h_p} = \lambda^2 \quad \ldots\ldots\ldots\ldots\ldots\ldots\ldots\ldots\ldots \quad 4.25$$

which is identical to Equation 4.20. Therefore, Equation 4.20 was used in modelling and designing the hydroelastic model. Table 4.4 presents the scaling factors for the hydroelastic model parameters together with the actual factors used to scale up the model values to the full-scale

ones. These factors include the effects of using different water density and structural stiffness.

4.3.2 Model Design

The modelling condition represented by Equation 4.20 is usually very hard to fulfill since a very low value of the modulus of elasticity, E and a very small thickness, h, are required. This makes the model extremely delicate and hence difficult to fabricate and handle.

High impact polystyrene plastic sheets were chosen for modelling the columns, pontoons and deck structure while cellulose acetate butyrate (CAB) tubes were used to simulate the bracing members. Polystyrene was selected because: i) it has a very low modulus of elasticity (the lower the better as indicated by Equation 4.20), ii) sheets were available in small thicknesses, and iii) it can be easily cemented. The CAB was selected because it has a similar modulus of elasticity to the polystyrene. In addition, the CAB has a common cementing material with the polystyrene.

The modulus of elasticity of the polystyrene sheets and CAB tubes, as determined by tension tests according to the ASTM standards (1981), were 1890 MPa and 1834 MPa, respectively. The stress-strain curves of both the polystyrene and the

CAB exhibited linear behaviour (constant E) up to the yield point (Figure 4.8). Table 4.5 presents the mechanical and physical properties of the polystyrene sheets and the CAB tubes.

The model scale was chosen to be 1/75. Since the ratio of the elastic modulus of the plastics (model) to that of the steel (prototype) is about 1/110 (which is much lower than the linear scale), this will allow using relatively thicker sheets, according to Equation 4.20.

To reduce the complex structural detailing of the model columns and pontoons, (Figures 4.6 and 4.7) 'equivalent' plate thicknesses were used to account for the contribution of the local stiffeners to the global stiffnesses of the cross-section using Equations 4.13 to 4.16. The equivalent thicknesses (for global structural response) for the pontoons and columns were 25 mm and 22 mm, respectively. The bracings, deck girders, bulk-heads and compartment walls were modelled without any changes.

For a full-scale equivalent pontoon thickness of 25 mm, the required model thickness according to Equation 4.20, is 0.48 mm. The smallest available nominal thickness of the polystyrene sheet that could be used for building the model was about 0.03 inch (0.75 mm). The actual thickness of two sets of polystyrene sheets was 0.86 mm and 0.78 mm. Using

the thicker sheets for the pontoons and the other ones for the columns, the structural stiffnesses of the model were 1.72 and 1.78, times higher than the required ratios, respectively. For the bracing and deck girders the values were 1.67 and 1.70, respectively.

This increase in structural stiffness in the model will only affect the structural response near structural resonance. However, the range of the wave frequencies are very much lower than the structural natural frequencies. For response to bergy-bit impact, the frequency content of the impact force was not close to any structural natural frequency. Therefore, no significant effects on the structural response are to be expected.

The relative stiffnesses of the structural members at any joint in the prototype were kept almost the same in the model. This ensured that force and moment distribution in the model members would be similar to that in the prototype. Figures 4.9a and 4.9b present the model configuration and dimensions while Figures 4.9c to 4.9e present the structural detailing of the column.

4.4 Fabrication of the Model

As mentioned earlier, except for bracing, the model was fabricated of polystyrene sheets. The columns and the

curved parts of the pontoons were made using a thermal forming process. The different parts of the model were joined together using solvent cement. Details of the construction techniques are presented by the model builder, Foster (1985).

The interior of the pontoons, columns and deck girders were divided into compartments by bulkheads made of polystyrene sheets (Figures 4.9c to 4.9e); these internal compartments simulated bulkheads present in the prototype semi-submersible. Figure 4.10 presents a view of the bulkheads in the pontoon of the model.

To compensate for the low density of the plastics, lead sheets and strips were attached internally to all the structural members in a manner such that the correct mass distribution was simulated without affecting structural stiffness. The ballast of the platform was provided in the form of removable weights, connected by a flexible bar, to provide the required draft. Each ballast component represented the equivalent weight of water in each ballast tank and was placed in the centre of the tank using special arrangements so that the effect of each ballast component was transferred locally to the pontoon. The weights of the platform deck buildings, mudhouse, derrick floor, heliport, etc., were simulated by placing lead sheets on blocks of styrofoam so that the positions of the horizontal and

vertical centre of gravity of the vessel were maintained properly. Plastic casings were then placed over the styrofoam and leads weights, to give an aesthetic appearance to the model. The derrick was also constructed from the plastic with extra weight provided by lead sheets glued to the inside of the plastic frame. Similar care was taken to properly simulate the weights of mud and fuel tanks, cranes, windlasses, etc. Figure 4.11 presents a general view of the completed model.

The simulation of mass distribution was so accurate that only very minor adjustments had to be done to achieve the required C.G. position. The measured radii of gyration were almost identical to the computed values.

A drainage system made of copper tubing and powered with a high-volume high-vacuum air pump was built-in to remove water that may seep in through the joints; however, very limited leakage took place in only one pontoon. Sealing the model seams with a paste, made by dissolving plastic sheets in a solvent liquid, proved to be effective. Figure 4.12 presents a view of a part of the drainage system before being installed inside the pontoon.

Since the model was very delicate, special arrangements were made for its handling. The model was built on a platform that was used later as a carrying and launching

platform (Figure 4.13). The model could not be carried by any other means. When it was required to put the model on the tilting platform (for measuring static properties), the transfer was done through water, using it as an intermediate 'carrying' medium. The tilting platform was specially designed to be able to lift the model from and launch it back into the water.

In order to obtain the stresses and forces in various locations of the semi-submersible, strain gauges were installed on the inside of the pontoons and columns, and on the outside of the braces and deck as shown in Figures 4.14 and 4.15. The outside gauges had fully encapsulated water proof grids. Therefore, no coating, which would have increased the thickness at the strain gauge location, was needed for additional water proofing (Figure 4.15).

A total of thirty gauges - eight in one of the pontoons, four at the base of one corner column, eight at the base and top of one secondary column, six in the braces and four on a platform girder - were used to monitor the structural response to waves and ice impact forces. Figure 4.16 presents the arrangements of the strain gauges in each section and the system of local principal axes of each section.

4.5 Modelling of the Mooring System

Figures 4.17 and 4.18 present the mooring system profile and arrangements for the prototype in the vertical and horizontal planes. Figure 4.19 presents the tension - excursion characteristics of the 3 in. (7.6 mm) chain as obtained from catenary equations provided by Korkut and Herbert (1970) and Rothwell (1979). Based on these curves, the restoring forces due to the mooring system configuration presented in Figure 4.18 were computed for all six motions.

The mooring system was simulated using four mooring lines with linear springs as shown in Figure 4.20. The values of the spring stiffness and the horizontal and vertical mooring angles were chosen so that the restoring forces in heave, pitch (roll), surge (sway) and yaw were simulated properly.

Figure 4.21 presents the actual and simulated restoring forces for heave and surge/sway motions. These plots cover the whole range of the model motion during the tests in regular and irregular waves (including the drift component). Figure 4.21 indicates that the mooring stiffness was modelled properly.

4.6 Model Characteristics

4.6.1 Mass Properties

Since, during the construction of the model, each part was weighted accurately and was compensated for the difference in density by the attached lead sheets as described earlier, the total mass of the model was very close to the modelled mass. Only minor adjustments had to be done to obtain the correct model mass and the C.G. location.

A tilt platform was specially designed to: i) handle the delicate model, ii) set the centroid position, and iii) check the radii of gyration (gyradii) for pitch and roll motions. Figure 4.22 presents a layout of the tilt platform while Figure 4.23 presents a general view of the model while being tested on the platform.

To set the centre of gravity of the model, the distance KG (Figure 4.22) was adjusted to the required value. Before placing the model on the tilt table, the counter weight heights were adjusted so that the table balances (stays in neutral condition) on the knife edge, signifying that the vertical centre of gravity of the table was at the same level as the knife edge. The model was then placed on the tilt table with the longitudinal centre of gravity placed in line with the knife edges. The ballast weights in the

model columns were then adjusted until the model and platform together assumed the neutral position again. This meant that the vertical centre of gravity was set to the required position.

The gyradius of the model was determined by measuring the period of oscillation of the model on the tilt table. Springs were attached to the tilt platform as shown in Figure 4.22 to provide a restoring force. The period of oscillation of the table alone and then the table with the model were determined using an accelerometer, mounted on the platform, and a HP Fourier analyzer. This provided the period to the nearest 0.01 sec.

The gyradius of the model in pitch or roll, depending on the model orientation, was calculated using the following equation.

$$R^2 = \frac{S}{4\pi^2 M}(P_2^2 - P_1^2) \quad \ldots\ldots\ldots\ldots\ldots\ldots\ldots\ldots \quad 4.26$$

where

R = gyradius

M = mass of the model

P_2 = period of oscillation of the table and model

P_1 = period of oscillation of the table only

S = rotational stiffness of the spring system

= Σkd^2

k = stiffness of one spring

d = distance between the spring and the knife edge (see Figure 4.22).

The measured gyradii were almost identical to the computed ones. The position of the centroid and the gyradii in full-scale values are presented in Table 4.2.

4.6.2 Metacentric Height

The longitudinal and transverse metacentric heights of the model for the survival and operating drafts were determined using the static stability test (Figure 4.24).

The heel angle-restoring moment relationship (Figure 4.25) was determined by using a couple applied to the model deck

and measuring the heel angle. The metacentric height, $\overline{GM}$ was determined from

$$\overline{GM} = RM/W \sin\theta$$

RM = applied moment

W = model weight

θ = heel angle

The values of the metacentric heights are presented in Table 4.2.

4.6.3 Natural Periods

The natural periods of oscillation in heave, roll and pitch motions of the free floating (unmoored) model were measured in the 'deep water tank' using accelerometers and a Fourier analyzer (Figure 4.26). The natural periods of the six motions of the moored model were measured in the 'wave tank' using the accelerometers. Another set of measurements was obtained using the potentiometers that measured the motion respones (see Section 4.7). The values obtained from both methods for the moored model were identical. A view of the test set-up for the deep water tank tests is presented in Figure 4.26. The results are presented in

Table 4.2. Only the heave period falls in the range of wave periods of interest. The rest of the motions have periods outside that range. The natural frequencies of the moored model were significantly higher than those of the unmoored model.

4.7 Testing Program

4.7.1 Test Set-Up

The tests were carried out in the 58 m long by 4.6 m wide wave tank at a water depth of 1.6 m, equivalent to 120 m in full scale. Waves were generated by the translatory motion of a piston-type vertical unarticulated waveboard controlled by a closed-loop servo-controller mechanism.

A detailed description of the wave tank and its performance characteristics has been provided by Muggeridge and Murray (1981). Figure 4.27 presents an outline of the test set-up while Figure 4.28 presents an overall view of the model and the wave tank. Wave profiles were measured at two locations as shown in Figure 4.20 (along the longitudinal and transverse axis of the model) using conductivity probes. The motion of the model was monitored using four potentiometer devices that provided translatory and angular motions to the nearest 0.1 mm and 0.05 degrees, respectively.

The strains in the model were monitored using conditioner and amplifier units that provided strains to the nearest 0.1 microstrain. The output of the motion and strain measuring devices was stored in an analogue form on a HP 8-track tape and processed later using the HP Fourier Analyzer. All tests were also recorded on video tapes.

Figure 4.29 presents part of the data acquisition system including HP 8-track recorders, strain gauge conditioner and amplifier units, and video recording equipment. All the measuring and recording devices were calibrated and the signal to noise ratio was kept at the lowest possible level so that the error in the measurements would be minimized.

4.7.2 Regular Wave Tests

The model was tested in regular and irregular head sea and beam sea waves at survival and operating drafts. Figures 4.30 and 4.31 present the model while being tested at survival and operating drafts. For regular wave tests, the wave height was 7 cm and the wave period varied from 1 to 2.5 sec. This is equivalent to a full scale wave height of 5.25 m (17.2 ft.) and a wave period range of 8.7 to 21.7 sec. To check system linearity, one series of tests was repeated at survival draft using a 10.5 cm wave (7.8 m or 25.8 ft. at full scale).

To study the changes in the structural and motion responses of the model after a corner column was punctured due to bergy-bit or supply boat collision, one corner column compartment (3.6 m high) near the water surface was assumed to be flooded. The corresponding mass was placed at the centre of the column compartment. The 'flooding' of the compartment caused the model to have a list of 6° in the longitudinal direction and 7.5° in the transverse direction (Figure 4.32). The 'damaged' column was facing the incoming waves. Motion and strains in all sections were measured for all the above tests.

Another series of regular wave tests was carried out to study the effect of varying the mooring cable stiffness on the motion response. The tests were carried out at survival draft under the following mooring conditions:

i) original mooring system (100% stiffness)
ii) slack leeward mooring (60% stiffness)
iii) slack mooring system, (25% stiffness), and
iv) without mooring system (zero stiffness)

4.7.3 Irregular Wave Tests

Two sets of irregular waves were generated using the Pierson-Moskowitz spectrum for sustained winds of 44 knots (22 m/sec) and 33 knots (16.5 m/sec). The length of the

irregular wave record in each set was 30 minutes of prototype time. The full-scale characteristics of the wave train generated by each spectrum are presented below:

	Spectrum #1	Spectrum #2
Wind speed (m/sec)	22	16.5
Maximum wave height (m)	20	10
Significant wave height (m)	10.5	5.5
Peak frequency (Hz)	0.06	0.077
Peak period (sec)	16.7	13

Motion and structural responses of the model were obtained for each irregular wave set for head sea and beam sea waves at survival draft.

4.7.4 Simulated Impact Tests

'Small' fragments of icebergs (growlers and bergy-bits) of masses up to 2000 tonnes may escape radar and visual detection, especially in heavy seas (Paschke, 1983), and pose a great hazard to semi-submersible members. Recent analytical and experimental studies on bergy-bit motion in waves reported by Doyle and Arockiasamy (1984), Lever et al (1984) and Murray et al (1983) indicated that bergy-bits could oscillate with speeds very close to the particle velocity of the wave. Considering that the drift speeds of icebergs due to current, wind and wave drift forces could

be as high as 1.3 m/sec (El-Tahan et al, 1983) the maximum speed of a bergy-bit could reach 4-5 m/sec. The impact velocity, being the relative bergy-bit/semi-submersible velocity could even be higher than this value. On the other hand, the diffraction of short waves near the SSM may reduce the bergy-bit velocity.

The above information on bergy-bit mass and velocity was used to design the impact tests. To determine the elevation of impact, the relative structure/bergy-bit motion in regular waves was studied using ballasted styrofoam models of 1000 and 2000 tonne bergy-bits. The bergy-bit model in most of the cases hit the semi-submersible model when the bergy-bit was at the crest of the wave. Depending on the wave period, the elevation of the impact point varied from a few meters above the still water level on the corner column to the tip of the pontoon (Figures 4.33 and 4.34). It was decided to carry out the simulated impact at about four meters below the sea level. Although the impact of the styrofoam bergy-bit models did not cause any damage to the model, it was decided to strengthen the impact zone on the outside of the corner and the secondary columns using thin (0.8 mm) steel shield (Figure 4.35). This shield protected the model against any damage caused by high impact speeds. The added stiffness of the shield simulated the stiffness of the column when strengthened for ice impact by introducing an inner wall having a diameter of 7 m.

The model was subjected to a simulated impact by 1000 and 2000 tonne bergy-bits moving and oscillating in waves with horizontal impact velocities of 0.5-5 m/sec. Figure 4.36 presents the relative sizes of the bergy-bits and the SSM. The impact tests were carried out using lead weights swinging in a pendulum mode in still water (Figure 4.37) and impacting a corner column or a secondary column. A parametric study was carried out to investigate the effect on the model response of: i) impact speed, ii) mooring system stiffness, and iii) impact direction.

The measured data for these simulated impact tests were the motion of the semi-submersible and bergy-bit models, strains at selected sections, and the impact force (measured by an accelerometer mounted on the impacting weight).

As the test results may be affected by the degree of strengthening of the impact zone, it was decided to study the effect of the impact interface stiffness on impact forces and semi-submersible responses. A series of impact tests were carried out using a two-degrees-of-freedom rigid body model on a test bench. Interface elements were used to represent the impact interface characteristics. The stiffness of these elements was varied by about six orders of magnitude. A description of the model and the study are presented in Chapter 6.

CHAPTER V

RESPONSE TO WAVES

This chapter presents the results of the model tests in regular and irregular waves, including the verification of the hydroelastic modelling. An analysis of the model response to waves and the results of the parametric study are also presented.

5.1 Model Response in Regular Waves

Figure 5.1 presents measured wave profiles for wave periods of 1, 1.75 and 2.5 sec. The wave height was uniform and the effect of reflection from the beach was negligible. The model motion reached a steady state after 4-5 wave cycles as shown in Figure 5.2. Model heave, pitch and roll motions showed only first order effects while the surge and sway motions indicated second order effects for wave periods up to 1.75 sec (15.2 sec full scale).

Figures 5.2 and 5.3 present the first order and the second order (drift) components of the surge motion. The second order effect was negligible at wave periods longer than 1.75 sec.

Figure 5.4 presents typical strain time histories measured at the top of the secondary column (ST4), the bottom of the main column (MB2) and the pontoon middle (PM2). The steady component of the measured strain is due to thermal effects. Since the plastic is a poor heat conductor, the heat generated by the electrical current in the strain gauge does not dissipate easily. The plastic temperature rises causing it to expand till the temperature stabilizes. When the test starts the forced water convection caused by wave particle motion cools the plastic. The plastic shrinks and the strain gauge indictes negative strain. The strains reach a steady state after few wave cycles.

This cooling effect was not noticed in the measured strains of above water sections (Figure 5.4) due to the poor heat convection capability of air as compared to water. When the stresses in the model reached the steady state, the structural response in regular waves appeared to be almost perfectly harmonic. However, when the model had a list (damaged condition test) a second order effect was noticed in the structural response. This point will be discussed later.

Figure 5.5 presents a view of the model being tested at survival draft in a 7 cm wave having a period of 1 sec. while Figure 5.6 presents the same for a wave period of 2.5 sec. Wave diffraction was noticed for short waves (Figure

5.5) while the model did not disturb the wave field for long waves (Figure 5.6).

5.1.1 Comparison of Model Test Results

To check the accuracy of the measured motion response, the prototype motion response obtained from the present model tests was compared with the corresponding values obtained from available computer analysis, model tests and field measurements on the SEDCO-700 series semi-submersibles.

The computed motion response under operating draft conditions was obtained by Opstal et al (1974) using the integrated motion and strength analysis system (MOSAS computer program) . The hydrodynamic forces were computed using potential flow method and accounting for viscous damping and frequency dependency on added mass coefficients, while the wave damping was neglected. A brief description of the MOSAS program is presented in Section 2.2.5.2. The reported results for the SEDCO-700 SSM were obtained at operating draft for a water depth of 120 m, identical to that simulated in our model tests.

The model test results were obtained from the Marine Operations Manual of the SEDCO-710 SSM (SEDPEX INC, 1983). Motion response curves (RAO plots) were obtained from models of the SEDCO-700 and SEDCO 707 SSM's at operating

draft. Information on the water depth and mooring system was not available.

The field measurement of heave response was obtained by Forristal et al (1979) for the SEDCO 706 SSM at operating draft in the Gulf of Alaska (see Section 2.2.5.1). The heave motion and wave profile were measured using accelerometers and wave staffs, respectively. The heave transfer function was obtained by cross-spectral analysis of wave profile and heave measurements.

Figures 5.7 to 5.10 present the full-scale response amplitude operators (RAO's) for heave in a head and beam sea, surge, sway, roll and pitch respectively as obtained from the hydroelastic model tests and the above mentioned sources. A very good agreement can be observed between test results and the motion obtained from the other sources. This agreement is less near the natural heave period of the SSM (23.6 sec.) probably due to drag and viscous damping effects as well as differences in mooring stiffness.

As mentioned earlier, field measurements from the SEDCO-706 were available for heave motion only. In fact almost all of the available studies on the field measurement on semi-submersible platforms also reported on heave motion only (Watts and Faulkner, 1968, Rey-Grenge, 1971, Vugts, 1971,

and Forristal et al, 1979). Therefore, no SSM motion (other than heave) whether obtained from model tests or computer analysis has been verified by field measurements for any SSM and reported in the open literature.

Heave, pitch and roll measurements are routinely recorded as part of the environmental data gathering from the Sedco-706 SSM which was drilling on the Grand Banks of Newfoundland. These data were made available by special permission from Husky/Bow Valley, the SSM operators, for the period February to June 1984. The data set consisted of wave period, significant height, maximum height and the maximum double amplitude values of heave and single amplitude values of pitch and roll, provided at intervals of one hour. Wave characteristics were obtained from a 20 minute wave record measured every hour by a waverider buoy. Maximum heave during the observation time was estimated to the nearest foot (0.3 m) from the relative SSM/marine riser vertical motion. The maximum roll and pitch motions were measured to the nearest 0.1 degree using an air bubble-type inclinometer. Since a significant amount of scatter in the data was observed it was decided to deal with the data on a statistical basis.

Figure 5.11 presents the frequency distribution plots for the wave characteristics and SSM motion using about 2000 data points. About 80% of the time the wave period varied

from 6-9 sec., significant wave height 1-4 m, maximum wave height 2-6 m, heave 0-1 m, pitch 0.5-1 degree and roll 0.5-1.5 degrees. The RAO's for the heave, pitch and roll were obtained as the double amplitude (or maximum range) of motion divided by the corresponding maximum wave height.

Figure 5.12 presents the frequency distribution of the measured heave, pitch and roll RAO's. The range of corresponding values obtained from the hydroelastic model results at corresponding wave periods is indicated on each plot. The results indicate good agreement between the motion obtained from model tests and full scale measurements. The measured roll motion is slightly higher than that obtained from model tests probably due to current and wind effects. The steady SSM tilt due to wind and currents could not be isolated since roll and pitch values were provided as the maximum angle of tilt to one side only.

The results presented in Figures 5.7 to 5.12 demonstrate the accuracy of the model motion response. Having established the accuracy and validity of motion response results, the next step is to check the validity of the structural response values and the hydroelastic modelling.

Figures 5.13 to 5.15 present the full-scale structural response (stresses) in the bracing members and pontoon section as measured by the hydroelastic model and computed

by two different programs. The results reported by Opstal et al (1974) were obtained for the Sedco-700 using the MOSAS program while those reported by Dao and Baily (1982) were computed for the Sedco-710 using SEADYN (1981). SEADYN is based on the Morison equation approach.

By comparing the experimental and analytical values, it is notour intention to establish the degree of accuracy of the experimental results since the accuracy of the computed structural response is not established yet. The review presented in Chapter 2 revealed that unlike the computed motion response, which was reported to be in good agreement with that obtained from model tests or field measurements, the computed structural response was consistently higher than that obtained from limited full-scale measurements, especially at short wave periods. The best way to establish the accuracy of the model structural response is to compare it with full-scale measurements. Due to the lack of such full-scale data, we can only check the validity of the hydroelastic structural response.

The results presented in Figures 5.13 to 5.15 indicate that the measured stresses are generally lower than the computed values at small wave periods. The same observation was reported for full-scale measurements by Bell (1974), Langfeldt et al (1975) and Olsen and Verlo (1976). At long wave periods, the measured stresses in the bracing members

were higher than the computed ones and had a minor peak near the wave period of 20 sec. Two possible reasons could explain it: increasing drag forces at longer periods, and a heave resonance effect near the 20 sec. period. Predictions by other computer programs show such 'minor peaks' because of large heave motion (Chung, 1985).

The above discussion indicates that there is a general agreement between the measured and computed stresses and that the differences are consistent with those found between the computed and full-scale values. This finding is based on the results of stress computations available for three sections only (one pontoon section and two bracings). To further check the validity of the measured structural response, we compared our data with another set of computed stress RAO's obtained for the Tim-77 semi-submersible at survival draft during the course of the study reported by Arockiasamy and Reddy (1982). Motion and structural responses of the SSM were obtained using Brown and Root's proprietary programs DAMS, TENMOT and LOADGEN. The hydrodynamic forces were computed using a strip theory method and the structural response was obtained using space frame analysis.

Each pontoon was divided into 28 strips for hydrodynamic calculations while each column was divided into eight

strips. For structural analysis, the structure was idealized as a space frame having 384 members and 254 nodal points. Details of the SSM idealization for hydrodynamic computation and structural analysis are presented by Arockiasamy and Reddy (1982).

First we examine the computed motion response. The results of the heave response presented in Figure 5.16 indicate good agreement between the computed and measured values for wave periods of less than 15 sec. The computed values become several times higher than the measured ones at longer periods. The same is true, but with smaller differences, for the pitch and roll motions presented in Figure 5.17. While the measured and computed sway responses, presented in Figure 5.18, are in good agreement, the computed surge response is very much lower than the measured values.

As presented earlier, the accuracy of the model motion response was verified by other model test results, computed values and field measurements. Therefore, the discrepancies in Figures 5.16 to 5.18 are due to errors in the computed values. These errors are probably due to computational or formulation errors since errors in input data could not cause this kind of motion response discrepancy (Yoshida, 1985).

Figures 5.19 to 5.23 present the computed and measured maximum stresses in the secondary column, main column, braces and pontoon, respectively. The computed stresses fluctuated significantly from one wave period to the other while the measured ones varied gradually with wave period. The same observation was reported by Bell (1974) who indicated that the computed transfer function of the stresses in the Sea Quest SSM had a 'series of humps and hollows' a feature he did not observe on the transfer function of measured (from full scale SSM) stresses.

The computed stresses (Figures 5.19 to 5.23) are in reasonable agreement with the measured ones for wave periods up to 12 sec. For longer waver periods, the computed values become several times higher than the measured ones in almost all the sections. Similar features were observed in the RAO plots of the measured and computed motion presented in figures 5.16 to 5.18. The high values of computed motion and structural responses at wave periods longer than 12-15 sec. are probably caused by over-estimation of wave forces.

Considering all the facts, the results presented in this section demonstrate the viability and reliability of the hydroelastic modelling of semi-submersibles.

5.1.2 Response at Different Draft and Listing Conditions

Strains measured by strain gauges at each section were used to compute axial stresses (due to axial force) and bending stresses (due to bending moments) about each principal axis of the section. The local axis system for the instrumented sections is presented in Figure 4.16.

Figures 5.24 to 5.29 present full-scale RAO plots for axial and bending stresses at the instrumented sections at survival draft in head and beam sea waves. Stresses in the pontoon, column and girder sections were generally dominated by bending stresses (Figures 5.24 to 5.28). Axial stresses contribute a significant portion to the total stresses in these sections. In beam seas the stresses in bracing members were dominated by axial stresses (Figures 5.28 to 5.30) while in head seas, bending stresses were higher due to direct wave action on these bracings (Figure 5.30).

Figures 5.31 to 5.33 present the full-scale motion responses at survival draft, operating draft and at survival draft in listing (damaged) condition. As expected, the motion response values are higher at survival draft than at operating draft (the pontoon is closer to the higher wave action near the surface). When the model

developed a list at survival draft, its motion was reduced. The model motion and structural response remained linear and harmonic. However, a harmonic component with a period several times higher than the wave period was observed in both the motion and structural responses (Figures 5.34 and 5.35). This phenomenon may be attributed to increased second order wave effects due to the listing of the model.

Although the motion decreased after the model developed a list (Figures 5.31 to 5.33), the stresses increased in almost all the sections (Figures 5.36 to 5.41). Stresses increased by up to 30% in the damaged condition. Stress increase is generally higher at lower wave periods.

The results in Figures 5.36, 5.39 and 5.41 indicate that the stresses, like the motions, were lower at operating draft than at survival draft.

5.2 Response in Irregular Waves

Two sets of irregular wave profiles were generated using the Pierson-Moskowitz spectrum. Figure 5.42 presents a plot of each spectrum while Figure 5.43 presents the measured wave profiles. The characteristics of each wave train are presented in Section 4.7.3. All the results presented in this section are in full-scale values at survival draft.

5.2.1 Motion Response

Figure 5.44 presents an extended portion of the wave profile and the corresponding segment of time histories for heave, pitch and surge responses in a head sea. Figures 5.45 and 5.46 present the measured power spectral density (P.S.D.) plots for wave profile #1 and the motion response in head and beam seas, respectively. Figure 5.47 presents the P.S.D. plots for wave profile #2 and the corresponding motion response in a beam sea.

The results presented in Figures 5.44 to 5.47 indicate second-order, low frequency response, at frequencies outside the wave spectra, for all the SSM motion except the heave. The same results were observed by Lundgren and Berg (1982) who pointed out that the motion in irregular waves obtained using RAO's for regular waves will be underestimated since the second order wave effects are not included in the regular wave RAO's. The spectra of the motion response contain a significant amount of energy due to second order effects as compared to the first order effects, especially for surge and sway motions.

Each spectrum has two peaks, one near the peak frequency of the wave spectra and the other very close to the natural frequencies of the semi-submersible. This is another

verification of the natural period measurements reported in Section 4.5.

5.2.2 Structural Response

The results presented in this section are for wave profile #1 only. Figures 5.48 and 5.49 present sample time history plots for measured stresses in SSM columns, pontoon and deck girder in head and beam sea waves respectively. Comparing these results with the wave profile presented in Figure 5.43 it can be noticed that the maximum structural response usually occurs due to the highest wave. Second order effects are noticed in the structural response.

These second order effects are also evident in the P.S.D. plots of measured stresses presented in Figures 5.50 to 5.55. The stress spectra have peaks at freqencies corresponding to the natural frequency of the SSM-motion.

This means that stresses are significantly affected by the resonant motion of the SSM. For example, axial and bending stresses in the main (corner) column have spectral peaks at frequencies near the natural frequencies of all the semi-submersible motions (Figure 5.50). Bending stresses at the middle section of the pontoon have spectral peaks at the heave and roll resonance frequencies (Figure 5.51 and 5.52). The axial stresses in the horizontal braces in beam

seas increase significantly near the natural frequency of sway (Figure 5.54).

The low frequency contents of the P.S.D. of stresses in some sections was almost non-existent, especially in beam seas (Figures 5.50, 5.53 and 5.55). In other instances, the low frequency contents may constitute a significant part of the spectra (Figures 5.50 and 5.54).

5.3 Linearity of Semi-Submersible Respones

To check the linearity of the response of the semi-submersible with respect to wave height, the motion RAO plots were obtained from regular wave tests for wave heights of 5 m and 7.5 m, and from the irregular wave tests for the two wave profiles. Figure 5.56 presents the P.S.D. of wave profile #1 and sample plots of the curves representing the square values of the heave and pitch transfer functions in a head sea. These curves were obtained by dividing the P.S.D. values of the motion by the wave spectral value at the corresponding frequency. The transfer function of each motion was obtained as the square root of these values.

The results presented in Figures 5.57 to 5.59 indicate that for beam seas, the RAO values obtained from the regular and irregular wave tests were very close at wave periods less

than 21 sec. However, for head sea te
differences in the RAO values obtained from regular and irregular wave tests. In head seas, the motion RAO values obtained from irregular wave tests (wave profile #1) were consistently lower than those of the regular waves especially for the surge motion (Figure 5.59). Again the difference is larger at longer periods due to viscous effects. Viscous effects become significant at low member-diameter-to-wave-length ratio.

The visible non-linear effects for head sea tests are due to the drag forces on the bracing system of the SSM. The TIM-77 SSM has a large number of bracing members that have small diameter-to-wave-length ratios (less than 0.015 for the waves used in the test). Therefore, the wave drag forces on the bracing members are predominant in the total wave force. These bracing members are more exposed to head sea waves than to beam seas where they become 'hidden' behind the larger columns.

Figure 5.60 presents the effect of wave height on the stress RAO plots at the middle of the pontoon and the top and bottom sections of the secondary columns. The results indicate that the non-linear effect are negligible for wave periods up to 20 sec. These results are identical to the ones obtained for the motion response and consistent with the results of theoretical, experimental and field studies

reported in Section 2.2. Therefore, it was decided not to investigate this point for the structural response any further.

5.4 Effect of Mooring Stiffness

Figures 5.61 and 5.62 present the effect of varying the mooring system stiffness on the motion response in head seas. The results indicate some decrease in SSM motion as the mooring stiffness decreased. The larger motion resulting from higher stiffness can be explained easily since the natural frequency of the motion will increase by increasing the mooring stiffness. And since the natural frequencies of the SSM motion are usually lower than the wave frequencies, an increase in the natural frequency will bring the system closer to the resonant state. This will increase the dynamic amplification factor, and hence, the SSM motion.

The overall effect of mooring stiffness does not seem to be significant but is expected to be larger near motion resonance and in the low frequency ranges of the second order wave effects since the natural frequencies of the SSM usually fall within this low frequency range. Similar results have been reported by Lundgren and Berg (1982), Yoneya (1984) and Price and Wu (1983).

5.5 Summary

The motion and structural responses of the model to regular and irregular waves have been presented. The accuracy of the measured motion response values was checked using available values obtained from numerical models, other model tests and full-scale measurements.

A general agreement between the measured and computed stresses was observed. The differences were consistent with those found between full-scale and computed values. The results demonstrate the utiltiy and validity of hydroelastic modelling.

The stresses in pontoon, column and girder sections were generally dominated by bending stresses while those in the bracing members were dominated by axial stresses.

Motion and structural response values at survival draft were higher than those at operating draft. After the model developed a list (due to simulated column rupture) the motion decreased but the stresses increased by as much as 30%. The motion and structural responses of the model in the listing (damaged) condition to regular waves contained a low frequency (second order) component, a phenomenon not observed for level-keel position in regular waves.

In irregular waves, the spectra of the motion and structural responses exhibited second order, low frequency (outside wave frequencies) components. Both motion and stress spectra had peaks at frequencies corresponding to the natural frequencies of the motion. The stresses were found to be significantly affected by the resonant motion.

Motion and structural responses to beam sea waves were linear for periods up to 21 sec. For head sea tests, however, some non-linearities in the motion were observed over the whole range of wave frequencies due to the direct wave effects on the multiple bracing system.

The motion of the model slightly decreased after the mooring system was removed. The stiffness of the mooring cable does not seem to significantly affect the motion or the structural response in regular waves.

CHAPTER VI

RESPONSE TO IMPACT

The evolution of numerical impact models and a review of the available work on the impact of offshore structures have been presented in Section 2.3. The following Section presents an outline of the latest version of the impact model developed by the Structures Group at Memorial University.

6.1 Equations of Motion

When a semi-submersible is subjected to the impact of small bodies it behaves as an elastically restrained body. The global equations of the six-degrees-of-freedom motion, without considering the local deformation at the point of impact, can be expressed in a matrix form as:

$$([M] + [A])\{\ddot{U}\} + [B]\{\dot{U}\} + [C]\{U\} = \{F(t)\} \quad \ldots\ldots\ldots\ldots 6.1$$

where

[M], [A], [B] and [C] are 6 x 6 matrices representing mass, added mass, damping and restoring force coefficients, respectively,

$\{U\}$, $\{\dot{U}\}$ and $\{\ddot{U}\}$ are the six motion components and their time derivatives; and

$\{F(t)\}$ the impact force vector.

The impact forces cannot be computed explicitly without solving the equations of motion. The impact forces depend on the global response of the impacting bodies and are strongly affected by the characteristics of the local impact interface. To account for the local effects on the impact forces, an impact interface model (Figure 6.1) was developed by Swamidas et al (1984). The local impact forces are assumed to act in any direction only in a horizontal plane since the ice will impact a vertical surface and the maximum ice velocity is horizontal. It is also assumed that the local impact is central and therefore the rotations of the ice mass are neglected.

The local equations of motions at these points of impact can be expressed as (Swamidas et al, 1984):

$$m_2 \ddot{\delta}_2 + c_2(\dot{\delta}_2 - \dot{\delta}_1) + k_2(\delta_2 - \delta_1) = 0$$

$$m_1\ddot{\delta}_1 + (c_1 + c_2)\dot{\delta}_1 + (k_1 + k_2)\delta_1 - k_2\delta_2 - c_2\dot{\delta}_2 - k_1\chi - c_1\dot{\chi} = 0 \quad \ldots\ldots\ldots 6.2$$

where m_1, m_2, c_1, c_2, k_1, k_2, δ_1, δ_2, and χ are as shown in Figure 6.1. χ represents the component of the rigid-body motion of the semi-submersible at the point of impact.

The two equations in 6.2 were combined to get the coefficients for an equivalent single-degree-of-freedom system to represent the combined characteristics of the impact zone. After incorporating the local stiffness equation and substituting for the impact force, the equations of motion for the system become:

$$(a_{11}D^2+b_{11}D+{}_cc_{11})\xi+(a_{15}D^2+b_{15}D)\theta-(b_{77}D+c_{77})(\delta-\chi)$$
$$\times \cos(180°-\gamma) = 0$$

$$(a_{22}D^2+b_{22}D+{}_cc_{22})\eta+(a_{24}D^2+b_{24}D)\phi-(b_{77}D+c_{77})(\delta-\chi)$$
$$\times \sin(180°-\gamma) = 0$$

$$(a_{33}D^2+b_{33}D+c_{33}+{}_cc_{33})\zeta = 0$$

$$(a_{24}D^2+b_{24}D)\eta+(a_{44}D^2+b_{44}D+c_{44}+{}_cc_{44})\phi-z_1(b_{77}D+c_{77})(\delta-\chi)$$
$$x\cos(180°-\gamma) = 0$$

$$(a_{15}D^2+b_{15}D)\xi+(a_{55}D^2+b_{55}D+c_{55}+{}_cc_{55})\theta-z_1(b_{77}D+c_{77})(\delta-\chi)$$
$$x\sin(180°-\gamma) = 0$$

$$(a_{66}D^2+b_{66}D+{}_cc_{66})\psi-(b_{77}D+c_{77})(\delta-\chi)\{y_1\cos(180°-\gamma)$$
$$-x_1\sin(180°-\gamma)\} = 0$$

$$(a_{77}D^2)\delta+(b_{77}D+c_{77})(\delta-\chi) = 0 \quad \ldots\ldots\ldots\ldots\ldots\ldots \quad 6.3$$

where

$D = \frac{\partial}{\partial t}$

a_{ij}, b_{ij}, c_{ij} = inertial, damping, and restoring coefficients for the semi-submersible for values of i and j less than 7. For $i=j\neq 7$ these coefficients represent the combined local degree-of-freedom.

c^{c}_{ij} = the contribution from the mooring system stiffness

ξ, η, and ζ = the translatory motions of surge, sway and heave, respectively,

ϕ, θ and ψ = the rotational motions of roll, pitch and yaw, respectively,

δ = the local degree of freedom in the direction of motion of the bergy bit at the zone of impact,

x_1, y_1, z_1 = the coordinates of the point of impact with respect to the semi-submersible centre of gravity

γ is the angle between the direction of the bergy bit motion and the surge direction of the semi-submersible.

$$\chi = (\eta+z_1\phi+x_1\psi)\sin(180°-\gamma)+(\xi+z_1\theta+y_1\psi)\cos(180°-\gamma) \quad \ldots\ldots 6.4$$

In equation 6.3 only the strong coupling coefficients are taken into account, while the other coefficients which have insignificant effects on the motion are neglected. The impact force F(t) is substituted in equation 6.1 as:

$$F(t) = (Db_{77}+c_{77})(\delta-\chi) \quad \ldots\ldots 6.5$$

The equations of 6.3 are solved in time domain using the Wilson-θ numerical integration method, subject to the initial condition

$$\dot{\delta}(0) = \text{impact velocity}$$

The local spring represented by the coefficient c_{77} has a tension cut-off property which permits separation of the colliding bodies and rebound of the bergy bit when the contact force, F(t) becomes zero. The analysis then continues to determine the post-impact motion of the semi-submersible.

The validity of the numerical model, representing equations 6.3 and 6.5 was checked using the results of the test program as outlined in the next section.

6.2 Verification of Numerical Model Results

All the results presented in this section and the following sections are scaled up to the full-scale values.

Impact forces and motion of the semi-submersible and bergy bit were computed using the numerical model described above under an impact of 1,000 and 2,000 tonne bergy bits with the instrumented corner column and at impact speeds of 1 and 4 m/sec in the direction of the surge motion. The added mass and damping coefficients were computed according to the method reported by Vugts (1968). The experimental results were used to tune some of the numerical parameters (i.e. hydrodynamic damping). The experimental results helped to locate a minor post-impact algorithm error and correct the tension cut-off (rebound) condition.

Figure 6.2 presents the computed and measured impact forces for the four mass/velocity combinations. The results indicate very good agreement between the measured and computed impact force. The peak impact force was almost linearly proportional to the bergy-bit mass and velocity.

Figure 6.3 presents the computed and measured semi-submersible surge and yaw motions due to the impact of a 1,000 tonne iceberg with a speed of 4 m/sec. All the rest

of the components of semi-submersible motion were negligible.

The results in Figures 6.2 and 6.3 demonstrate the validity and accuracy of the numerical model results. Further verification of the numerical model results are presented in Section 6.6.4 using the experimental results of the two-degrees of freedom model.

6.3 Case Study

This section presents detailed results of the impact test for a sample case. For the rest of the tests only a summary of the results will be given in a following section. The case under consideration is the simulated impact test on the semi-submersible by a 1,000 tonne bergy bit moving at a speed of 4 m/sec. The impacted member was the instrumented corner column. The impact point was 4 m below the water surface and the impact direction was parallel to the surge motion (head sea impact).

Figure 6.4 presents time histories of the measured bergy bit deceleration and velocity. The velocity was obtained by integrating the deceleration. The bergy bit rebounded after impact with a velocity of about 1.8 m/sec, 45 % of the initial velocity. The impact force obtained from the deceleration time history is presented in Figure 6.2 while

Figure 6.3 presents the yaw and surge motions of the semi-submersible after impact. The peak impact force was 79 MN, about 8 times the bergy bit weight. Impact duration was 110 ms which corresponds to a frequency of about 4.5 Hz. After this impact, the semi-submersible had a maximum yaw and surge motion of 3 degrees and 2.4 m, respectively. This motion is within the motion response under normal operating conditions and will not increase the mooring forces significantly (Fig. 4.21). The other motions (heave, pitch, etc.) were very small and virtually immeasurable.

Figure 6.5 presents sample plots of stress time histories as measured by the strain gauges at the base of the impacted corner column (Section MB). The stresses measured at the four strain gauges were used to determine the time histories of maximum axial and bending stresses about the principal axis of the section (Figure 6.6). The stresses at the column base were so high (about 60% of yield strength) that damage to the column may not be restricted to the local impact zone. Combined stresses from wave and impact may cause yielding in the column. Actually, this value was several times higher than the expected maximum stresses in this section due to a 20 m wave.

High stresses were also measured at the horizontal bracings connected with the impacted column (Section HBO), and the bracings connecting the secondary columns (HBI). Although

these bracing members were not subjected to direct impact, stresses as high as 65 MPa were produced in them due to the corner column impacts (Figure 6.7). This value, is equivalent to the stresses caused by the direct action of a 20 m head sea wave on these bracings (see Figure 5.30).

The stresses presented in Figures 6.6 and 6.7 indicate strong interactive vibrations in the whole semi-submersible when a corner column was hit by a bergy bit. This suggests that a significant part of the energy may be absorbed by structural vibrations. Actually, analysis of test results indicated that about 36% of the kinetic energy was absorbed by structural vibrations of the members not directly impacted. This point will be discussed later in detail.

The impact was in the direction of the local Y-axis (Figure 6.6) which should cause bending stresses, Z, if the column was connected at its ends only. But due to the multiple bracing system connected to the column (two horizontal and one vertical bracing), the interaction with the bracings caused the column to vibrate in the axial direction and in bending modes about the principal axes. It also had torsional vibrations, evident by the flexural vibrations of the horizontal bracings.

Figure 6.8 presents power spectral density plots for the axial and flexural stresses at the column base (presented

in Figure 6.6). The P.S.D. of the flexural stress, Z, (major stress) has a peak near the frequency of 5 Hz, the impact force frequency. All the structural vibrations have frequency components lower than 5 Hz. The axial stresses and flexural stresses about the axis have a dominating frequency slightly lower than 2.5 Hz. This frequency component exists also in the measured stresses in the horizontal bracings as presented in Figure 6.9. The P.S.D. plots in Figure 6.9 demonstrate the interactive effect between the stresses in the column and the two bracings. Except for the impact frequency (near 5 Hz) and the frequency near 3.8 Hz (likely a natural frequency for the column), each peak frequency of the stresses at the MB-3 strain gauge location has a corresponding peak in the two bracing stresses.

The results in Figures 6.8 and 6.9 indicate that the frequencies contained in the impact impulse were higher than the natural frequencies of the structural members and are not likely to cause resonance in the global structural response.

Since the stiffness of the hydroelastic model was about 70% higher than required, the natural frequencies of the prototype are expected to be about 30% lower than those obtained from the model. This means that the natural

frequencies of the prototype fall even farther from the dominating frequency of the impact impulse.

As indicated earlier the impact zone in the model was strengthened to prevent structural failure. For the unstrengthened columns the actual local stiffness is much smaller than the simulated one, and therefore, the impulse frequency is likely to be lower than the measured one. The effect of varying the local stiffness on the impact force and duration is investigated in Section 6.6.

6.4 Energy Dissipated by Structural Vibrations

Analysis of the results for the case study indicated that 18% of the kinetic energy of the bergy bit was returned in the form of bergy-bit rebound and 9% was spent in the surge and yaw motions of the semi-submersible. About 37% of the input energy was absorbed by the local deformation of the impacted column. The rest of the energy (about 36%) was apparently absorbed by the vibration of all the semi-submersible structural members. This finding can be supported by the fact that the numerical model, although it predicted similar impact forces and semi-submersible motion, also predicted much higher rebound velocity. The measured rebound velocity was 45% of the initial velocity (Figure 6.2), while the computed value represented 70%. Therefore, the experimental rebound energy represented

about 20% of the input energy while the numerical value was about 50%. The numerical model considers the semi-submersible as a rigid body (except at the local impacted zone); therefore, energy dissipated by global structural vibrations is not accounted for.

The experimental energy spent in local deformation and global semi-submersible motion was almost equal to that obtained from the numerical model. Therefore, the remaining energy (30% of input energy) was turned back into the system in the form of higher rebound velocity. It is interesting to note that the extra rebound energy (30%) is close to the amount of energy believed to be spent in structural vibration by the hydroelastic model (36%).

The above values are based on an impact velocity of 4 m/sec. The same value of structural vibration energy (36% experimental, 30% numerical) was obtained for input velocities of 3 and 2 m/sec. For an impact velocity of 1 m/sec, this value was only 24% from experimental and 20% from numerical models.

These results are based on the assumption that the impact zone is strengthened well enough to prevent any local damage. Otherwise, redistribution of stresses will occur and more energy will be absorbed in denting or rupturing of the column.

6.5 Parametric Study

This section presents the results of a parametric study carried out to investigate the effect of varying bergy-bit mass and velocity, impact direction and location, and the stiffness of the mooring system on the semi-submersible response (using the hydroelastic model).

6.5.1 Impact Force

Table 6.1 presents the variation in the impact force versus bergy-bit mass and velocity. It also presents the effect of mooring stiffness on the impact force. The values given in Table 6.1 present the ratio of the maximum impact force to the bergy-bit weight. The results indicate that the impact force is almost linearly proportional to the impact velocity and bergy-bit mass. The impact force is slightly affected by the mooring system stiffness. The impact force was reduced by about 10% when the mooring stiffness was reduced by 80%. The impact impulse duration did not vary with impact velocity but increased significantly as the bergy-bit mass increased.

The impact force is affected by the global stiffness of the column. The impact force on the corner (main) column was 38% higher for the tranaverse collision (sway direction) than for the longitudinal collision (surge direction) for

the 4 m/sec impact velocity. The difference was lower at lower velocities. The column has more stiffness in the transverse direction due to the support provided by the vertical diagonal bracing member (DBO) near the impact zo[illegible]

The impact forces on the secondary column were also higher than those on the main column. Although the cross-section of the secondary column is smaller than that of the main column, the vertical diagonal bracing provides support at almost the same level as the impact force. This increased the rigidity of the column and hence, the impact forces were higher.

6.5.2 Motion Response

Table 6.2 presents the variation in surge and yaw motions with bergy-bit mass, impact velocity and mooring system stiffness, due to a head impact (in surge di[illegible]ion) with the corner column.

The motion is significantly affected by impact speed. Doubling the mooring stiffness has little effect on the surge and yaw motions, while reducing the stiffness by 80% significantly increased the motion.

6.5.3 Impact Stresses

For the corner column impact in the direction of surge motion, strains were measured at sections at the base of the main column (section MB) and the middle of the horizontal bracings (sections HBO and HBI). For the impact in the direction of sway motion, the strains were measured at section MB, diagonal bracing section DBO, and deck girder section DG. The secondary column impact in the direction of sway motion was at the same elevation as the impact for the main column (4 m below the still water level). The strains were measured at the top (section ST) and base (section SB) of the secondary column. The variations in the maximum impact stresses at these sections with bergy-bit mass, impact velocity and mooring cable stiffness are presented in Tables 6.3 to 6.5.

Generally speaking, the impact stresses were proportional to the impact velocity. However, impact stresses did not double in value when the bergy-bit mass was doubled. For example, for corner column impact, the stresses increased by 26% to 40% when the bergy-bit mass was doubled at original mooring stiffness; less effect was observed for the secondary column impact.

Impact stresses increased only slightly when the mooring stiffness was doubled for the 1,000 tonne bergy-bit impact.

However, the impact stresses increased significantly when the mooring stiffness was doubled for the 2,000 tonne bergy-bit impact.

The results presented in Tables 6.3 and 6.4 indicate that high stresses (up to 87 MPa) were measured in the members not directly hit by the bergy-bit (bracings and deck girder). Very high stresses (up to 281 MPa) were measured at the ends of impacted columns. Stresses in the corner column were generally higher than those in the secondary column under similar conditions, although the secondary column has a smaller diameter. The reason is that the secondary column was supported at the level of impact by a diagonal bracing and therefore less global bending took place due to impact.

The amount of global stresses and structural vibrations is expected to be less than the above values if local failure occurred allowing more energy to be absorbed by local denting and rupture.

To allow local failure to occur, the local structural detailing and strength properties have to be properly simulated. This can only be done by using a detailed large scale (e.g., 1:10) model of a column portion. However, such an elaborate investigation is beyond the scope of this study. Instead, the effect of varying local stiffness on

the results can be investigated using a simplified model as presented in the following section.

6.6 Effect of Local Stiffness

Since the local impact zone was artifcially strengthened to prevent local damage to the model, it was decided to investigate the effect of varying the local stiffness on the impact force (impulse) and semi-submersible motion.

6.6.1 Model Description

The results of the hydroelastic model indicated that about 9% of the input energy was absorbed by global semi-submersible motion. Most of this energy (more than 7% of the input energy) was dissipated through surge (or sway) motion alone, less than 2% by the yaw motions and almost none by the other motions. Therefore, it was decided that it would be sufficient to represent the surge motion as the only degree-of-freedom for global motion, plus one local degree-of-freedom to represent the stiffness of the impact interface. Springs were placed at the back of the impacted body to simulate the restoring force for the surge motion. A cylindrical (3.8 cm diameter, 3.2 cm long) stiffness element representing the local stiffness of the impact interface was placed in the impact zone to transfer the impact loads to the semi-submersible model (Figure 6.10).

This two-degrees-of-freedom model was made of oak wood, both the impacted body (representing the semi-submersible) and the impacting sphere (representing the bergy-bit). The region of impact was made flat on both bodies. The impact forces were monitored using three instruments: i) an accelerometer mounted on the impacting spherical pendulumn, ii) an accelerometer on the impacted block, and iii) an impact force transducer placed between the block and the stiffness element (Figure 6.10). Very good agreement was found between the impact impulses obtained from these three different instruments (Figure 6.11). In addition to these transducers, a LVDT mounted alongside the rectangular prism was used to measure the impacted body displacement.

The stiffness elements were made of steel, oak, paraffin wax and two grades of synthetic packing material (foam). The stiffness of these elements varied from 79,000 KN/cm to 0.107 KN/cm.

The dynamic forces, accelerations and displacement were recorded on a high speed magnetic tape that can record frequencies up to 60 KHz. A magnetic-activated system was used to record a signal to trigger the data acquisition process by the computer. Figures 6.12 and 6.13 present a general view of the test set-up and the data acquisition system.

6.6.2 Modelling Parameters

The model parameters were chosen in such a way that the modelled local stiffness can be represented by available material. This was achieved by choosing λ (the length scale) as the stiffness scale as opposed to λ^2 for Froude scaling. This modelling distorts the gravitational acceleration but gravitational forces are not involved in this model. The principal scaling parameters are listed below:

dimension	λ
velocity	1
acceleration	$1/\lambda$
forces	λ^2
stiffness	λ
mass	λ^3
time	λ
frequency	$1/\lambda$
damping ratio	1
stresses	1
elasticity modulus	1

The linear scale λ is 1:98.

6.6.3 Test Program

The impact tests were carried out for three ball masses (representing 1000, 2000 and 4000 tonne bergy-bits). The stiffness of the springs were varied to simulate i) one half, ii) double, and iii) the original mooring system stiffness for the surge motion.

Impact speeds varied from 0.5 m/sec to 2 m/sec. Effect of local stiffness was investigated using the six stiffness elements for original mooring stiffness, impact velocity of 1 m/sec and bergy-bit mass of 2000 tonnes.

A total of 30 tests were carried out, each test involving 3 to 6 repeated hits under the same conditions.

6.6.4 Further Verification of Numerical Model

The equation of motion of the two-degrees-of-freedom rigid-body model shown in Figure 6.10 is given by:

$$m_1 \ddot{v}_1 + c_1 \dot{v}_1 + k_1 v_1 - k_1 v_2 - c_1 \dot{v}_2 = 0$$

$$m_2 \ddot{v}_2 + (c_1+c_2)\dot{v}_1 + (k_1+k_2)v_1 - c_1 \dot{v}_1 - k_1 v_1 = 0 \quad \ldots\ldots \quad 6.6$$

where (m_1, m_2), (c_1, c_2) and (k_1, k_2) are the mass, damping and stiffness properties of the two-degrees-of-freedom model,

v_1 and v_2 are the local and base (global) displacements, respectively

$$\dot{v}_1(0) = \text{impact velocity}$$

The equations are solved numerically using Wilson - θ method.

Equations 6.6 were used to obtain the impact force and global motion for 3 selected stiffness elements: the oak, wax and black foam plugs with full-scale stiffness of 40, 5.2 and 0.0107 MN/cm, respectively. Figure 6.14 presents the full-scale computed and measured impact forces for the three stiffness elements due to impact of a 2,000 tonne bergy-bit at 1m/sec. Good agreement was obtained between the experimental and numerical values. These values were scaled up to the prototype values.

It is interesting to note that the impact force obtained for the wax element is similar to that obtained from the hydroelastic model for the same bergy-bit mass and impact speed (Figure 6.2). The stiffness of the wax element was close to the local stiffness of the semi-submersible column used in the seven-degrees-of-freedom numerical model.

The computed surge motion was also close to the measured one. It is also interesting to note that the maximum surge motion measured from the two-degrees-of-freedom model was 1.76m while that obtained from the hydroelastic model was 1.8m (Table 6.2).

6.6.5 Parametric Study

This section presents the effect of local stiffness on the impact force and motion response as measured from the two-degrees-of-freedom model. Table 6.6 presents a summary of the full-scale results obtained for an impact of a 2,000 tonne bergy bit at 1m/sec. The results are given relative to the corresponding values of the wax element, since its stiffness is close to the local stiffness of the strenghened column of the semi-submersible.

The local stiffness values varied by about 6 orders of magnitude. However, the impact force varied only by a factor of 70 and the impact duration by a factor of about 1/45. When the stiffness increased by a factor of 7.8 (oak element) from the original value (for wax), the impact force was doubled. However, further increase of the stiffness did not affect the impact force significantly. For example, by increasing the stiffness by more than 3 orders of magnitude (steel element), the impact force increased by a factor of only 2.6. The impact force,

however, was more sensitive to stiffness variation at lower stiffness values.

For example, when the stiffness was reduced to 1.1% of the original value, the impact force became about 5% of its value at original stiffness.

The increase in the impact force was accompanied by a decrease in the impact duration and vice versa. Although both the force and duration varied significantly with variation in local stiffness, the value of impulse almost remained constant. This is evident since there was very little variation in the rebound velocity. Nor did the maximum surge displacement vary with variation in local stiffness.

This means that the response was a function of the impulse value only (impact duration is very much shorter than natural period of motion). Therefore, it is expected that the global semi-submersible motion and bergy bit rebound obtained from the locally stiffened hydroelastic model tests represent the same for the actual semi-submersible (without extra local stiffening). This is based on the fact that the impulse value almost did not change over the wide range of values of local stiffness including the actual stiffness.

However, the global impact stresses may vary significantly from the values presented in Section 6.5.3, since the structural response will be affected by both the impact force and duration (principal frequency of impact is not very far from the natural structural frequencies).

The results presented in Table 6.6 indicate that although the local stiffness varied by about six orders of magnitude, the energy absorbed by local deformation and global motion remained almost constant.

The maximum surge motion obtained from the two-degrees-of-freedom model (1.76m) was close to the value obtained from the hydroelastic model (1.8m). The bergy bit velocity rebound obtained from the 2 D.O.F. model was 0.68m/sec while that obtained from the hydroelastic model for the same conditions (2,000 tonne and 1m/sec) was 0.5m/sec. This corresponds to rebound energies of 46% and 25% of the input kinetic energy, respectively. The difference, 21%, must have been absorbed by structural deformation in the hydroelastic model.

It is interesting to note that analysis of the results of the hydroelastic model impact tests indicated that 20% of the input energy was believed to be absorbed by structural vibrations of the semi- submersible for an impact of 1m/sec (Section 6.4).

6.7 Practical Application

As stated earlier, the main objective of this research program is to investigate the global response of the semi-submersible to wave forces and ice impacts. Therefore, the impact zone in the column was assumed to be strengthened well enough to prevent local damage. The local deformations in the hydroelastic model and the two-degrees-of-freedom model were elastic ones. Accurate estimates of the extent of permanent deformation and rupture involve either: i) large scale-model tests where the local structural detailing and material properties are properly simulated, or ii) a detailed dynamic non-linear finite element analysis of the portion of the column subjected to impact using isoparametric shell elements. Such elaborate investigations are beyond the scope of the present study.

However, an approximate analysis, based on simplified methods, can be carried out using the impact forces obtained from the experimental models to see if permanent deformation will take place in the ice-strengthened and unstrengthened columns.

First we compare the numerical impact forces of a bergy-bit on a semi-submersible obtained by Kitami et al (1984) using a non-linear load-deformation relationship for the impact interface (both for ice and a well-strengthened column).

The load deformation curve for the 2,000 tonne bergy-bit was obtained from indentation tests on sea ice sheets (impact strength of iceberg ice was not ayailable to them). The load-deformation curve of the double-walled column was obtained using elasto-plastic analysis. The outer diameter of the column was 12.5 m while that of the inner cylindrical wall was 9.5 m. Horizontal ring stiffeners joining the two cylinders were placed 1.03 m apart. The initial stiffness of the column was 3.5 MN/cm. An outline of the numerical model developed by Kitami et al has been presented in Section 2.3.

The results were presented for the impact of a 2,000 tonne bergy-bit and 1 m/sec impact velocity. The peak impact force was about 15 MN and occurred 100 ms from impact starting time. The peak impact force obtained from the hydroelastic model (Figure 6.2) and the 2.D.O.F. model (Table 6.6) for the 2,000 tonne bergy-bit, 1 m/sec impact velocity and local stiffness of 5.2 MN/cm was about 38 MN. The results of Kitami et al will be used to check the validity of the approximate analysis as outlined below.

The simplified analysis is based on the assumption that the local column stiffness can be approximated by the stiffness of a thin ring loaded by two equal and opposite forces acting along the ring diagonal. The moment of inertia of the ring section is taken equivalent to that of a segment

of the column section having a height equal to the thickness of the ice at the contact area. According to this method the stiffness of the column and ice used by Kitami et al were 2.07 MN/cm and 3.8 MN/cm, respectively. The combined stiffness of the impact interface is, therefore, 1.34 MN/cm. By interpolation from Table 6.6, the impact force corresponding to interface stiffness of 1.34 MN/cm is 19 MN. The corresponding column deformation can be computed as

$$19(\text{MN})/2.07(\text{MN/cm}) = 9.2 \text{ cm}.$$

The impact force and column deformation reported by Kitami et al were 15 MN and 8 cm, respectively.

They indicated that since the local displacement was less than 1% of the column diameter (12.5 m), no permanent deformation would occur. Using the simplified ring model the load needed to develop a plastic hinge in the column was 23.4 MN (higher than the impact force).

Comparing the numerical values obtained by Kitami et al (1984) with the results of the simplified ring model, it can be seen that the simplified model can provide a reasonable approximation of failure load and local displacement.

We will apply this simple model to get a general idea of the conditions that may cause local failure for the stiffened and unstiffened column of the Tim-77 semi-

submersible. As mentioned earlier no damage took place in the strengthened columns of the model. However, this does not necessarily mean that permanent deformation in the strengthened columns of the prototype will not occur. The measured impact forces will represent full-scale forces since the stiffness is properly simulated. However, since the strength of the material used to strengthen the model (steel) is about 110 times higher than required for the prototype, failure to the prototype may occur although no failure took place in the model. Another difference between the model and prototype is that the impact tests were carried out using lead weights. Deformation of ice is expected to influence the value of the forces in the prototype.

The computed stiffness of the strengthened column was 6.87 MN/cm. The stiffness of ice obtained, assuming 4 m high vertical ice surface in the impact zone and an average impact strength of ice of 8 MPa (obtained from impact tests reported in Chapter 3), was 10.1 MN/cm. Therefore, the combined stiffness of the column and ice will be 4.1 MN/cm. Interpolating from Table 6.6, the impact force is obtained as 34.2 MN. The corresponding local displacement is 5 cm. The indentation in ice will be 3.4 cm and the contact area 4.28 m^2 (4 m high, 1.07 m wide). This means that failure will take place in ice.

The load needed to develop a plastic hinge in the column (as computed from the ring model) is 53.6 MN. Therefore, the strengthened column will probably suffer no permanent deformation for the 2,000 tonne bergy-bit with impact speeds up to 1.5 m/sec, or for a 1,000 tonne bergy-bit with impact speeds up to 3 m/sec. For higher combinations of mass and speed, permanent deformation is expected to take place.

Following the same procedure, the following values were obtained for the unstiffened column:

column stiffness	=	0.08 MN/cm
ice stiffness	=	10.1 MN/cm
combined stiffness	=	0.079 MN/cm
impact force	=	2.53 MN
column deformation	=	31.6 cm
ice deformation	=	0.25 cm
yield load	=	1 MN

The above values indicate large column deformation (about 3.5% of column diameter) and large impact force (about 2.5 times higher than the yield load). Therefore, permanent deformation of the column is expected to take place for mass and velocity combinations higher than 1,000 tonne and 0.5 m/sec (500 tonne and 1 m/sec. etc.). The ice deformation is very small and crushing may not occur.

The above values represent only rough estimates, especially since the stresses due to waves and gravitational/buoyancy loads were not taken into account. Better estimates of the extent of damage can be obtained using detailed non-linear finite element analysis of the local structure of the column in the impact zone.

6.8 Summary

The results of impact tests on the elastic model and the two-degrees-of-freedom model of the semi-submersible have been presented. Impact forces; stresses in the columns, bracings and a deck girder; and bergy-bit and semi-submersible motion during and after impact have been presented for a combination of bergy-bit masses, impact speed and mooring stiffness.

The effect of varying local stiffness on the impact forces and motion response was also investigated. The experimental values were in good agreement with those obtained from two numerical models that use a linear load-deformation relationship for the impact interface.

Estimates of the impact conditions that may cause permanent local deformation were obtained using a simplified numerical method. The validity of the method was checked using available results of a numerical model that utilizes a non-

linear load-deformation relationship and uses an elasto-plastic analysis of the column.

The results indicated that impact forces and stresses are significantly affected by bergy-bit mass, impact velocity and local stiffness, but not sensitive to mooring system stiffness. A significant amount of energy is believed to be absorbed by global structural vibrations.

The strengthened column can withstand an impact of a 1,000 tonne bergy-bit for impact speeds up to 3 m/sec without noticeable damage. The column designed for wave forces (without ice strengthening) will not be able to resist impact without a considerable amount of damage.

The study demonstrated the usefulness of the elastic model in determining impact stresses since, to our knowledge, no finite element model is available yet to directly perform such an analysis for a semi-submersible.

CHAPTER VII

CONCLUSIONS

The main objective of this study was to develop a model that was structurally and dynamically similar to a typical semi-submersible and use it to measure the stresses developed in all the structural members due to wave forces and impact loads. The literature review shows development of such a model might not be feasible since the model would be very delicate and there would be enormous problems in modelling, construction, handling, and testing of the model. This study presents the techniques used to overcome these problems.

The modelling techniques were developed to achieve similarity of local mass distribution and the axial, bending, shear and torisonal stiffnesses of the structural members. The local mass distribution was perfectly simulated and the relative stiffnesses of the structural members were kept the same in the model and the prototype. The absolute value of modelled stiffness was only 70% higher than that required for the members. Therefore, the developed hydroelastic model represents a new generation of structural models which is several steps ahead of the best available semi-submersible model.

Due to increased structural rigidity of the previously available models, strains were measured in bracings and deck girders only, while the strains were measured in all the structural members from the hydroelastic model.

The slight increase in model stiffness did not affect the structural response to waves. However, the natural frequencies obtained from the model are about 30% higher than the actual values. Since impact involves natural vibrations and dynamic response, the results may vary slightly due to the difference in stiffness.

The delicate model survived about 150 regular wave tests; four irregular wave tests with maximum wave height of 26 cm (20 m full scale); and about 50 impact tests with modelled bergy-bits representing masses up to 2,000 tonnes and impact speeds up to 5 m/sec. This is an indication of the reliability of design, construction, handling and testing techniques.

The accuracy of the motion response of the model in waves was verified using results obtained from numerical models, earlier model tests and field measurements. The measured structural response values were validated using computer analyses. The accuracy of structural response obtained from elastic models should be checked using full-scale measurements.

The first attempt to develop a structurally similar model was a successful one. The results demonstrated that developing a 100% structurally and dynamically similar model is quite feasible. For example, the same material used to construct the hydroelastic model can provide a perfect stiffness similarity for a scale of about 1:50. Structural damping similarity may be a problem since the damping of plastics is higher than that of steel.

The results of model response in regular waves indicated that the motion will slightly decrease and stresses increase by up to 30% after the model developed a list. The motion and structural response of the model in the listing condition contained a low frequency component, a phenomenon not observed for level-keel position.

Second order low-frequency components were also observed in both the motion (except heave) and structural responses of the model in irregular waves. The stresses were significantly affected by the resonant motion. The results also demonstrated the linearity of the motion and structural responses.

The results of impact tests carried out on the elastic model of the semi-submersible indicated that impact forces and stresses are significantly affected by bergy-bit mass and speed; forces are more affected than stresses.

A significant portion of input energy is absorbed by elastic vibration of the structure. This structural vibration may be less in semi-submersibles with a smaller number of bracing members. Local stiffness was found to significantly affect impact forces but motion was not affected. The study demonstrated the usefulness of the elastic model to investigate the problems of bergy-bit collision with semi-submersibles.

Local failure of the impacted zone was not permitted to occur in the model. To account for local failure, a replaceable 'failure' element, similar to the stiffness element used in the two-degrees-of-freedom model, can be developed and placed on the column of the elastic model. The failure element should simulate the load-deformation characteristics of both the column and ice. The load-deformation characteristics of the column can be obtained using a detailed non-linear finite element analysis of the impacted part of the column, using appropriate boundary conditions.

The load-deformation characteristics of ice in the impact zone can be established using the results of the impact tests on iceberg and snow ice presented in Chapter III. These results represent the only available data on impact strength of isotropic ice.

The results of numerical impact models were verified using the results of impact tests. The models provide a good estimate of impact forces and motion. The models should be modified to account for non-linear load deformation characteristics and for elastic vibration in the semi-submersible structure (e.g., by adding an extra degree-of-freedom). The three degrees-of-freedom representing heave, roll and pitch may be eliminated from the numerical models without affecting the accuracy of the results.

Strengthened columns will withstand the impact of a 1,000 tonne bergy-bit at 3 m/sec impact velocity, while columns designed for wave forces only may not withstand the impact of a bergy-bit. These results are based on simplified analysis. Better estimates of the extent of damage can be obtained using non-linear finite element analysis as described above.

Overall, the study demonstrated the viability and reliability of hydroelastic modelling of semi-submersibles. The model was successfully designed, built and tested; it survived all the tests, and performed well beyond all expectations.

REFERENCES

1. American Society for Testing and Materials, 1981, "Annual Book of ASTM Standards", Part 35, Plastics - General Test Methods, ASTM, Philadelphia, pp. 228-388.

2. Arockiasamy, M, and Reddy, D.V., 1982, "Analysis of Certain Offshore Structural Concepts: Analysis of Results", Vol. II, Project Report submitted to Petroleum Directorate, Govt. of Newfoundland and Labrador, August, 251 pp.

3. Arockiasamy, M., El-Tahan, H., Swamidas, A.S.J., Russell, W., and Reddy, D.V., 1983a, "Semi-Submersible Response to Bergy Bit Impact", Proceedings of the RINA International Symposium on Semi-submersibles; The New Generations, London, March 17-18.

4. Arockiasamy, M., Reddy, D.V. and Muggeridge, D.B., 1983b, "Dynamic Respone of Moored Semi-sumbersibles in an Ice Environment", Preprint SC-12, ASCE Structures Congress, Oct. 17-19, 16 pp.

5. Bain, J.A., 1964, "Extension of MOHOLE Platform Forces and Motion Studies", Project MOHOLE Report by General Electric Co.

6. Bainbridge, C.A., 1981, "Strength Analysis of Semi-submersible Production Platforms", Proceedings of the Symposium on 'Production and Transportation Systems for the Hibernia Discovery', Petroleum Directorate, St. John's, Newfoundland, February 16-18, pp. 322-336.

7. Bell, A.O. and Walker, R.C., 1971, "Stresses Experienced by an Offshore Mobile Drilling Rig", Proceedings OTC 1971, Paper No. 1440, Houston, Texas, April 19-21.

8. Bell, A.O., 1974, "Service Performance of a Drilling Unit", Ahnual Meeting of the Royal Institue of Naval Architects, London, April 24, pp. 243-258.

9. Brakel, J., Reinhardt, H.W. and Oostlander, L.J., 1979, "Concentrated Loading on a Thick Walled Concrete Cylinder", Proceedings of the International Symposium on Offshore Structures, COPPE, Federal Univ. of Rio de Janeiro, Brazil, October, pp. 171-187.

10. Burke, B.G., 1969, "The Analysis of Motion of Semi-submersible Drilling Vessels in Waves", Proceedings of the Offshore Technology Conference, Houston, Texas, May 18-21, Paper No. OTC 1024.

11. Burke, B.G., 1970, "The Analysis of Motions of Semi-submersible Drilling Vessel in Waves", Transactions of the Society of Petroluem Engineers, Vol. 249, pp. 311-318.

12. Butkovich, T.R., 1955, "Crushing Strength of Lake Ice", CRREL Research Report 15, March.

13. Butkovich, T.R., 1956, "Strength Studies of High Density Snow", CRREL Research Report 18, Oct.

14. Butkovich, T.R., 1959, "Some Physical Properties of Ice from the Tuto Tunnel and Ramp, Thule, Greenland", CRREL Research Report 47, May.

15. Caldwell, D. and Billington, C.J., 1981, "Major Ship Collision Damage to the Pre-stressed Concrete Cylinder Towers of Offshore Gravity Structures", Proceedings of Second International Symposium on Integrity of Offshore Structures, University of Glasgow, Scotland, July 1-3, pp. 339-361.

16. Cammaert, A.B. and Tsinker, G.P., 1981, "Impact of Large Ice Floes and Icebergs on Marine Structures", Proceedings of the 6th International Conference of Port and Ocean Engineering under Arctic Conditions, Quebec, Canada, July 27-31, Vol. II, pp. 653-667.

17. Carlsen, C.A., 1977, "Simplified Collapse Analysis of Stiffened Plates", J. of Norwegian Maritime Research, Vol. 5, No. 4, pp. 20-36.

18. Carlsen, C.A. and Mathisen, J., 1980, "Hydrodynamic Loading for Structural Analysis of Twin-Hull Semi-submersible", American Society of Mechanical Engineering, Applied Mechanical Symposium Series, Vol. 37, pp. 35-48.

19. Carter, D., 1970, "Brittle Fracture of Snow Ice", Proc. IAHR Symposium, Reykjavik, Iceland, Section 5.2.

20. Chakrabarti, S.K., 1980, "Impact of Analytical Model and Field Studies on the Design of Offshore Structures", International Symposium on Ocean Engineering - Ship Handling, Sept. 17-18, Gothenburg, Sweden, pp. 6:1 - 6:79.

21. Chakrabarti, S.K. and Cotter, D.C., 1984, "Interaction of Waves with a Moored Semi-submersible", Proceedings of Third International Offshore Mechanics and Arctic Engineering Symposium, New Orleans, LA, February 12-17, pp. 119-127.

22. Chao, J.C., 1978, "Dynamic Responses of Floating Structures", Journal of the Waterway, Port, Coastal and Ocean Division, ASCE, Vol. 104, No. WW2, May, Proceedings Paper 13769, pp. 105-118.

23. Chung, J.S., 1975, "A Note on the Two Force Equations for a Floating Platform", Journal of Hydronautics, Vol. 9, No. 4, October, pp. 170-172.

24. Chung, J.S., 1976, "Motion of a Floating Structure in Water of Uniform Depth", Journal of Hydronautics, Vol. 10, No. 3, July, pp. 65-73.

25. Chung, J.S., 1977, "Forces on Submerged Cyclinders, Oscillating Near or Free Surface", Journal of Hydronautics, Vol. 11, No. 3, July, pp. 100-106.

26. Chung, J.S., 1985, Personal Communication.

27. Cole, D.M., 1979, "Preparation of Polycrystalline Ice Specimens for Laboratory Experiments", Cold Regions Science and Technology, Vol. 1, No. 2, pp. 153-159.

28. Corona, E.N. and Yashima, N., 1983, "Development of a Novel Ice-Resistant Semi-Submersible Drilling Unit", Proceedings of Offshore Technology Conference, Houston, Texas, Paper No. OTC 4602.

29. Croteau, P., Rojansky, M., and Gerwick, M., 1984, "Summer Ice Floe Impacts against Caisson-Type Exploratory and Production Platforms", Presented at the Third International Symposium on Offshore Mechanics and Arctic Engineering, New Orleans, Louisiana, U.S.A., February 12-16, pp. 228-237.

30. Curtis, D.D., Cammaert, A.B., Wong, T.T. and Bobby, W., 1984, "Numerical Analysis of Impact of Small Icebergs on Semi-Submersibles", Proceedings of Cold Regions Engineering Speciality Conference, April 4-6, Montreal, Quebec, pp. 415-430.

31. Dao, B.V. and Baily, D.C., 1982, "Redundancy Analysis of Semi-Submersible Vessels Operating in the North Sea", Proceedings of Offshore Mechanics and Arctic Engineering Symposium, March 7-10, New Orleans, LA, pp. 23-31.

32. Davies, I.L. and Mavrides, A., 1981, "Assessment of the Damage Arising from Collision between Ships and Offshore Structures", Proceedings of Second International Symposium on Integrity of Offshore Structures, University of Glasgow, Scotland, July 1-3, pp. 363-380.

33. Doyle, R. and Arockiasamy, M., 1984, "Bergy-Bit Motion under Wind, Wave and Current Excitation", paper presented at the 41st Eastern Snow Conference, 7-8 June, Maryland, U.S.A.

34. Diemand, D., 1984, "Temperatures of Near Shore Icebergs in St. John's Area - 1983", C-CORE Publication No.84-14, November, 55 p.

35. El-Tahan, H., 1979, "IRWAF - A Computer Program for Irregular Wave Forces on Cylindrical Elements", Internal Report, Faculty of Engineering, Memorial University of Newfoundland, 61 p.

36. El-Tahan, M., El-Tahan, H. and Venkatesh, S., 1983, "Forecast of Iceberg Ensemble Drift", Offshore Technology Conference, Houston, Texas, May 2-5, Paper No. OTC 4460, Vol. I, pp. 151-158.

37. El-Tahan, H., Arockiasamy, M. and Swamidas, A.S.J., 1985, "Motion and Structural Response of a Hydro-Elastic Semi-Submersible Model to Waves and Ice Impacts", Proceedings of Fourth International Symposium on Offshore Mechanics and Arctic Engineering, Dallas, Texas, February 17-21, 9 pp.

38. Fenco, German and Milne, 1971, "Iceberg Impact on Drillship", Project sponsored by Eastcoast Petroleum Operations Association, August, 40 pp.

39. Fenco, "Effects of Ice Floe Impact on Semi-Submersible Drilling Vessels", Project Report submitted to BPOG Operations Ltd., Calgary, 38 pp.

40. Fenco, 1975, "Spring Field Ice Survey Offshore Labrador", Report prepared for Eastcan Exploration Limited, July.

41. Fenco, 1976, "Winter Field Ice Survey Offshore Labrador", Report prepared for Eastcan Exploration Limited, December.

42. Forristal, G.Z., Kreider, J.R. and Reece, A.M., 1979, "Semi-Submersible Rig Motion Studies Offshore Alaska and Southern California", Proceedings of the Offshore Technology Conference, Houston, Texas, April 30-May 3, Paper No. OTC 3557.

43. Foster, S., 1985, "Constructing a Hydroelastic Model of a Semi-Submersible Platform from the Model Builder's Standpoint", presented at SEMINAR '85, the American Engineering Model Society, Boston, Massachusetts, May 13 - 16.

44. Frankenstein, G.E., 1959, "Strength Data on Lake Ice", CRREL Technical Report 59, December.

45. Furness, O. and Amdahl, J., 1980, "Computer Simulation Study of Offshore Collisions and Analysis of Ship-Platform Impacts", Norwegian Maritime Research, No. 1, pp. 2-12.

46. Gammon, P., Gagnon, R., Bobby, W. and Russell, 1983, "Physical and Mechanical Properties of Icebergs", Proc. 15th Annual Offshore Technology Conference, Houston, Texas, May 2-5.

47. Garrison, C.J., 1984, "Wave-Structural Interaction", Speciality Conference on Computer Methods in Offshore Engineering, Technical University of Nova Scotia, Halifax, May 23-25, pp. 1-73.

48. Glen, I.F., and Comfort, G., 1983, "Ice Impact Pressure and Loads, Investigation by Laboratory Experiments and Ship Trials", Proc. of POAC 1983, Helsinki, April.

49. Halvorsen, L.K., 1959, "Determination of the Modulus of Elasticity of Artificial Snow Ice in Flexure", CRREL Research Report 31, February.

50. Hammett, D.S., 1981, "Semi-Submersible Operating Experience in Rough Seas and Occasional Icebergs", Proceedings of the Symposium on 'Production and Transportation Systems for the Hibernia Discovery' Petroleum Directorate, St. John's, Newfoundland, February 16-18, pp. 70-90.

51. Hammett, D.S., 1983, "Future Semi-Submersible Drilling Units", Proceedings of International Symposium on 'Semi-Sumbersibles: The New Generation', RINA Offshore Engineering Group, London, U.K., March 17-18, 19 pp.

52. Hawkes, I. and Mellor, M., 1972, "Deformation and Fracture of Ice Under Uniaxial Stress", Journal of Glaciology, Vol. 11, No. 61, pp 103-131.

53. Haynes, F.D., 1978, "Effect of Temperature on the Strength of Snow-Ice", CRREL Report 78-27, December.

54. Hogben, N., Miller, B.L., Searle, J.W., and Ward, G., 1977, "Estimation of Fluid Loading on Offshore Structures", National Maritime Institute Report No. NMI R11, Feltham, Middleaex, U.K., April, 57 pp.

55. Hooft, J.P., 1971, "A Mathematical Method of Determining Hydrodynamically Induced Forces on a Semi-Submersible", Proceedings of Annual Meeting of the Society of Naval Architects and Marine Engineering, New York, November, 36 pp.

56. Hsiung, C.C., 1984, "Computing Response (Motion and Wave Loads) for Floating Marine Structures in Waves - A-State-Of-The-Art Review", Speciality Conference on Computer Methods in Offshore Engineering, Technical University of Nova Scotia, Halifax, May 23-25, pp. 101-139.

57. Huang, X., Hoff, J.R., and Naers, A., 1982, "Loads and Motions Measured on a Semi-Submersible having a Large Permanent List Angle", Norwegian Maritime Research, No. 2, pp. 24-33.

58. Huang, X., and Naess, A., 1983, "Dynamic Response of a Heavily Listed Semi-Submersible Platform", Second International Symposium on Ocean Engineering and Ship Handling, Gothenburg, Sweden, pp. 375-392.

59. IAHR, 1980, "Standardization of Testing Methods for Ice Properties", Working Group on Ice Problems, Journal of Hydraulic Research, Vol. 18, No. 2, pp. 153-165.

60. Incecik, A., 1981, "Structural Response of Floating Offshore Structures", Department of Naval Architecture and Ocean Engineering, University of Glasgow, Report No. NAOE-HL-81-03, October, 118 pp.

61. Jones, H.E., 1982, "Surveying Offshore Canada Lands for Mineral Resources Development", Department of Energy, Mines and Resources, Third Edition, December, pp 4-8.

62. Kallstrom, G.G., 1983, "Mooring and Dynamic Positioning of a Semi-Submersible - A Comparative Simulation Study", Proceedings of the Second International Symposium on Ocean Engineering and Ship Handling, Gothenburg, Sweden, pp. 417-442.

63. Katayama, M., Unoki, K., Hatakenaka, K., Ujiara, T., 1978, "On Structural Response Analysis of Semi-Submersible Offshore Structures in Waves", Japan Shipbuilding and Marine Engineering, Vol. 12, No. 3, pp. 11-20.

64. Kheisin, D.E., and Likhomanov, V.A., 1975, "An Experimental Determination of The Specific Energy of Mechanical Crushing of Ice by Impact", Problemy Arktiki i Antarktiki, Vol. 41, pp 55 - 61.

65. Kheisin, D.E., Likhomanov, V.A., and Kurdmov, V.A., 1975, "Determination of Specific Crushing Energy and Contact Pressures Due to Impact of Rigid Body on Ice", Works, Vol. 326, pp 210-219.

66. Kim, C.H., 1973, "Motions of a Semi-Submersible Drilling Platform in Head Seas", Journal of Marine Technology, Vol. 10, No. 12, April.

67. Kim, C.H., 1976, "Motion and Loads of a Catamaran Ship of Arbitrary Shape in a Seaway", Journal of Hydraulics, Vol. 10, No. 1, January, pp. 8-17.

68. Kim, C.H., 1980, "On the Motions of a Multi-Member Supported Semi-Submersible in Seas", Proceedings IMT 80, Paper No. IMT 121.

69. Kistler, E.L. and Nash, J.M., 1975, "Influence of Draft on Wave Steepness Effect in the Dynamics of Semi-Submersibles", Proceedings of Offshore Technology Conference, Houston, Texas, Paper No. OTC 2367.

70. Kitami, E. et al, 1984, "Iceberg Collision with Semi-Submersible Drilling Unit", Proceedings of IAHR Ice Symposium, Hamburg, W.G., August 27-31, pp. 45-53.

71. Klosner, J.M. and Chen, Y.K., 1980, "Boundary Integral Methods Applied to Hydro Dynamic Force Calculations", American Society of Mechanical Engineers, Applied Mechanics Symposium Series, Vol. 37, pp. 9-21.

72. Kobus, L.C.S., Meyers, H.M. and Haines, S.W., 1977, "Super-Sized Semi-Submersible Performance in the North Sea", Proceedings of Offshore Technology Conference, Houston, Texas, May 2-5, Paper No. OTC 2973.

73. Korkut, M.D. and Hebert, E.J., 1970, "Some Notes on Static Anchor Chain Curve", Proceedings of Offshore Technology Conference, Houston, Texas, April 22-24, Paper No. OTC 1160.

74. Kovacs, A., Weeks, W.F., and Michitti, F., 1969, "Variations of Some Mechanical Properties of Polar Snow. Camp Century, Greenland", CRREL Research Report 276, December.

75. Kovacs, A., 1978, "Axial Double Point-Load Tests on Snow and Ice", CRREL Report 78-1, March.

76. Langfeldt, J.N., Verlo, P.O. and Olsen, 1975, "Compare Performance of Aker H-3, Full Scale Field Measurements to Theoretical Calculations", Presented at the BSSM/RINA Joint Conference, Heriot-Watt University, Edinburgh, September 8-11, 53 pp.

77. Larsen, C.M. and Engseth, A.G., 1978, "Ship Collision and Fendering of Offshore Concrete Structures", Proceedings of European Offshore Petroleum Conference and Exhibition, Paper No. EUR 17, Vol. 1, pp. 145-154.

78. Legenko, A.P., Chuguj, I.V., and Yeremin, N.N., 1974, "Results of Temperature Measurements on the Drifting Island North Pole 19", Proc. of IEEE Int. Conf. on Eng. in the Ocean Environment, Ocean '74, Halifax, Nova Scotia, Vol. 1, pp. 137-139.

79. Lever, J.H., Reimer, E. and Diemand, D., 1984, "A Model Study of the Wave Induced Motion of Small Icebergs and Bergy-Bits", Proceedings of the Third International Symposium on Offshore Mechanics and Arctic Engineering, February 12-16, New Orleans, Louisiana, U.S.A., pp. 282-290.

80. Likhomanov, V.A., and Kheisin, D.E., 1971, "Experimental Investigation of Solid Body Impact on Ice", Problemy Arktiki i Antarktiki, Vol. 38, pp 105-111.

81. Lipsett, A.W., and Gerard, R., 1980, "Field Measurements of Ice Forces on Bridge Piers", Alberta Research Council, Edmonton, Report SWE 80-3, December.

82. Lundgren, J. and Berg, A., 1982, "Wave Induced Motion on a Four-Column Semi-Submersible Obtained from Model Tests", Proceedings of Offshore Technology Conference, Houston, Texas, Paper No. OTC 4230.

83. Maeno, N., Narita, H., Araoka, K., 1978, "Measurements of Air Permeability and Elastic Modulus of Snow and Firn Drilled at Mizuho Station, East Antarctica", Memoirs of National Institute of Polar Research, Tokyo, Special Issue No. 10, pp 88-94, December.

84. Mathisen, J. and Carlsen, C.A., 1980, "A Comparison of Calculation Methods for Wave Loads on Twin Pontoon Semi-Submersibles", International Symposium on Ocean Engineering - Ship Handling, September 17-18, Gothenburg, Sweden, pp. 7:1 - 7:11.

85. Mathisen, J., Borresen, R. and Lindberg K., 1982, "Improved Strip Theory for Wave-Indu Loads on Twin-Hull Semi-Submersible", First national Offshore Mechanics and Arctic neering Symposium, March 7-10, pp. 1-9.

86. Mavrikios, Y. and Oliveira, J.G., 1983, "Design Against Collision for Offshore Structures", Report No. MITSF 83-7, Sea Grant College Program, M.I.T., Cambridge, Massachusetts, April, pp. 164.

87. Mellor, M., and Cole, D.M., 1983, "Stress/Strain/Time Relations for Ice Under Uniaxial Compression", Cold Regions Science and Technology, Vol. 6, No. 2, pp 207-230.

88. Mitsui Engineering, 1979, "A Design and Analysis Program System for Offshore Structures", Journal of Japan Ship Building and Marine Engineering, Vol. 13, No. 1, pp. 5-33.

89. Muggeridge, D.B. and Murray, J.J., 1981, "Calibration of a 58 m Wave Flume", Canadian J. of Civil Engineering, Vol. 8, pp. 449-455.

90. Murray, J.J., Guy, G.B., and Muggeridge, D.B., 1983, "Response of Modelled Ice Masses to Regular Waves and Regular Wave Groups", Proc. of OCEAN '83, pp. 1048-1052.

91. Naess, A. and Hoff, J.R., 1984, "Time Simulation of the Dynamic Response of Heavily Listed Semi-Submersible Platforms in Waves", Norwegian Maritime Research, No. 1, pp. 2-14.

92. Nakaya, U., 1959, "Visco-elastic Properties of Snow and Ice in the Greenland Cap", CRREL Research Report 40, May.

93. Natvig, B.J. and Pendered, J.W., 1977, "Non-linear Response of Floating Structures to Wave Excitation", Proceedings Offshore Technology Conference, Houston, Texas, May 2-5, pp. 525-536.

94. Natvig, B.J. and Pendered, J.W., 1980, "Motion Reponse of Floating Structures to Regular Waves", Journal of Applied Ocean Research, Vol. 2, No. 3, pp. 90-97.

95. Noble, P.G. and Singh, D., 1982, "Interaction of Ice Floes with the Columns of a Semi-submersible", Proc. of the 14th Offshore Technology Conference, Houston, Texas, May 3-6, Paper No. OTC 4424.

96. Nojiri, N., 1981, "A Study of Hydrodynamic Pressures and Wave Loads on Three-Dimensional Floating Bodies", IHI Engineering Review, Vol. 14, No. 2, pp. 6-20.

97. Nojiri, N. and Inoue, Y., 1981, "Dynamic Behaviour of Semi-Submersible Platforms in Waves", IHI Engineering Review, Vol. 14, No. 2, pp. 31-42.

98. Nordenstrom, N. Faltinsen, O., Pendersen, B., 1971, "Prediction of Wave-Induced Motions and Loads for Catamaran", Proceedings of Offshore Technology Conference, Houston, Texas, Paper No. OTC 1418.

99. Ocean Industry, 1982, "SAFE DP 120-First of Three New Rig Concepts", May 1982, pp. 30-32.

100. Ocean Industry, 1983a, "Seven New Semis for SEDCO", February, pp 99-100.

101. Ocean Industry, 1983b, "New Generation Semi Design for 10,000 Ft. Waters", December, pp. 86-93.

102. Oliveira, J.G., 1981, "The Behaviour of Steel Offshore Structures and Accidental Collisions", Proceedings of Thirteenth Annual Offshore Technology Conference, Houston, Texas, May [illegible], Paper No. OTC 4136.

103. Olsen, O.A. and Verlo, P.O., 1976, "Comparison of Full-Scale Performance Measurements of Aker H-3 with Theoretical Predictions", Proceedings OTC, Houston, Texas, May 3-6, Paper No. OTC 2508.

104. Opstal, G.H.C., Hans, D., Salomons, J.W., and Van dervlies, J.A., 1974, "MOSAS: A Motion and Strength Analysis System for Semi-Submersible Units and Floating Structures", Proceedings of Offshore Technology Conference, Houston, Texas, May 6-8, Paper No. OTC 2105.

105. Paschke, P., Offshore Operations Supervisor, Fenco Newfoundland Limited, 1983, Personal Communication.

106. Pattersen, E. and Johnsen, K., 1981, "New Non-Linear Methods for Estimation of Collision Resistance of Mobile Offshore Units", Proc. of Offshore Technology Conference, Houston, Texas, May 4-7, Paper No. OTC 4135.

107. Pauling, J.R., Hong, Y.S., Chen, H.H. and Stianseh, S.G., 1977, "Analysis of Semi-Submersible Catara-ran-Type Platforms", Proceedings of the Offshore Technology Conference, Houston, Texas, May 2-5, Paper No. OTC 2975.

108. Pauling, J.R. Hong, Y.S., Stiansen, S.G., Chen, H.H., 1978, "Structural Loads on Twin-Hull Semi-Submersible Platforms", Proceedings of Offshore Technology Conference, Houston, Texas, May 8-11, Paper No. OTC 3246

109. Pawlowski, J.S., 1983, "A Short Note on Elastic Physical Models of Ships", National Research Council of Canada, AVMRI Report No. MTB-143, October, 27 pp.

110. Petersen, M.J. and Pedersen, P.T., 1981, "Collision Between Ships and Offshore Platforms", Proc. of Offshore Technology Conference, Houston, Texas, May 4-7, Paper No. OTC 4134.

111. Pincemin, M., Planeix, J.M., Huard, G., Dupuis, G. and Duval, G., 1974, "An Integrated Program for the Dynamic Structural Calculation of Mobile Offshore Units", Proceedings of Offshore Technology Conference, Houston, Texas, May 6-8, Paper No. OTC 2052.

112. Price, W.G. and Wu, Y., 1983, "Hydrodynamic Coefficients and Responses of Semi-Submersibles in Waves", Proceedings of the Second International Symposium on Ocean Engineering and Ship Handling, Swedish Maritime Research Centre, Gothenburg, pp. 393-415.

113. Popov, E.P., 1969, "Introduction to mechanics of Solids", Prentice-Hall, Inc., Englewood Cliffs, New Jersey, pp 169-171.

114. Ramseier, R.O., 1966, "Some Physical and Mechanical Properties of Polar Snow", CRREL Research Report 116, February.

115. Reddy, D.V., Muggeridge, D.B., Swamidas, A.S.J., Arockiasamy, M., Murray, J.J., El-Tahan, H. and Hsiung, C.C., 1982, "Dynamic Response of Moored Semi-Submersible to Bergy Bit Impact, Irregular Wave, Wind and Current Forces", Proceedings of the Offshore Technology Conference, Houston, Texas, May 3-6, Paper No. OTC 4425.

116. Rey-Grange, A.C., 1971, "Design and Actual Behaviour of Pentagone 81 Semi-Submersible Drilling Platform", Proceedings of the Offshore Technology

Conference, Houston, Texas, May, Paper No. OTC 1224.

117. Rodnight, T.V., "Development of the Modern Semi-Submersible Drilling unit", Proceedings of International Symposium on 'Semi-Submersible: The New Generations", RINA Offshore Engineering Groups, London, U.K., March 17-18, 15 pp.

118. Rothwell, A., 1979, "A Graphical Procedure for the Stiffness of a Catenary Mooring", Journal of Applied Ocean Research, Vol. 1, No. 4, pp. 217-219.

119. Salvesen, N., Tuck, E.O. and Faltinsen, O., 1970, "Ship Motions and Sea Loads", Trans. SNAME, Vol. 78, pp. 250-287.

120. Satake, M. and Katayama, M., 1977, "On Structural Response Analysis of Semi-Submersible Offshore Structures in Waves", Safety of Structures Under Dynamic Loading, V.2, International Conference on Finite Element in Non-linear Solid of Structure Mechanics at Geilo, Norway, August 29-September 1.

121. Seadyn, 1981, "Ocean Structure Design and Analysis Language", Earl and Wright Consulting Engineers.

122. SEDPEX Inc., 1983, "SEDCO 710 - Column Stablized Dynamically Positioned Drilling Unit", Marine Operations Manual, SEDPEX Inc., Calgary, Alberta, November.

123. Sharp, J.J., 1981, "Hydraulic Modelling", Chapter 6: Models of Hydraulic Structures, Butterworths, pp. 86-91.

124. Shoji, H. 1978, "Stress-Strain Tests of Ice Core Drilled at Mizuho Station, East Antarctia", Memoirs of National Institute of Polar Research, Tokoyo, Special Issue No. 10, December, pp. 95-101.

125. Sims, C.N. Langkamp, G., Alberts, J.C., Zingraf, H.L., and Hammett, D.S., 1976, "Sedco-709 - First Dynamically Stationed Semi-Submersible, Parts I-VI; Ocean Industdry, December 1976 to June 1977, 18 pp.

126. Sluijs, M.F. Van and Minkenberg, 1977, "A Review of Studies of Ocean Platform Motions", Journal of Ocean Engineering, Vol. 4, pp. 75-90.

127. Smith, N., 1969, "Determining the Dynamic Properties of Snow and Ice by Forced Vibration", CRREL Technical Report 216, June.

128. Soreide, T.H. and Amdahl, J., 1983, "Deformation Characteristics of Tubular Members with Reference to Impact Loads from Collision and dropped Objects", Norwegian Maritime Research, Vol. 10, No. 2, pp. 3-21.

129. Sorensen, K.A., 1976, "Behaviour of Reinforced and Prestressed Concrete Tubes under Static and Impact Loading", Proceedings of the First International Conference on Behaviour of Offshore Structures, BOSS '76, Norwegian Institute of Technology, pp. 798-813.

130. Standing, R.G., 1981, "Wave Loading on Offshore Structures: A Review", National Maritimes Institue Report No. NMI R102, Feltham, Middleses, U.K., February, 102 pp.

131. Suhara, T., Tasai, F. and Mitsuyasu, H., 1974, "A Study of Motion and Strength of Floating Marine Structures in Wave", Proceedings of Offshore Technology Conference, Houston, Texas, Paper No. OTC 2068.

132. Sun, F.Z., 1980, "Analysis of Motions of Semi-Submersible in Sea Waves", Proceedings of Offshore Technology Conference, Houston, Texas, May 5-8, Paper No. OTC 3899.

133. Sun, F.Z., 1982, "Analysis of Motions of a Semi-Submersible in Sea Waves", Journal of Energy Resources Technology, Transaction of the ASME, March, Vol. 104/29, 10 pp.

134. Swamidas, A.S.J., Arockiasamy, M. and Reddy, D.V., 1983, "Bergy-Bit Impact Forces on a Moored Semi-Submersible", presented at the VIIth International Conference on Port and Ocean Engineering Under Arctic Conditions, Helsinki, Finland, April 5-10, 25 pp.

135. Swamidas, A.S.J., Arockiasamy, M.A., Reddy, D.V. and El-Tahan, H., 1984, "Dynamic Response of Moored Semi-Submersibles to Ice-Floes and Bergy-Bits", Preprint 84-021, Spring Meeting, ASCI, Georgia, May, 18 pp.

136. Swamidas, A.S.J. and Arockiasamy, M., 1984, "Iceberg Impact Forces on Gravity Platforms", Third International Specialty Conference on Cold Regions Engineering, April 4-6, Edmonton, Alberta, 32 pp.

137. Tasai, F., Arakawas, H. and Kurihara, M., 1970, "A Study on the Motions of a Semi-Submersible Catamaran Hull in Regular Waves", Reports of Research Institute for Applied Mechanics, Kyushu University, Japan, Vol. XVII, No. 60, pp. 9-32.

138. Taylor, D.M., 1974, "Aker H-3 - The $750 Million Rig", Ocean Industry, April, pp 169-175.

139. Taylor, R.E., 1974, "Structural Dynamics of Fixed and Floating Platforms in Waves", Proceedings of International Symposium on the Dynamics of Marine Vehicles and Structures in Waves, London, Paper 24, pp. 234-247.

140. Timco, G.W., and Martin, R.A., 1979, "Impact Strength of Ottawa River Ice", National Research of Canada Report No. LTR-LT-97, 20 p.

141. Tse, C.C., 1984, "Computation of the Motion and Drift Forces for a Floating Body", M. Eng. Thesis, Memorial University of Newfoundland, April, 90 pp.

142. Vugts, J.H., 1968, "The Hdyrodynamic Coefficients for Swaying, Heaving, and Rolling Cyclinders in a Free Surface", Report No.1125, Netherlands Ship Research Center, TNO, Delft, May, 29 pp.

143. Vugts, J.H., 1971, "The Role of Model Tests and Their Correlation with Full Scale Observations", Symposium of Offshore Hydrodynamics, Wageningen, The Netherlands, August 25-26, pp. II.1-II.30.

144. Watts, J.S. and Faulkner, R.E., 1968, "A Performance Review of the Sedco 135-F Semi-Submersible Drilling Vessel", 19th Annual Technical Meeting of the Petroleum Society of CIM, Calgary.

145. Weeks, W.F. and Assur, A., 1969, "Fracture of Lake and Sea Ice", CRREL Research Report 269, December.

146. Weir, F.V., 1981, "The Comparative Environmental Risks Associated with Fixed Platforms and Floating Platforms and With Tankers and Pipelines", Proceedings of the Symposium on 'Production and Transportation Systems for the Hibernia Discovery', Petroleum Directorate, St. John's, Newfoundland, February 16-18, pp. 337-355.

147. Yoneya, T., 1984, "Experimental Study on Wave-Induced Structural Responses of Semi-Submersibles", Proceedings of the Third International Offshore Mechanics and Arctic Engineering Symposium, New Orleans, LA, February 12-17, pp. 253-259.

148. Yoshida, K., Ishikawa, K., and Iida, K., 1974, "Periodic Response Analysis of Floating Framed Structures", Journal of The Society of Naval Architects of Japan, Vol. 136, pp. 105-113.

149. Yoshida, K. and Ishikawa, K., 1975, "Periodic Responses Analysis of Floating Framed Structures (continued)", Journal of The Society of Naval Architects of Japan, Vol. 138, pp. 56-67.

150. Yoshida, K. and Ishikawa, K., 1980, "Structural Response Characteristics of Semi-Submersibles for Wave Loading", Journal of the Faculty of Engineering, The University of Tokyo (B), Vol. XXXV, No. 3, pp. 407-432.

151. Yoshida, K., Ozaki, M. and Oka, N., 1984, "Structural Response Analysis of Tension Leg Platforms", Proceedings of the Third International Offshore Mechanics and Arctic Engineering Symposium, New Orleans, LA, February 12-17, pp. 12-19.

152. Yoshida, K., Professor, Dept. of Naval Architecture, University of Tokyo, 1985, Personal Communication.

Table 1.1 Hibernia Development Environmental Criteria (Weir, 1981)

Parameter	Petroleum Directorate	Mobil	
	SI Units	SI Units	Traditional Units
Water Temperature	1°C	1.1 - 11.6°C	34 - 53°F
Air Temperature	(-)30 - (+)30°C	(-)26 - (+)31°C	(-)15 - (+)88°F
Wave Height	25 m	28 - 35 m	92 - 115 feet
Current	2 m/s	1 - 2 m/s	2 - 4 knots
Sea Ice			
- Rafted	4 m	2 - 3 m	7 - 10 feet
- Compressive Strength	1 - 12 MPa	1.6 - 10.3 MPa	225 - 1500 PSI
Icebergs			
- Mass	$5x10^6$ - $15x10^6$ Tonne	$5x10^6$ - $12x10^6$ Tonne	$5x10^6$ - $12x10^6$ L. Ton
- Scour Depth	4 - 8 m	9 m	30 feet
- Speed	1 m/s	0.4 - 1 m/s	0.8 - 2 knots
- No. of Bergs Crossing 47°N.	1000 - 1500	1200	1200

Table 3.1 Summary of Uniaxial Compressive Strength Test Results at a Temperature of -5°C.

Ice Type	Mean Strain Rate (sec^{-1})	Mean Strength (MPa)	Mean Tangent Modulus (GPa)	Mean Time to Failure (sec)	Mean Strain at Failure (%)
Iceberg Ice	0.82×10^{-3}	7.43	5.04	2.38	0.19
	0.59×10^{-2}	6.6	5.97	0.20	0.12
	0.58×10^{-1}	6.97	6.7	0.02	0.11
Snow Ice	0.88×10^{-4}	3.88	3.25	14.85	0.17
	0.87×10^{-3}	6.98	6.16	2.39	0.23
	0.78×10^{-2}	5.63	6.88	0.17	0.13
	0.39×10^{-1}	6.73	7.21	0.04	0.17

Table 3.2 Summary of Indentation Strength Test Results at a Temperature of -5°C:

Ice Type	Indentation Speed (mm/sec)	Indentor Shape	Confinement Condition	Mean Strength* (MPa)	Resistance to Penetration (kN/mm) Initial	Resistance to Penetration (kN/mm) Mean	Time to Failure (sec)	Mean Strain at Failure %	Mean Strain Rate (sec^{-1})
Iceberg Ice	0.041	Circular	Unc.	16.98	292	107	3.25	0.13	0.37×10^{-3}
	0.049	Cylindrical	Unc.	23.46	322	128	3.45	0.18	0.45×10^{-3}
	0.073	"	Conf.	28.43	127	53	7.96	0.59	0.66×10^{-3}
	0.481	"	Unc.	30.47	343	211	0.33	0.14	0.44×10^{-2}
	0.515	"	Conf.	33.97	137	69	0.64	0.34	0.47×10^{-2}
	10.560	"	Unc.	23.72	251	199	0.011	0.12	0.96×10^{-1}
	35.150	"	Conf.	27.41	165	110	0.008	0.27	3.20×10^{-1}
Snow Ice	0.051	Cylindrical	Unc.	21.28	337	113	3.56	0.18	0.51×10^{-3}
	0.059	Circular	Unc.	16.39	173	102	4.97	0.29	0.59×10^{-3}
	0.078	"	Conf.	20.52	115	46	9.22	0.71	0.77×10^{-3}
	0.491	"	Unc.	17.44	216	146	0.43	0.21	0.49×10^{-2}
	11.540	"	Unc.	17.98	192	138	0.019	0.22	1.10×10^{-1}

* Total force divided by the contact area.

Table 3.3 Summary of Impact Test Results

Sample No.	Type of Ice	Maximum Pressure* (MPa)	Failure Indent.** (mm)	Impact Period (sec)	Indentation Depth*** (mm)
G1	Iceberg Ice	18.17	0.30	0.016	8.77
G2		16.44	0.31	0.015	9.89
G3		21.63	0.32	0.02	6.6
G4		12.46	0.34	0.024	10.60
G5		13.84	0.35	0.017	10.85
G6		20.76	0.36	0.022	11.65
G7		18.17	0.32	0.021	9.7
Mean		17.35	0.329	0.019	9.73
S1	Snow Ice	20.07	0.81	0.021	9.1
S2		16.44	0.79	0.013	6.65
S3		17.30	0.75	0.013	6.6
S4		23.36	0.77	0.013	6.76
S5		24.22	0.79	0.02	5.2
S6		21.63	0.73	0.013	6.96
S7		20.76	0.72	0.014	6.75
Mean		20.54	0.76	0.015	6.86
SU1	Unconfined Snow Ice	17.30	0.52	0.016	10.3
SU2		16.44	0.56	0.021	12
F1	S2 Fresh Water Ice	20.76	0.63	0.018	11.1
F2		20.76	0..59	0.016	8.2

* Measured by the force transducer
** Indentation depth at initial failure.
***Measured after impact.

Table 3.4 Comparison of Uniaxial Compressive Strength of Isotropic Ice

Ice Type	Compressive Strength (MPa)	Temperature (kN)	Strain Rate (10^{-3}/sec)	Density (Mg/m^3)	Grain Size (mm)	Tangent Modulus (GPa)	Reference
Articifical Snow Ice	9.1	-7	2.1	0.911	0.6	13.2	Haynes (1978)
	10.1	-5	1.0	0.917	1.2	3.0	Mellor and Cole (1983)
	7.0	-5	0.9	0.861	0.85	6.2	Present Study
Iceberg Ice *	7.4	-5	0.9	0.904	7.4	5.0	Present Study
	5.53	-4.5	1.1	N/A	15	6.2	Gammon et al (1984)
Greenland Glaciers**	4.2-6.9	-5	N/A*	0.905-0.915	3-7	1.5-2.3	Butkovich (1959)

* Stress rate 0.05 MPa/sec.

** Five different types of glacier ice.

Table 4.1 Total Mass of the Semi-Submersible Components at Survival Draft

Component	Mass (tonne)	
	Fixed	Variable
Two Hulls	2,750	5,670
Four Main Columns	1,850	600
Four Secondary Columns	1,575	-
Bracing System	1,270	-
Deck	4,150	3,000

TABLE 4.2 Main Dimensions of the Prototype and Its Static and Dynamic Properties as Measured from the Model Tests

Dimensions		
Overall length		90 m
Length between column centers		69 m
Overall breadth		75 m
Breadth between column centers		60 m
Pontoon		
Height		6.5 m
Width		15 m
Corner radius		1 m
Column diameter		
4 corners		9 m
4 inners		5.5 m
Draft		
Survival (S.D.)		18.5 m
Operating (O.D.)		23.0 m
Displacement	at S.D. 20,800 t	at O.D. 22,000 t
C. G. height from keel	17.4	16.8 m
Metacentric height (moored)		
GM_L (measured)	3.3	3.5 m
GM_T (measured)	2.7	3.1 m
Radius of gyration		
Roll (measured)	31.2	31.2 m
Pitch (measured)	29.9	30.2 m
Yaw (computed)	36.9	37.5 m
Natural Periods (measured)	Free	Moored
Heave	24.5	23.6 sec.
Roll	71.0	59.1 sec.
Pitch	50.7	44.8 sec.
Surge		89.6 sec.
Sway		117.8 sec.
Yaw		88.6 sec.

Table 4.3 Basic Scaling Parameters According to Froude Modelling

Length	λ
Area	λ^2
Volume	λ^3
Density	1
Pressure	λ
Mass	λ^3
Force	λ^3
Moment	λ^4
Time	$\sqrt{\lambda}$
Frequency	$1/\sqrt{\lambda}$
Velocity	$\sqrt{\lambda}$
Acceleration	1
Linear Stiffness	λ^2
Rotational Stiffness	λ^4

Table 4.4 Scale Factors for the Hydroelastic Model

Parameter	Scale Factor (Prototype/Model)	Actual Scale-up Value
Length, L	$C_L = 1/\lambda$	75
Fluid density, ρ	C_ρ	1.025
Displacement	$C_\rho C_L$	76.9
Mass, M	$C_\rho C_L^3$	432,422
Force, F	$C_\rho C_L^3$	432,422
Time, t	$\sqrt{C_L}$	8.66
Frequency of Motion	$1/\sqrt{C_L}$	0.115
Velocity, u	$\sqrt{C_L}$	8.66
Acceleration	1	1
Cable Stiffness	$C_\rho C_L^2$	5,766
Young's Modulus, E	C_E	112
Thickness, h	C_h	30
Strain, ε	$(C_\rho C_L^2)/(C_h C_E)$	1.75
Stress, σ	$(C_\rho C_L^2)/C_h$	192
Sectional Forces	$C_\sigma C_L^2$	1,080,000
Bending Moments	$C_\sigma C_L^3$	81,000,000
Structural Deformation	$C_\varepsilon C_L$	131
Frequency of Structural Vibrations	$1/\sqrt{C_L C_\varepsilon}$	0.088

TABLE 4.5 Properties of Plastic Sheets and Tubes used in the Model

	High-Impact Polystyrene Sheets	Cellulose Acetate Butyrate Tubes
a) Measured		
Specific Gravity	0.997	1.096
Tensile Strength (MPa)	23.55	37.7
Elongation (%)	20 - 50	50
Modulus of Elasticity (MPa)	1890	1834
b) Supplied by Manufacturer		
Compressive Strength (MPa)	28 - 63	14.7 - 154
Flexural Yield Strength (MPa)	35 - 84	12.6 - 65.1
Thermal Expansion (10^{-5} cm/cm/°C	3.4 - 21	11 - 17
Resistance to Heat (°C continuous)	60 - 80	60 - 105
Water Absorption, 24 hr, 1/8 in. Thick (%)	0.05 - 0.6	0.9 - 2.2
Effect of Sunlight	Some strength lost, yellow slightly	Slight
Effect of Weak Acids	None	Slight
Effect of Weak Alkalies	None	Slight
Effect of Organic Solvents	Soluble in aromatic and chlorinated hydrocarbons	Soluble in ketones and esters

Table 6.1 Measured Impact Force on the Semi-Submersible

Impacted Column	Bergy Bit Mass (tonne)	Impact Direction	Mooring Stiffness	Maximum Impact Forces/B.B. Weight		
				Impact Velocity (m/sec)		
				1.0	2.0	4.0
Main Column	1,000	Surge	Original	2.2	3.9	7.6
			Very Slack	2.0	3.5	7.2
		Sway	Original	2.5	4.8	10.5
	2,000	Surge	Original	2.05	3.8	7.9
			Very Slack	2.0	3.5	6.8
Secondary Column	1,000	Sway	Original	3.9	7	11.5

Table 6.2 Surge and Yaw Motions After Impact of Corner Column

	Impact Velocity (m/sec)	1,000 Tonne Bergy-Bit			2,000 Tonne Original Mooring
		Original Mooring	Double Mooring Stiffness	Very Slack Mooring	
Surge (m)	1	0.3	0.36	0.5	1.0
	2	0.9			
	3	1.7			
	4	2.3	2.2	3.2	4.1
	5	2.9			
Yaw (°)	1	0.75	0.9	1.8	1.8
	2	1.4			
	3	2.2			
	4	3	3.5	4.8	5.2
	5	3.6			

Table 6.3 Impact Stresses in Main Column and Horizontal Bracings - Head Sea Impact on Main Column

Bergy-Bit Mass (tonne)	Mooring Stiffness	Maximum Impact Stress (MPa)								
		Section MB			Section HBO			Section HBI		
		1m/s	2m/s	4m/s	1m/s	2m/s	4m/s	1m/s	2m/s	4m/s
1,000	Original	38	73.5	168	18	39	70	17.5	31.5	66
	Double	38	70	161	17.5	49	77	14	28	52
2,000	Original	45	112	210	18	38	70	21.5	42	56
	Double	73.5	164	281	21	56	78	17	38	65
	Very Slack	56	157	259	21	45	60	12.5	25	49

Table 6.4 Impact Stresses in Main Column, Diagonal Bracing and Deck Girder — Beam Sea Impact on Main Column

Bergy-Bit Mass (tonne)	Mooring Stiffness	Maximum Impact Stress (MPa)								
		Section MB			Section DBO			Section DG		
		1m/s	2m/s	4m/s	1m/s	2m/s	4m/s	1m/s	2m/s	4m/s
1,000	Original	60	126	190	12	25	50	17.5	33	66
	Double	72	129	186	17.5	28	52	21	30	55
2,000	Original	84	129	240	28	28	72	25	32	87
	Double	122	157	280	17	28	75	21	42	84

Table 6.5 Impact Stresses at Top and Base Sections of the Secondary Column - Original Mooring System

Bergy-Bit Mass (tonne)	Impact Stress (MPa)					
	Section ST			Section SB		
	1m/s	2m/s	4m/s	1m/s	2m/s	4m/s
1,000	52.5	77	91	56	91	154
2,000	54	80	126	60	100	170

Table 6.6 Effect of Local Stiffness on Impact Force and Motion Response of the 2-D.O.F. Model - 2,000 Tonne Bergy-Bit at 1.0 m/s.

All Values are Scaled up to Full-Scale Values

Element Material	Stiffness MN/cm	Stiffness Ratio*	Impact Force (MN)	Force Ratio*	Impact Duration (ms)	Duration Ratio*	Rebound Velocity (m/s)	Maximum Displacement (m)
steel	7,900	1,500	100	2.63	115	0.58	0.64	1.76
oak	40	7.8	77	2.02	132	0.67	0.65	1.75
wax	5.2	1	38	1	198	1	0.68	1.76
white foam	0.06	0.0115	1.9	0.05	4,200	21.2	0.67	1.78
black foam	0.0107	0.002	1.5	0.04	5,100	25.8	0.65	1.80

* Values are given relative to the corresponding values of the wax element.

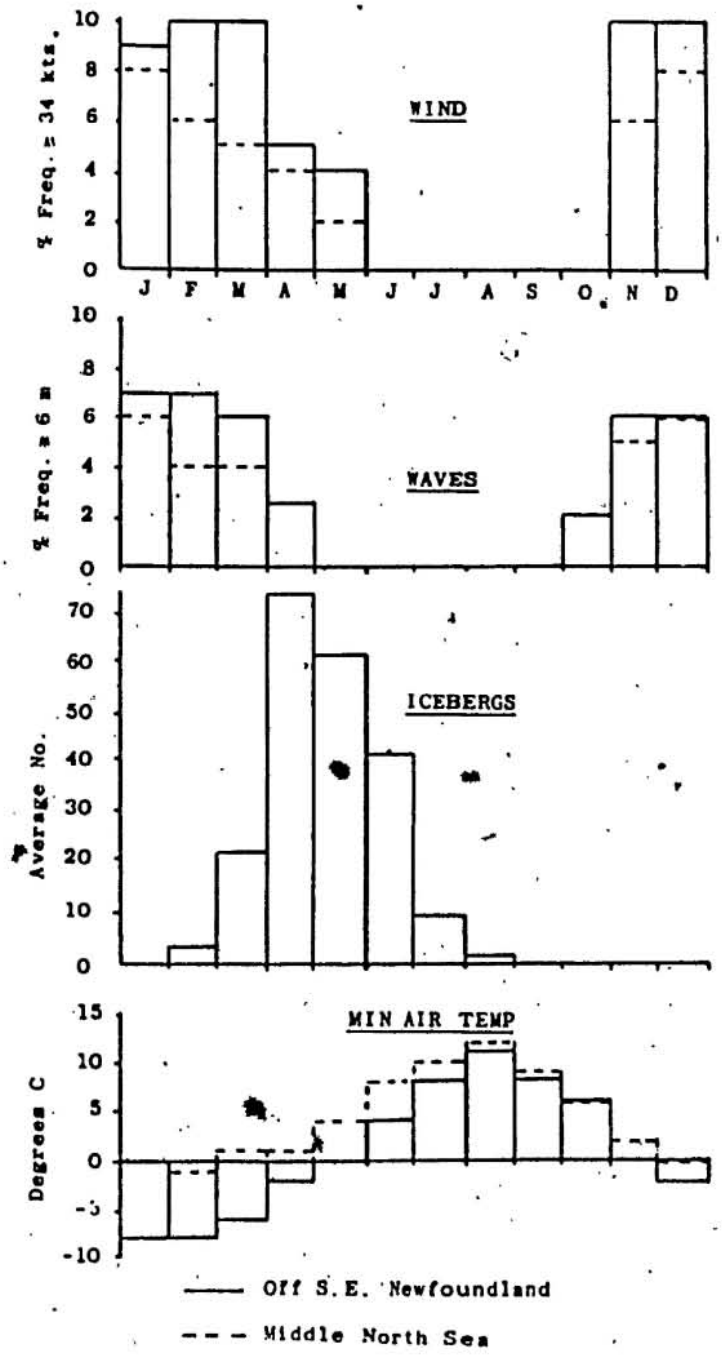

FIG. 1.1 COMPARISON OF THE ENVIRONMENTAL CONDITIONS OF THE GRAND BANKS AND THE NORTH SEA . (Bainbridge, 1981)

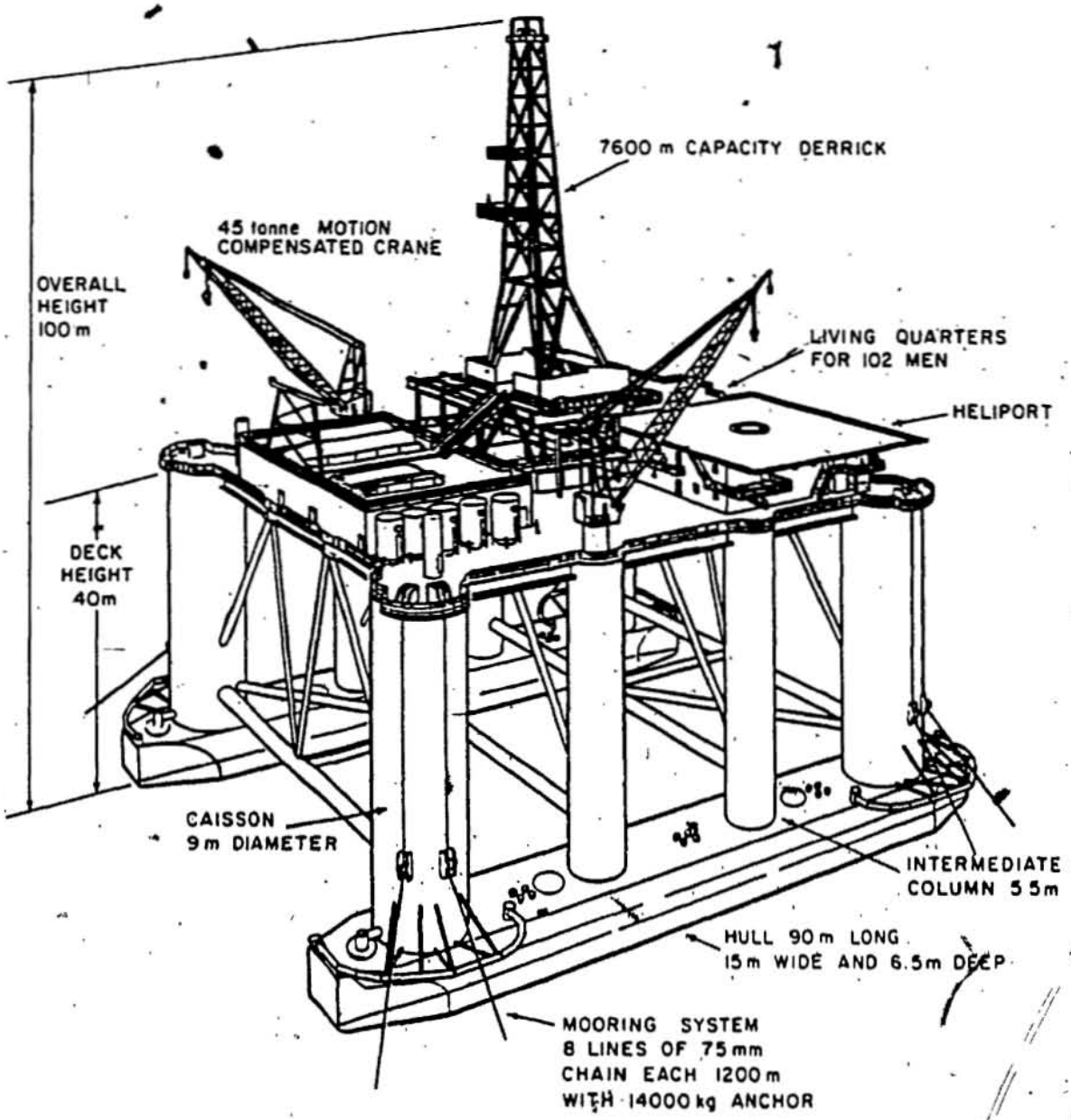

FIG. 2.1 TYPICAL SEMI-SUBMERSIBLE OFFSHORE DRILLING UNIT - SEDCO-700 SERIES. (Jones, 1982)

FIG. 2.2 SEDCO-711 SEMI-SUBMERSIBLE (OCEAN INDUSTRY, 1983a).

FIG. 3.1 THE PROCESS OF PRODUCING ARTIFICIAL SNOW

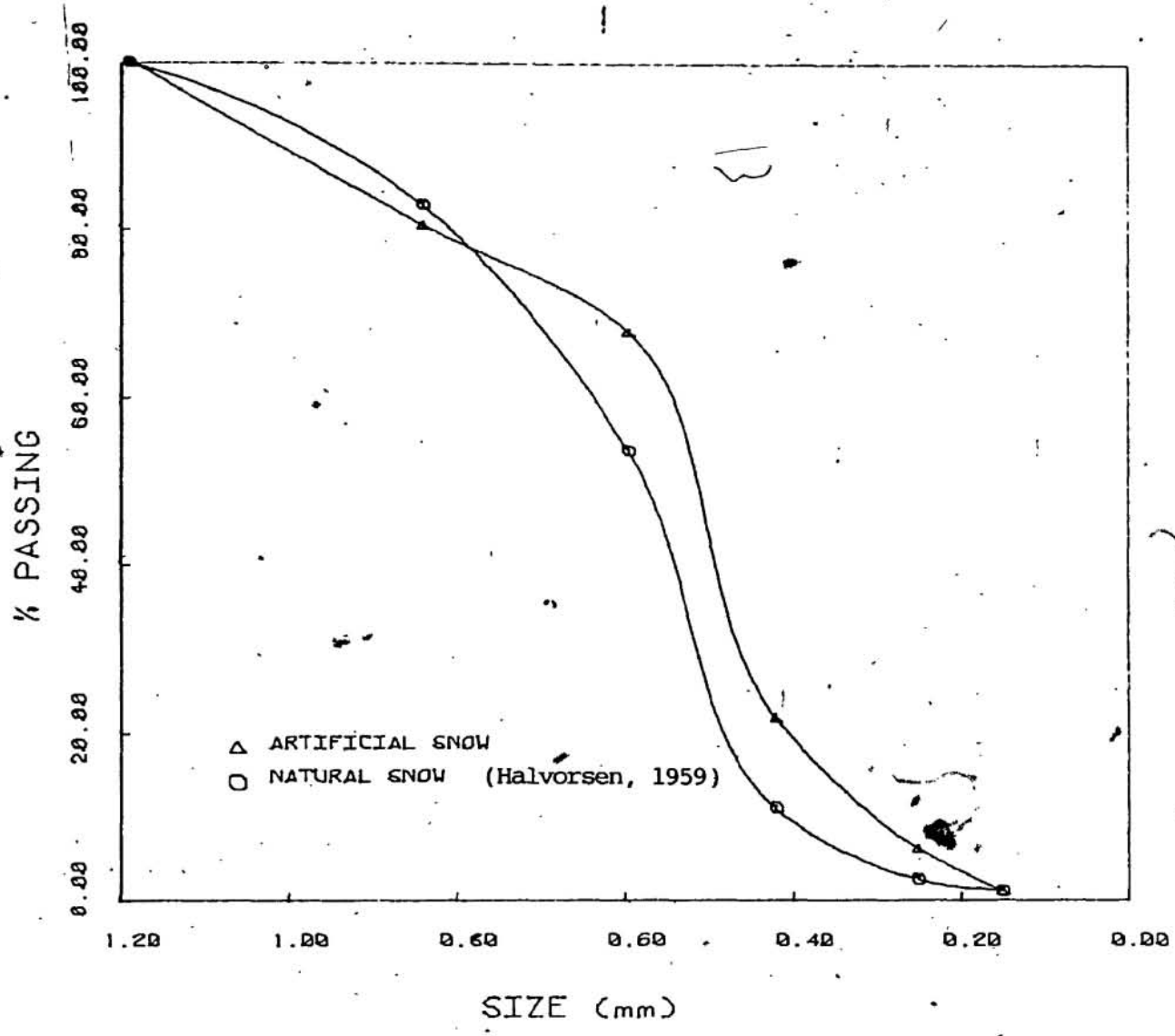

FIG. 3.2 : SIEVE ANALYSIS OF NATURAL AND ARTIFICIAL SNOW.

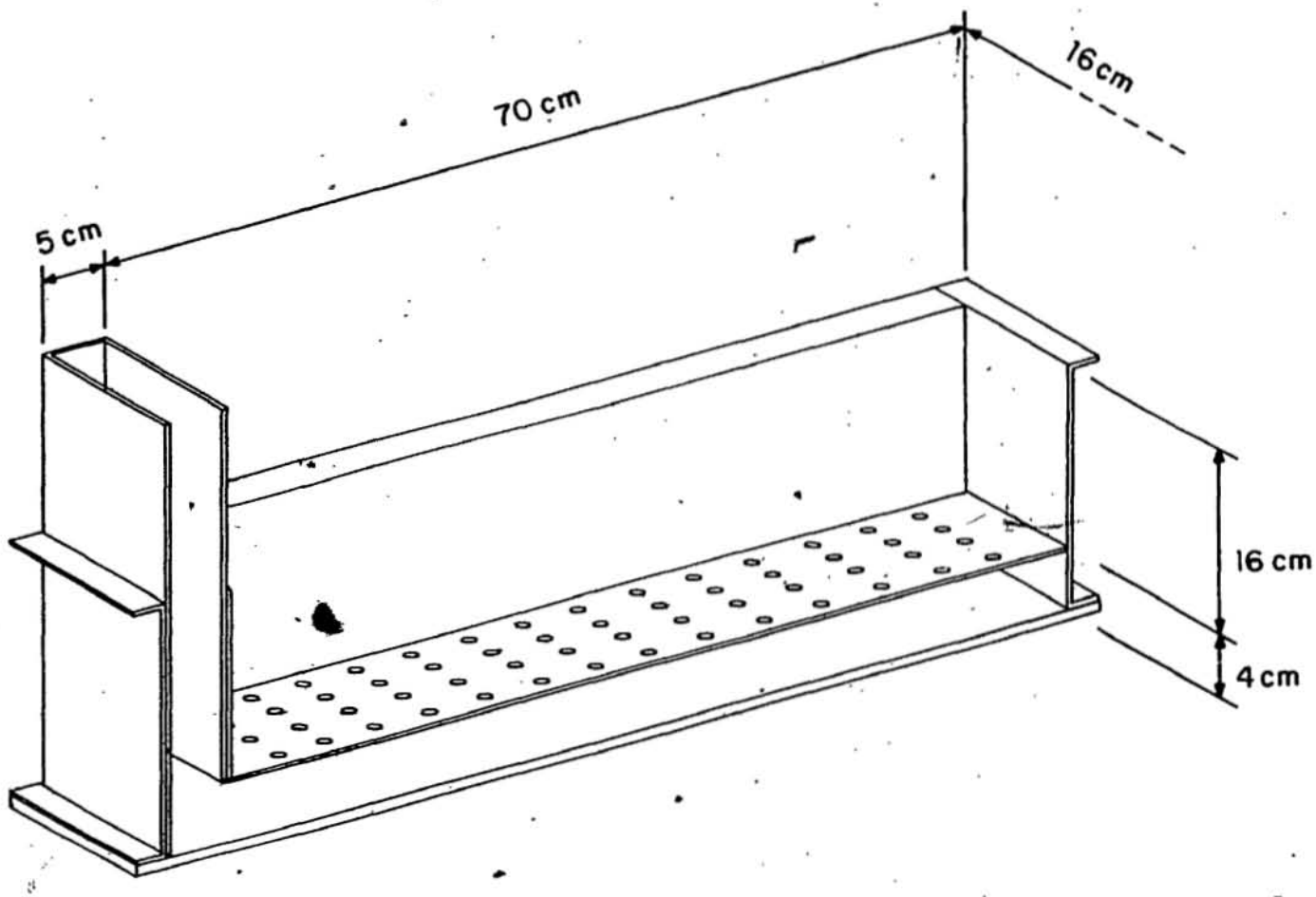

FIG. 3.3 SECTIONAL VIEW OF THE SNOW ICE MOULD

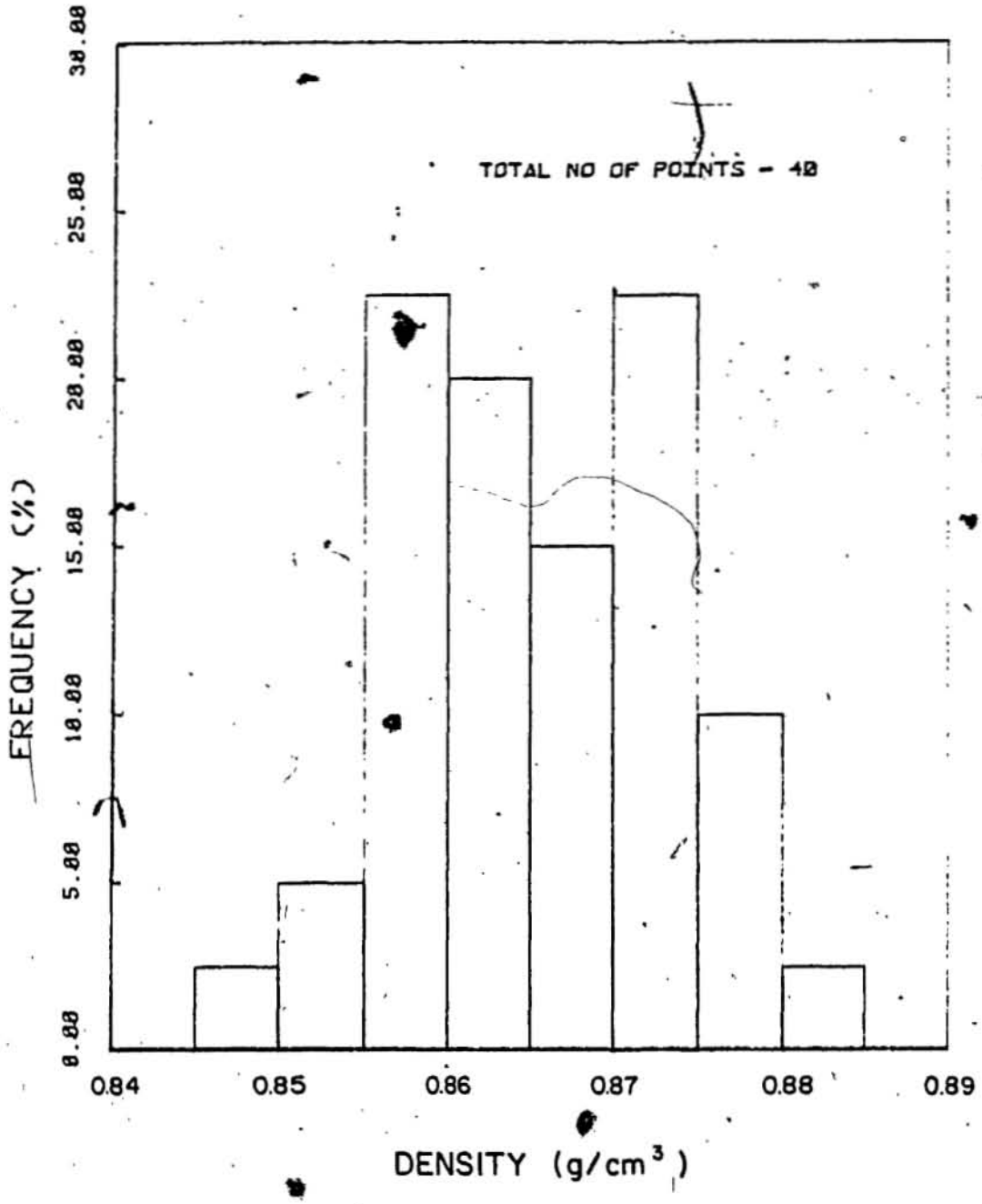

FIG. 3.4 FREQUENCY DISTRIBUTION OF SNOW ICE DENSITY.

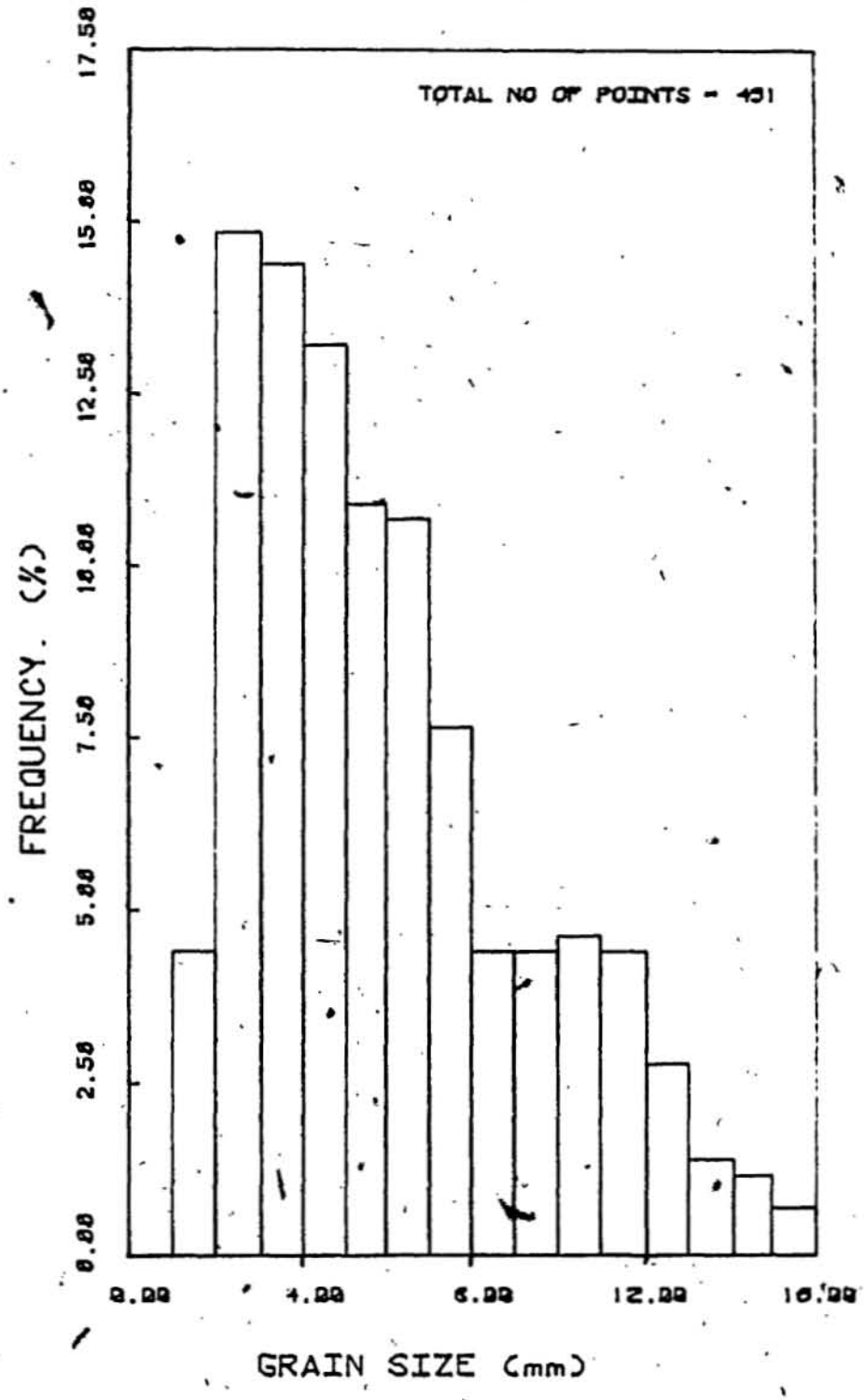

FIG. 3.5 GRAIN SIZE DISTRIBUTION OF GLACIER ICE.

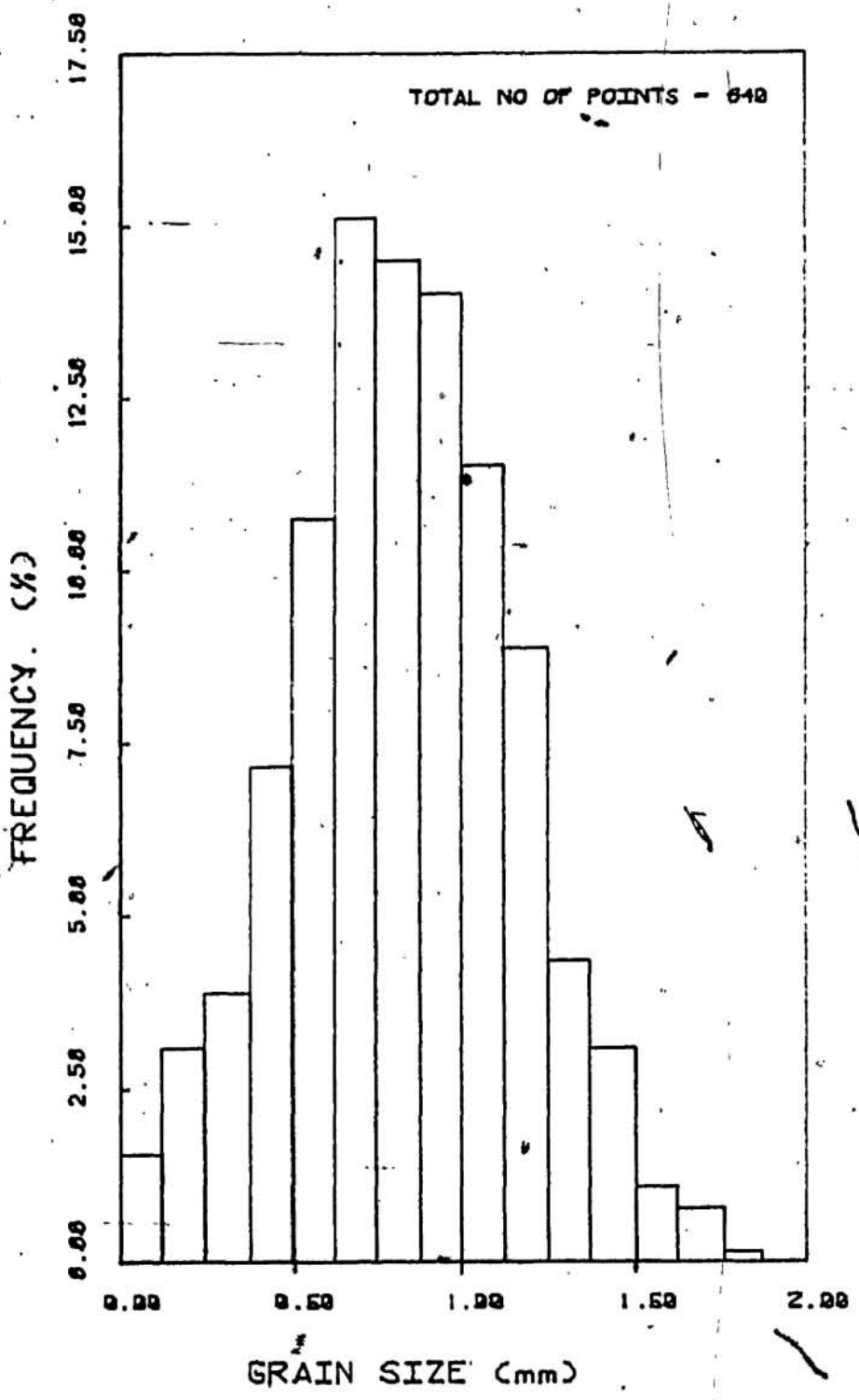

FIG. 5.6 GRAIN SIZE DISTRIBUTION OF SNOW ICE.

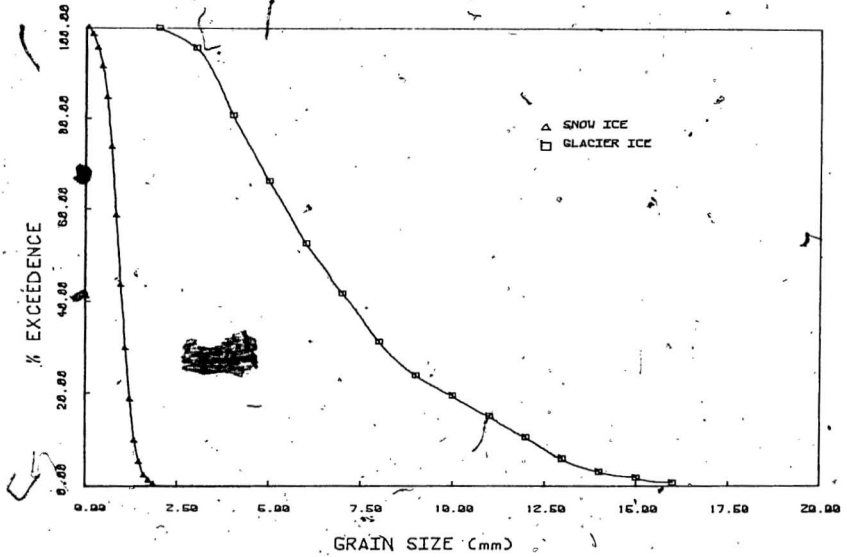

FIG. 37 EXCEEDENCE DIAGRAM FOR THE GRAIN SIZE DISTRIBUTION OF GLACIER AND SNOW ICE.

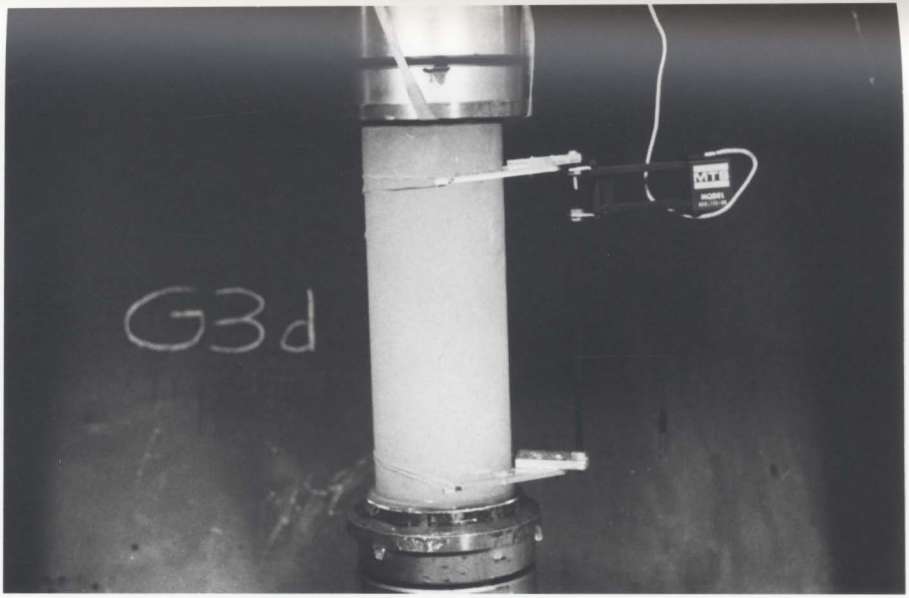

FIG. 3.8 UNIAXIAL COMPRESSION TEST FOR ICEBERG ICE

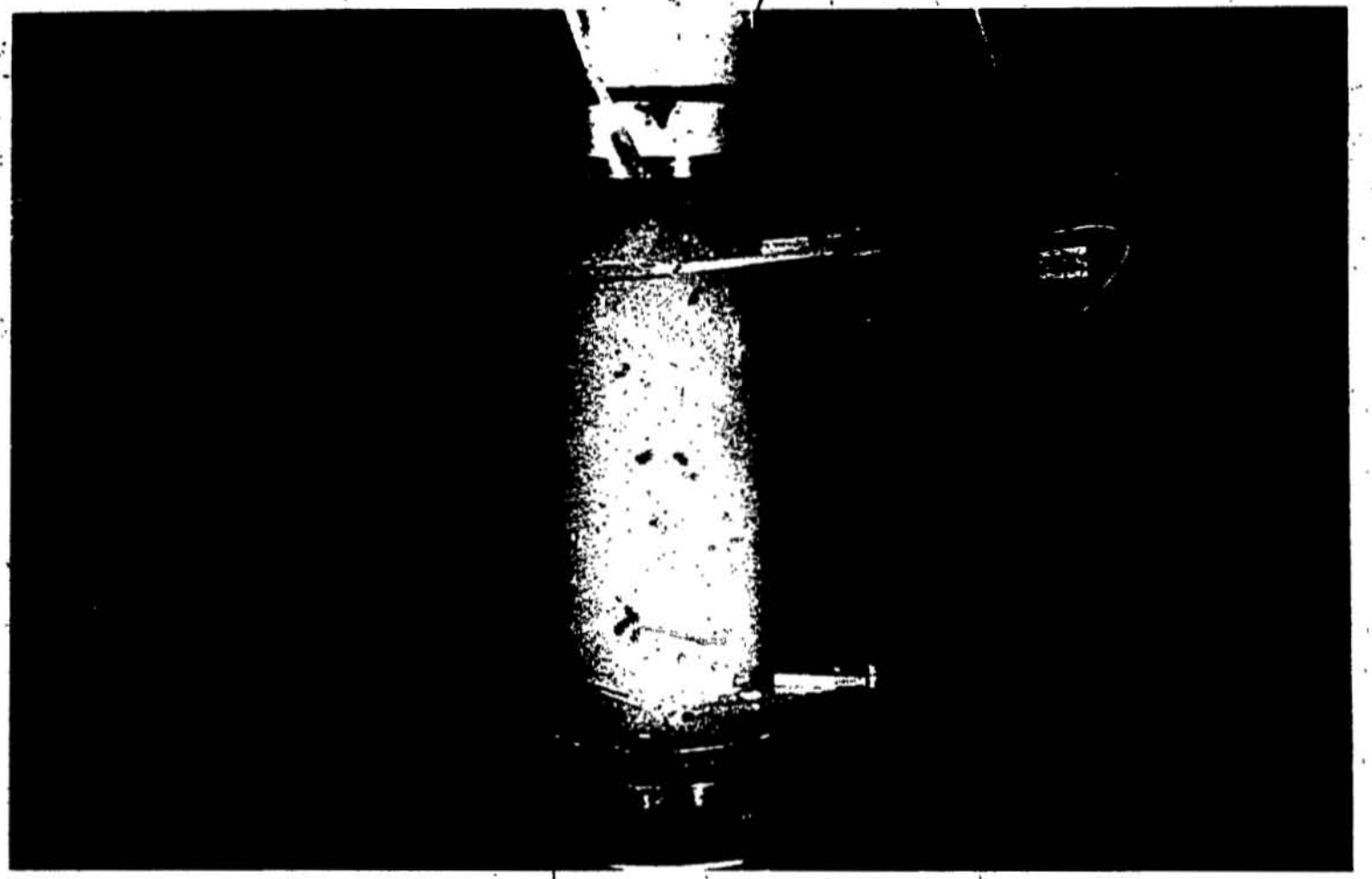

FIG. 3.8 UNIAXIAL COMPRESSION TEST FOR ICEBERG ICE

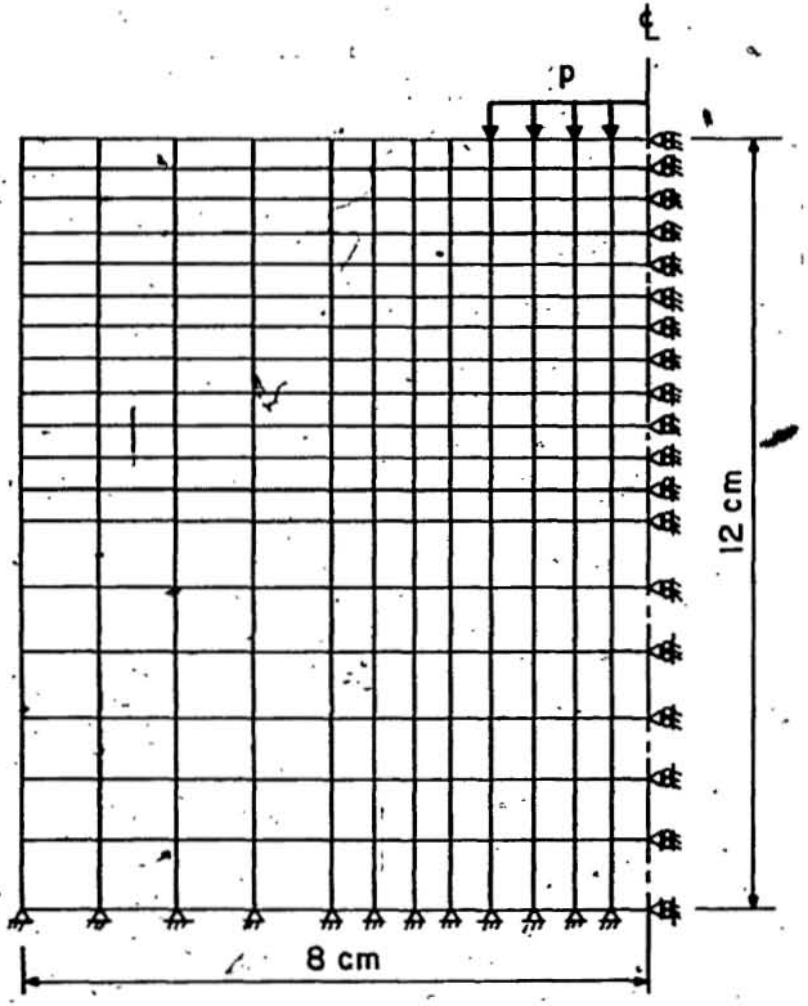

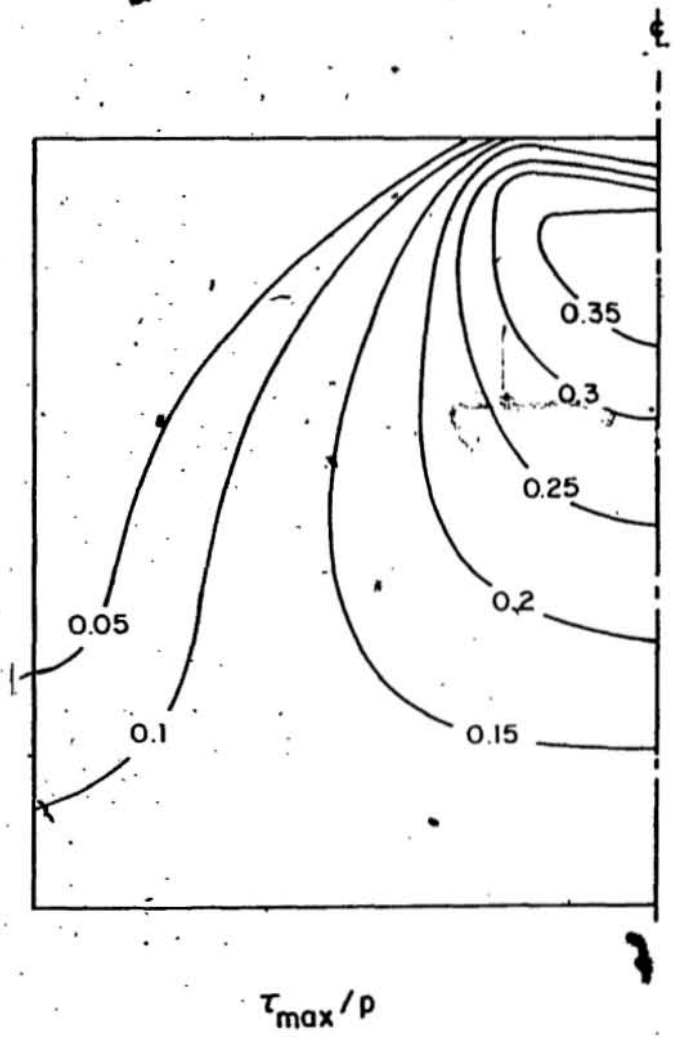

FIG. 3.9 FINITE ELEMENT DISCRETIZATION OF THE ICE BLOCK AND CONTOURS OF PRINCIPAL SHEAR STRESS

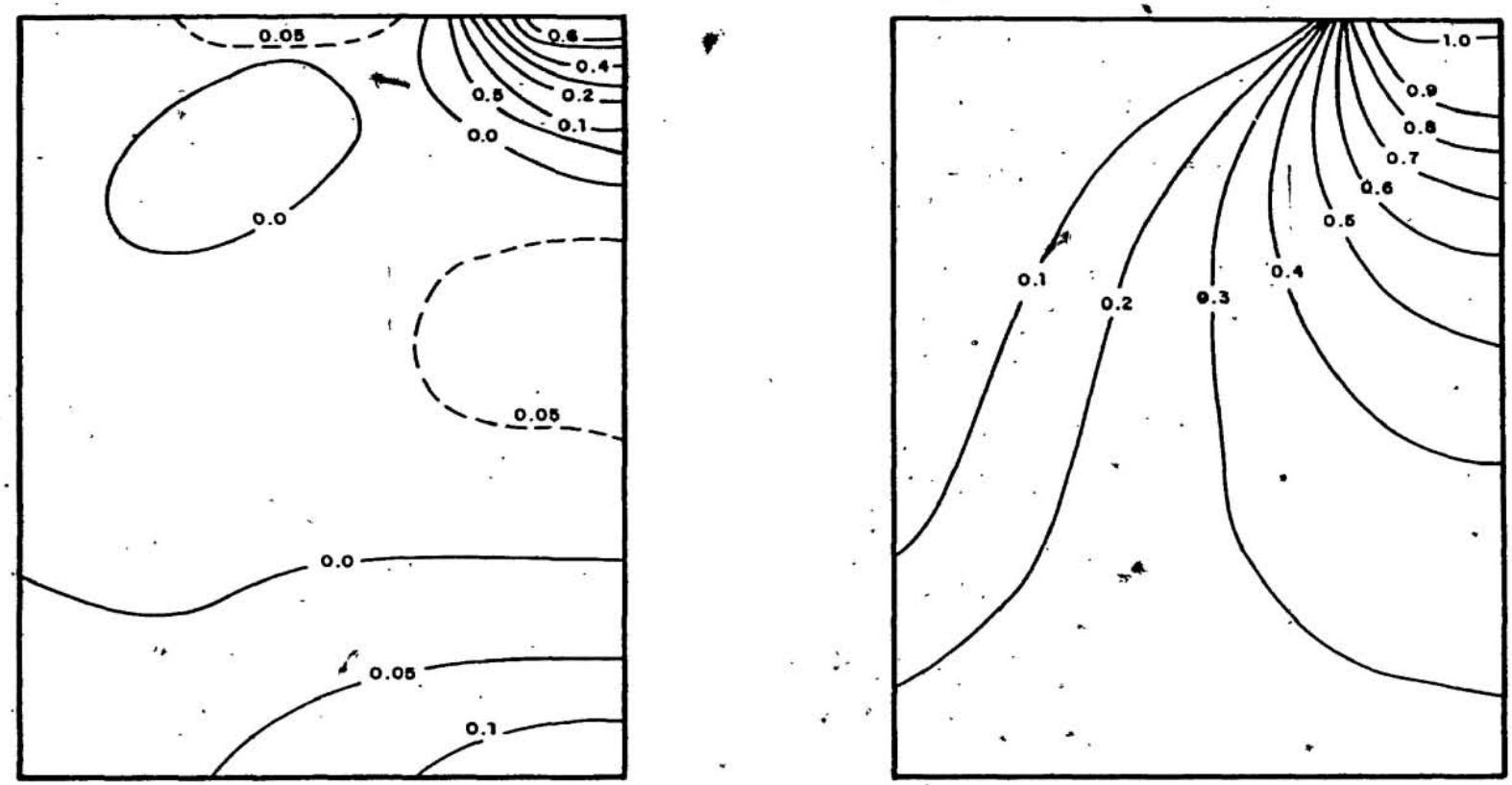

FIG. 310 CONTOURS OF THE PRINCIPAL NORMAL STRESSES IN THE ICE BLOCK.

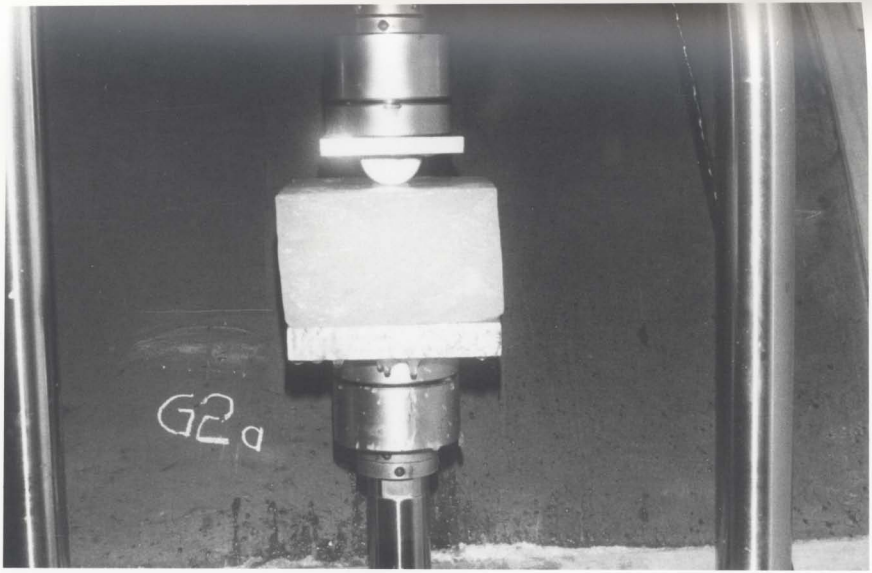

FIG. 3.11 INDENTATION TEST ON UNCONFINED ICEBERG ICE BLOCK.

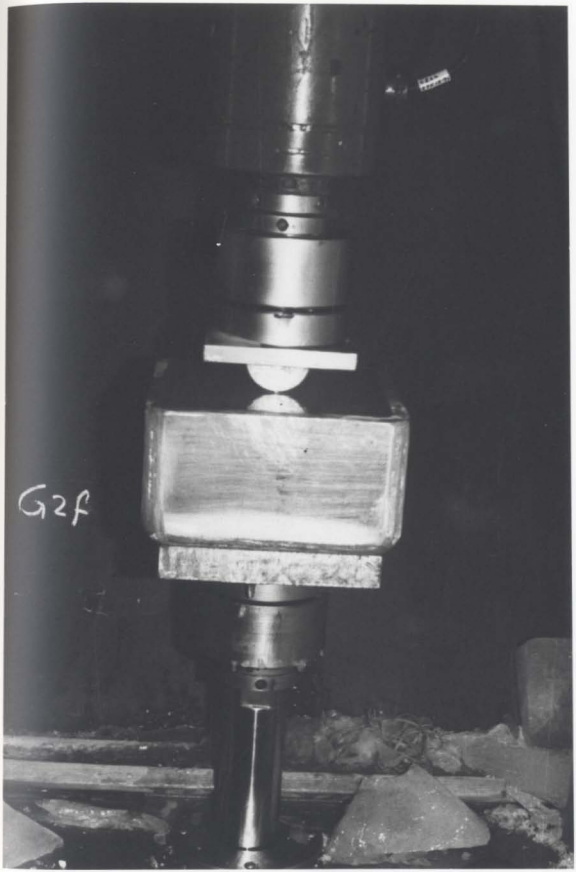

FIG. 3.12 INDENTATION TEST ON CONFINED ICEBERG ICE BLOCK.

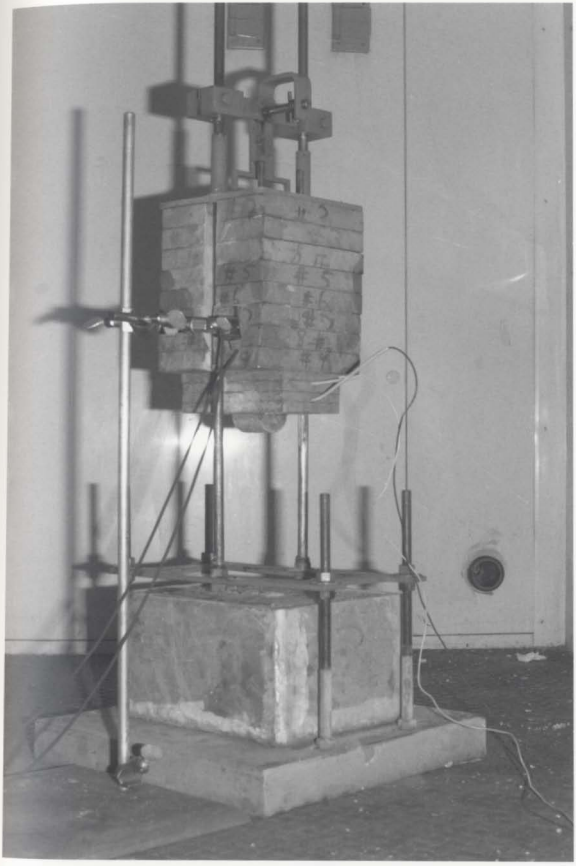

FIG. 3.13 GENERAL VIEW OF IMPACT TEST DEVICE

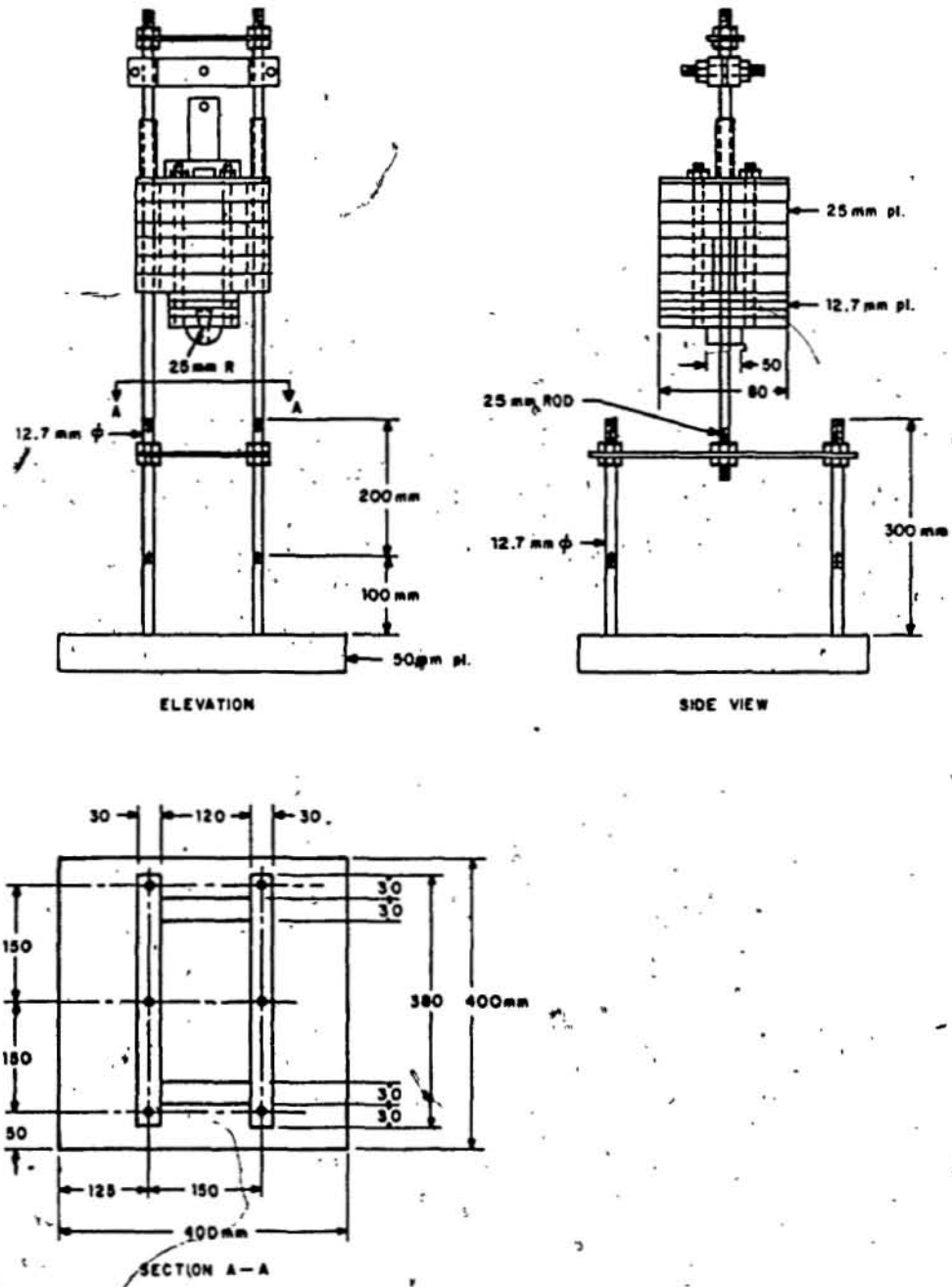

FIG. 3.14 IMPACT DEVICE

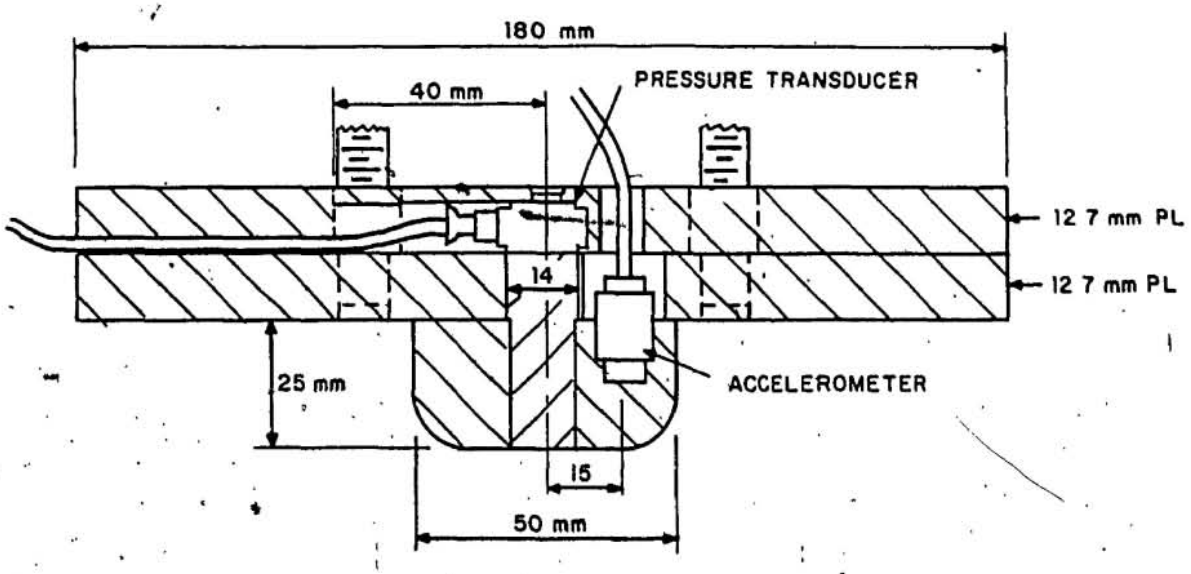

LONGITUDINAL SECTION

ALL DIMENSIONS IN mm.

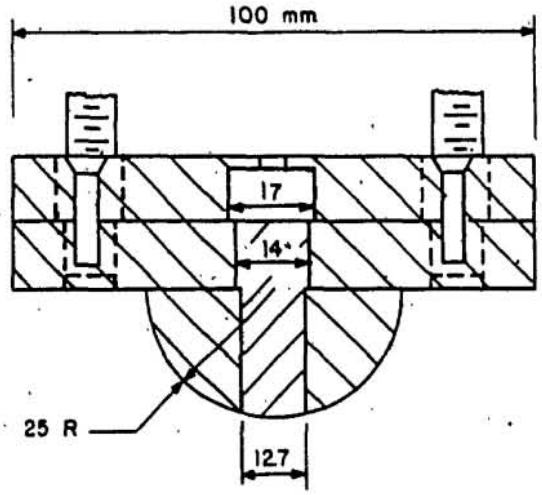

TRANSVERSE SECTION

FIG. 3.15 INSTRUMENTATION OF THE IMPACT TEST INDENTOR

FIG. 3.16 SNOW ICE SPECIMEN AFTER TEST - STRAIN RATE OF .001 AT -5° C.

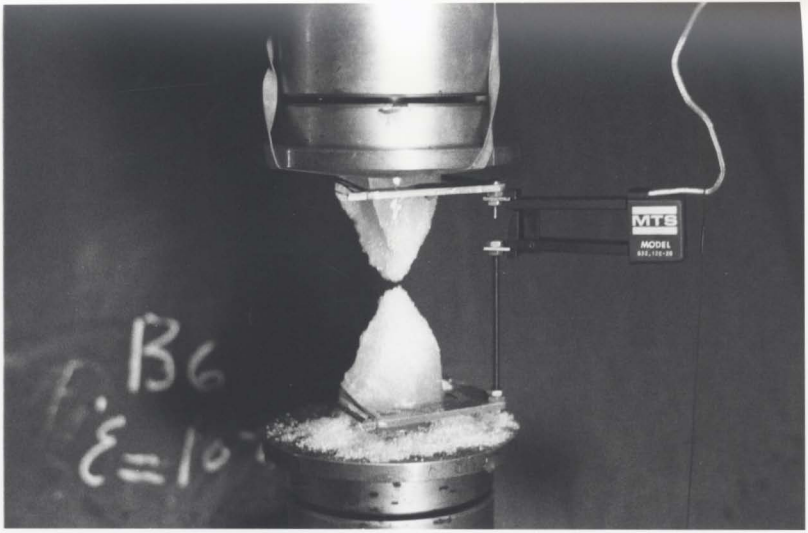

FIG. 3.17 SNOW ICE SPECIMEN AFTER TEST - STRAIN RATE .01 AT -5° C.

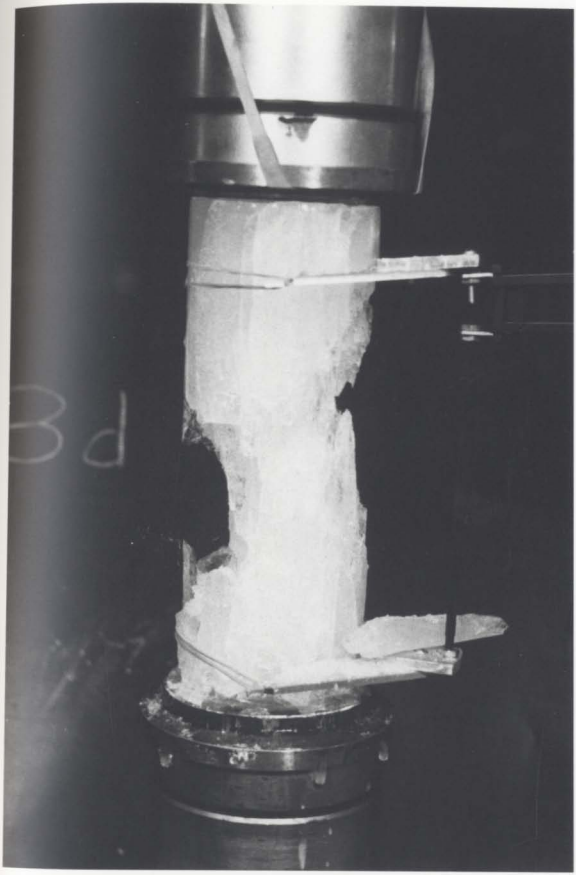

FIG. 3.18 TYPICAL FAILURE PATTERN OF ICEBERG ICE AT -5°C.

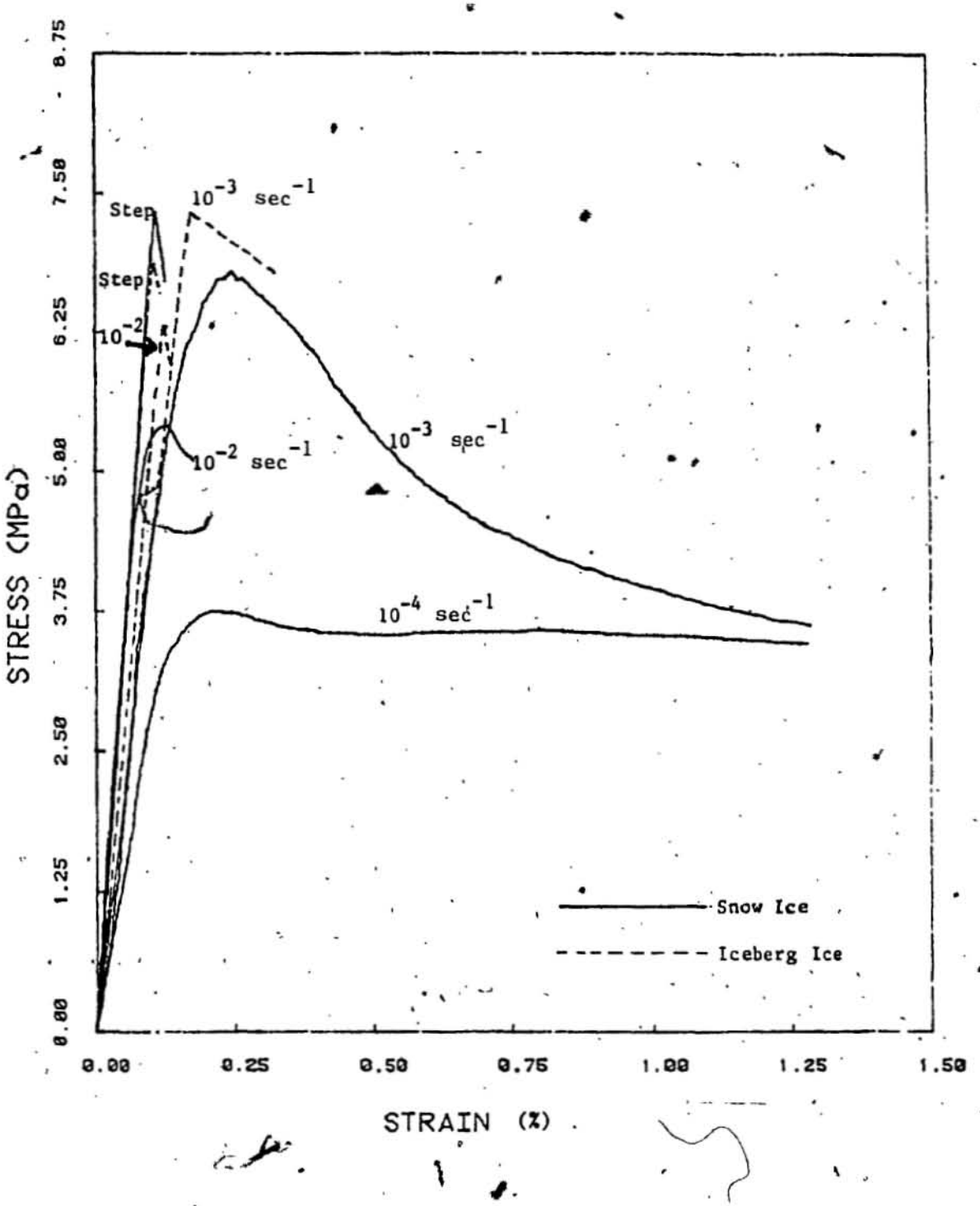

FIG. 3.19 STRESS-STRAIN CURVES FOR ICEBERG AND SNOW ICE AT DIFFERENT STRAIN RATES .

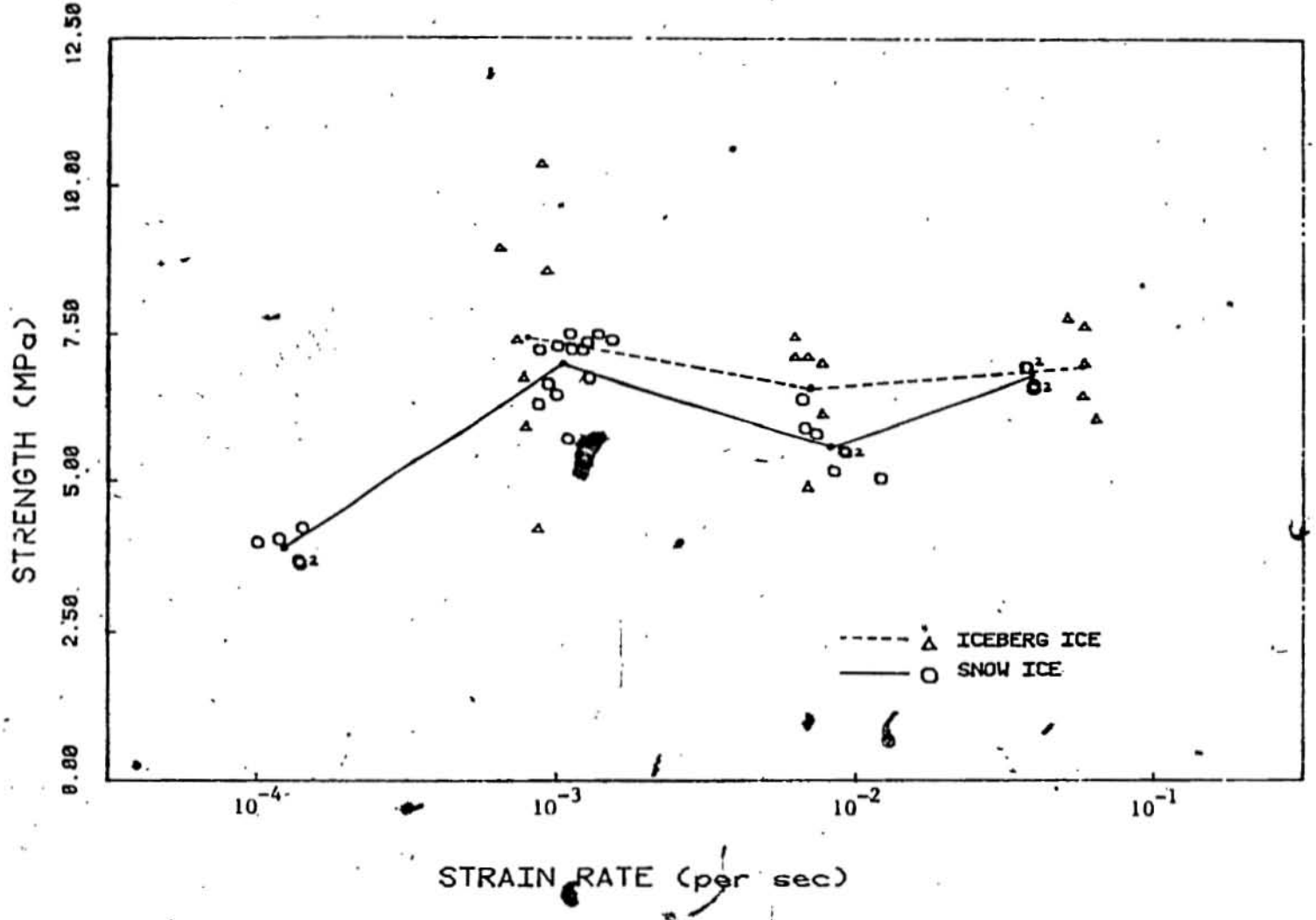

FIG. 3.20 UNIAXIAL COMPRESSIVE STRENGTH VS STRAIN RATE FOR ICEBERG AND SNOW ICE .

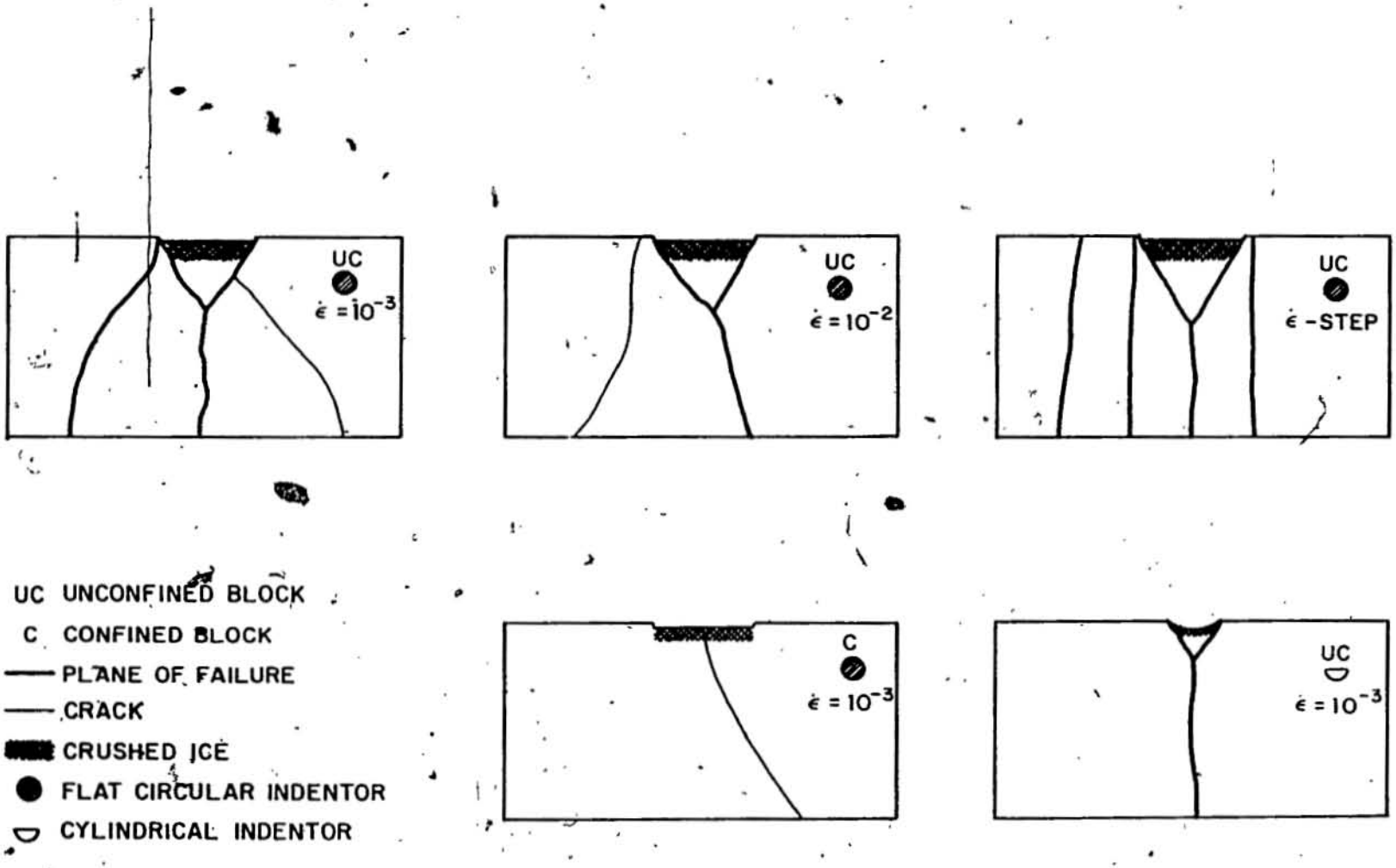

FIG.3.21 TYPICAL FAILURE PATTERNS IN A MIDDLE PLANE OF SNOW ICE BLOCKS – INDENTATION TEST

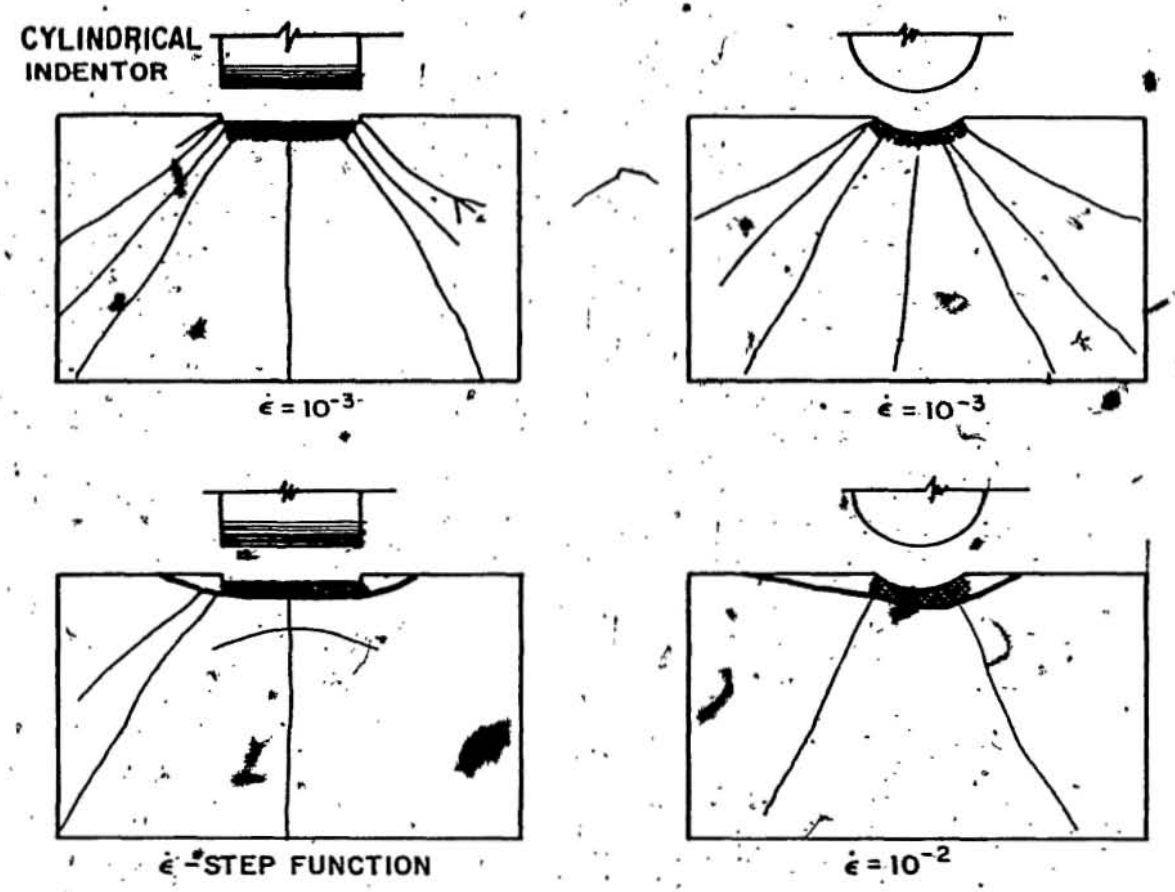

FIG. 3.22 TYPICAL FAILURE PATTERNS IN A MIDDLE PLANE OF CONFINED ICEBERG ICE BLOCKS - INDENTATION TESTS, CYLINDRICAL INDENTOR.

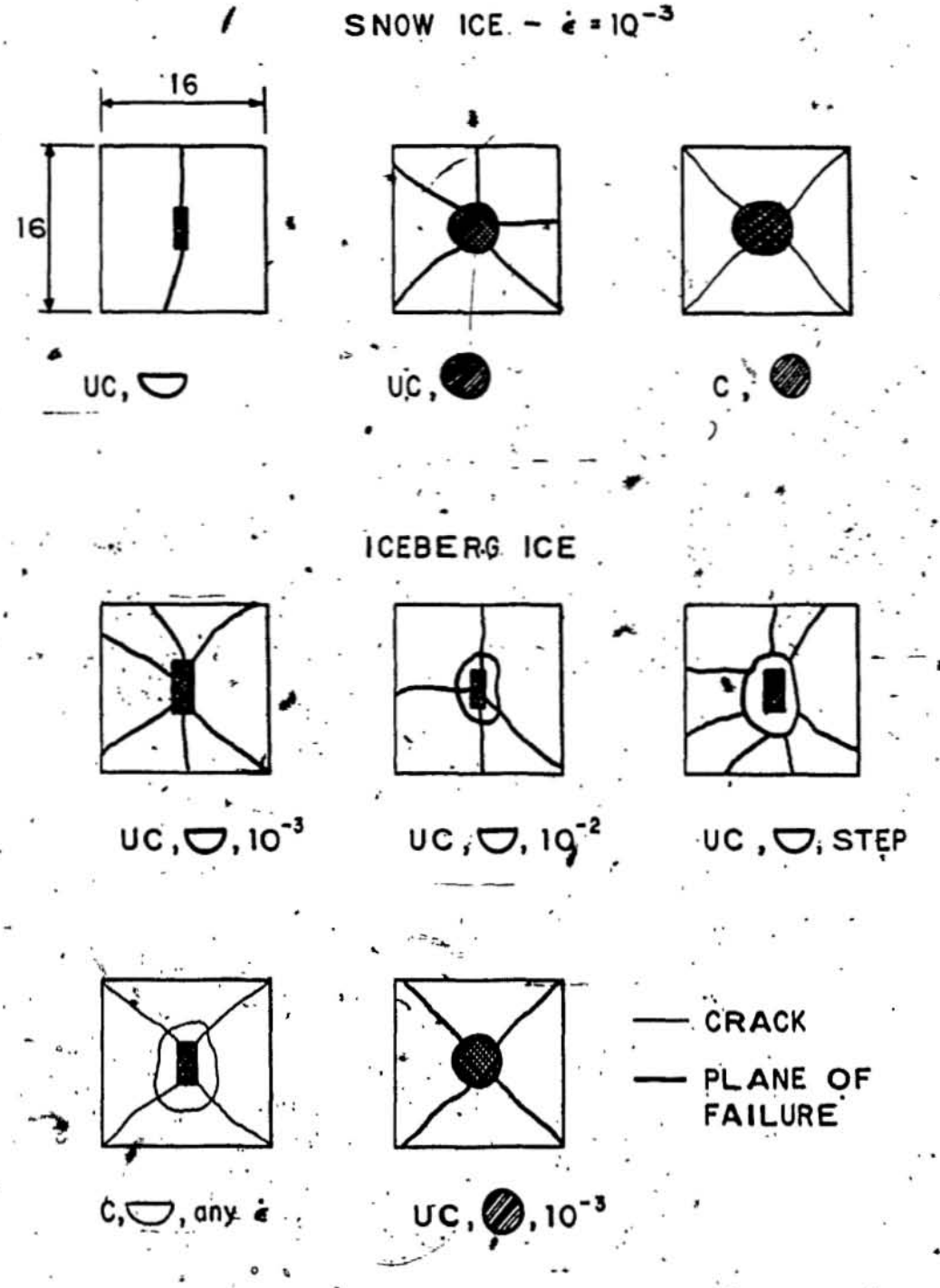

FIG. 3.23 FAILURE PATTERNS AT THE INDENTATION SURFACE OF ICE BLOCKS

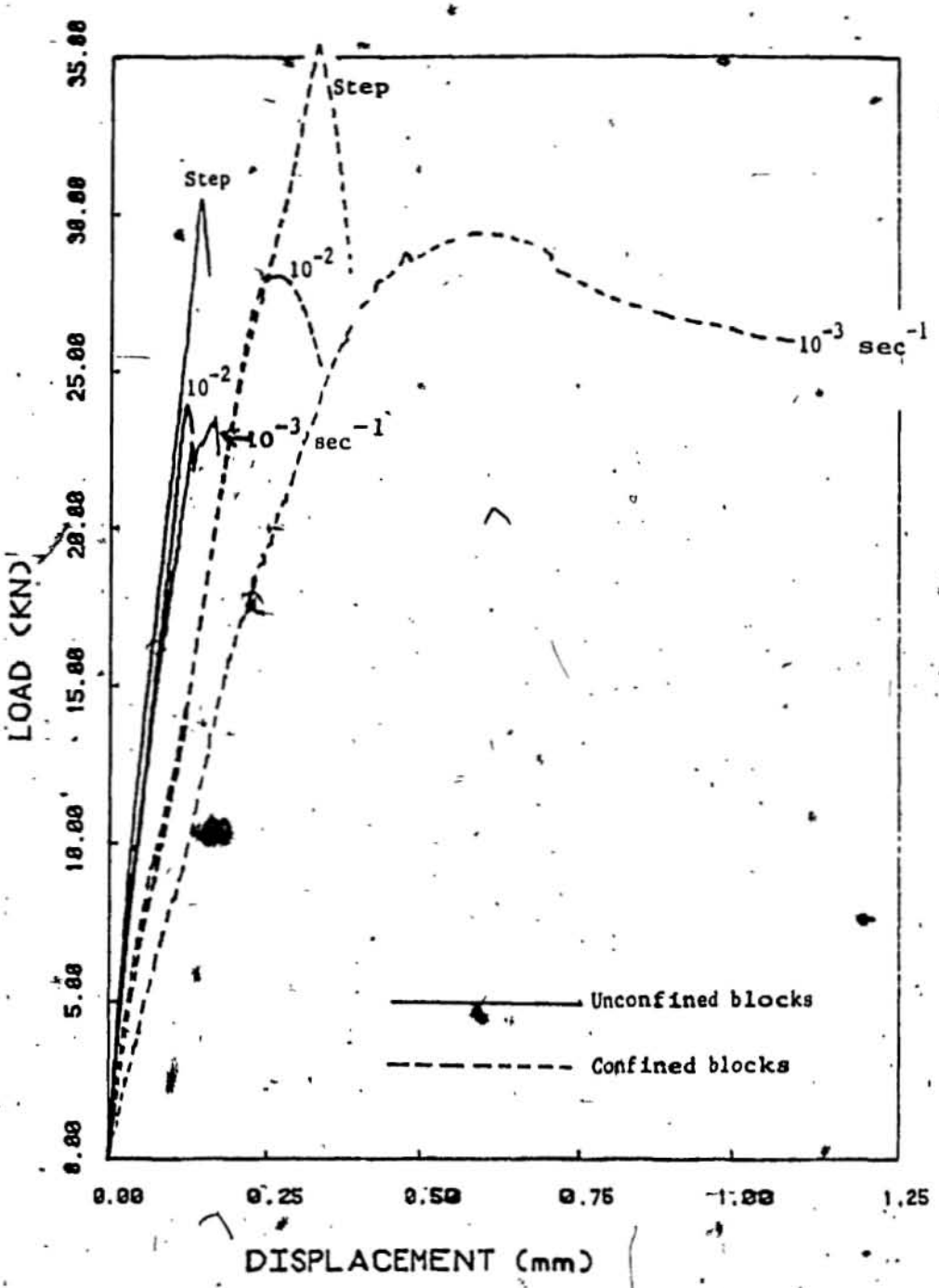

FIG. 3.24 EFFECT OF STRAIN RATE ON LOAD VS DISPLACEMENT CURVE FOR INDENTATION TEST OF ICEBERG ICE / CYLINDRICAL INDENTOR.

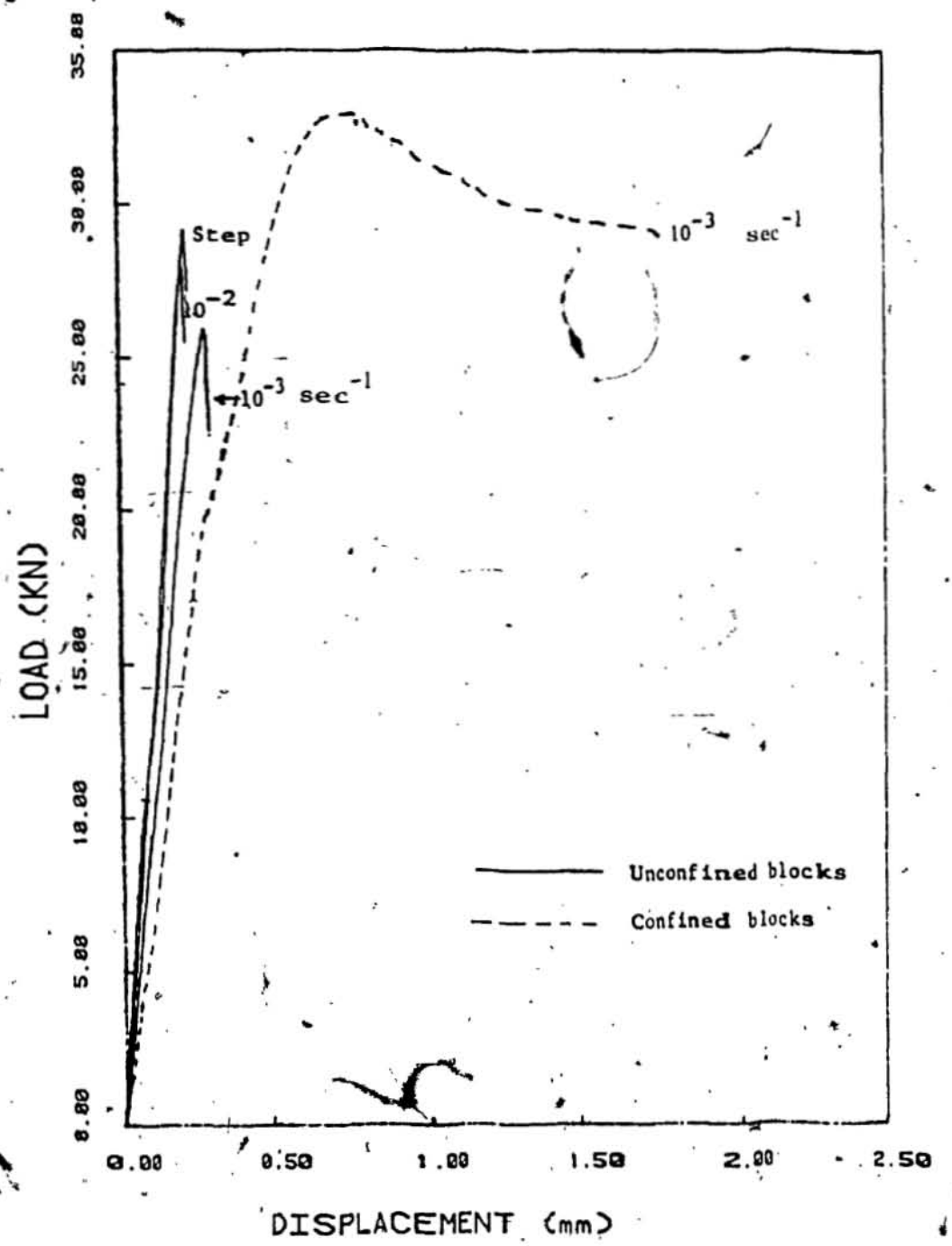

FIG. 3.25 EFFECT OF STRAIN RATE ON LOAD VS DISPLACEMENT CURVE FOR INDENTATION TEST OF SNOW ICE – CIRCULAR INDENTOR

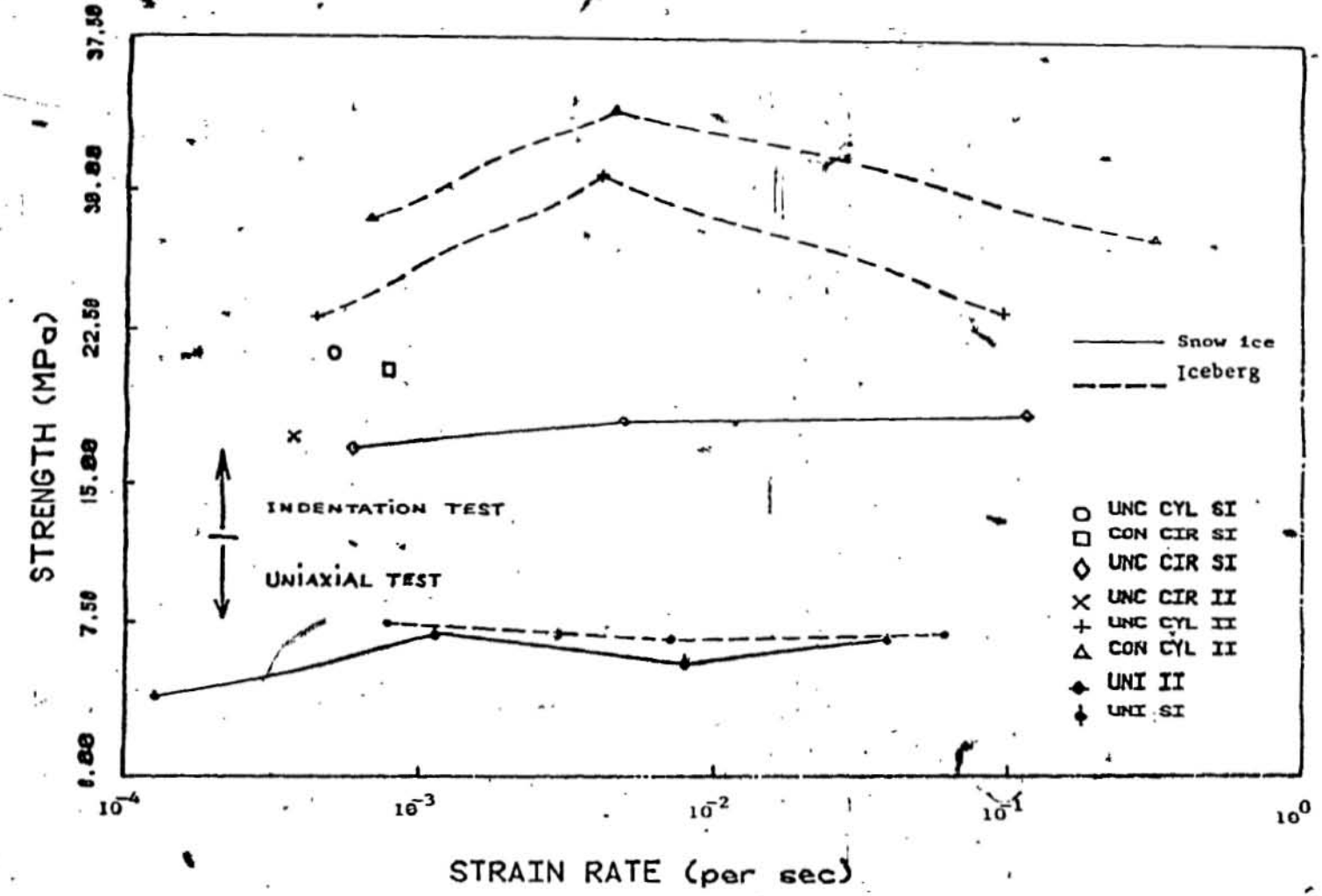

FIG. 3.26 AVERAGE STRENGTH VS STRAIN RATE FOR ICEBERG AND SNOW ICE

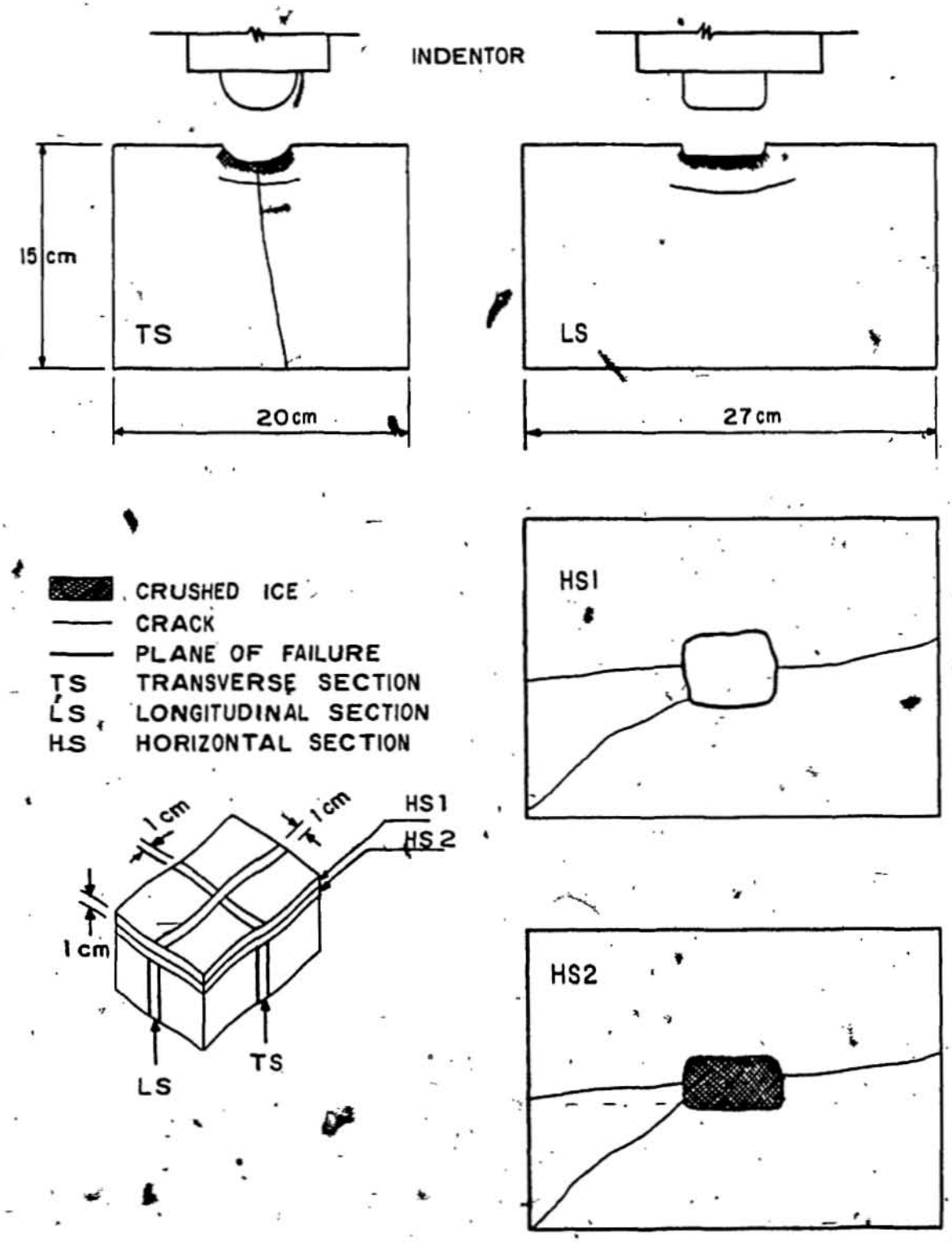

FIG. 3.27 FAILURE PATTERNS OF CONFINED SNOW ICE BLOCKS - IMPACT TEST

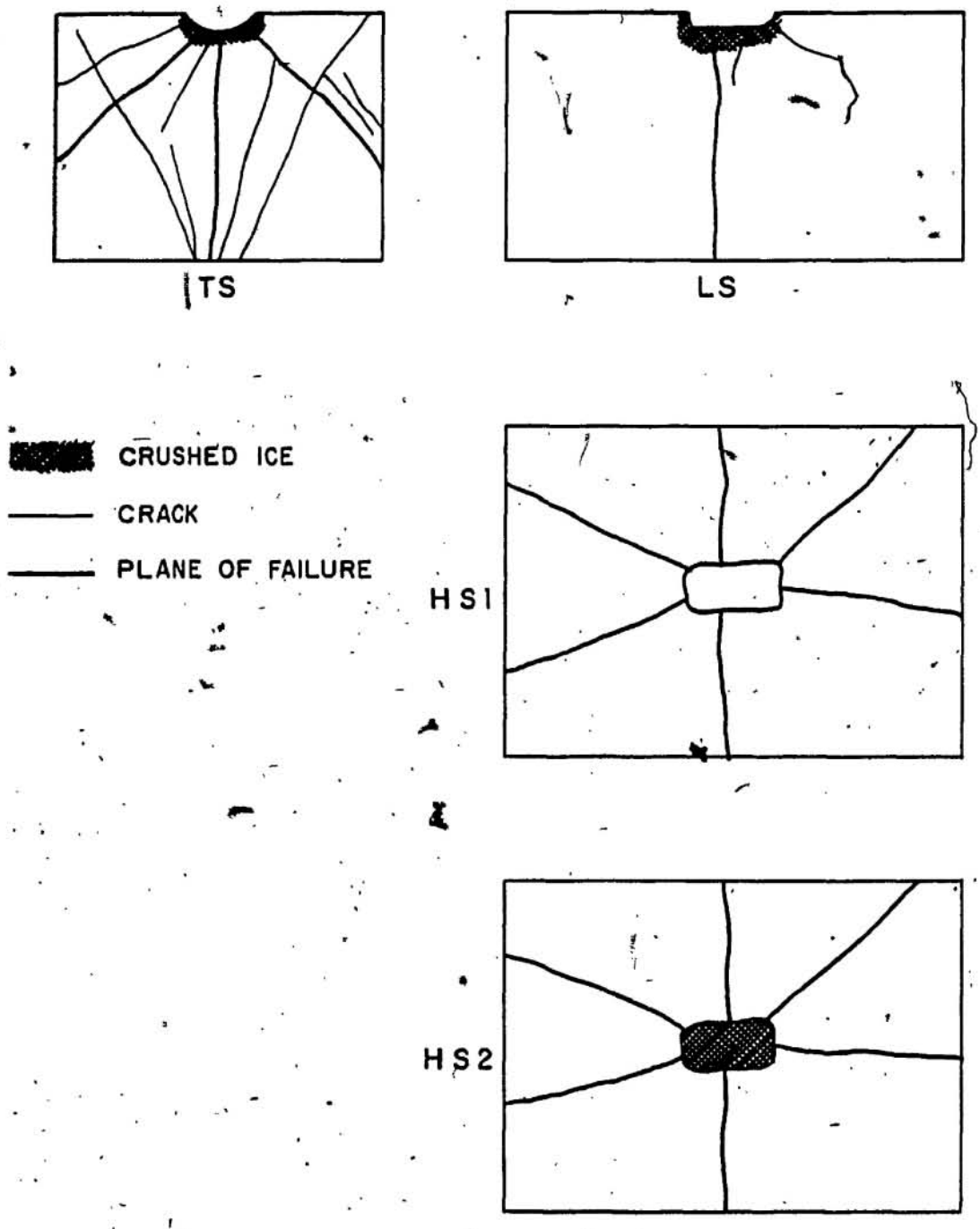

FIG. 3.28 FAILURE PATTERNS OF UNCONFINED SNOW ICE BLOCKS - IMPACT TEST

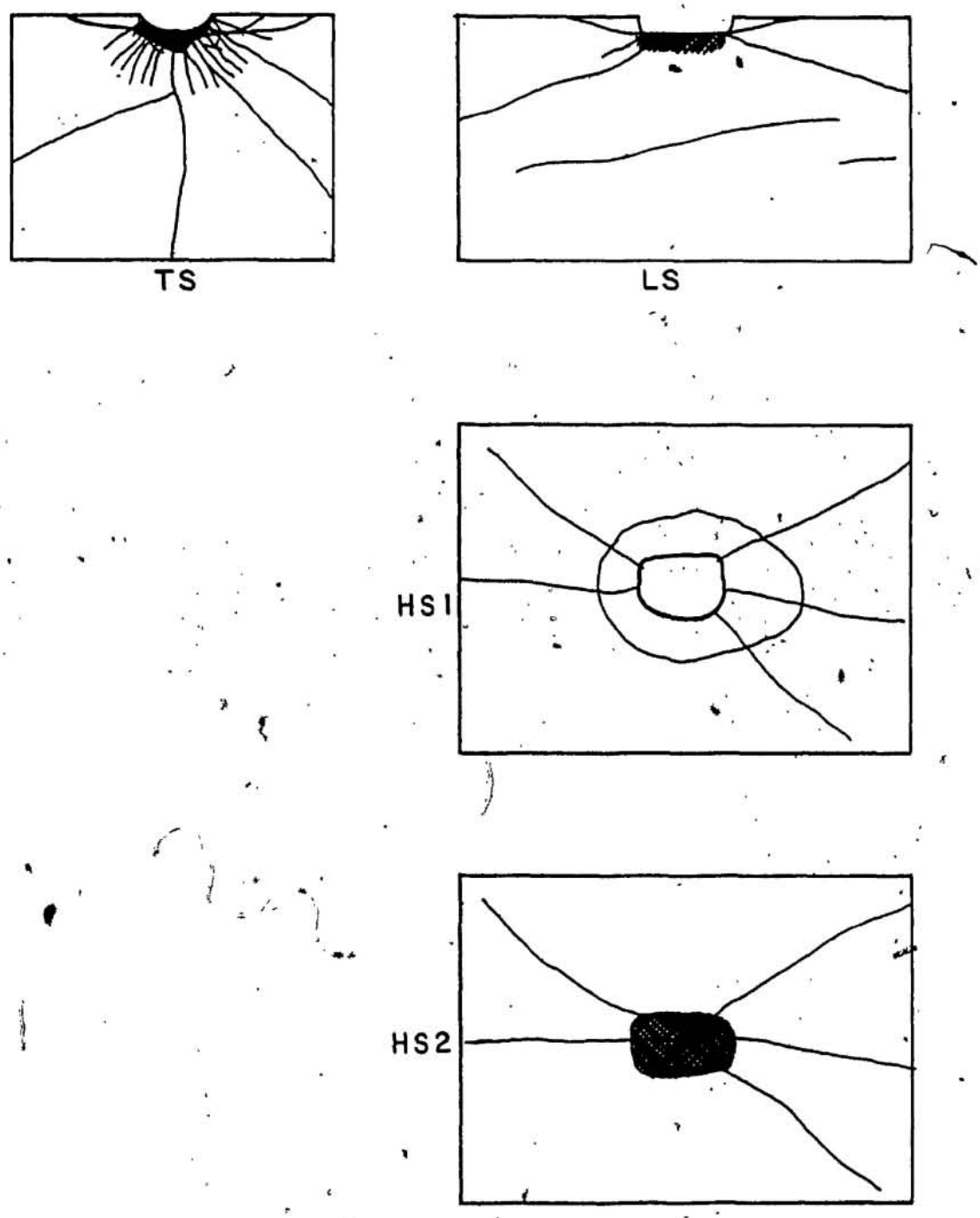

FIG. 3.29 FAILURE PATTERNS OF CONFINED ICEBERG ICE BLOCKS - IMPACT TEST.

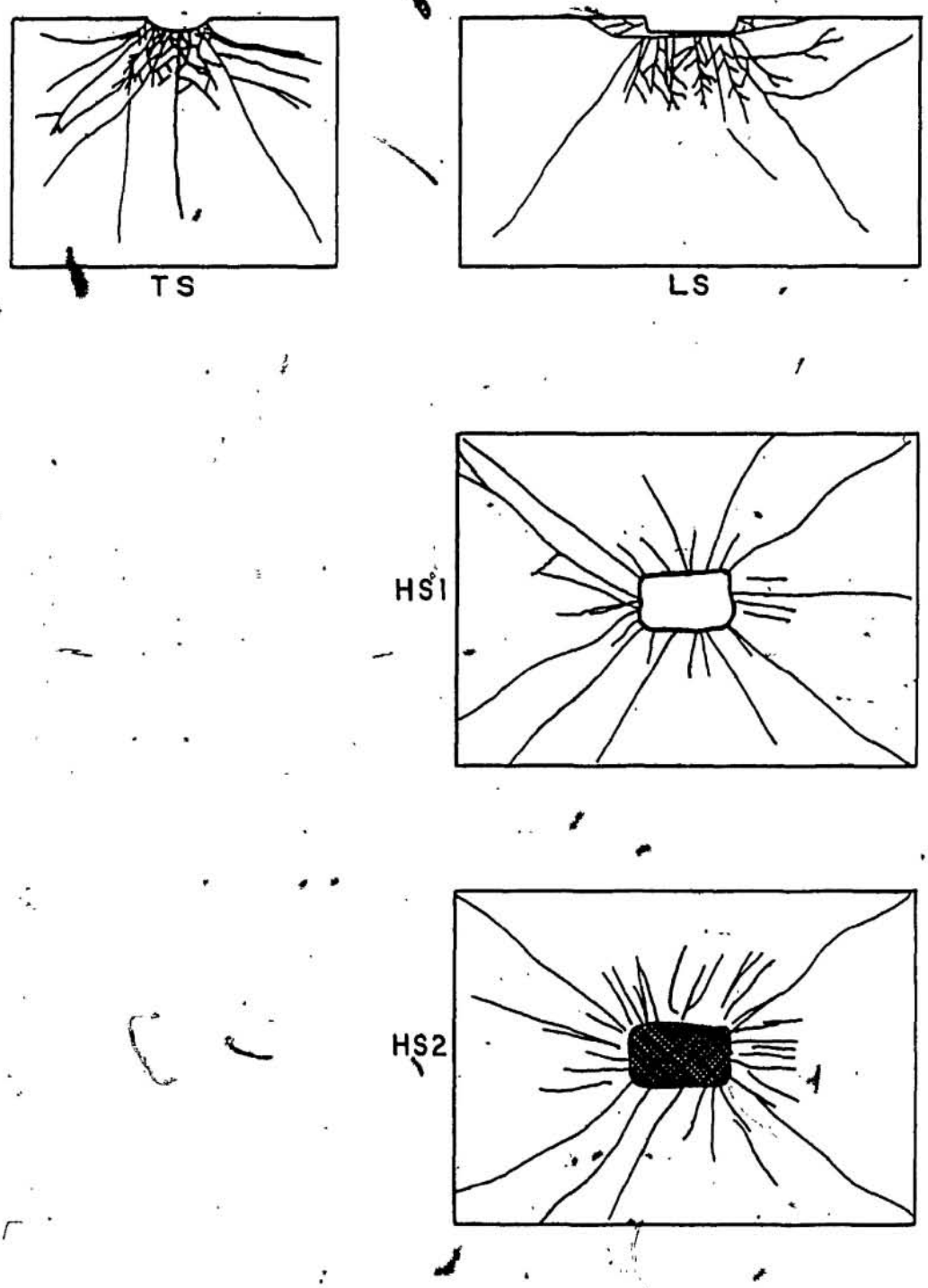

FIG. 3.30 FAILURE PATTERNS OF CONFINED S2 ICE BLOCKS- IMPACT TEST

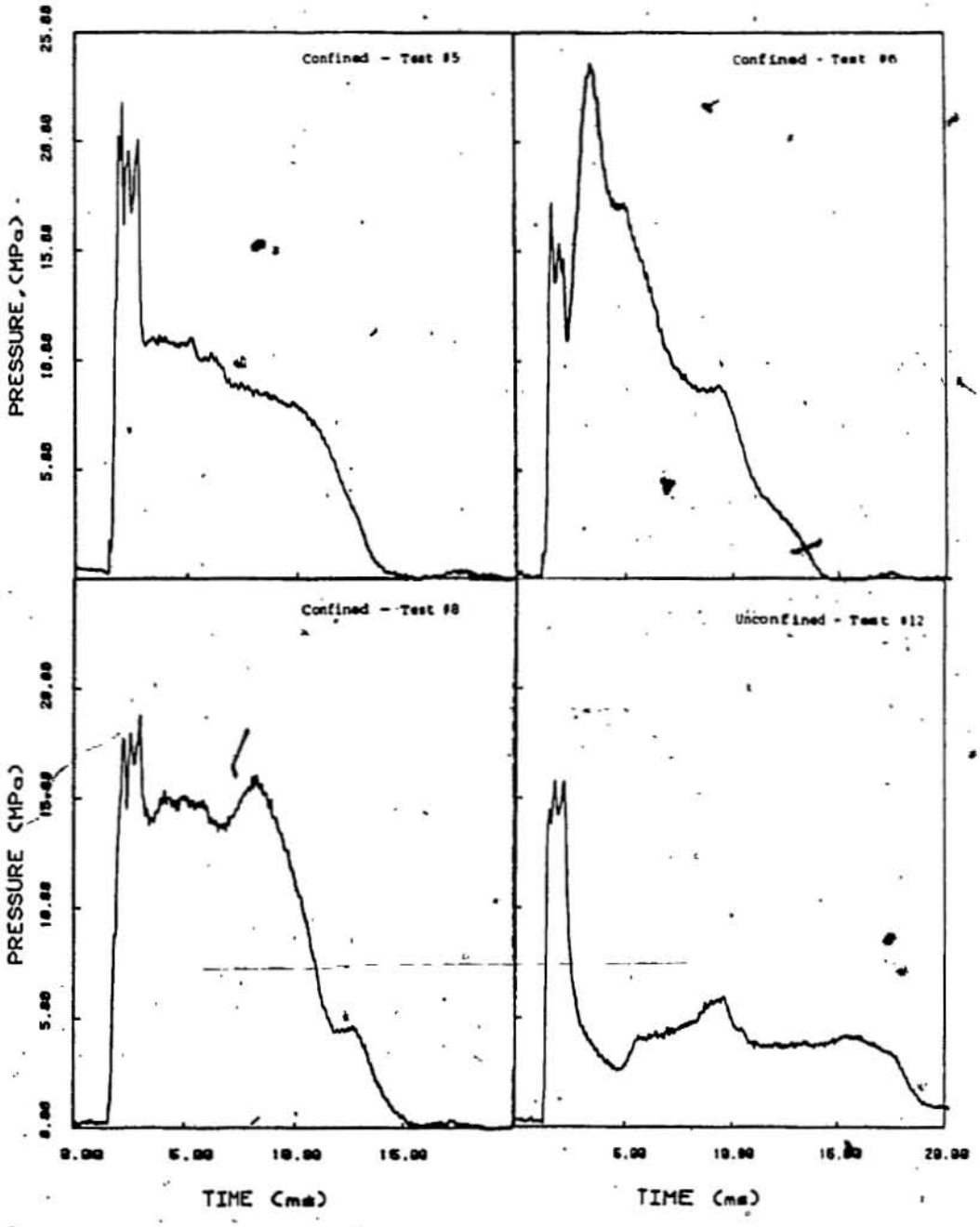

FIGURE 3.31 TIME HISTORY OF PRESSURE UNDER INDENTOR CENTRE DURING IMPACT - SNOW ICE.

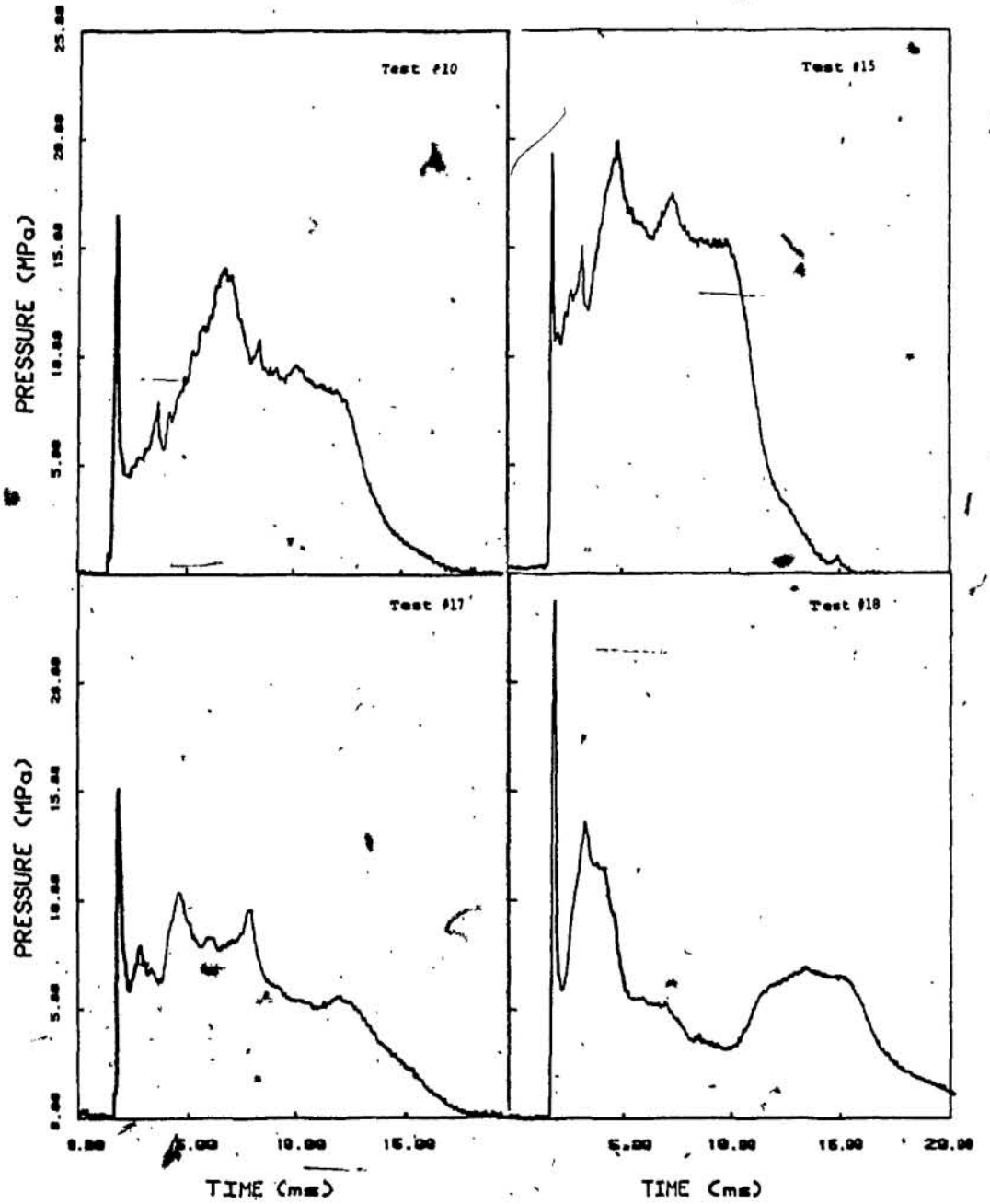

FIGURE 3.32 TIME HISTORY OF PRESSURE AT INDENTOR CENTRE DURING IMPACT - CONFINED ICEBERG ICE.

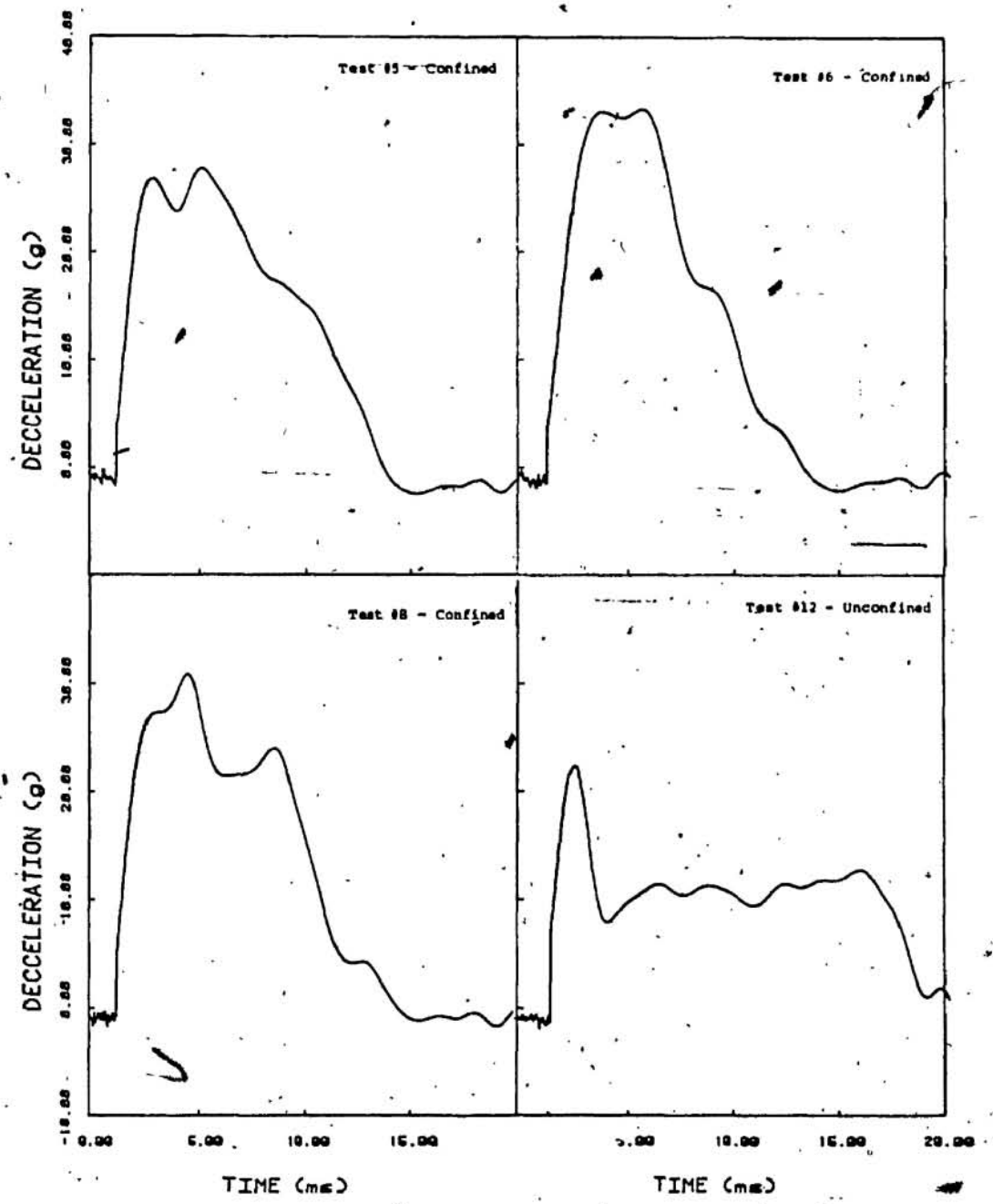

FIGURE 3.33 TIME HISTORY OF INDENTOR DECELERATION - SNOW ICE

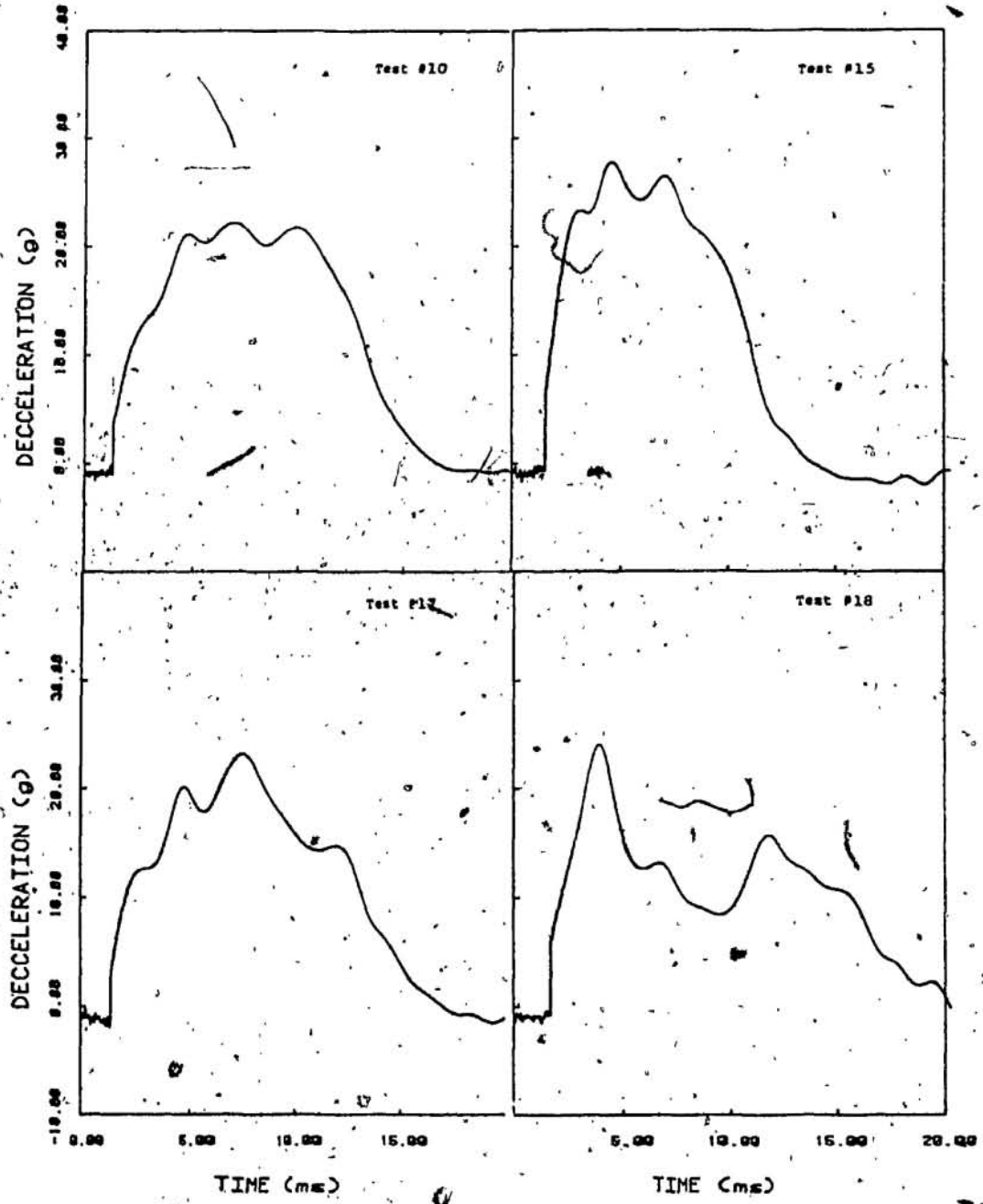

FIGURE 3.34 TIME HISTORY OF INDENTOR DECELERATION - CONFINED ICEBERG ICE.

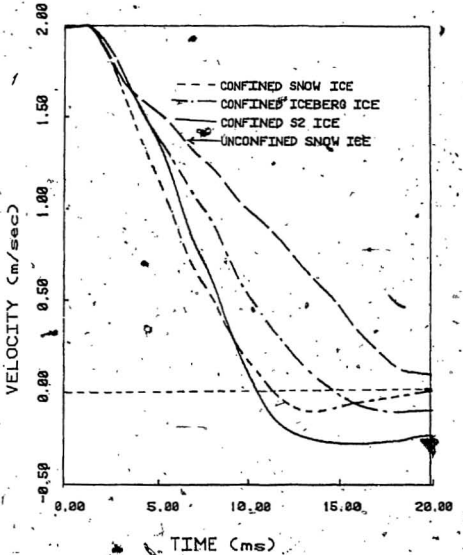

FIG. 3.35 TIME HISTORY OF INDENTOR VELOCITY DURING IMPACT TESTS.

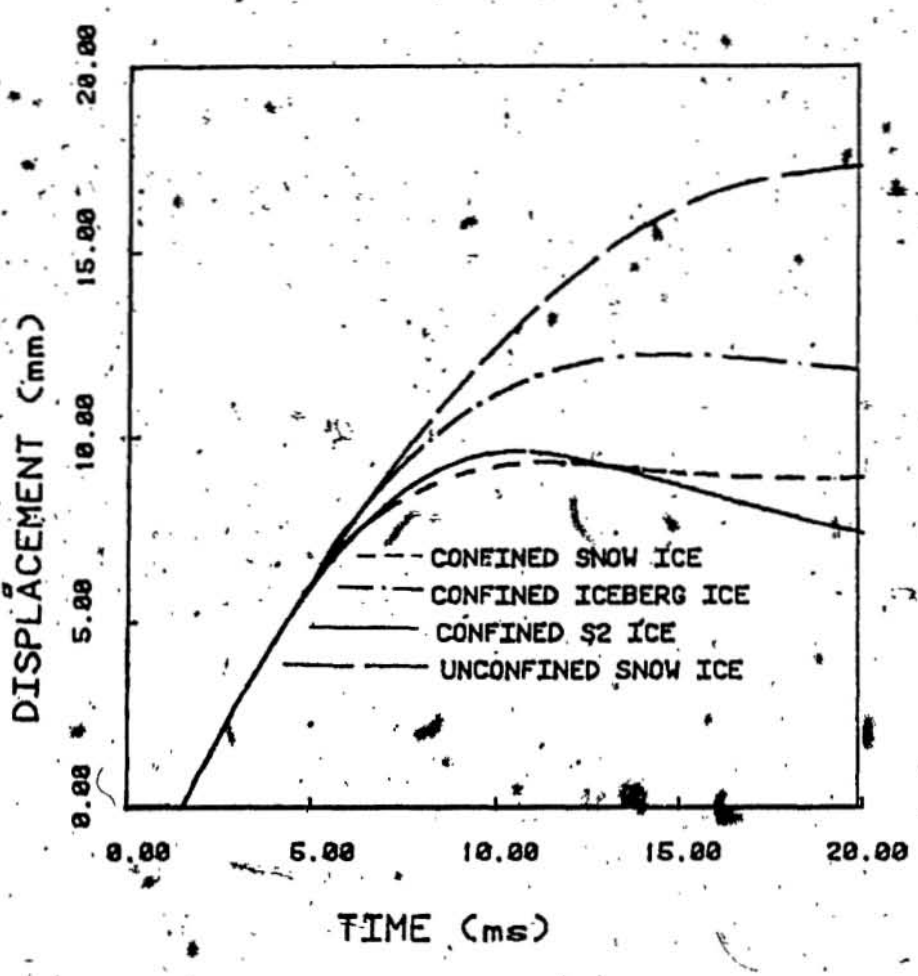

FIG. 3.36 INDENTOR DISPLACEMENT DURING IMPACT.

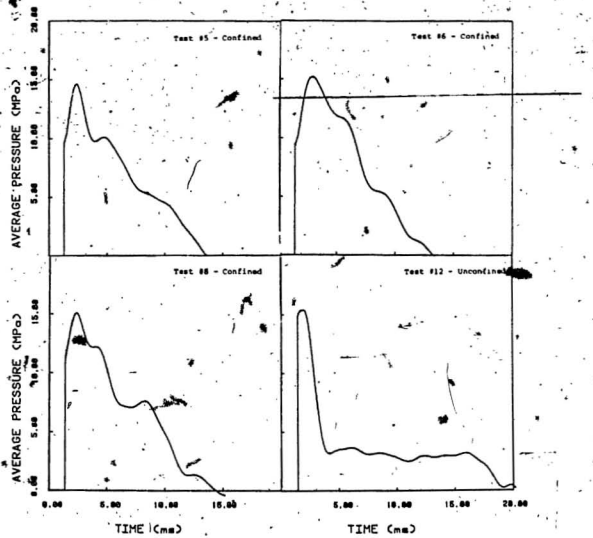

FIGURE 3.37 AVERAGE IMPACT PRESSURE - SNOW ICE.

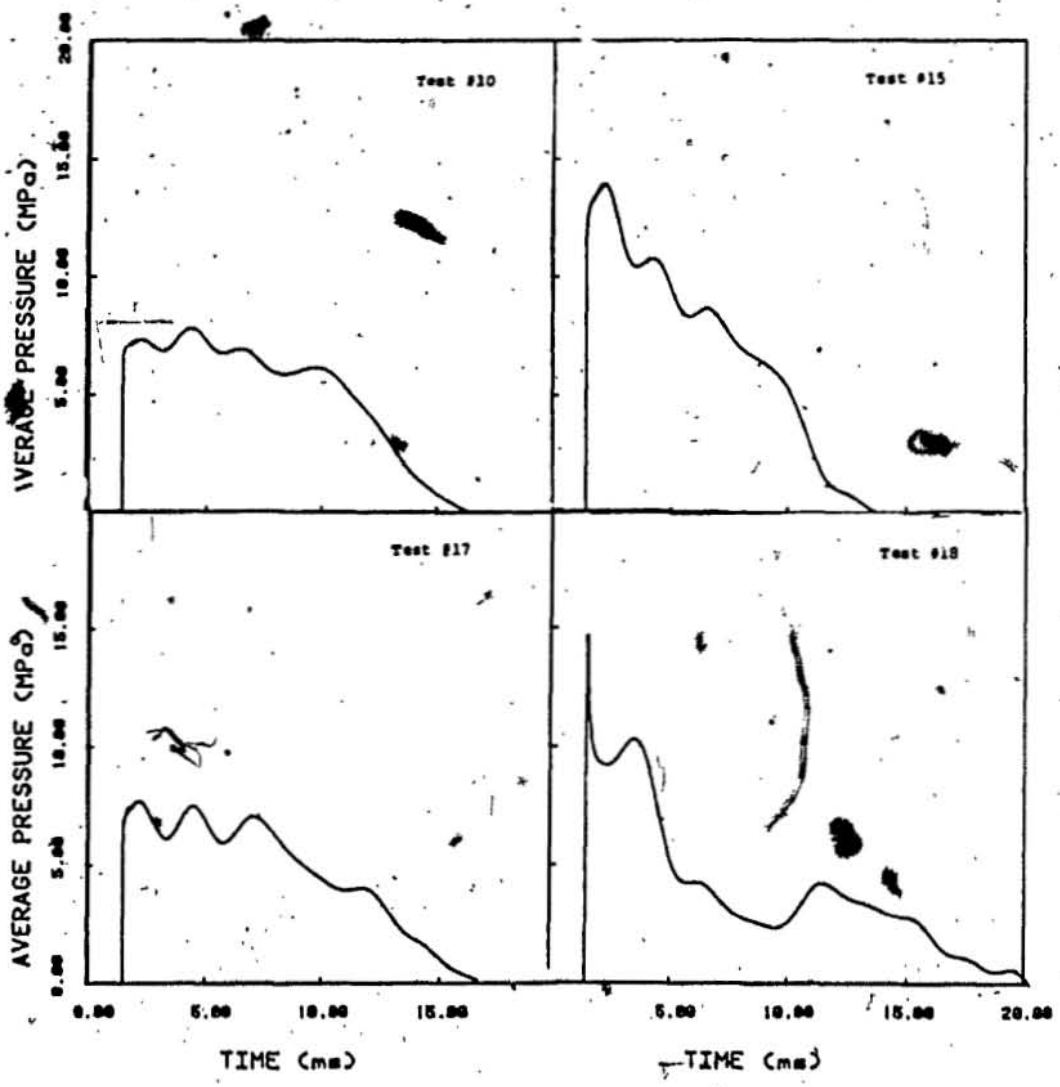

FIGURE 3.38 AVERAGE IMPACT PRESSURE - ICEBERG ICE.

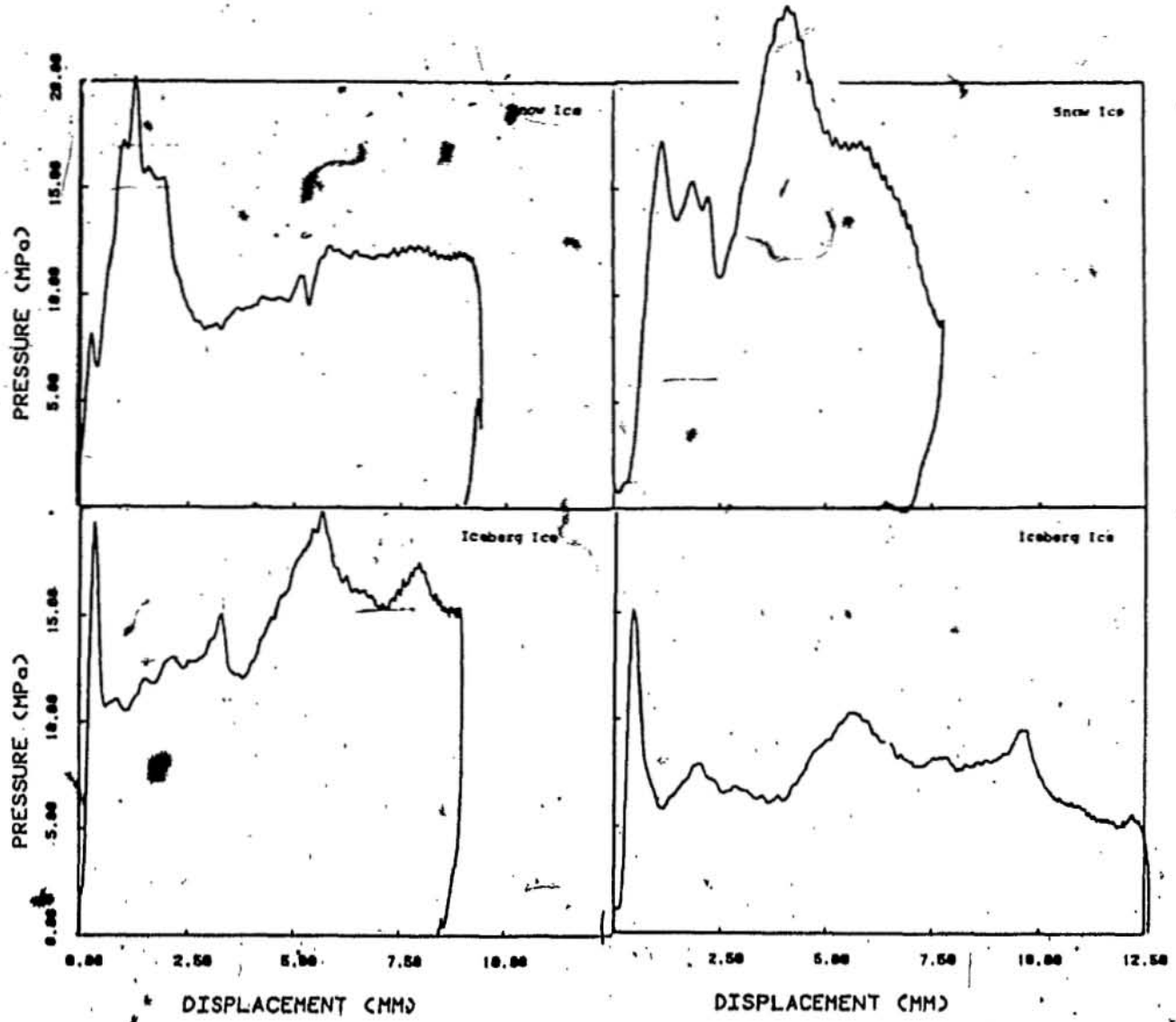

FIGURE 3.39 PRESSURE UNDER INDENTOR CENTRE VERSUS INDENTATION DEPTH.

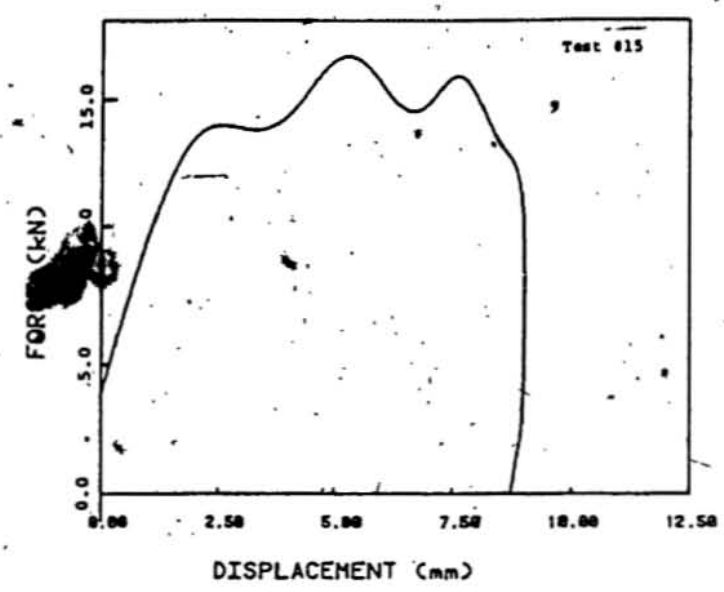

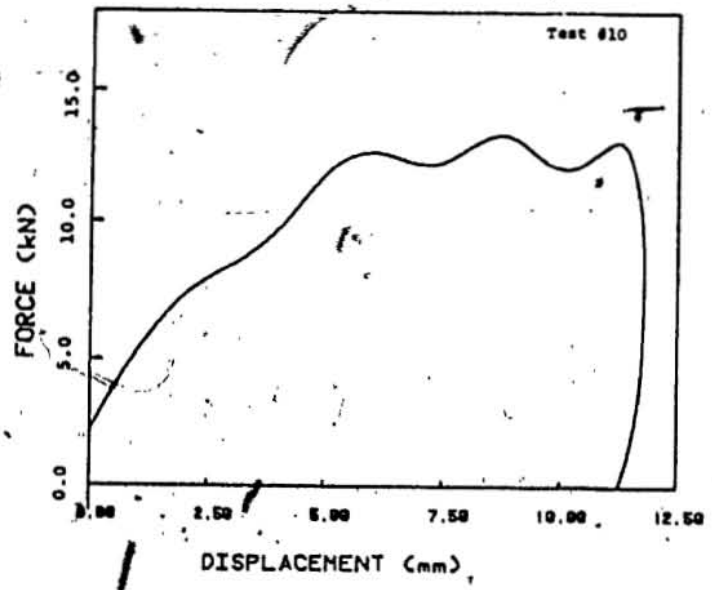

FIGURE 3.40 IMPACT LOAD VERSUS DISPLACEMENT FOR CONFINED ICEBERG ICE.

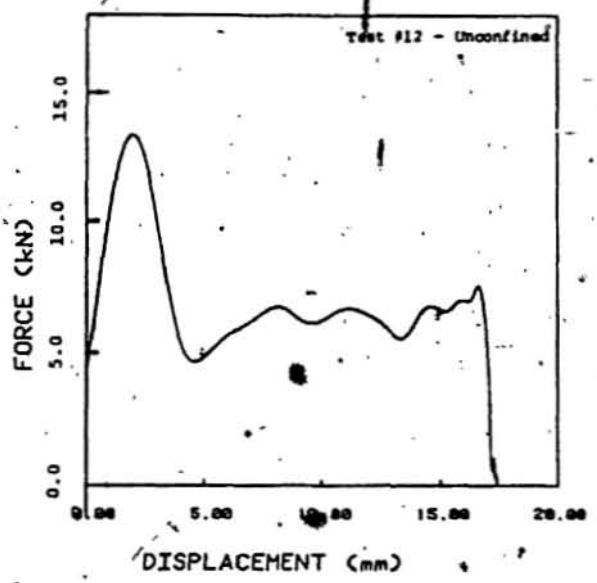

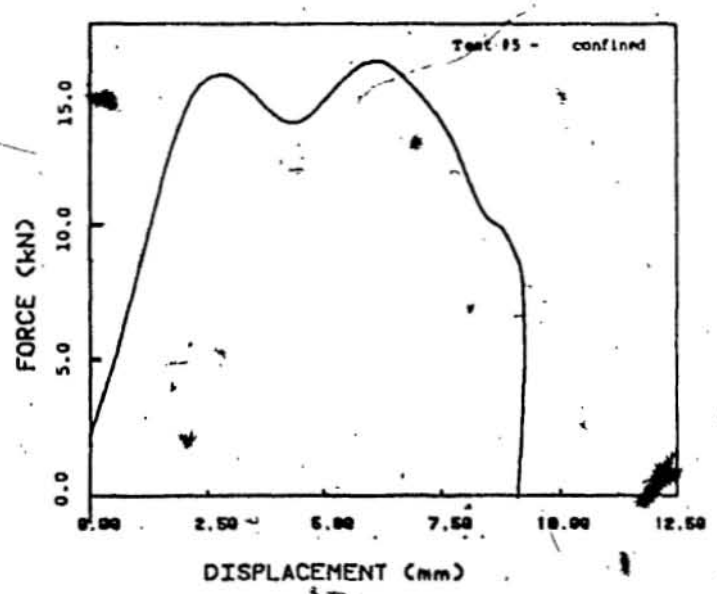

FIGURE 3.41 IMPACT LOAD VERSUS DISPLACEMENT FOR SNOW ICE

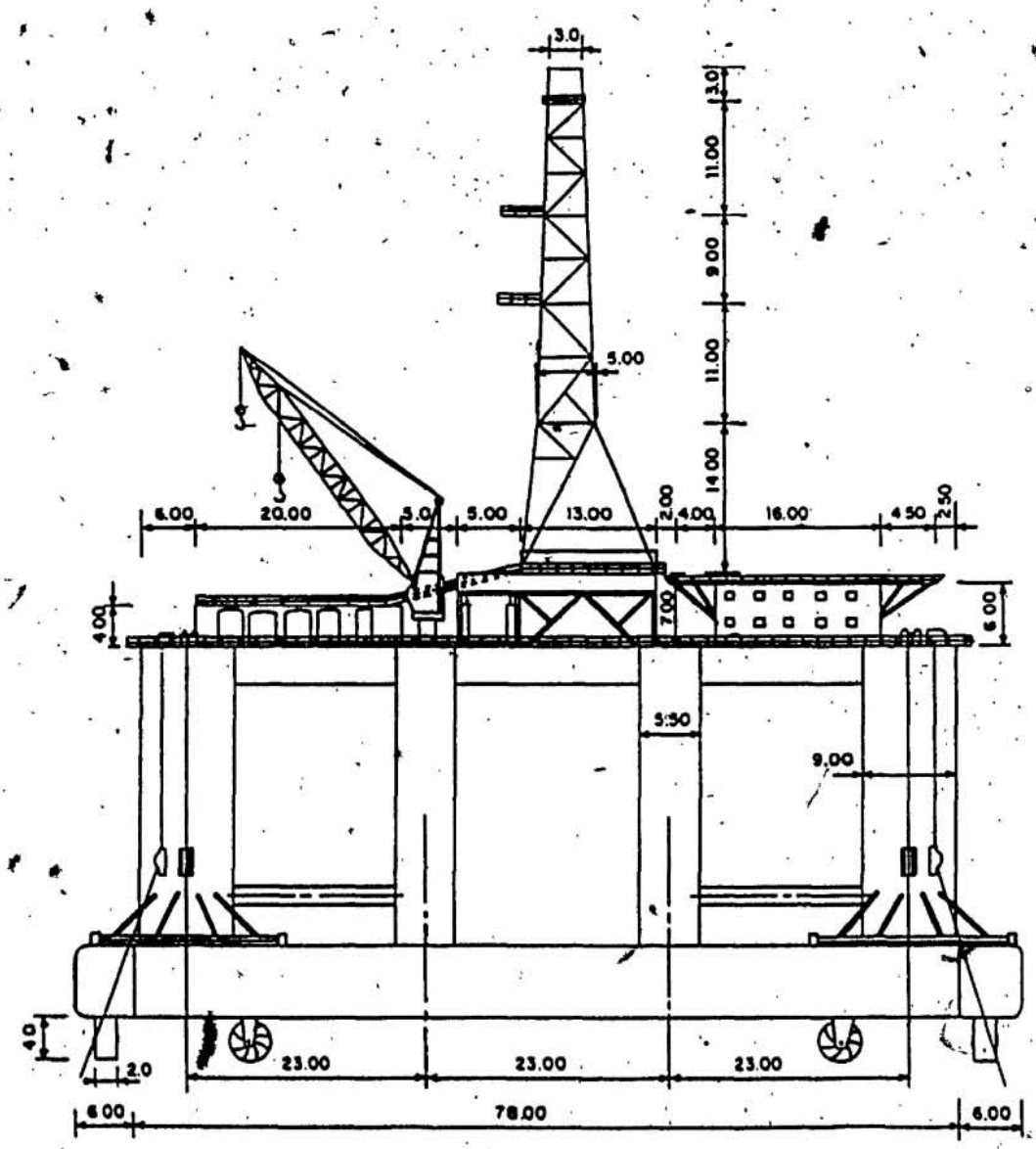

All dimensions in m

FIG. 4.1 SIDE VIEW OF THE TIM-77 SMI-SUBMERSIBLE

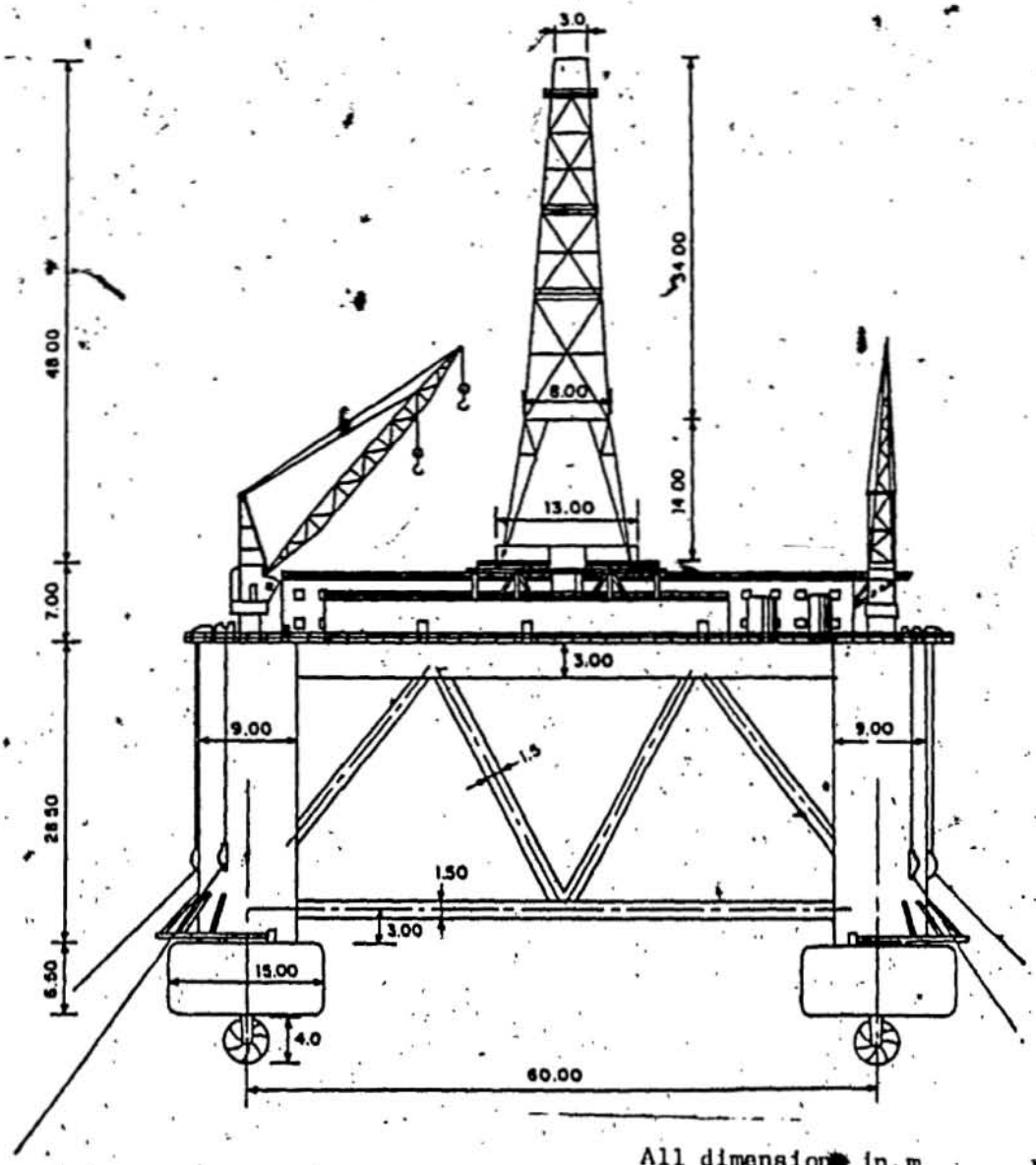

FIG. 4.2 END VIEW OF THE TIM-77 SEMI-SUBMERSIBLE

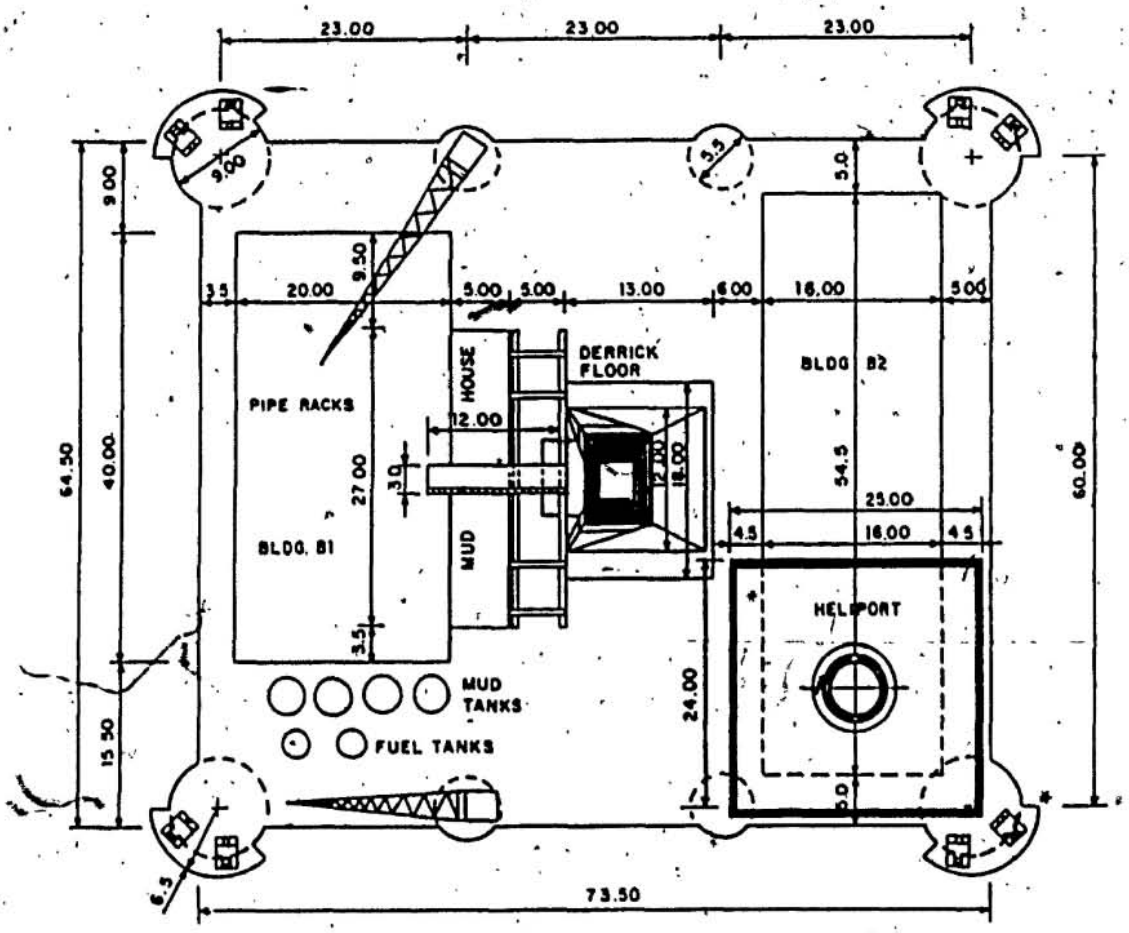

All dimensions in m

FIG. 4.3 DECK ARRANGEMENT FOR THE TIM-77 SEMI-SUBMERSIBLE

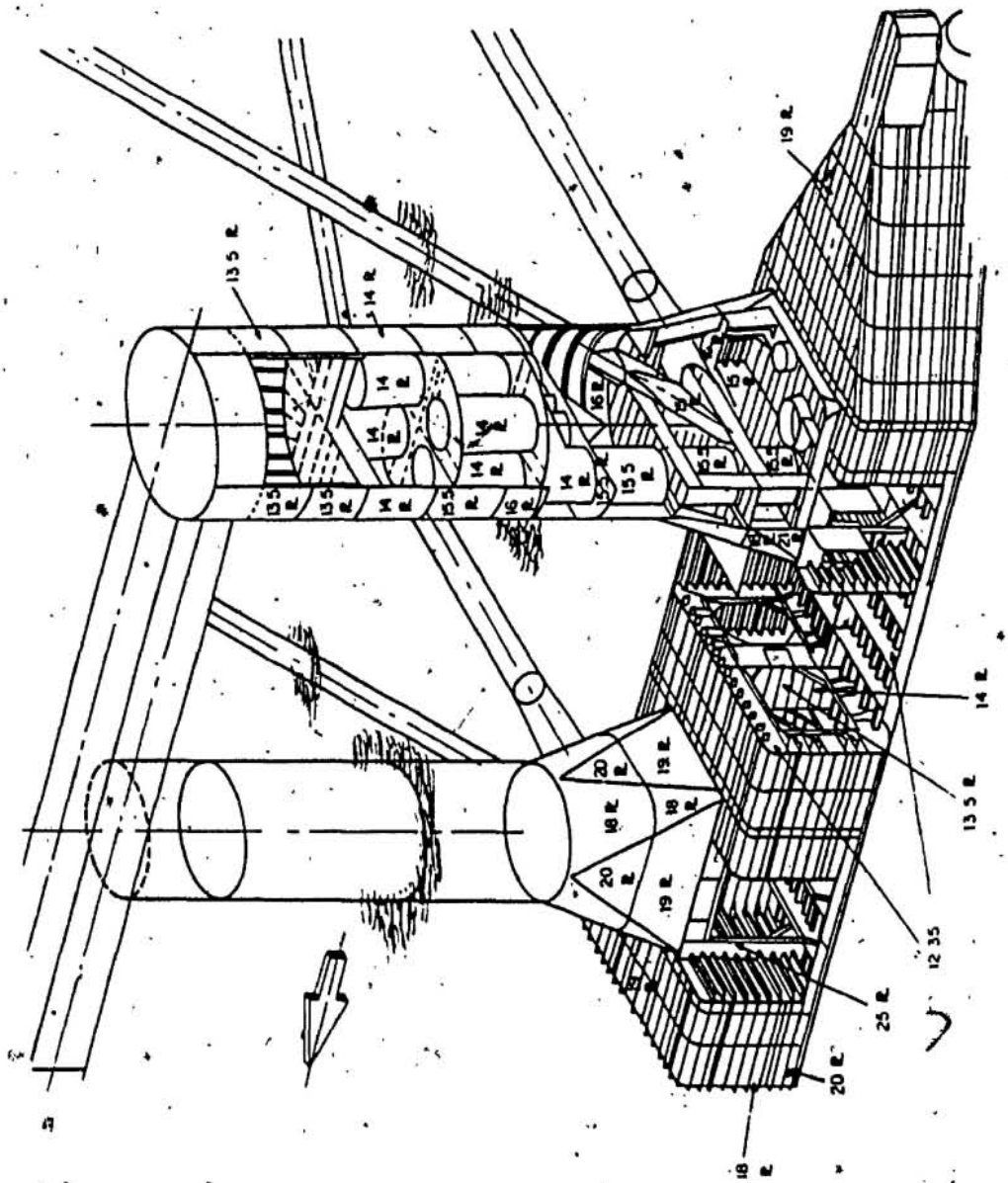

FIG. 4.4 STRUCTURAL DETAILS OF AKER-H3 SEMI-SUBMERSIBLE.

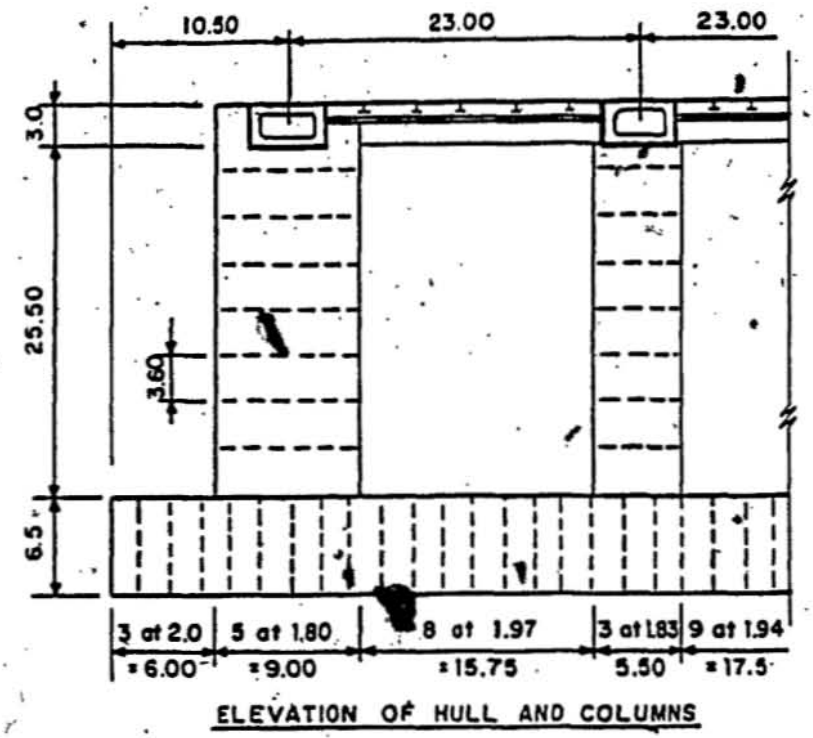

ELEVATION OF HULL AND COLUMNS

All dimensions in m

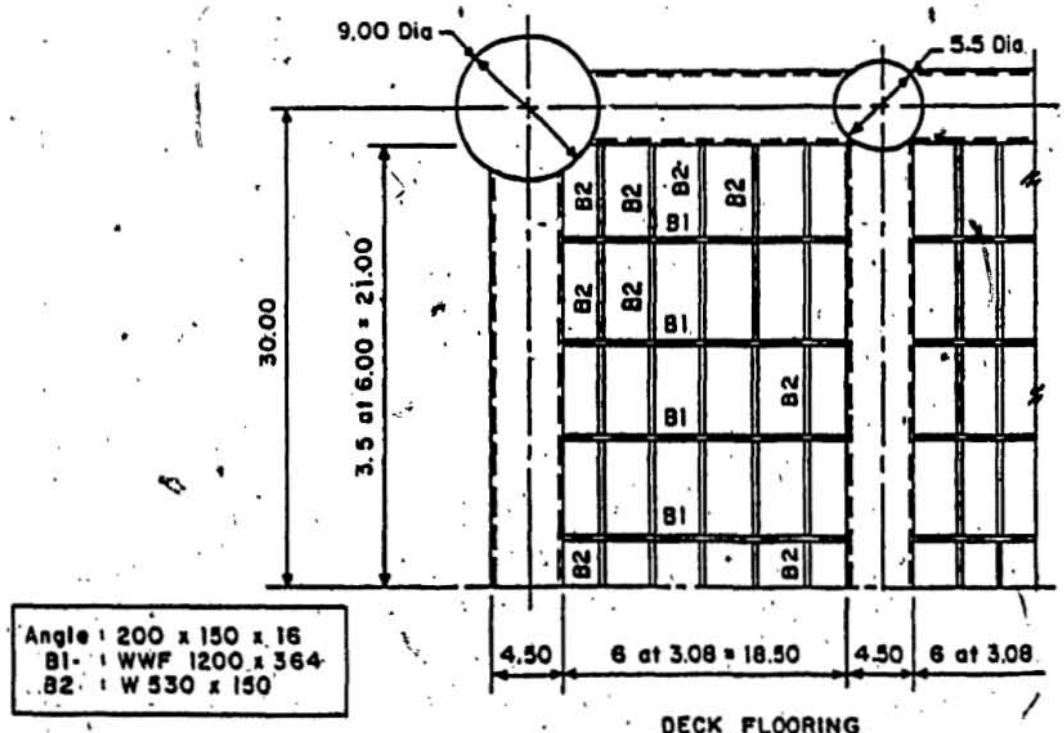

DECK FLOORING

FIG. 4.5 DETAILS OF DECK FLOORING, HULL AND COLUMNS OF THE PIM-77 SEMI-SUBMERSIBLE

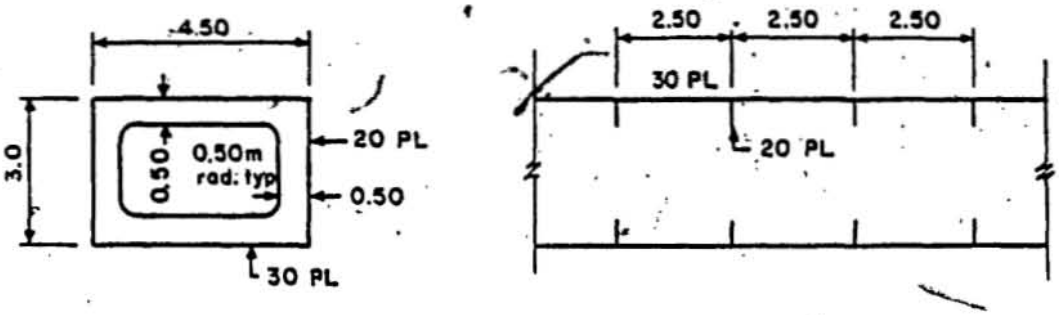

BOX GIRDER - (DECK BULKHEAD)

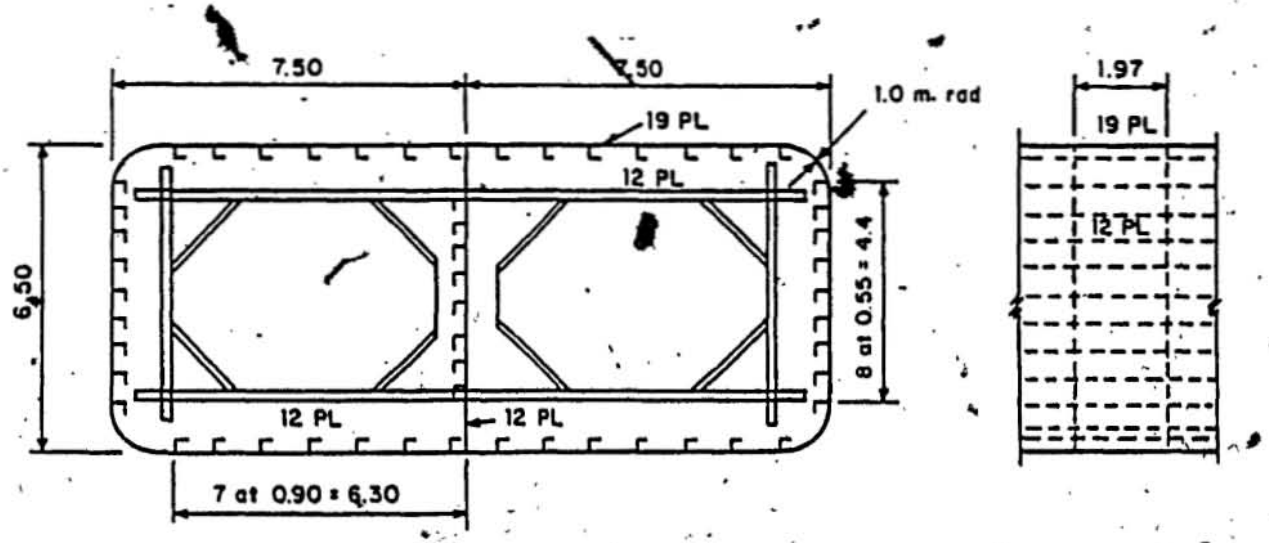

HULL

Note:

All angles in hull 200 x 150 x 16

All dimensions in m

FIG. 4.6 STRUCTURAL DETAILING OF HULL AND DECK GIRDER

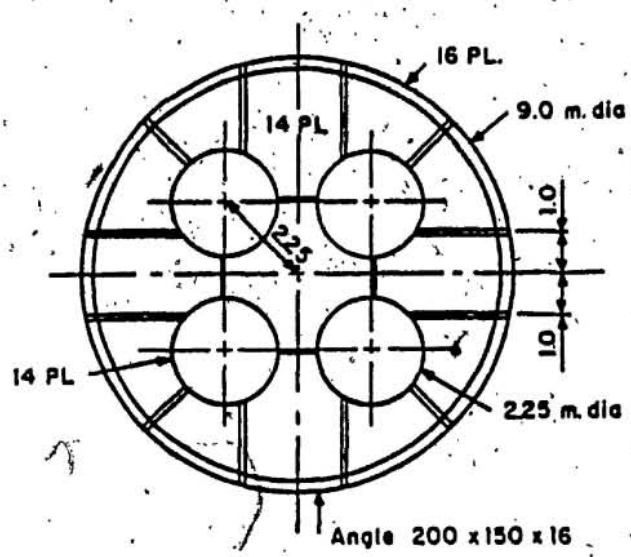

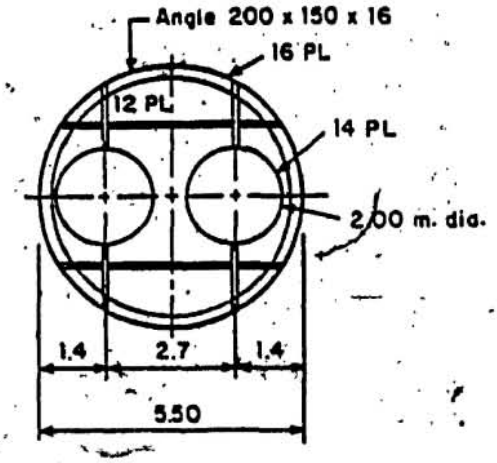

INTERMEDIATE COLUMN

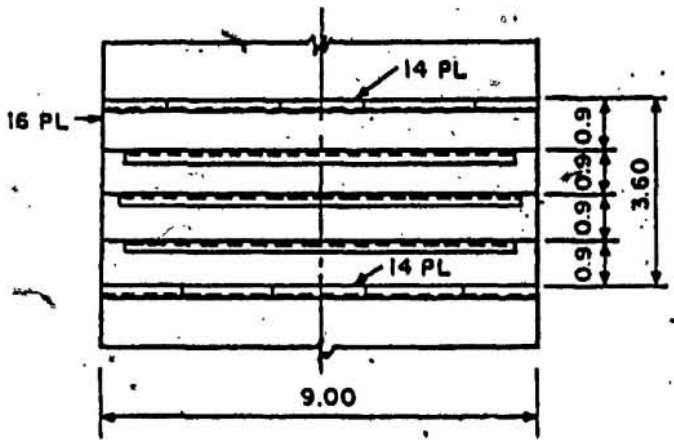

MAIN COLUMN

NOTE

1. Same detailing in elevation as main column
2. All angles in columns 200 x 150 x 16
3. All dimensions in m

FIG. 4.7 STRUCTURAL DETAILING OF COLUMNS

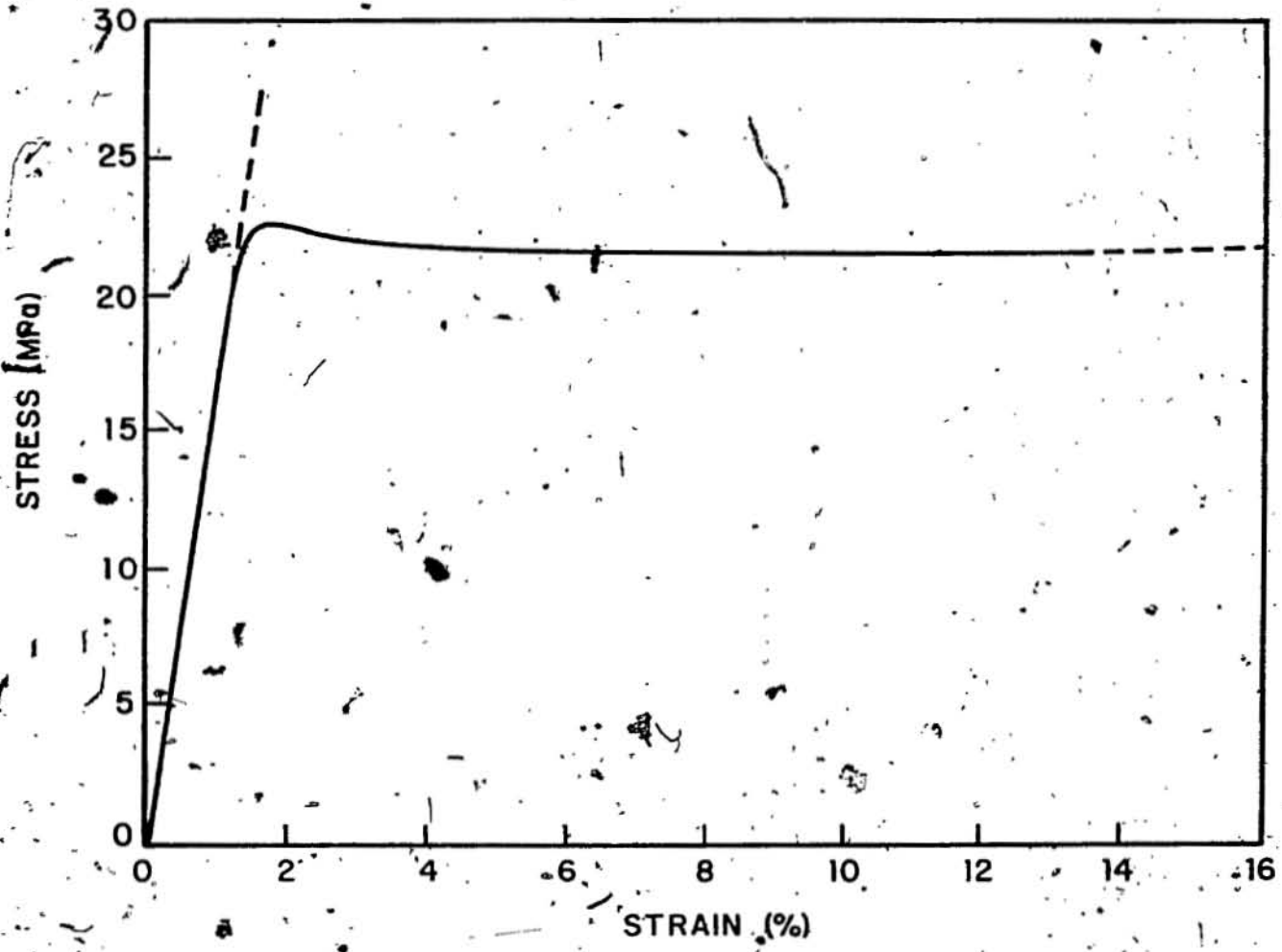

FIG. 4.8 TYPICAL STRESS-STRAIN CURVE FOR POLYSTYRENE SHEETS

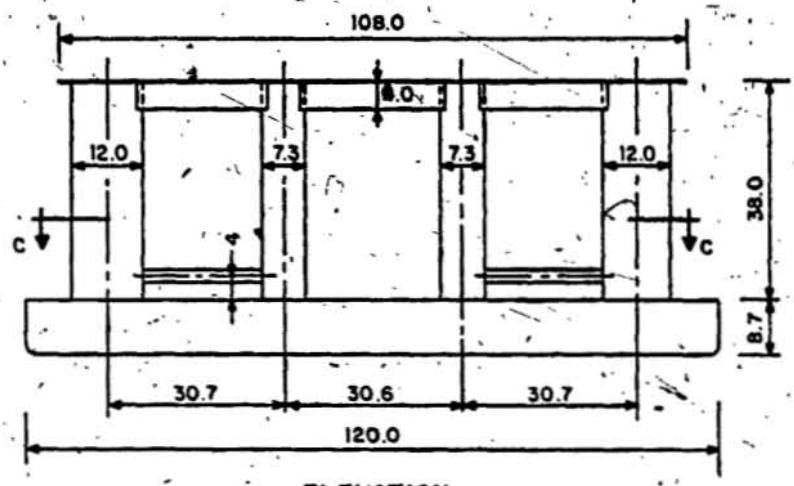

ELEVATION

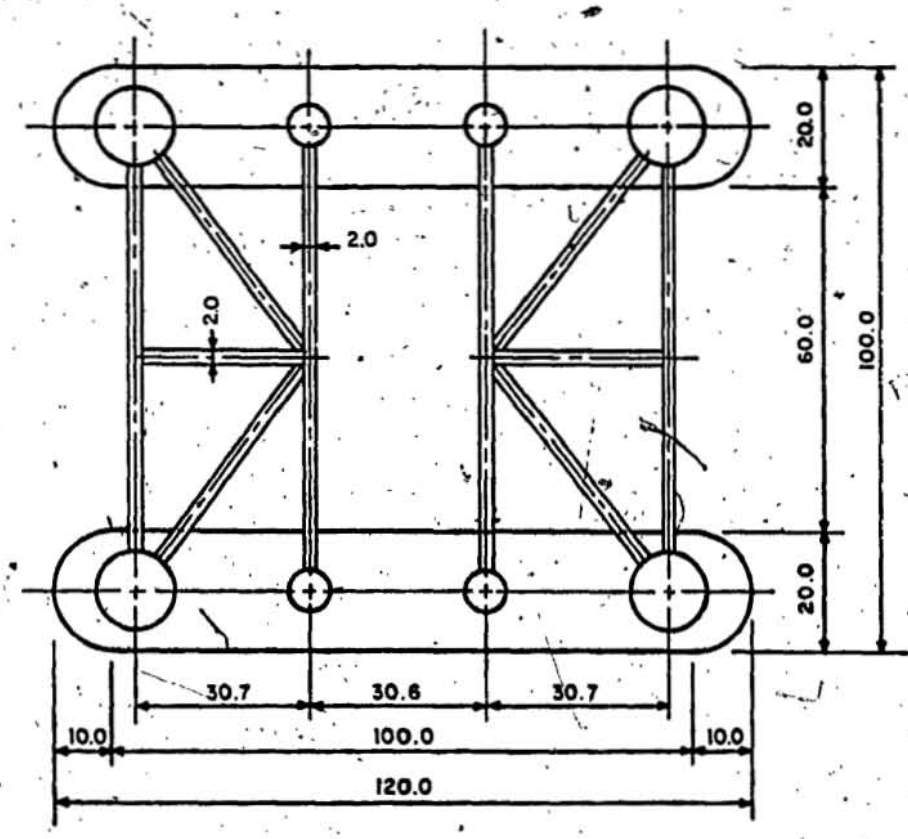

SECTIONAL PLAN C-C

ALL DIMENSIONS IN CM

FIG. 4.9 a MODEL DIMENSIONS

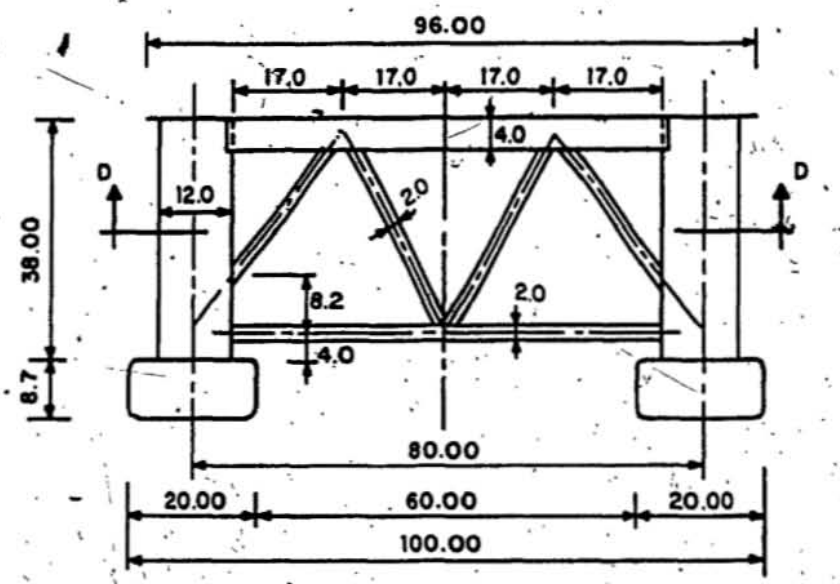

SIDE VIEW

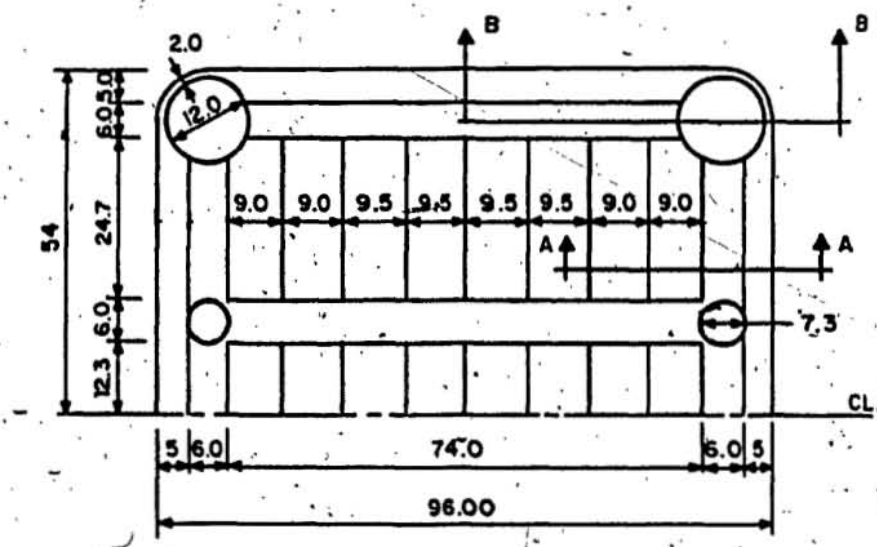

SECTION D-D

ALL DIMENSIONS IN CM.

FIG. 4.9 b ARRANGEMENTS OF MODEL DECK

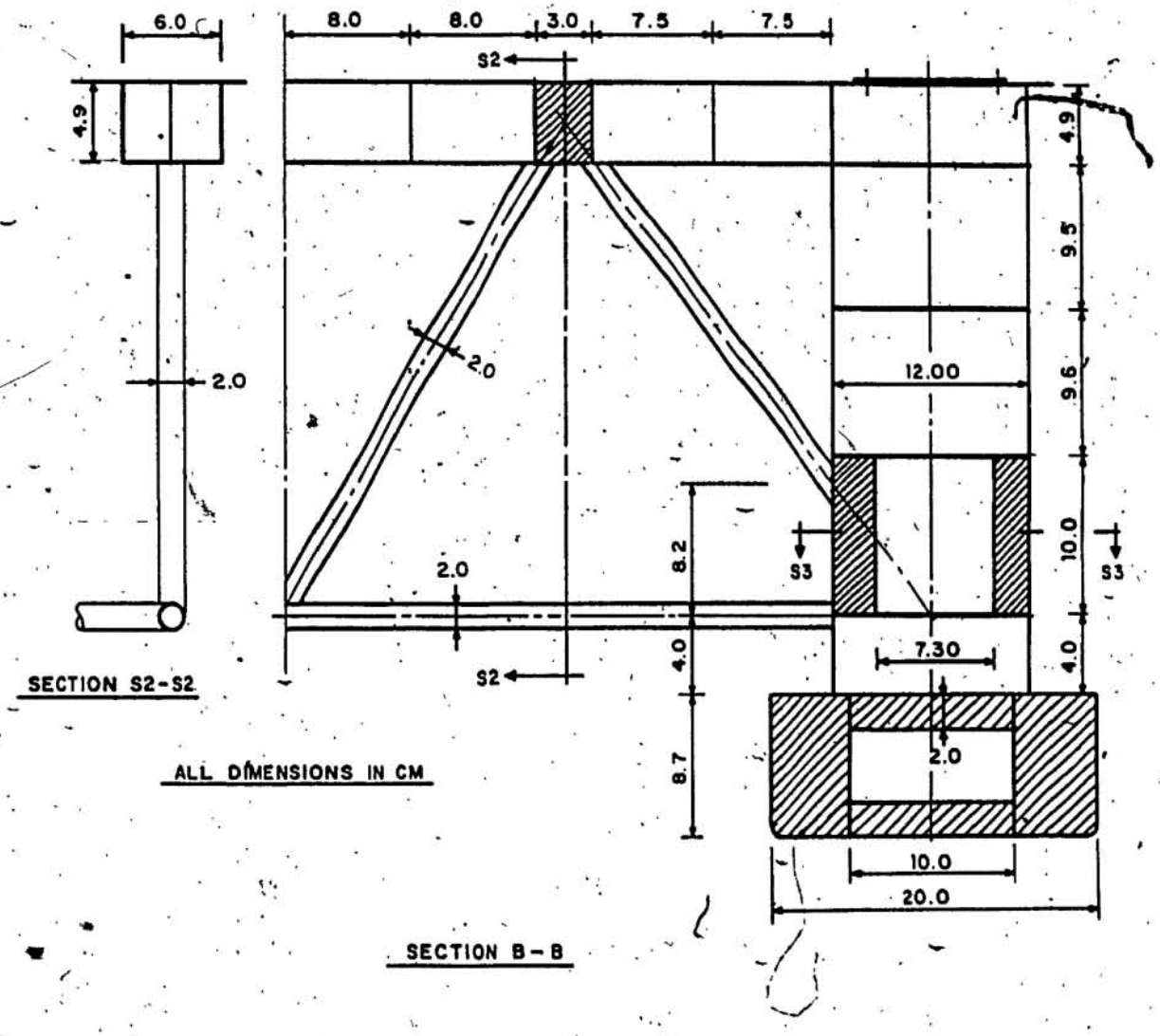

FIG. 4.9 c STRUCTURAL DETAILS OF THE MODEL

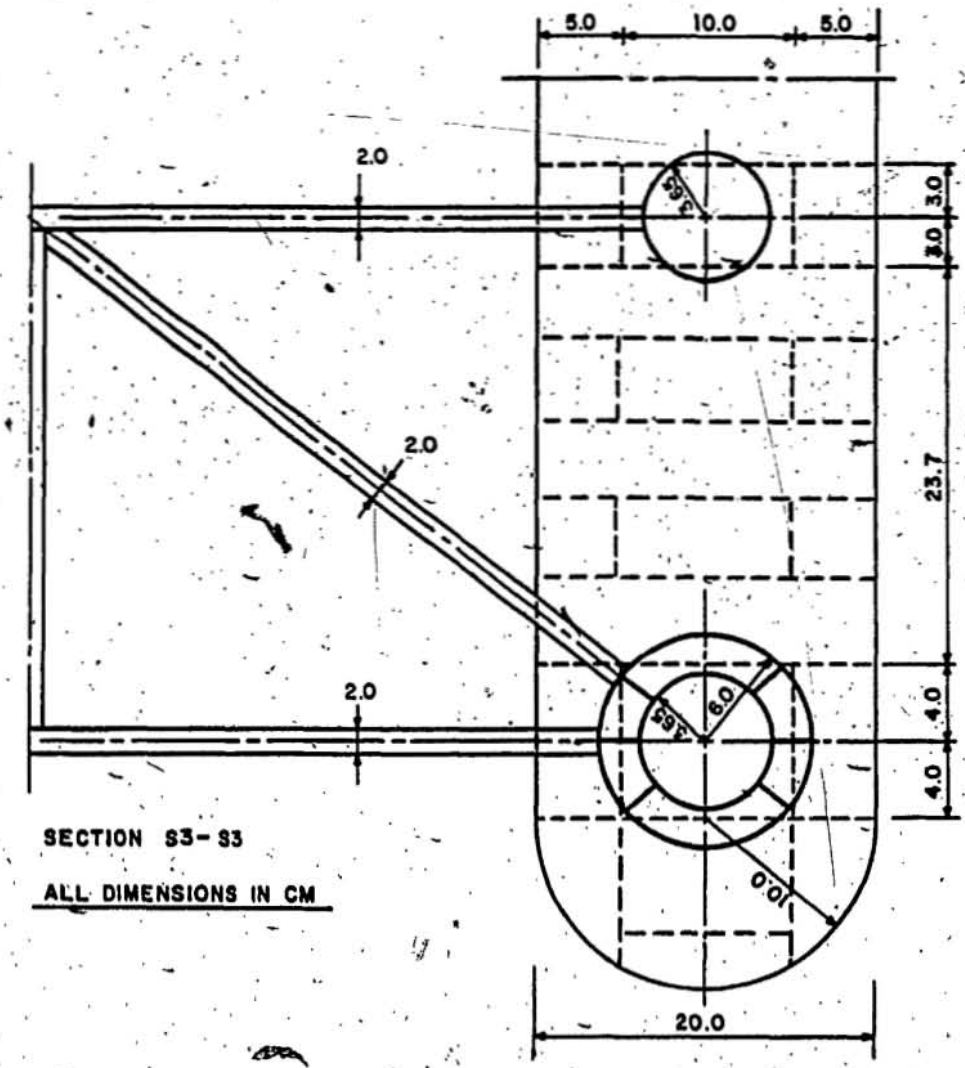

FIG. 4.9 d PONTOON COMPARTMENTS

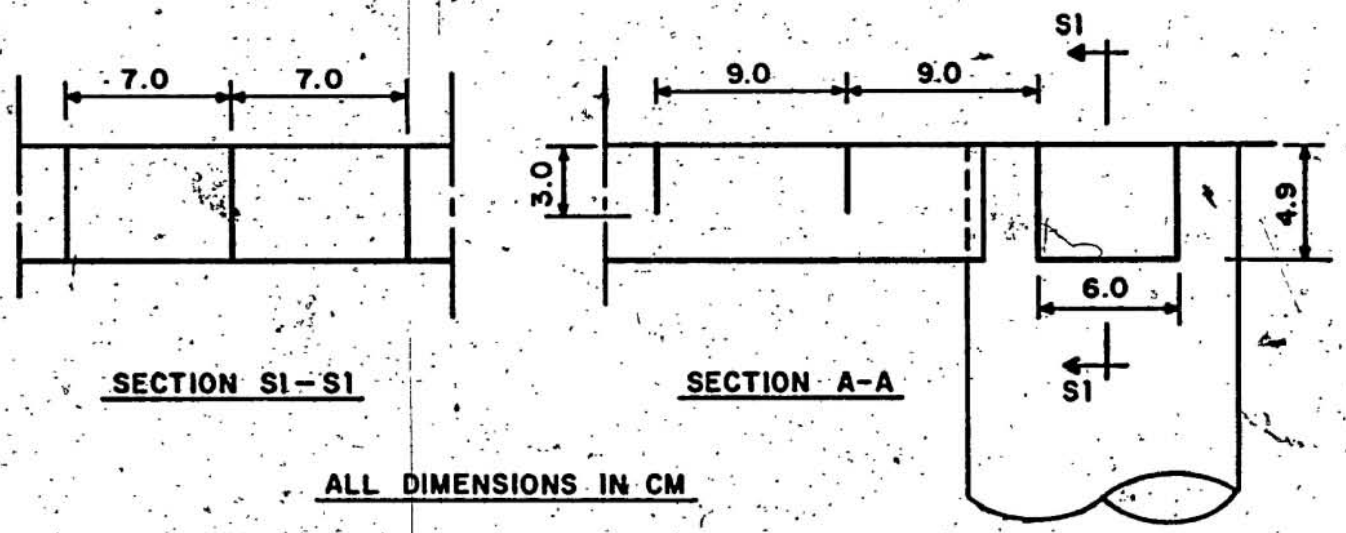

FIG. 4.9 e DETAILS OF MAIN GIRDER AND DECK FLOORING

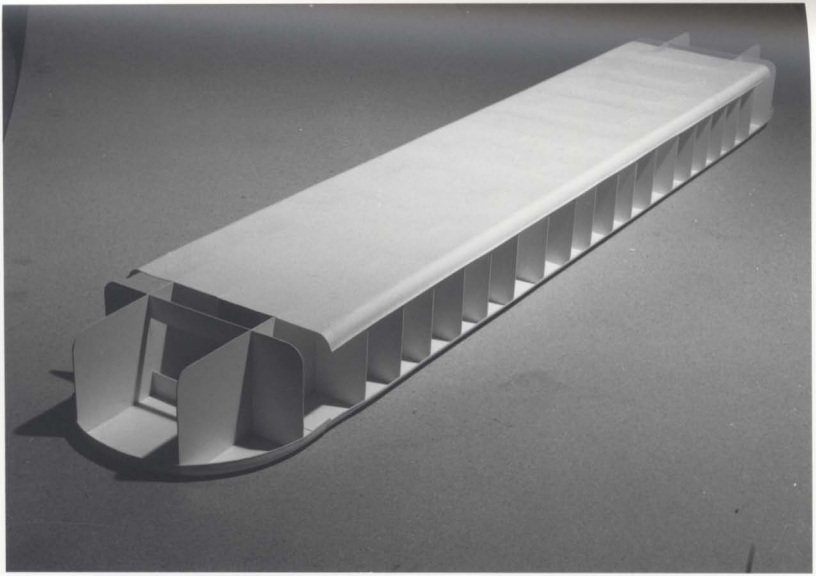

FIG. 4.10 INTERNAL ARRANGEMENTS OF THE PONTOON.

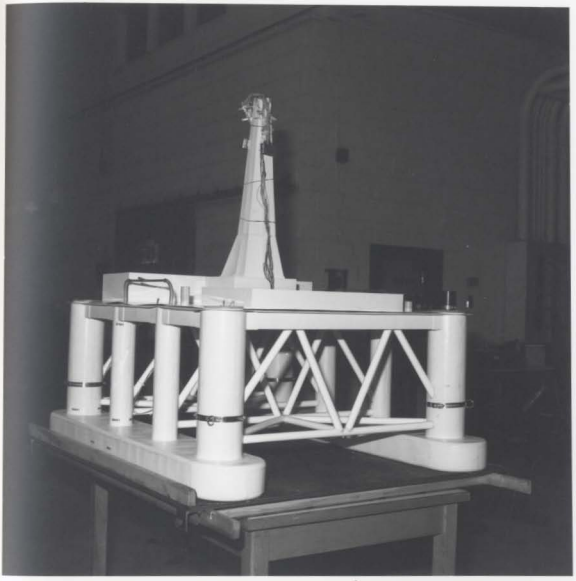

FIG. 4.11 THE HYDROELASTIC MODEL.

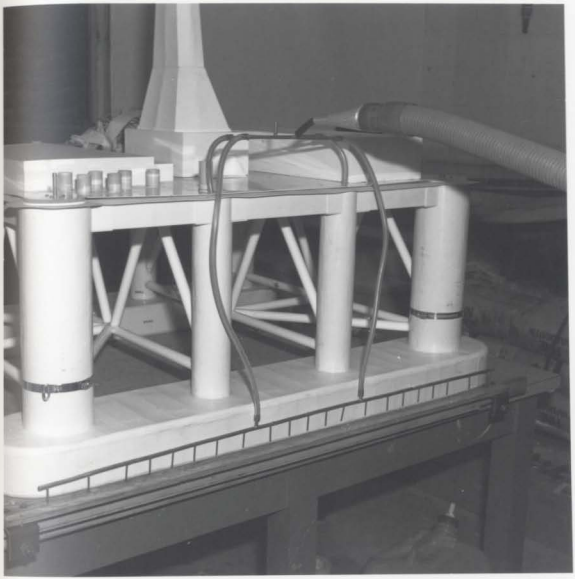

FIG. 4.12 THE DRAINAGE SYSTEM.

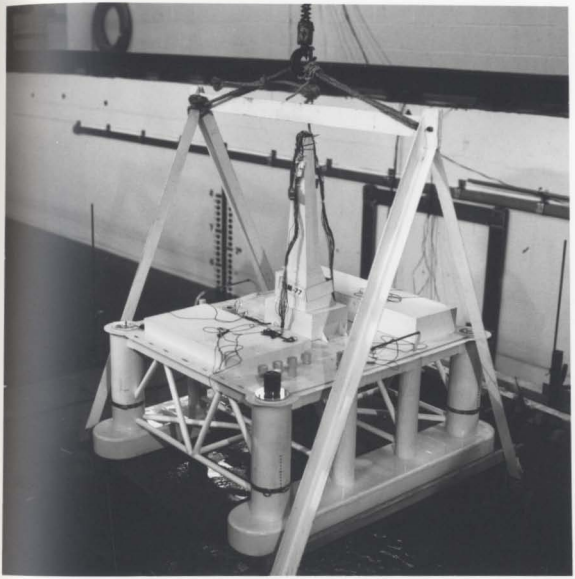

FIG. 4.13 THE CARRYING PLATFORM.

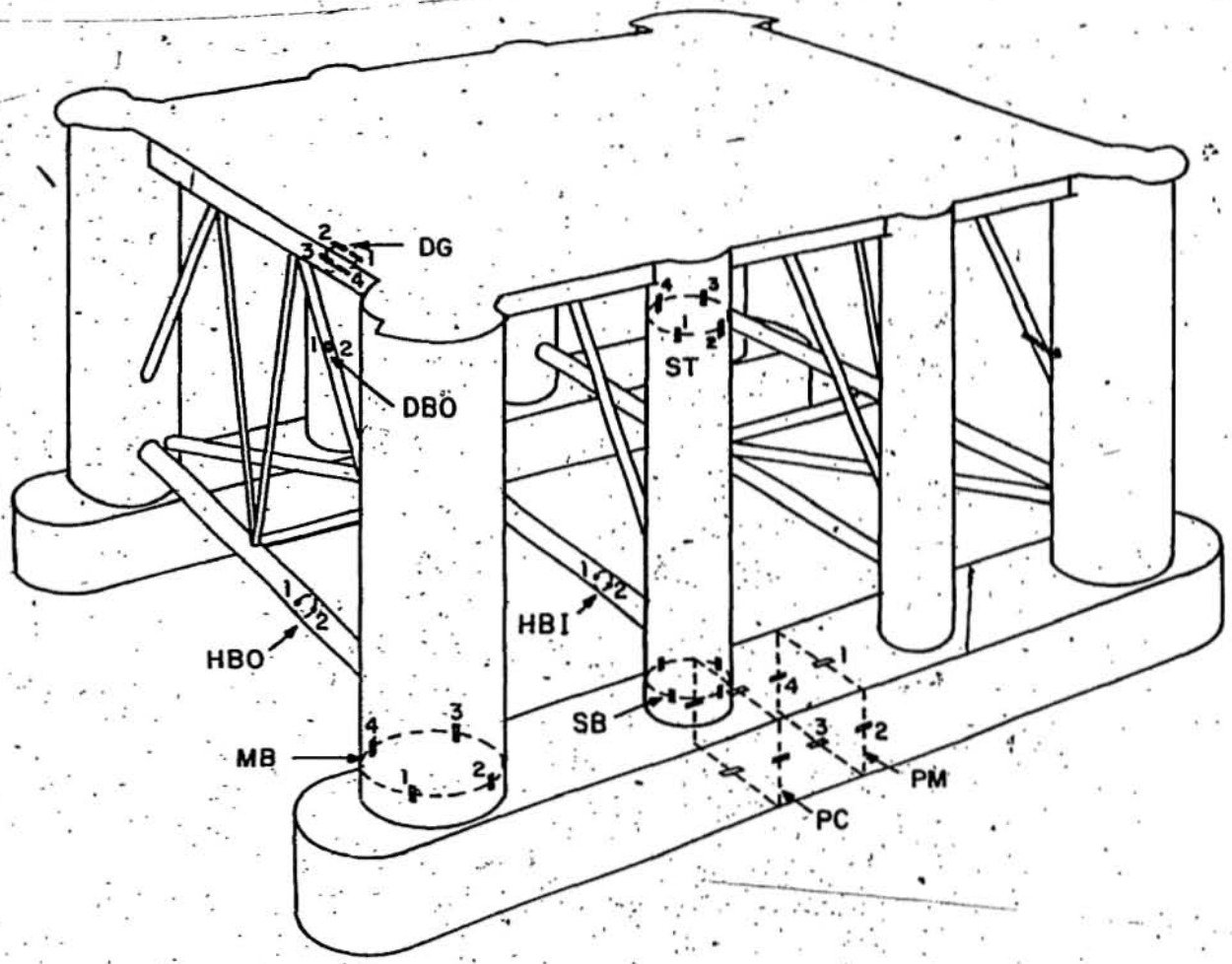

FIG. 4.14 STRAIN GAUGE LOCATIONS ON THE MODEL

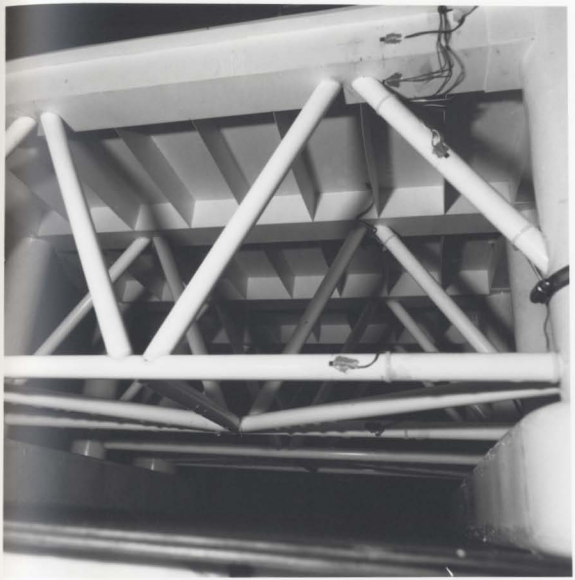

FIG. 4.15 STRAIN GAUGES ON THE DECK AND THE BRACINGS.

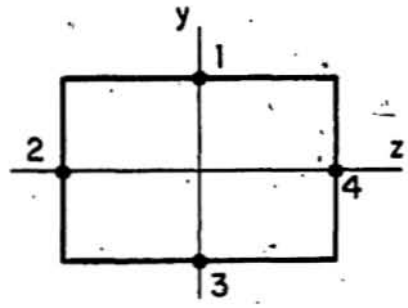

RECTANGULAR SECTIONS

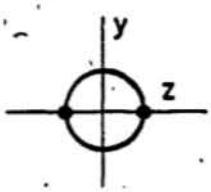

BRACING SECTIONS

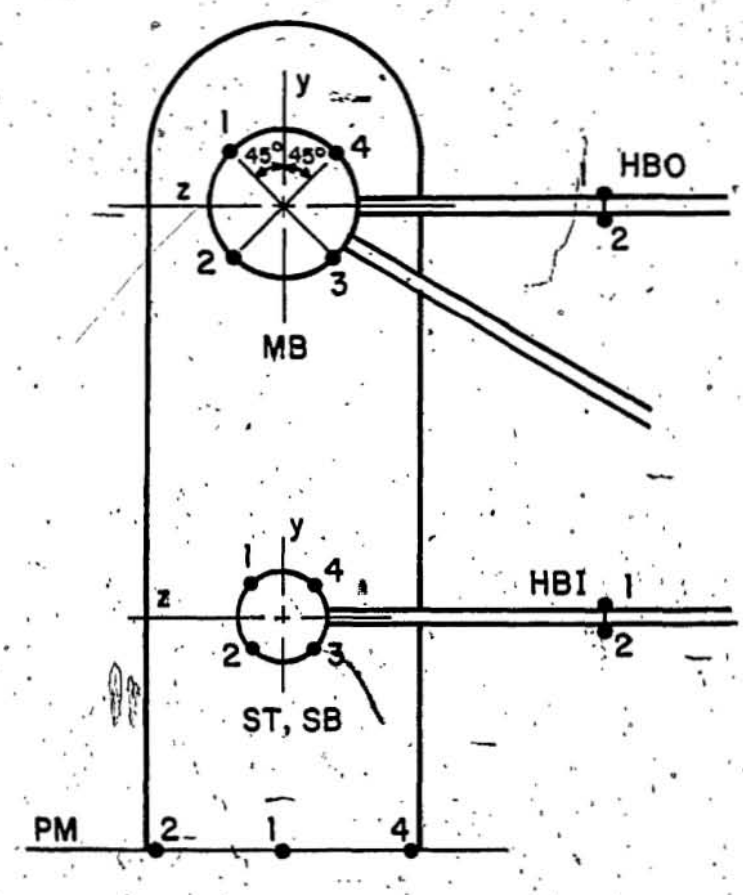

FIG. 4.16 LOCAL AXES FOR INSTRUMENTED SECTIONS

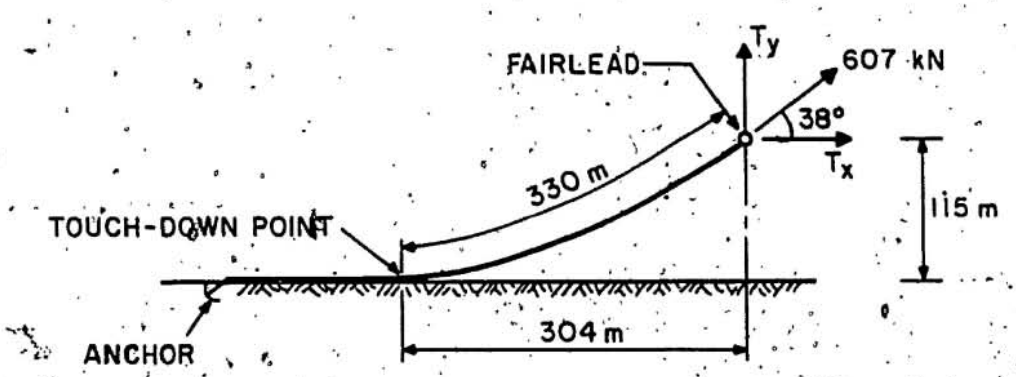

FIG.4.17. MOORING CHAIN PROFILE

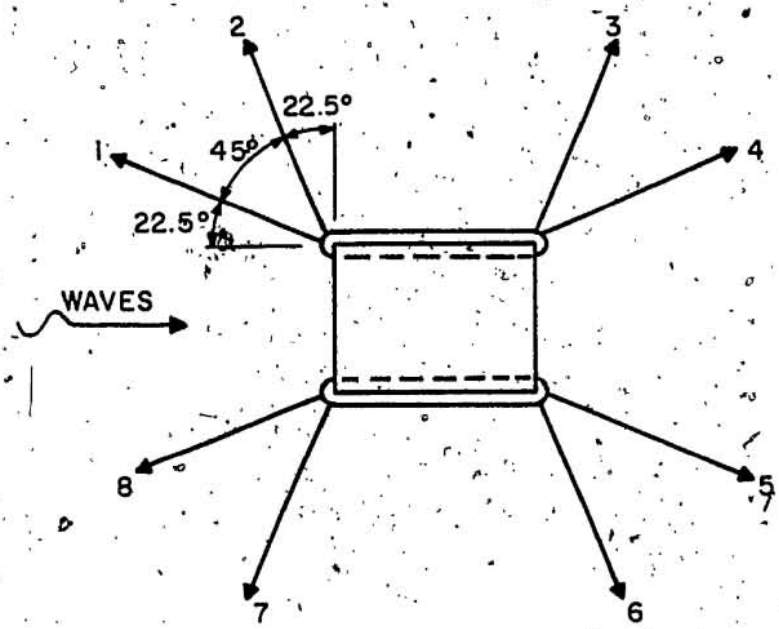

FIG.4.18 PROTOTYPE MOORING PATTERN

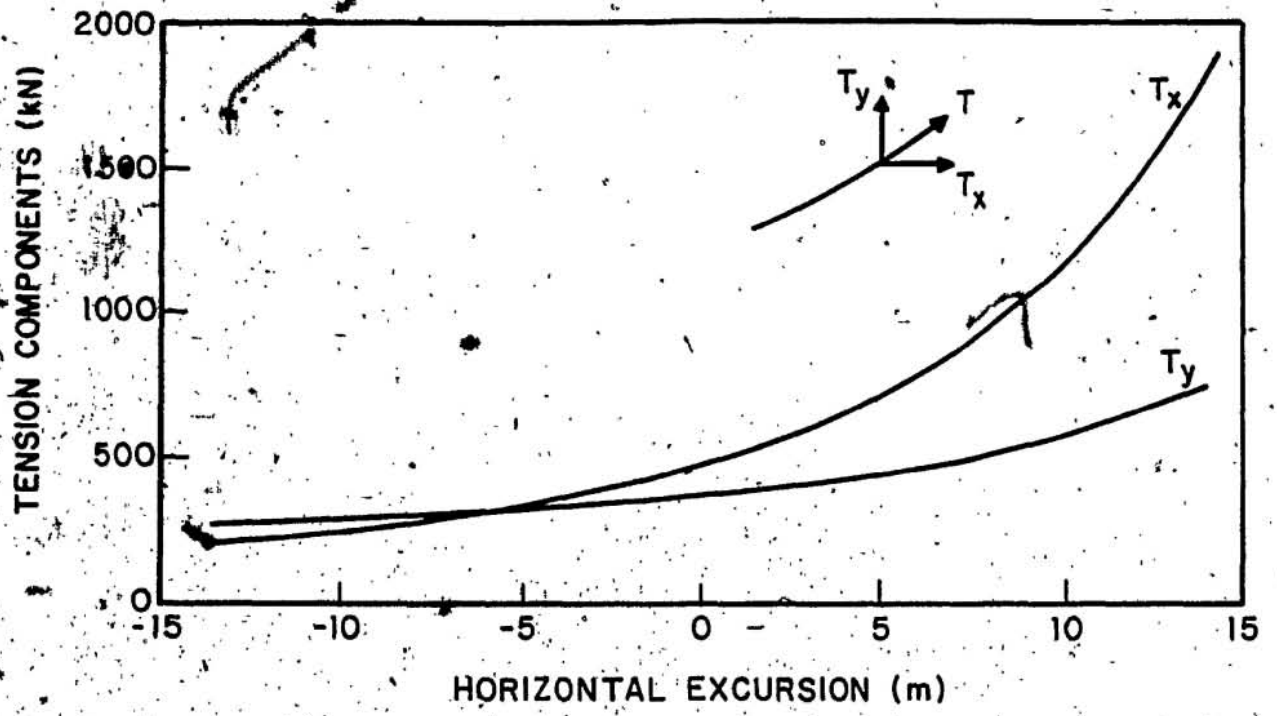

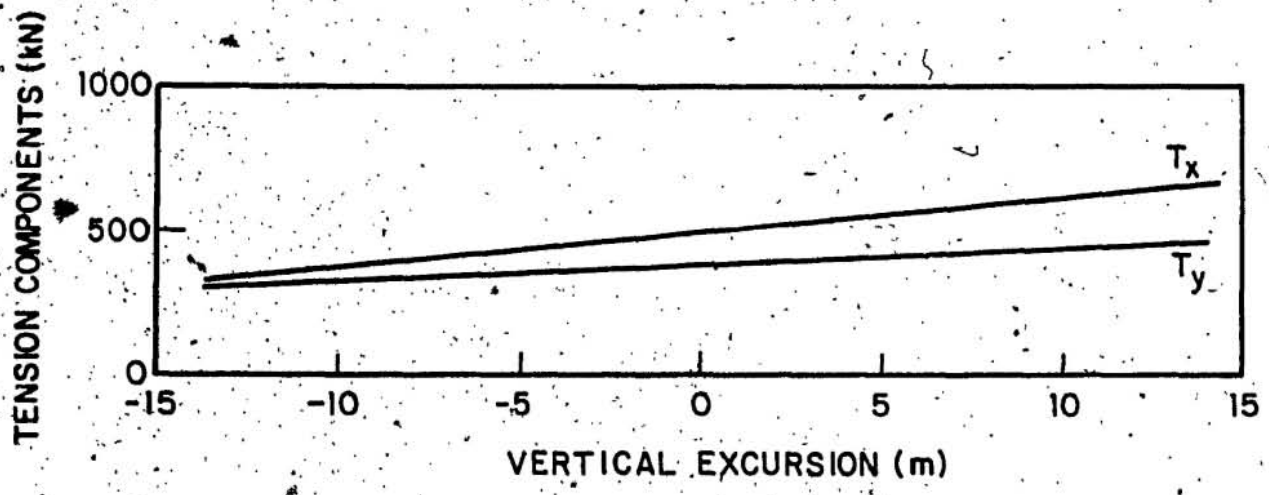

FIG. 4.19 COMPONENTS OF MOORING CHAIN FORCE AT THE FAIRLEADS VS. HORIZONTAL AND VERTICAL EXCURSION FROM PLATFORM NEUTRAL POSITION

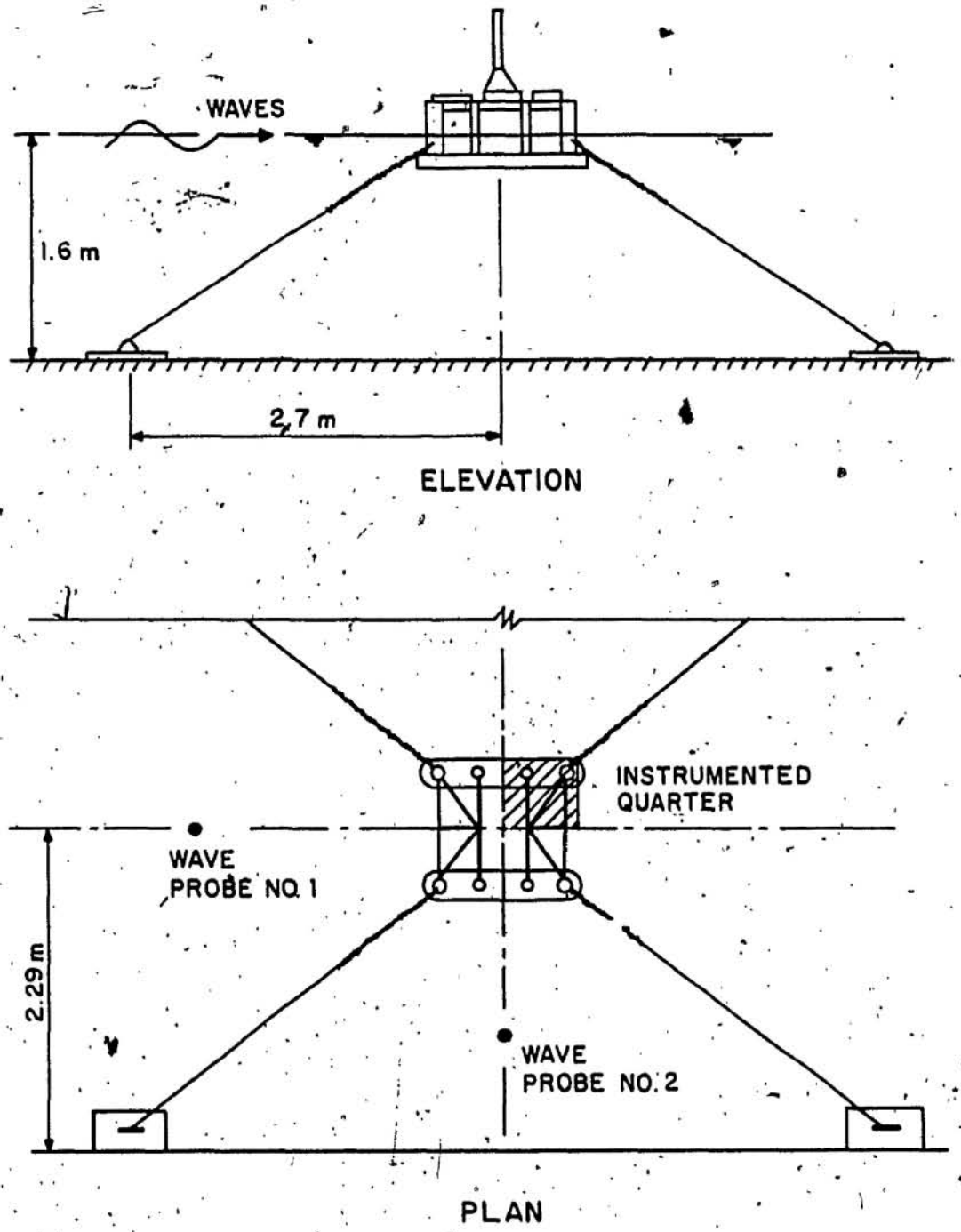

FIG. 4.20 MOORING SYSTEM FOR THE MODEL

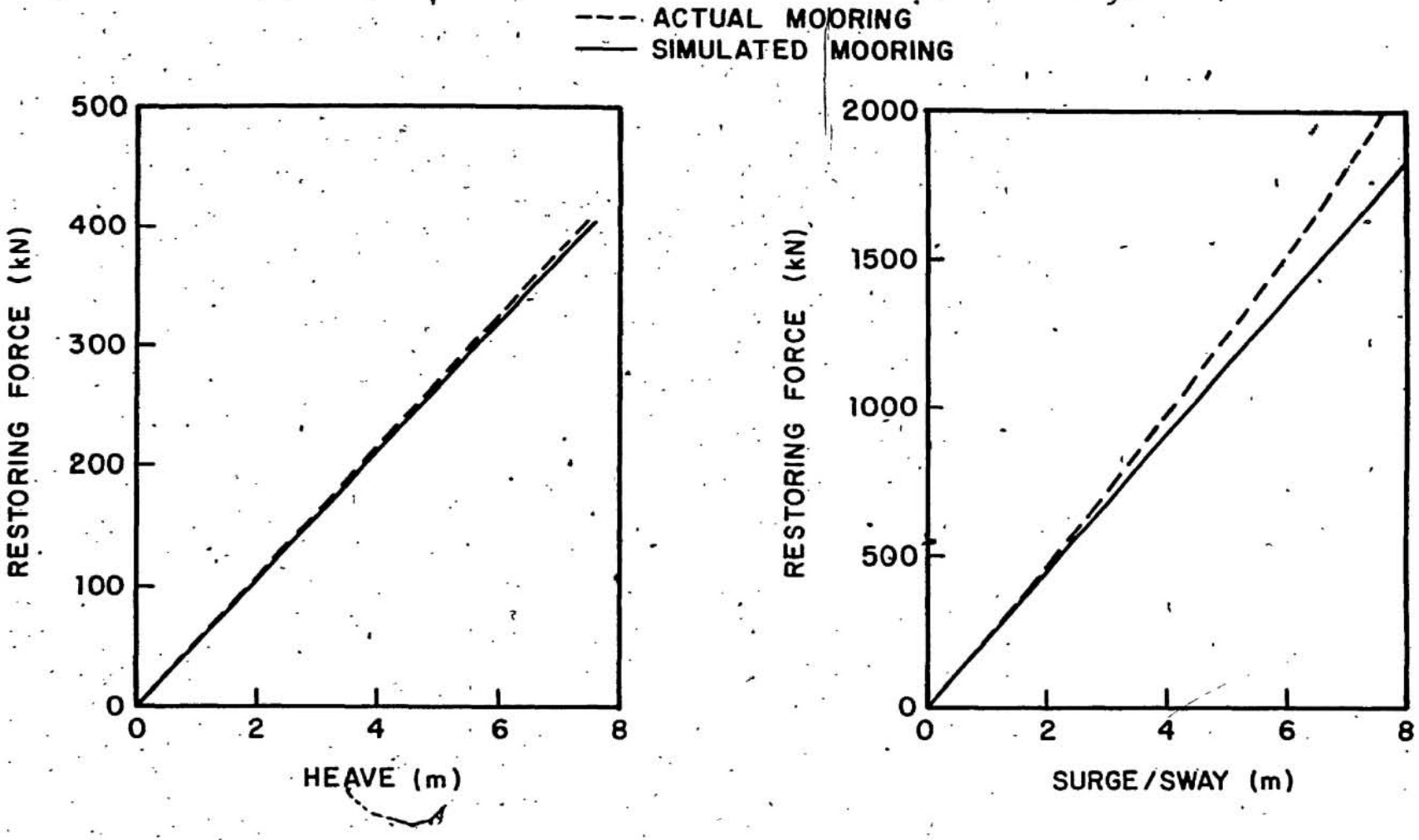

FIG. 4.21 ACTUAL AND SIMULATED RESTORING FORCES OF THE MOORING SYSTEM.

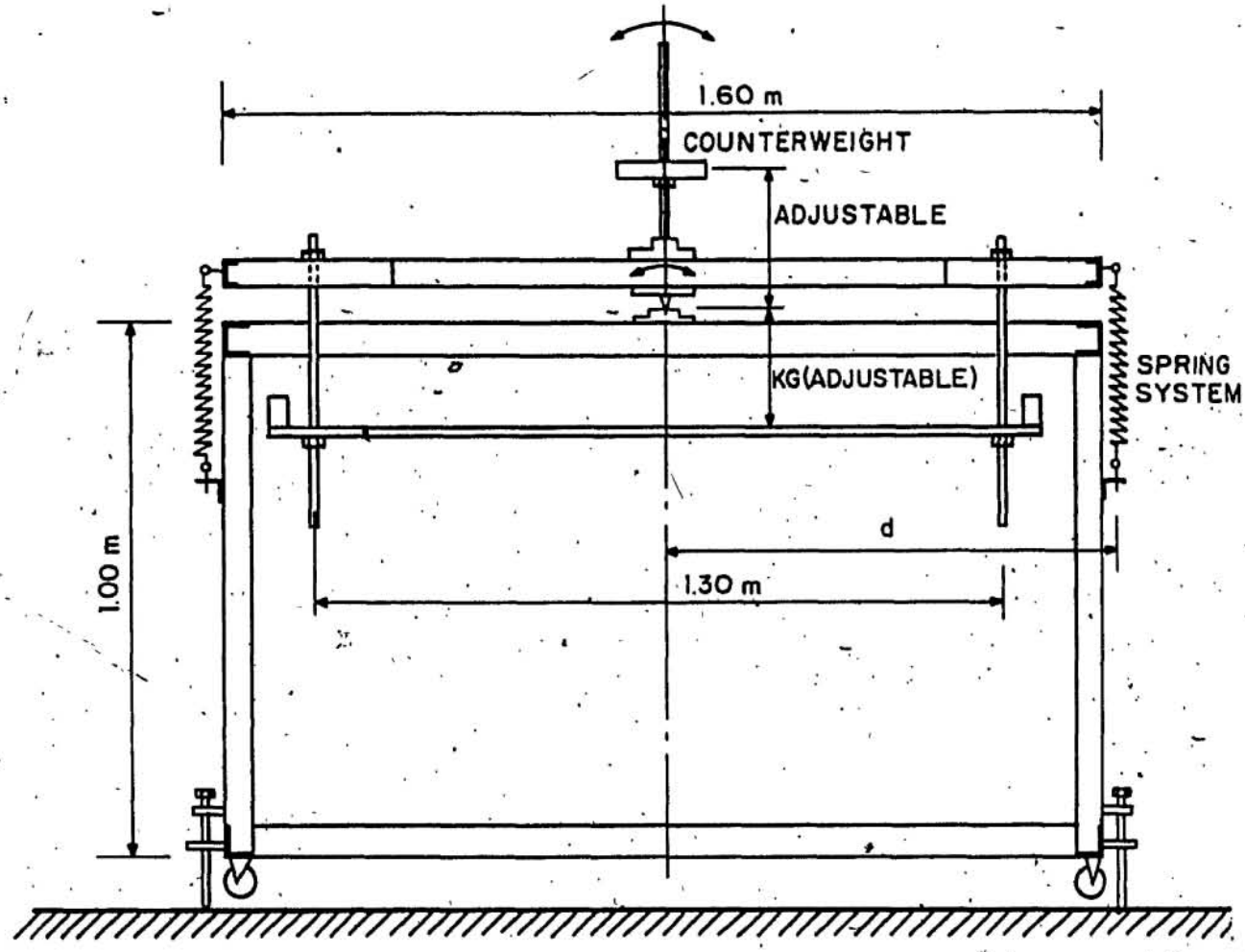

FIG.4.22 OUTLINE OF THE TILTING PLATFORM — (MIDDLE SECTION)

FIG. 4.23 SET-UP FOR STATIC PROPERTIES TEST.

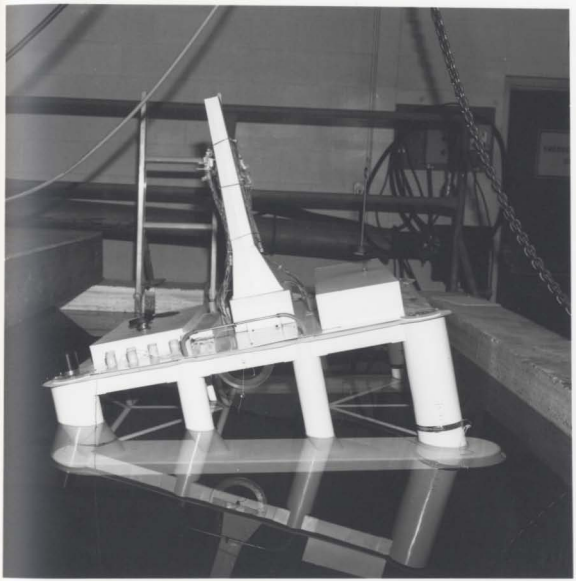

FIG. 4.24 STATIC STABILITY TEST.

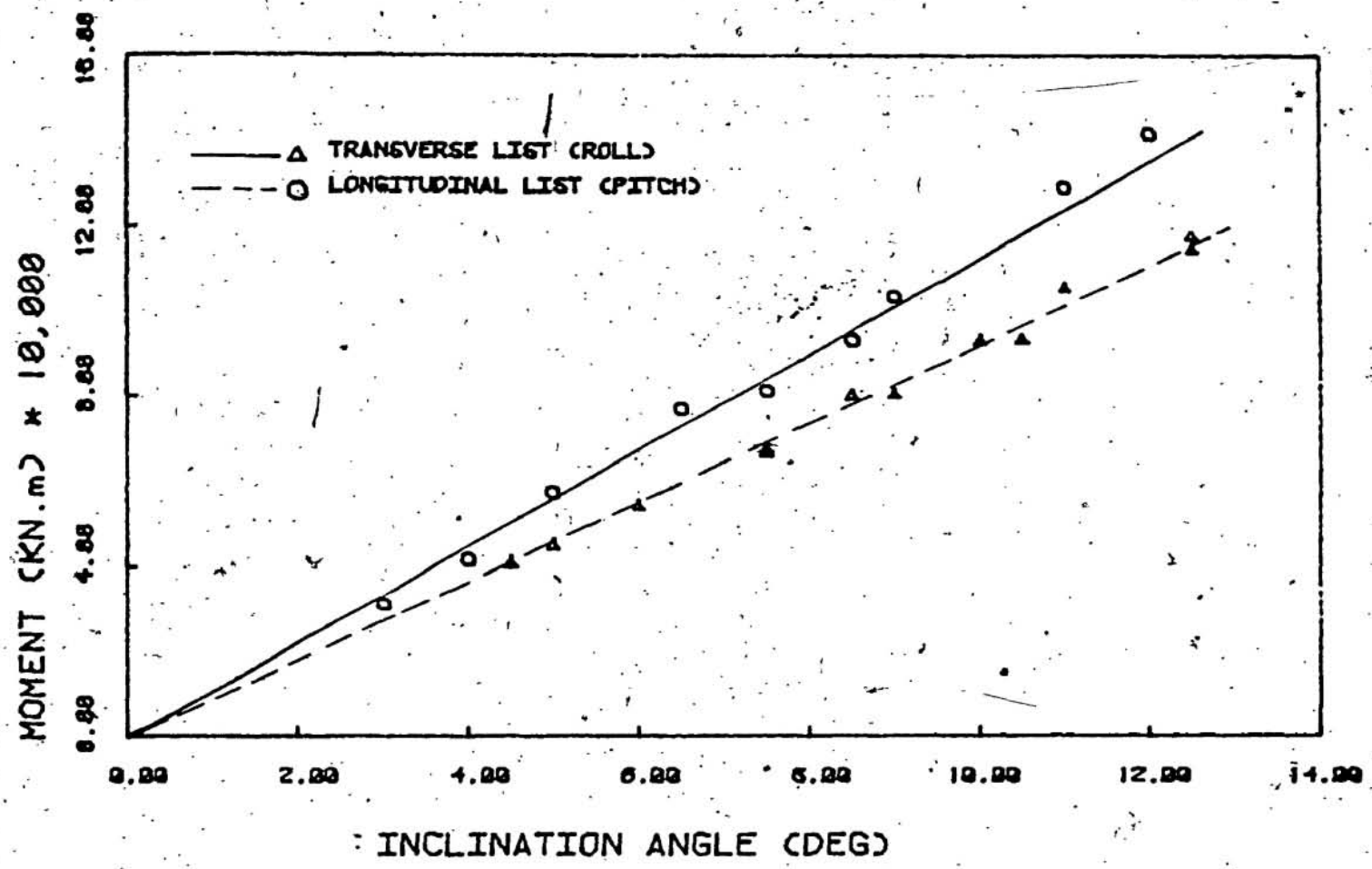

FIG. 4.25 MEASURED INCLINATION ANGLE VS MOMENT FOR THE TIM-77 SEMI-SUBMERSIBLE.

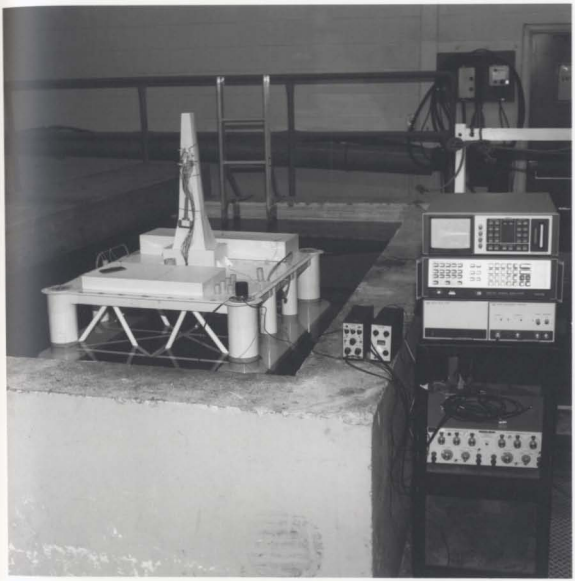

FIG. 4.26 SET-UP FOR MEASURING NATURAL PERIODS OF MOTION.

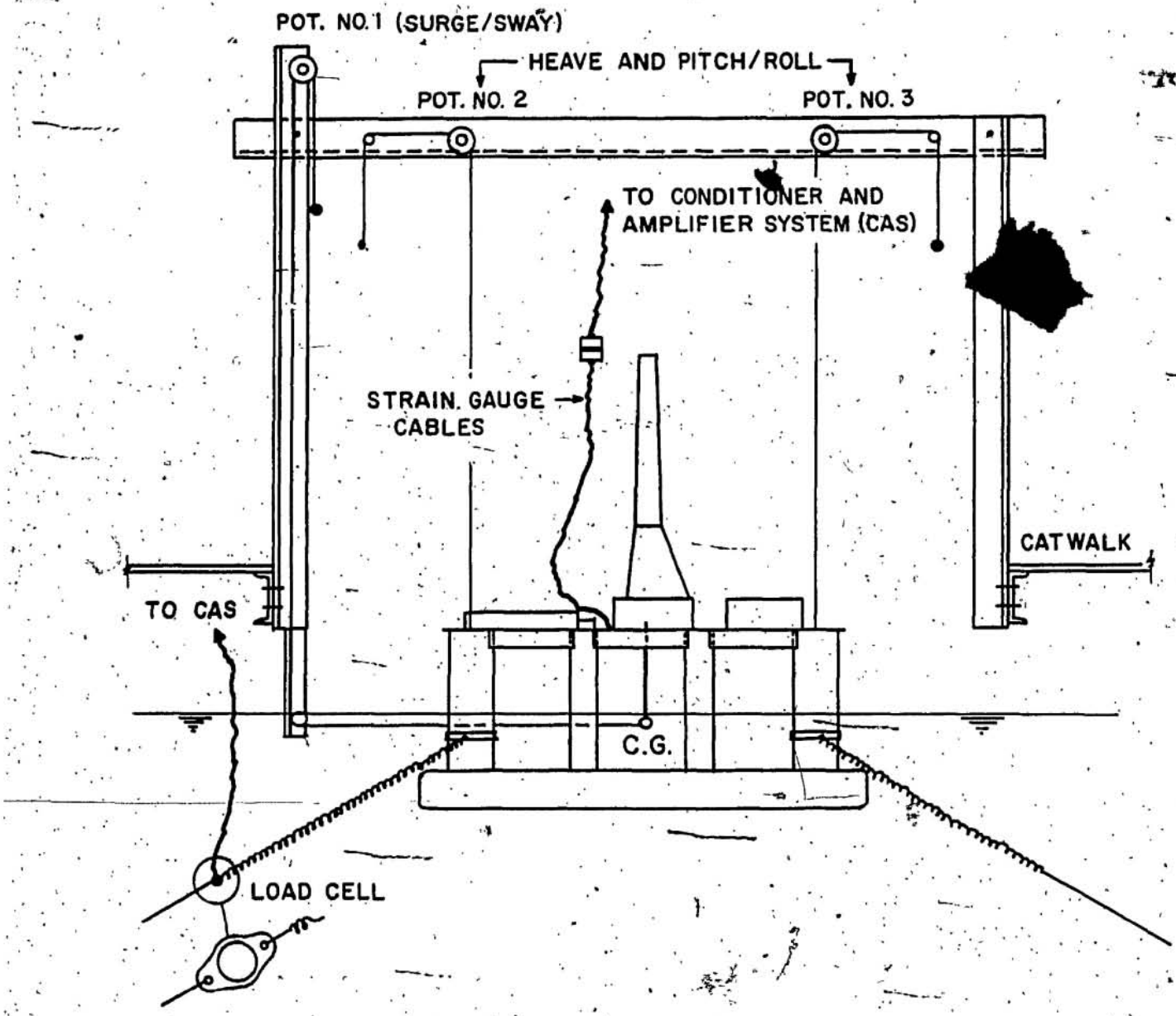

FIG. 4.27 SET-UP OF THE WAVE TANK TEST

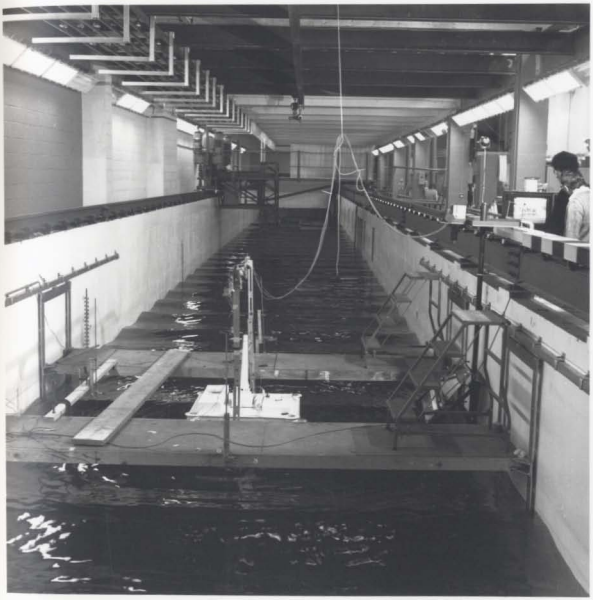

FIG. 4.28 GENERAL VIEW OF THE MODEL AND WAVE TANK.

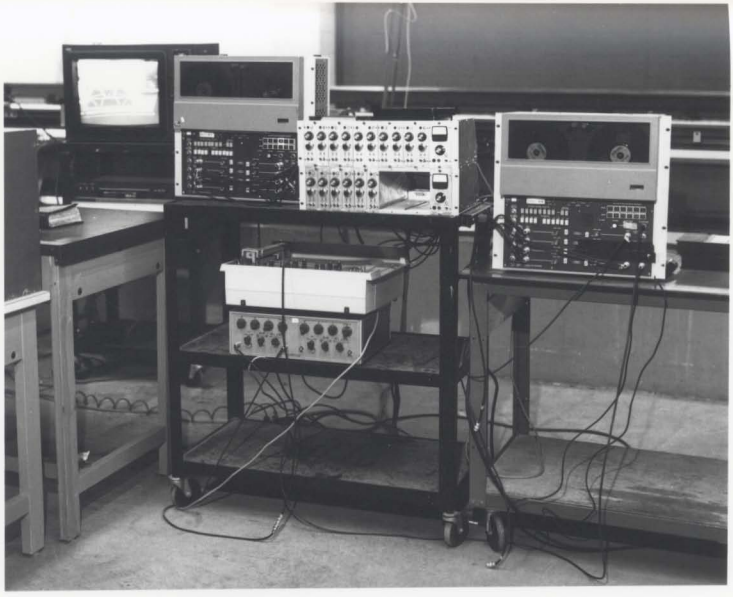

FIG. 4.29 DATA ACQUISITION SYSTEM.

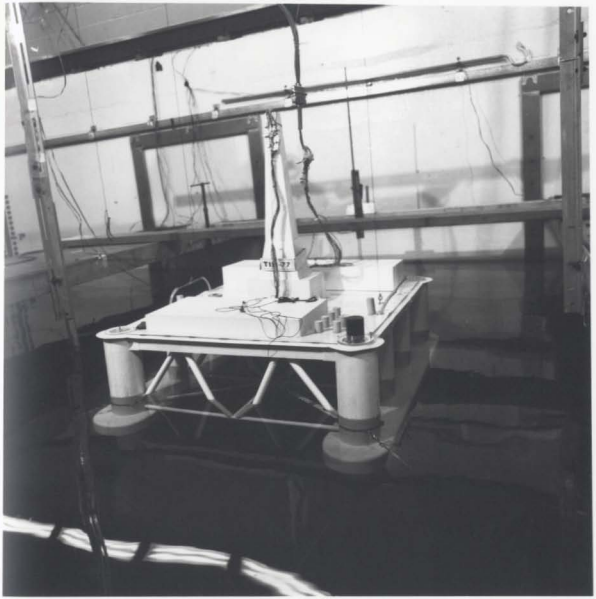

FIG. 4.30 MODEL AT SURVIVAL DRAFT.

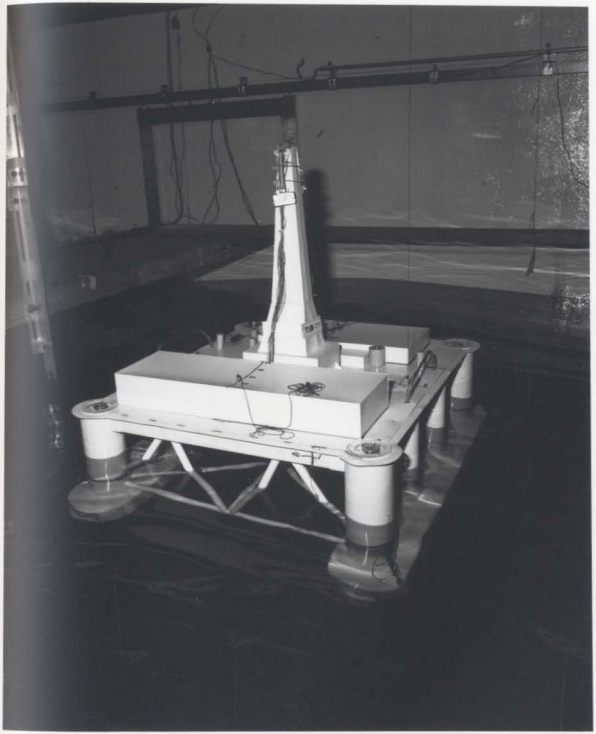

FIG. 4.31 MODEL AT OPERATING DRAFT.

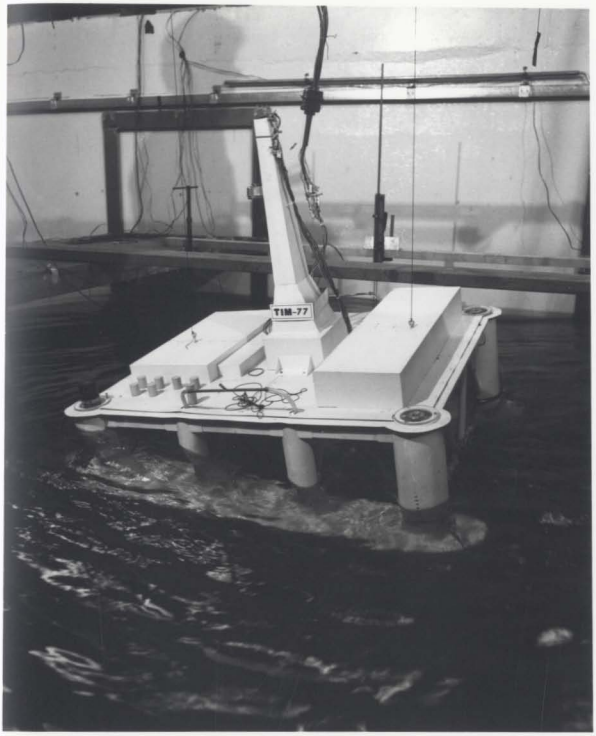

FIG. 4.32 MODEL IN THE DAMAGED CONDITION.

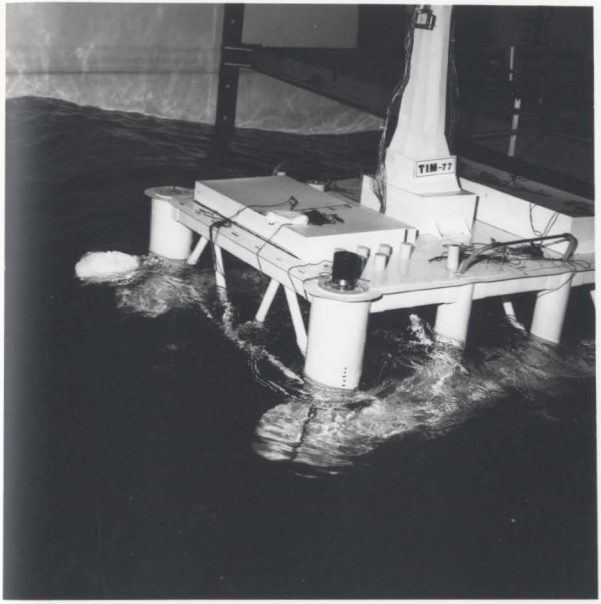

FIG. 4.33 RELATIVE POSITIONS OF THE MODEL AND THE 1,000 TONNE BERGY-BIT MODEL.

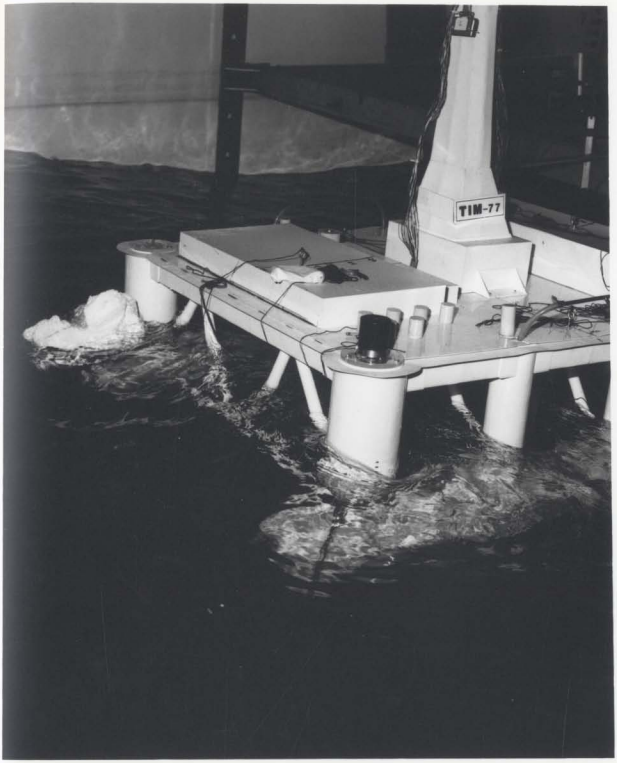

FIG. 4.34 RELATIVE POSITIONS OF THE MODEL AND THE 2,000 TONNE BERGY-BIT MODEL.

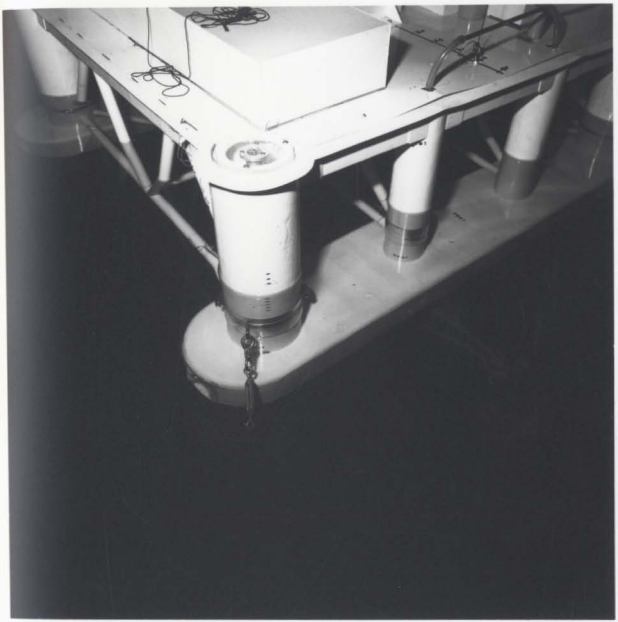

FIG. 4.35 PROTECTING SHIELDS.

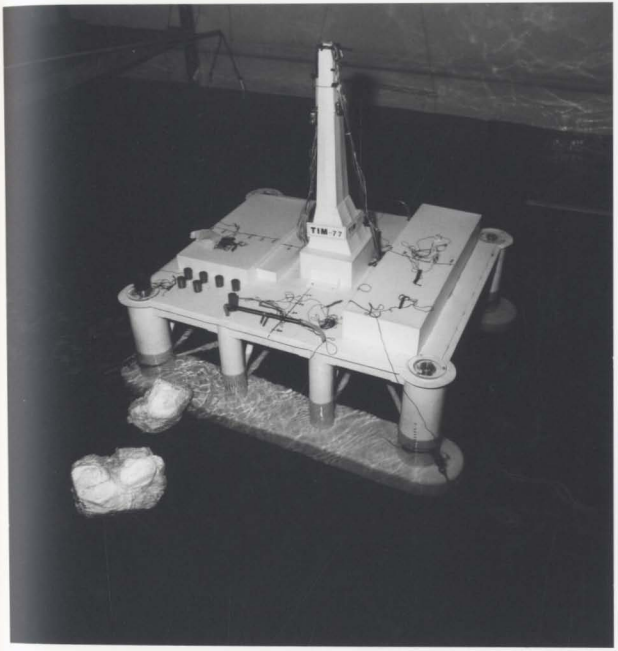

FIG. 4.36 RELATIVE SIZES OF THE BERGY-BITS AND THE MODEL.

FIG. 4.37 SIMULATED IMPACT TEST.

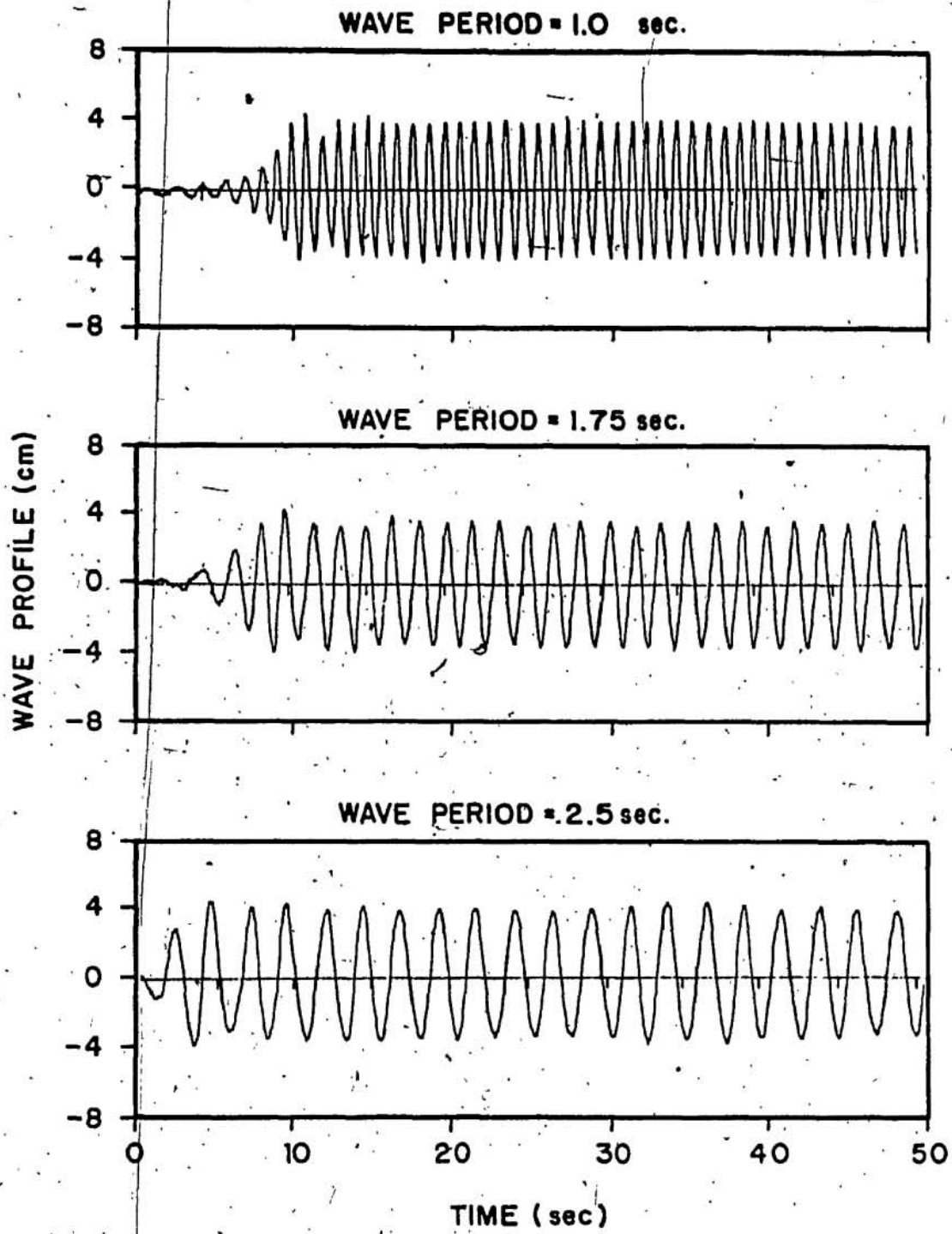

FIG. 5.1 TYPICAL WAVE PROFILES AS MEASURED BY WAVE PROBE #1.

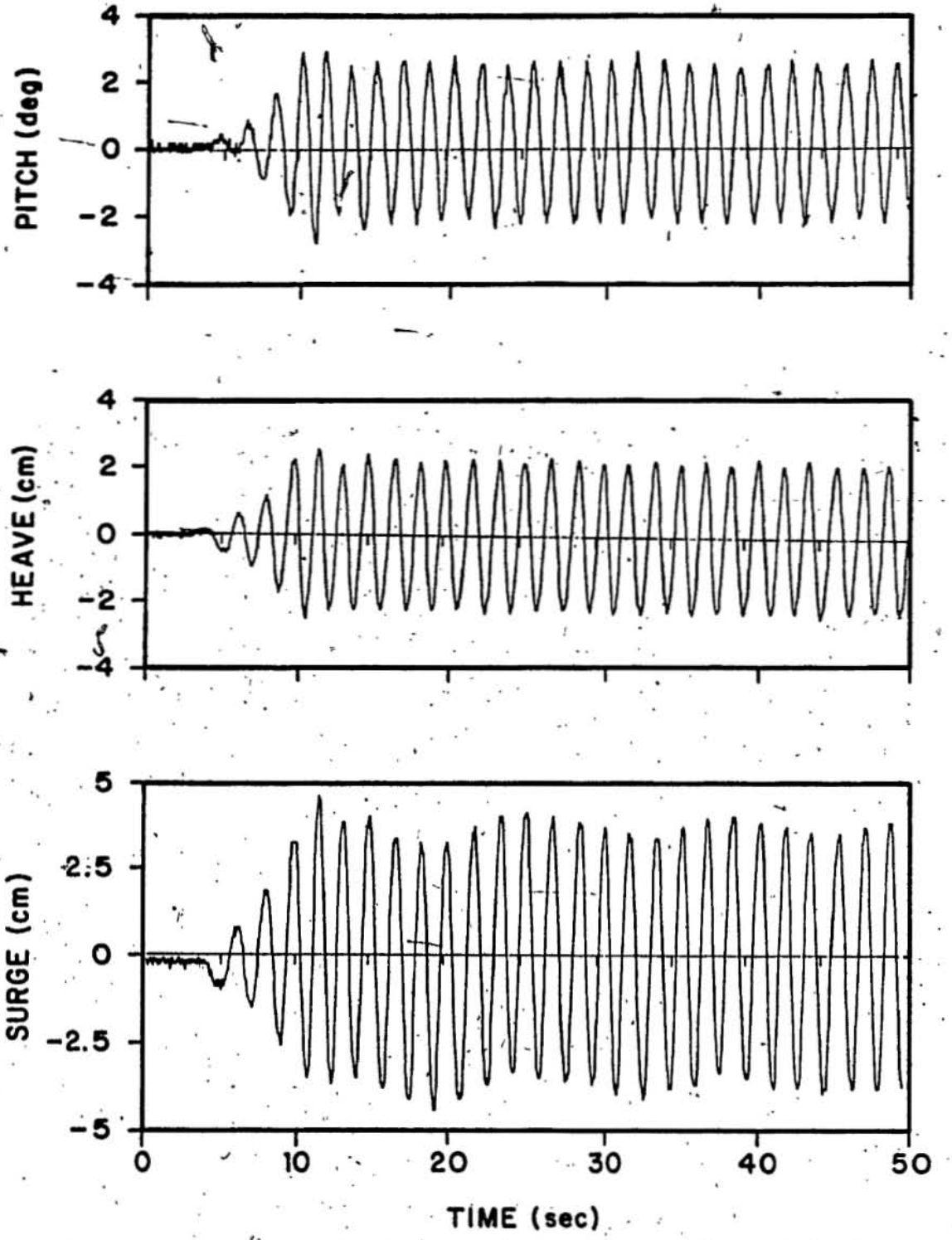

FIG. 5.2 MODEL MOTION IN 1.75 SEC. WAVE AS MEASURED BY POTENTIOMETERS.

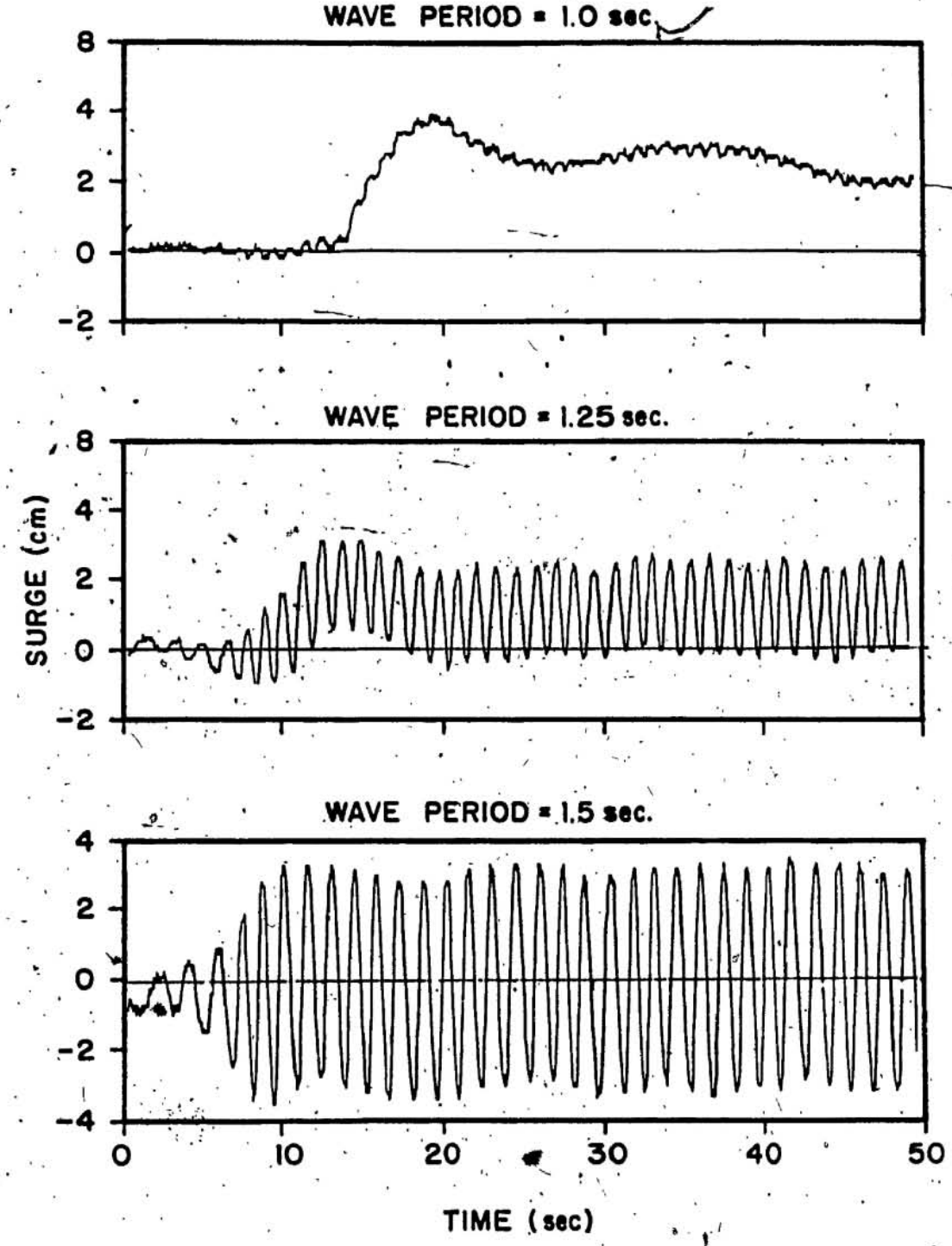

FIG. 5.3 OSCILLATORY AND DRIFT COMPONENTS OF THE MODEL SURGE MOTION.

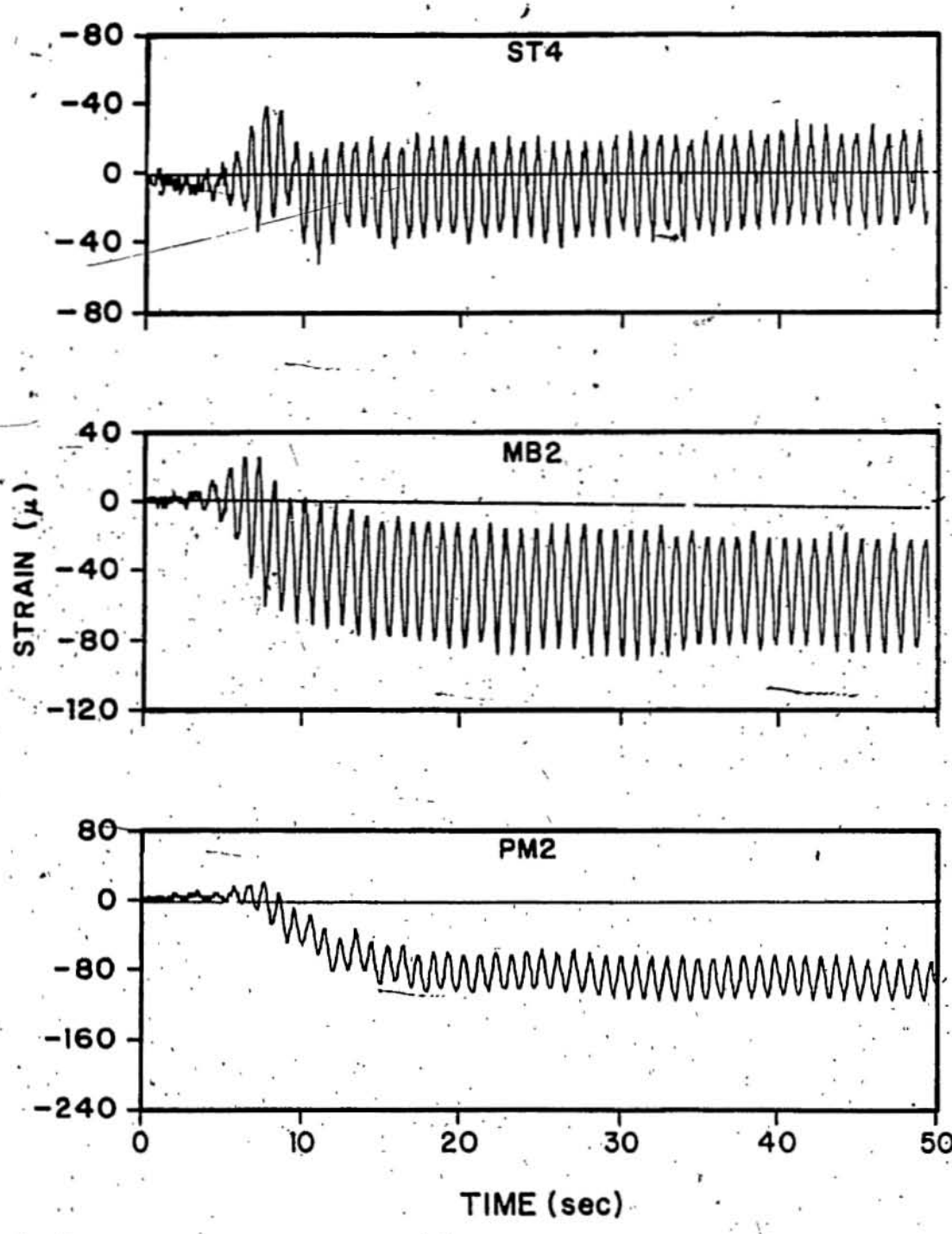

FIG. 5.4 MODEL STRAIN AS MEASURED BY INDICATED STRAIN GAUGES FOR 1 SEC. WAVE.

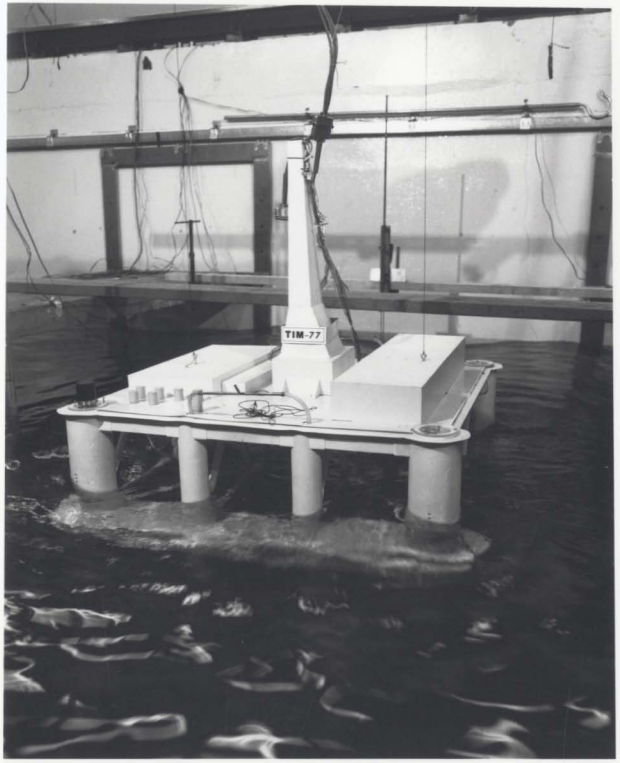

FIG. 5.5 MODEL IN 1 sec. WAVE.

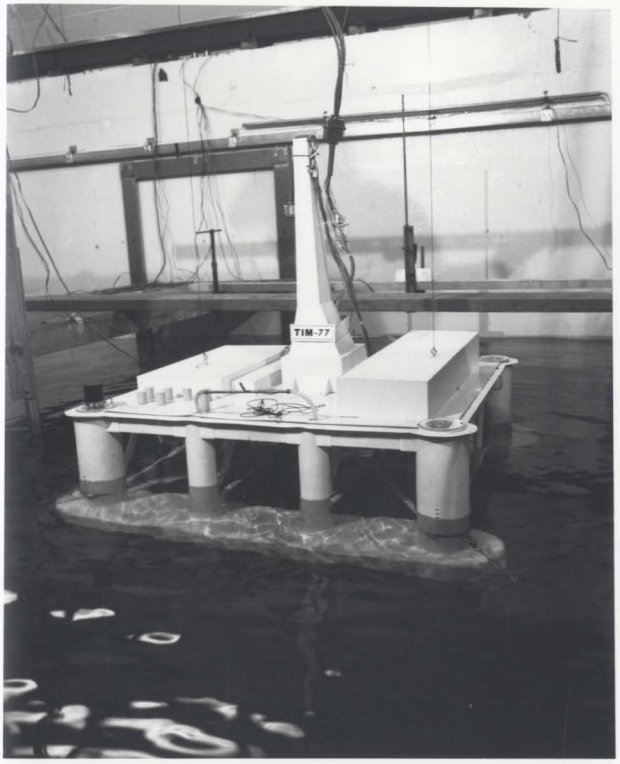

FIG. 5.6 MODEL IN 2.5 sec. WAVE.

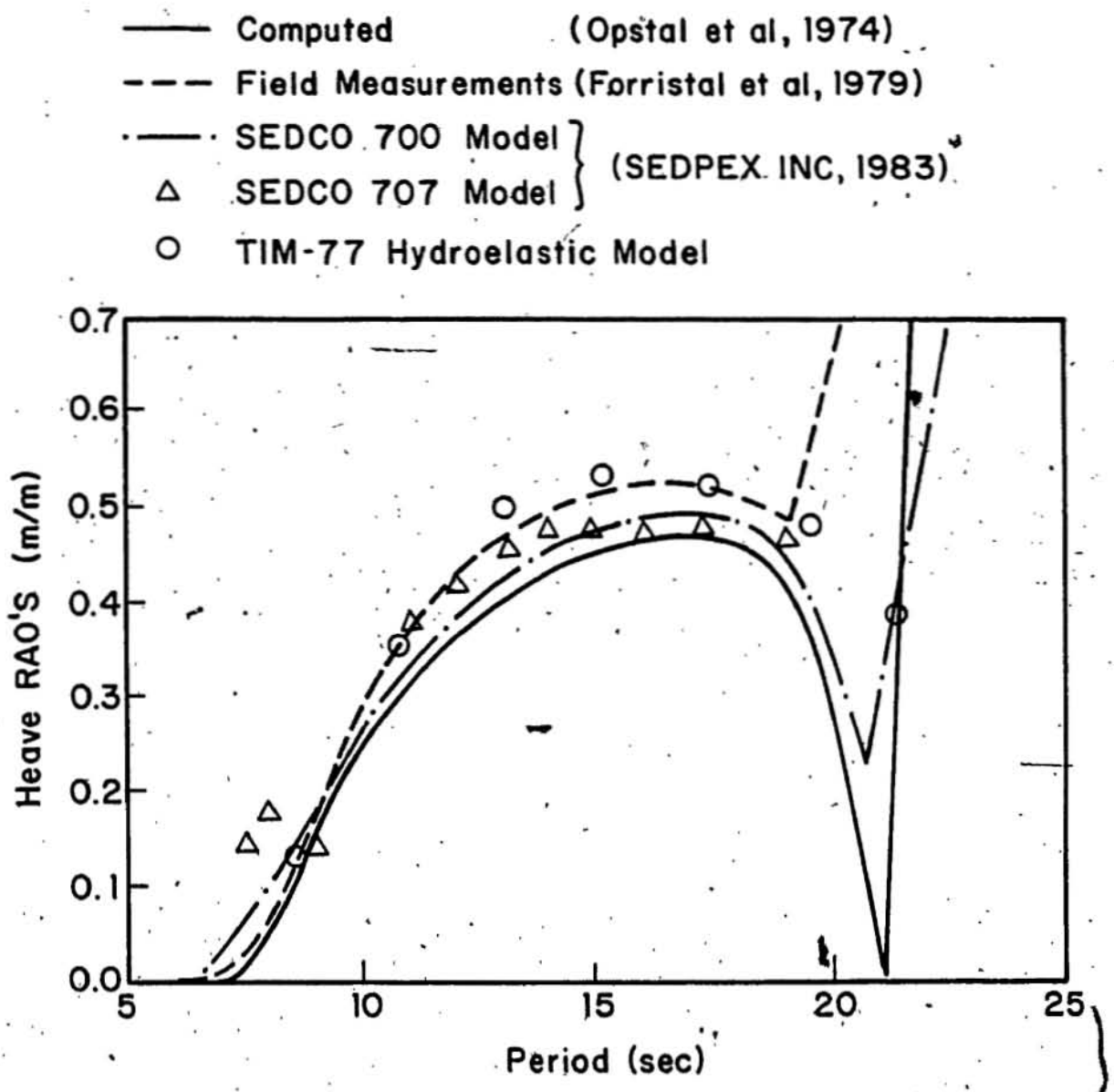

FIG. 5.7 HEAVE RESPONSE TO REGULAR HEAD SEA WAVES - OPERATING DRAFT

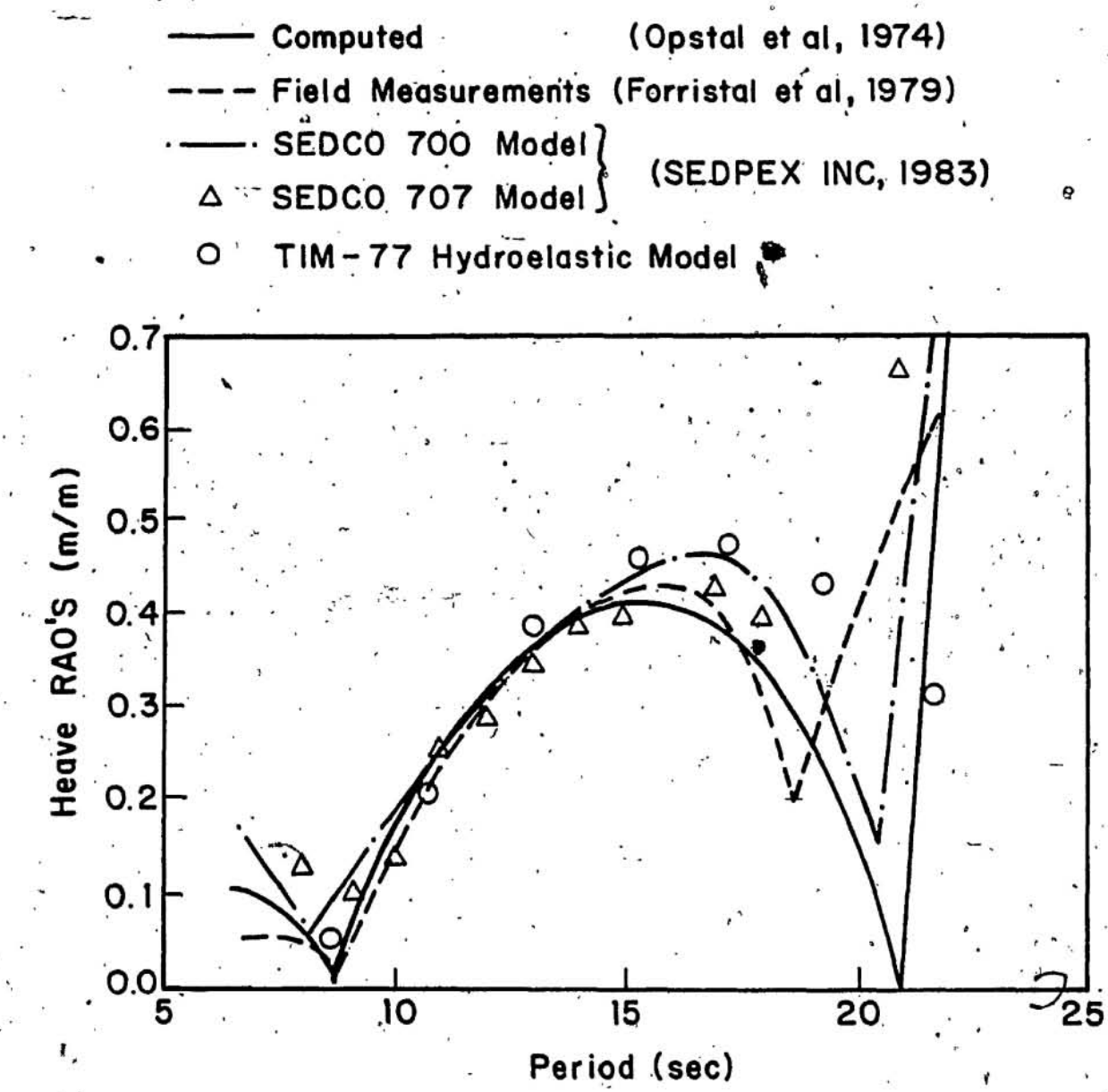

FIG. 5 HEAVE RESPONSE TO REGULAR BEAM SEA WAVES OPERATING DRAFT

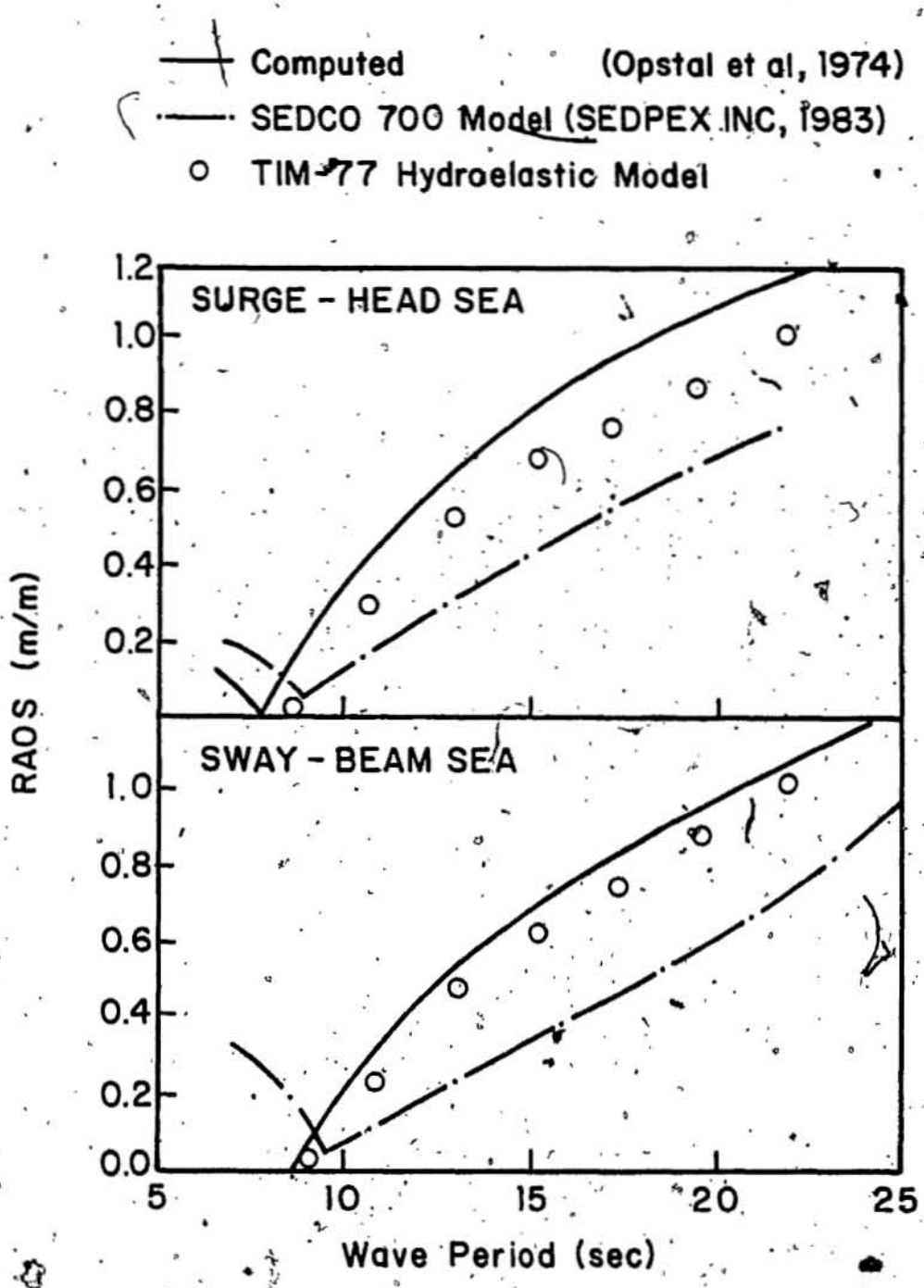

FIG. 5.9 SURGE AND SWAY RESPONSES TO REGULAR WAVES - OPERATING DRAFT.

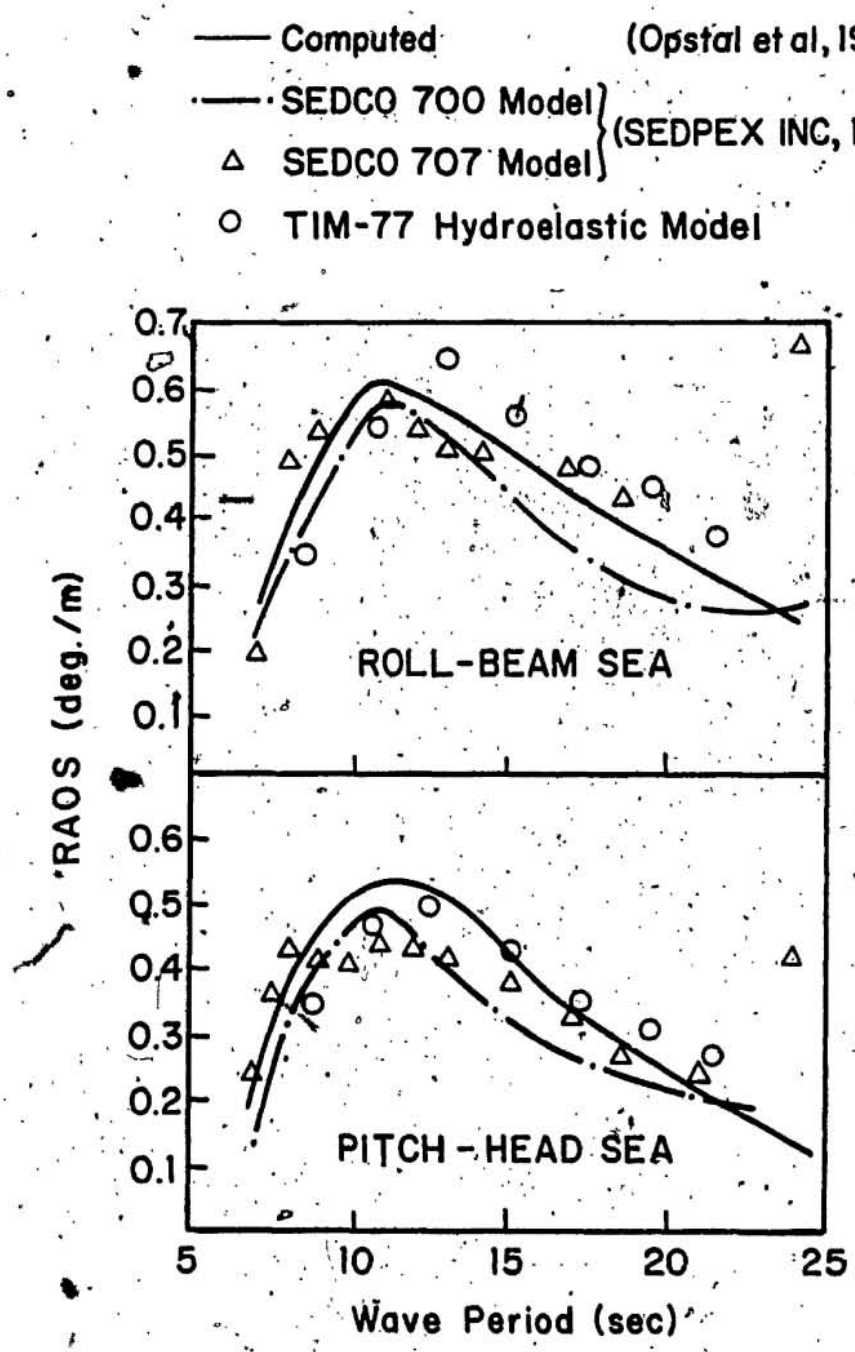

FIG. 5.10 ROLL AND PITCH RESPONSES TO REGULAR WAVES - OPERATING DRAFT.

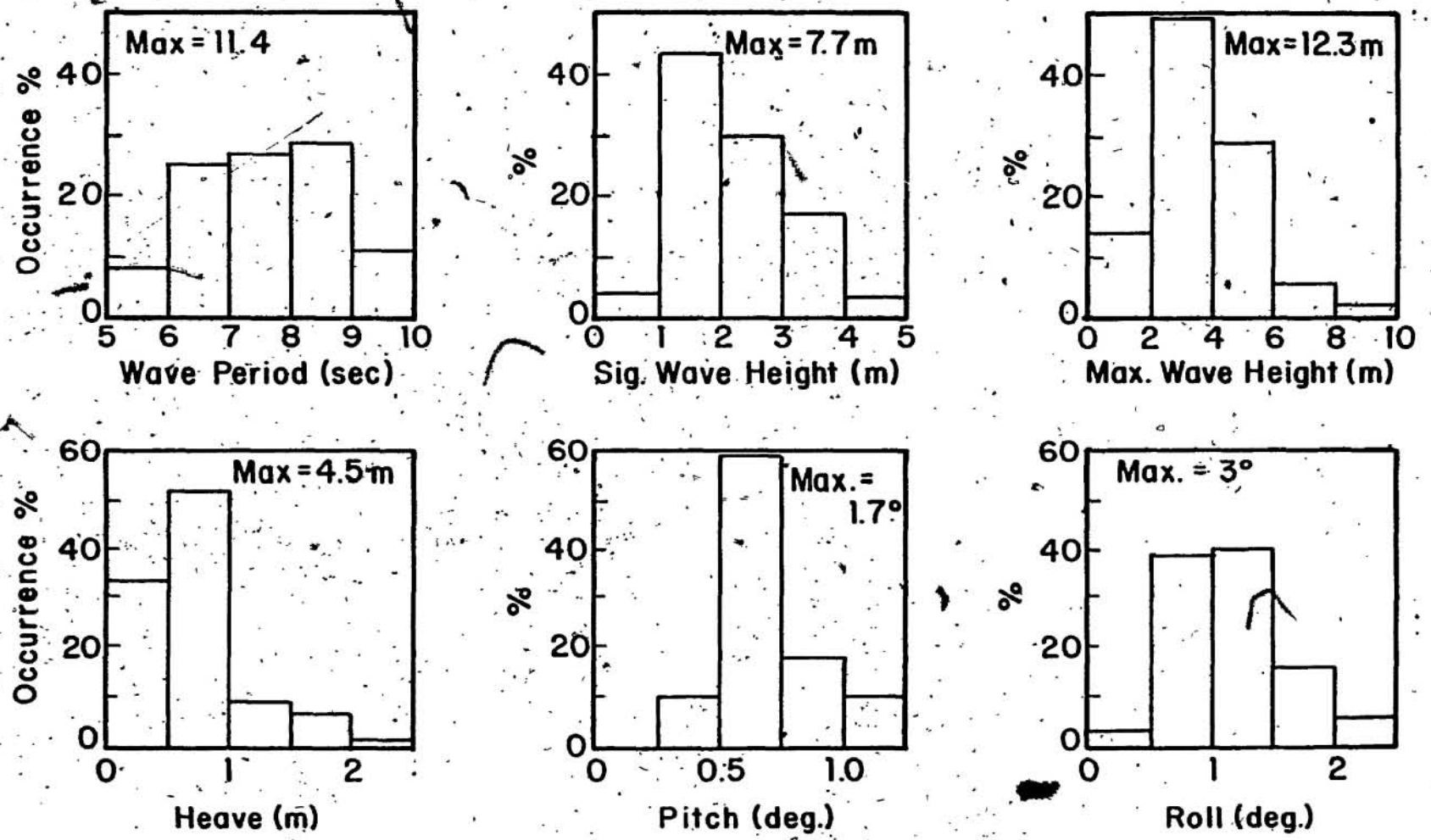

FIG. 5.11 FREQUENCY DISTRIBUTION OF MEASURED WAVE AND MOTION CHARACTERISTICS OF THE SEDCO-706

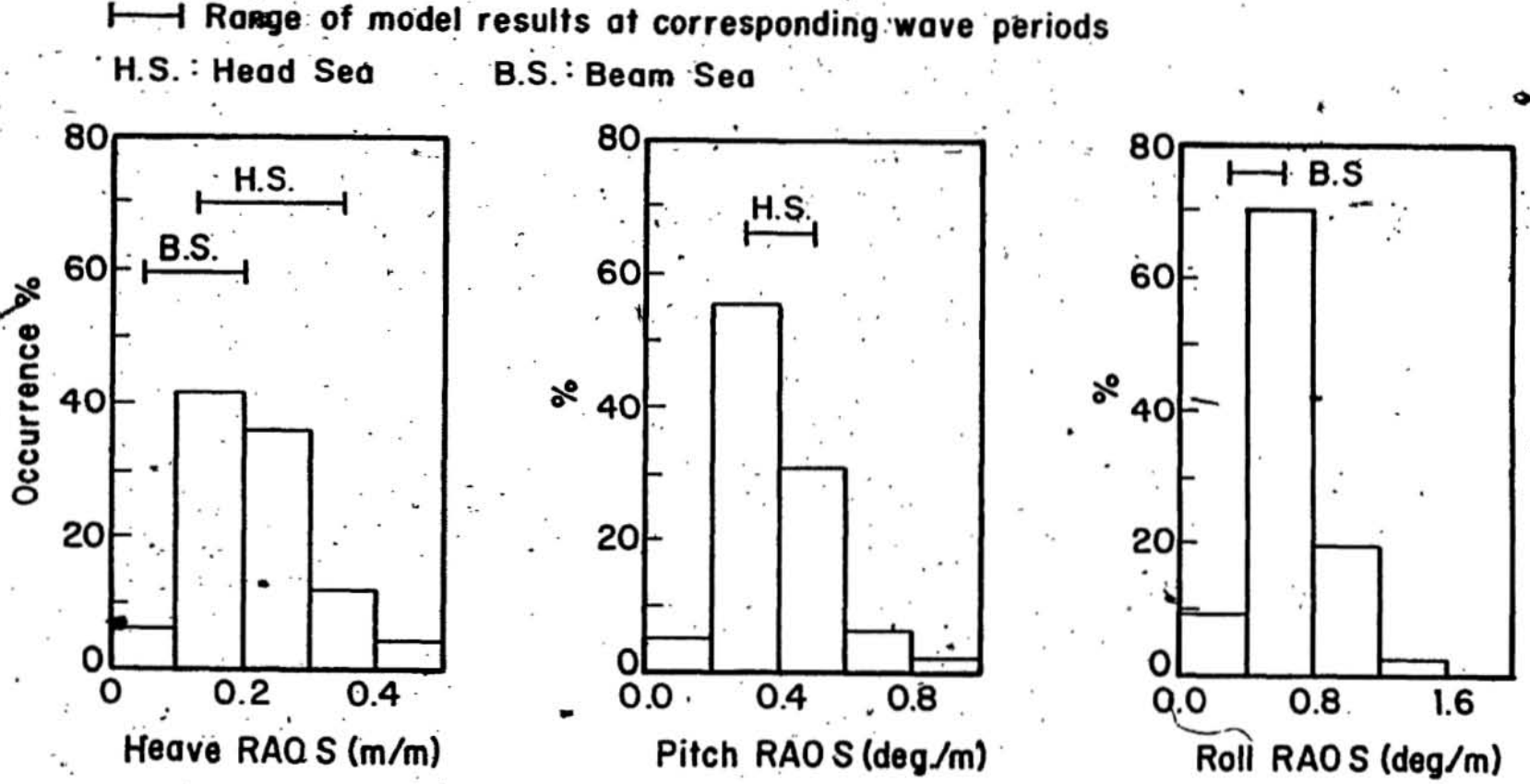

FIG. 5.12 FREQUENCY DISTRIBUTION OF RAO'S OF THE MEASURED SEDCO-706 MOTION

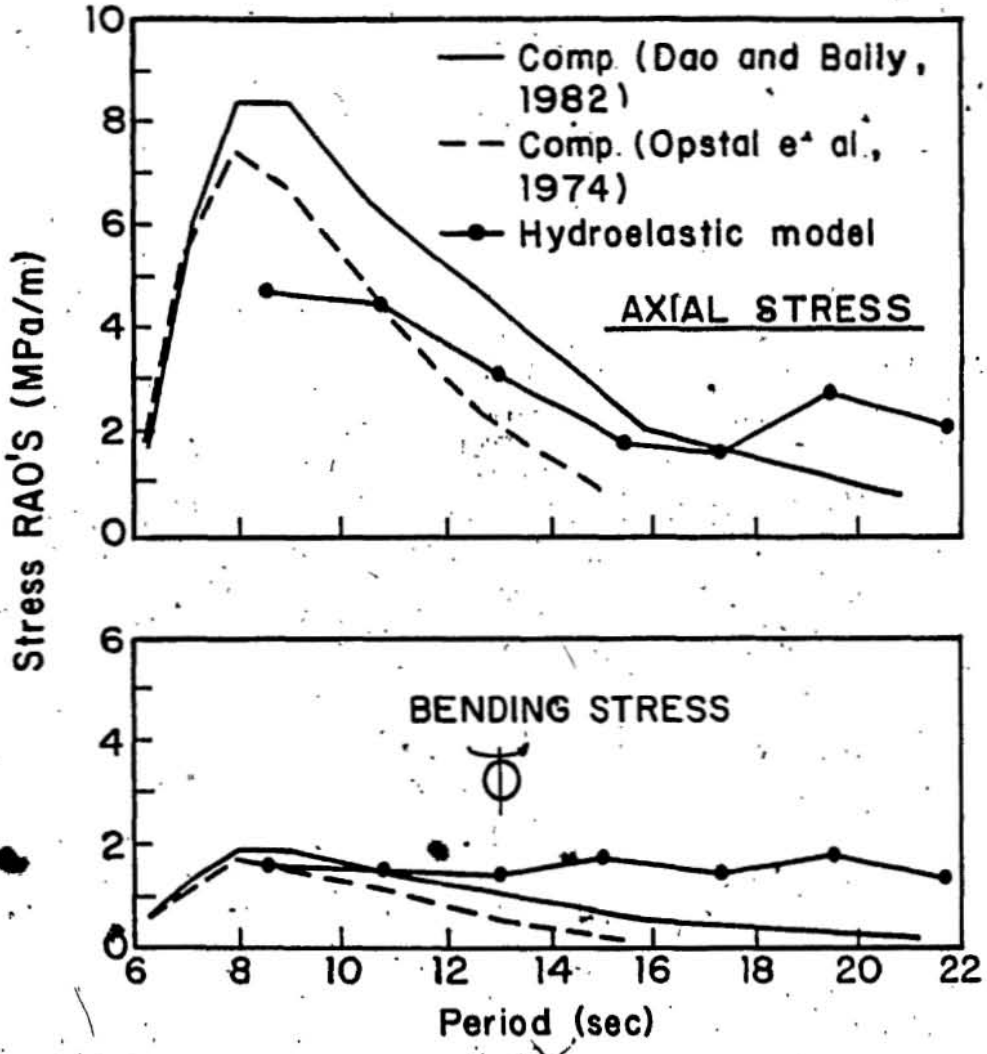

FIG. 5.13 RAO'S OF AXIAL AND BENDING STRESSES IN HORIZONTAL BRACING SECTION HBO-BEAM SEA AT OPERATING DRAFT.

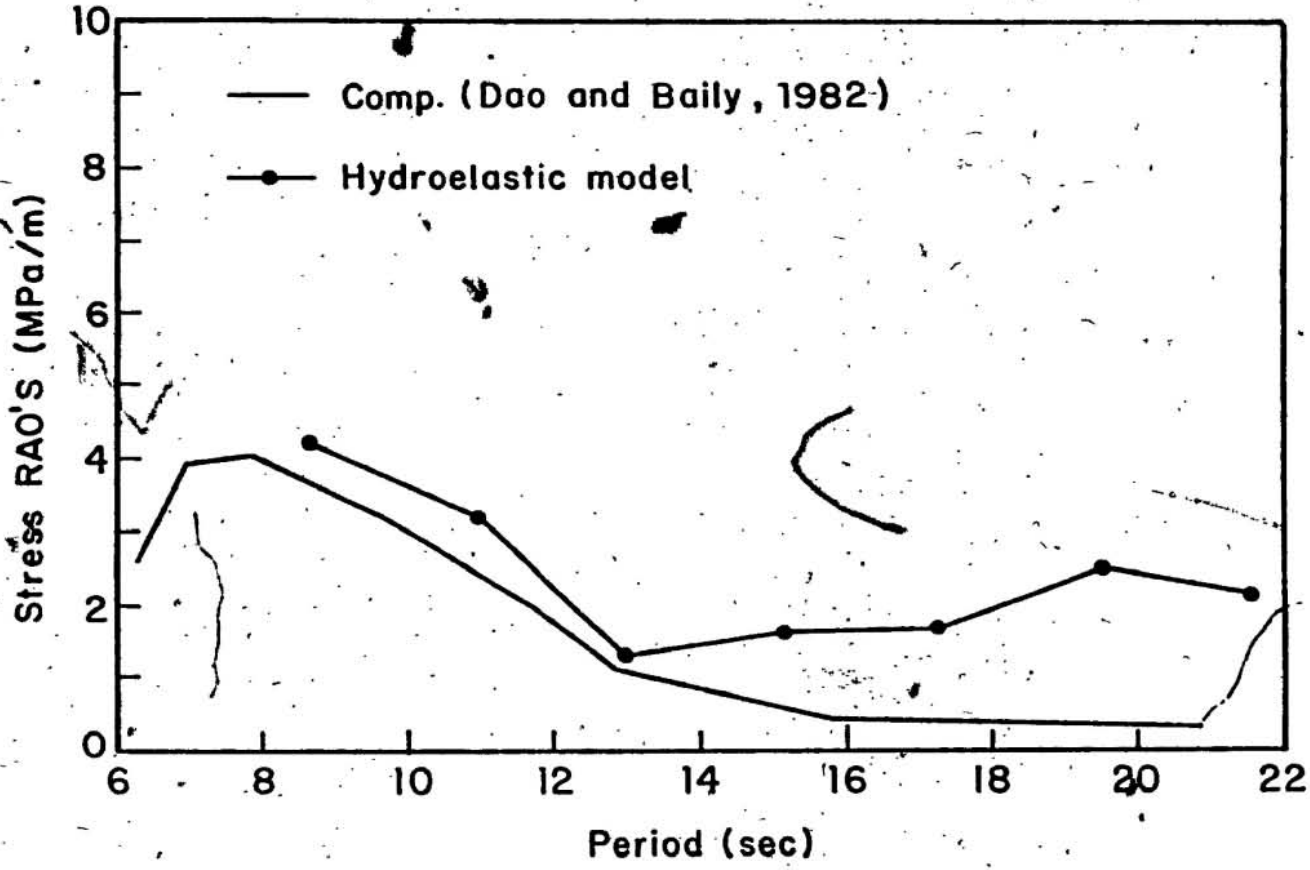

FIG. 5.14 RAO'S OF AXIAL STRESSES IN DIAGONAL BRACING SECTION DBO-BEAM SEA AT OPERATING DRAFT

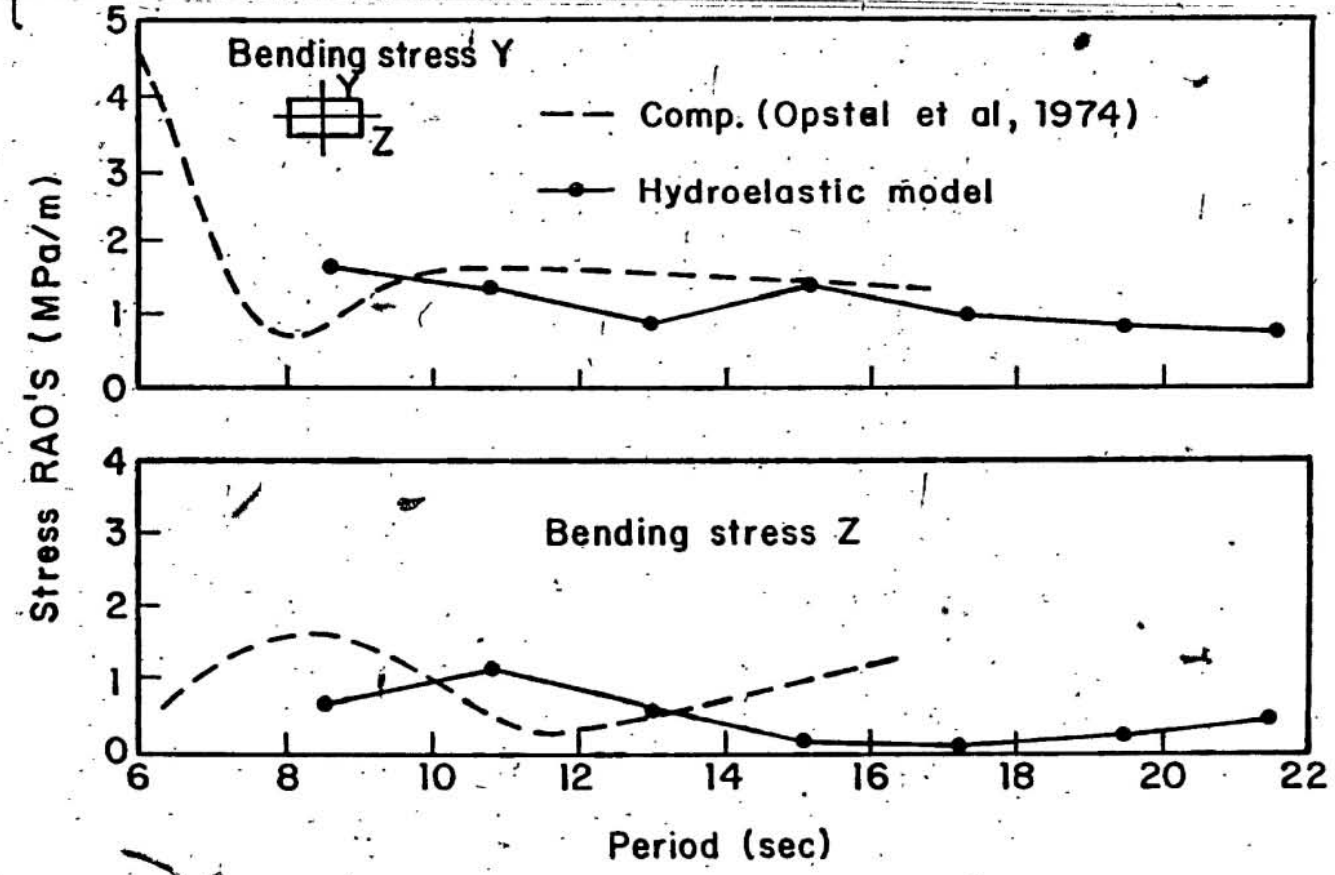

FIG.5.15 RAO'S OF BENDING STRESSES IN PONTOON SECTION PM-BEAM SEA AT OPERATING DRAFT

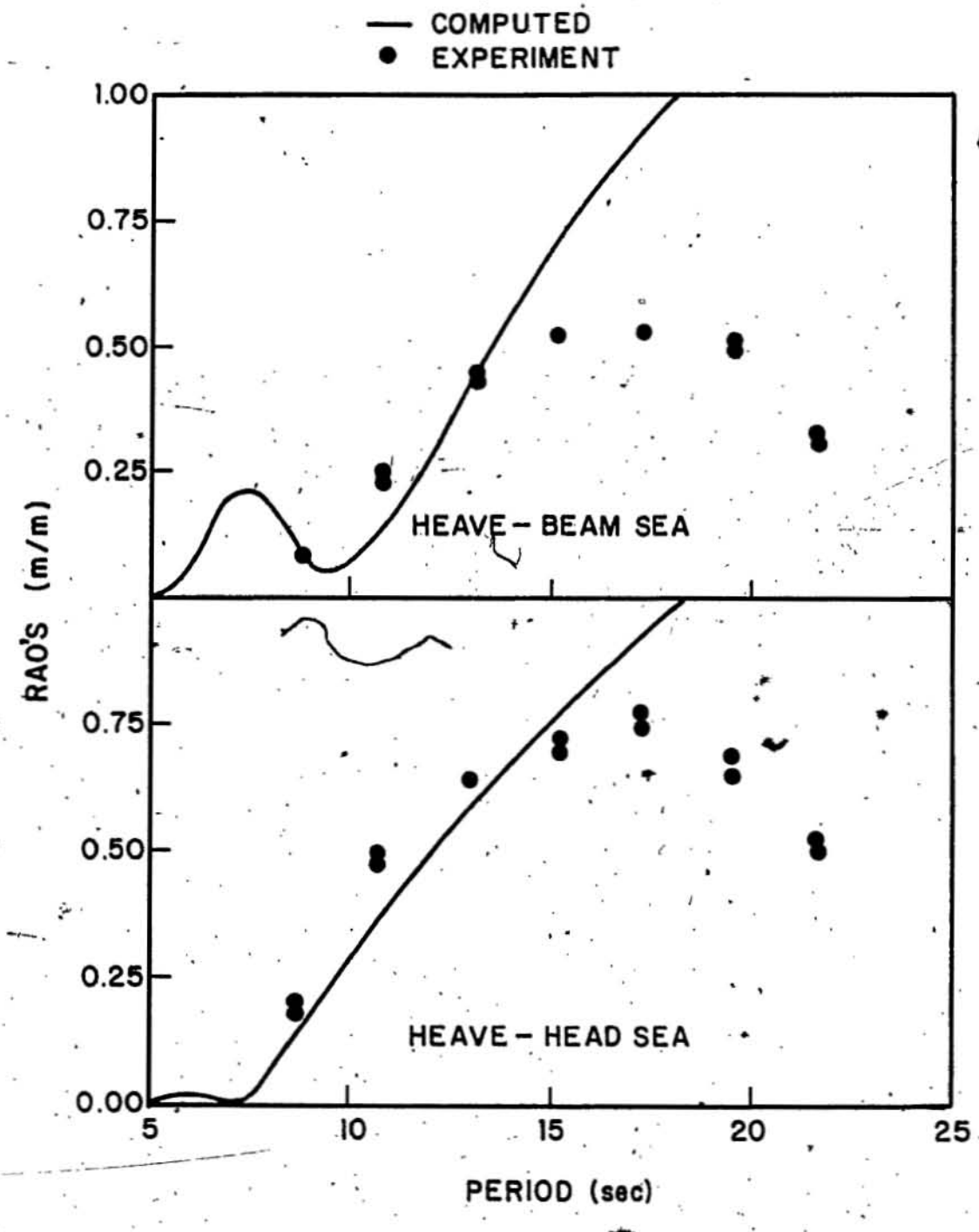

FIG. 5.16 HEAVE RESPONSE IN REGULAR WAVES — SURVIVAL DRAFT

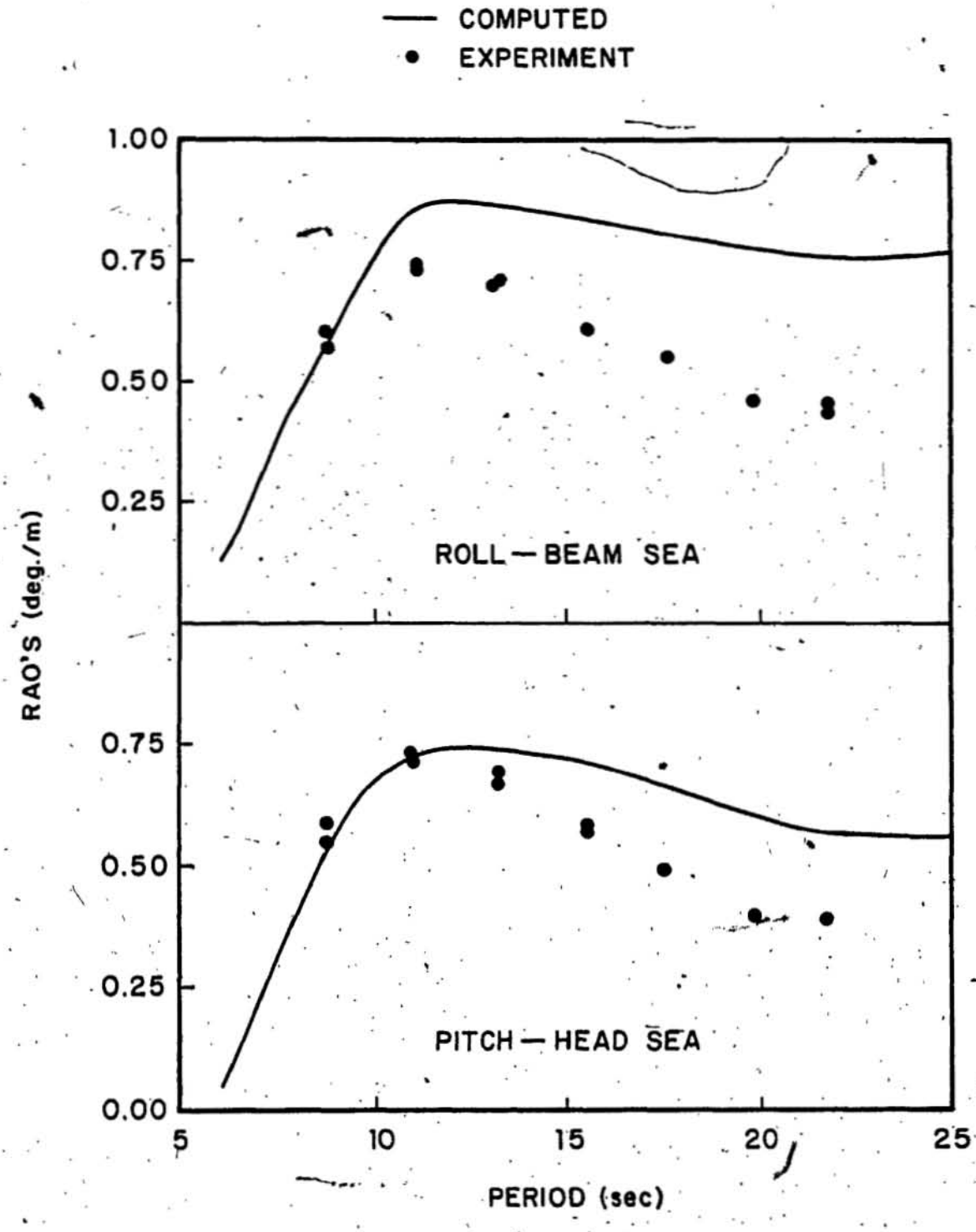

FIG. 5.17 ROLL AND PITCH RESPONSES IN REGULAR WAVES — SURVIVAL DRAFT.

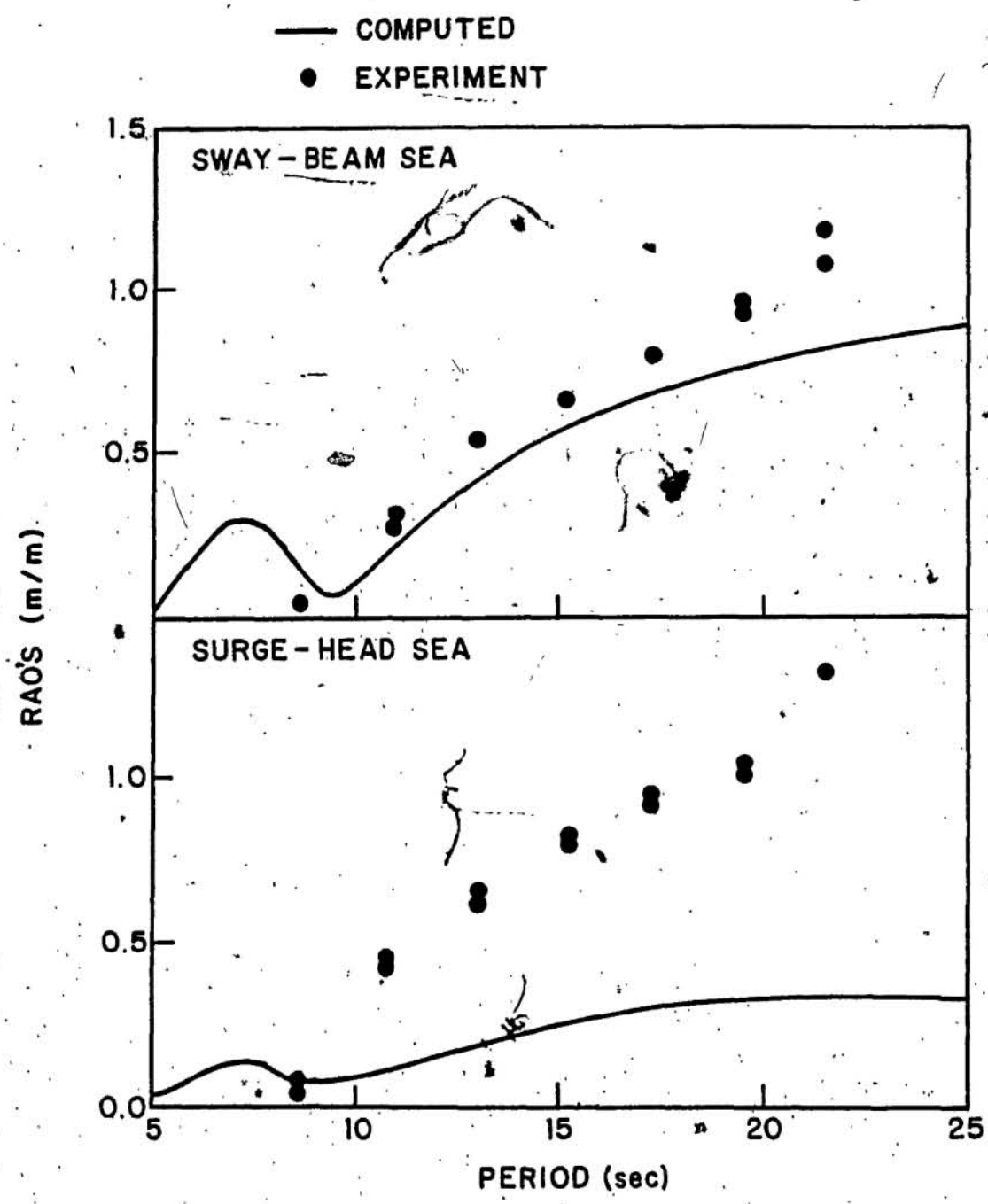

FIG. 5.18 SURGE AND SWAY RESPONSES IN REGULAR WAVES - SURVIVAL DRAFT

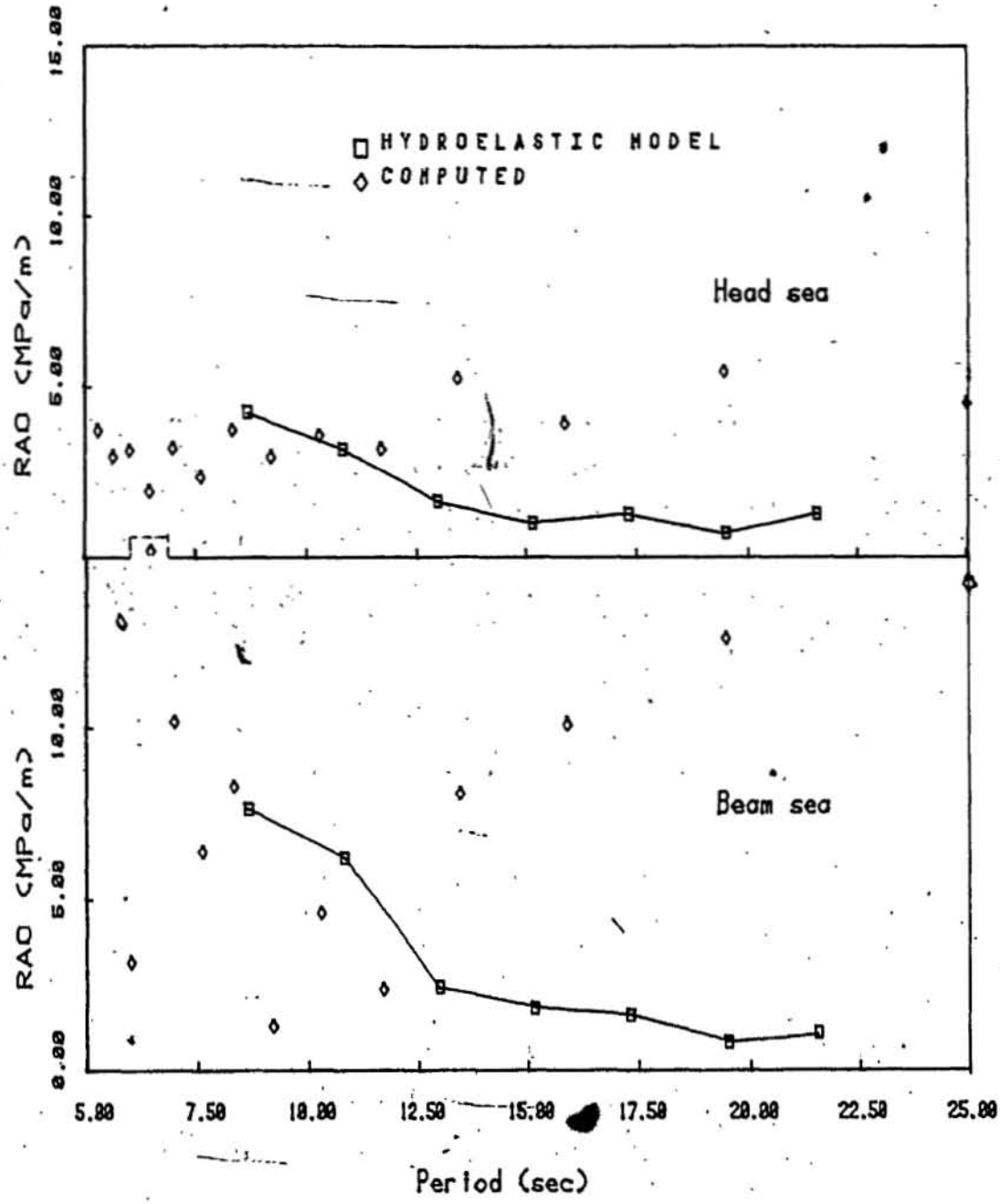

FIG. 5.19 COMPUTED AND MEASURED COMBINED STRESSES AT SECONDARY COLUMN SECTION SB - SURVIVAL DRAFT.

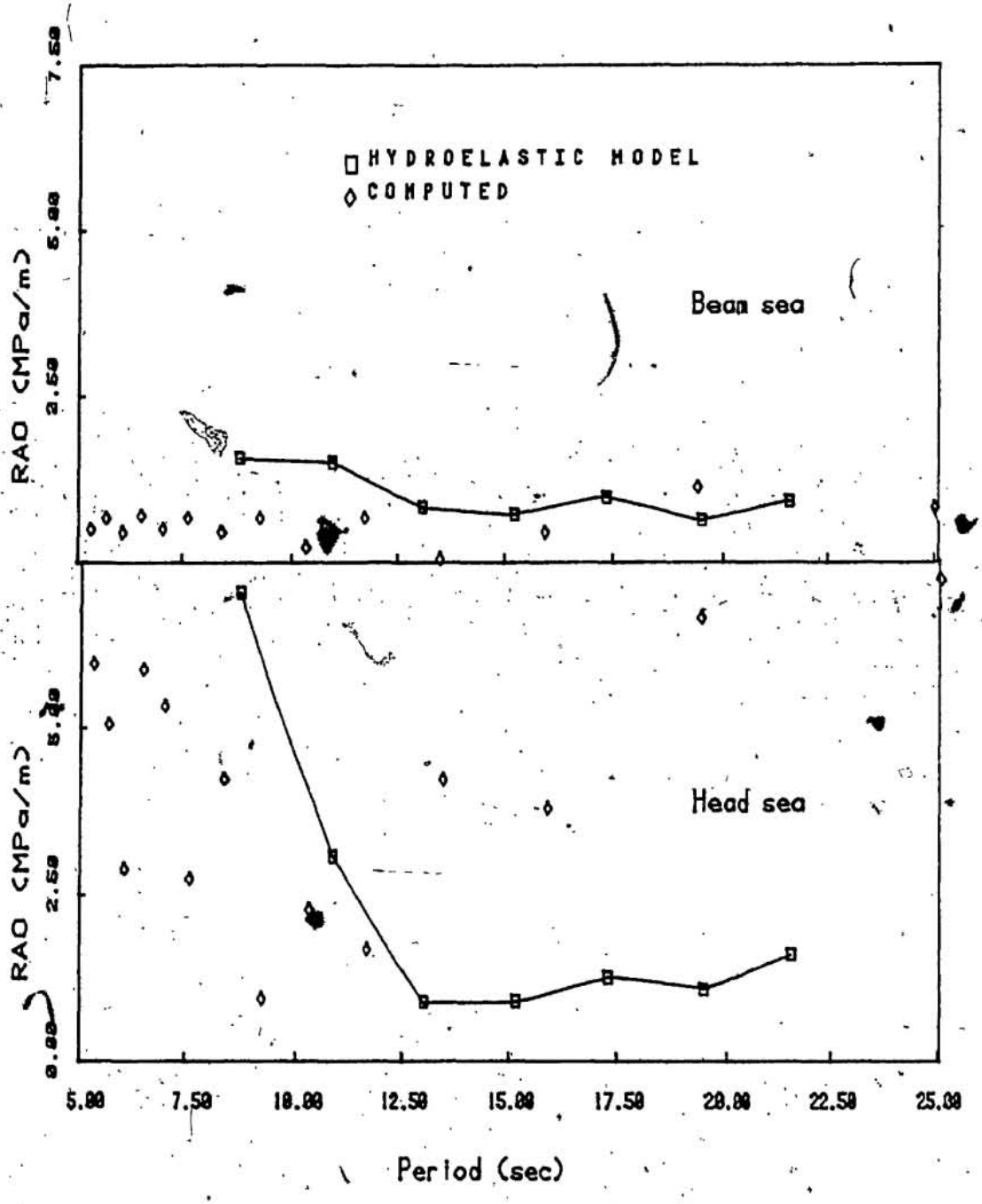

FIG. 5.20 COMPUTED AND MEASURED COMBINED STRESSES AT SECONDARY COLUMN SECTION ST - SURVIVAL DRAFT.

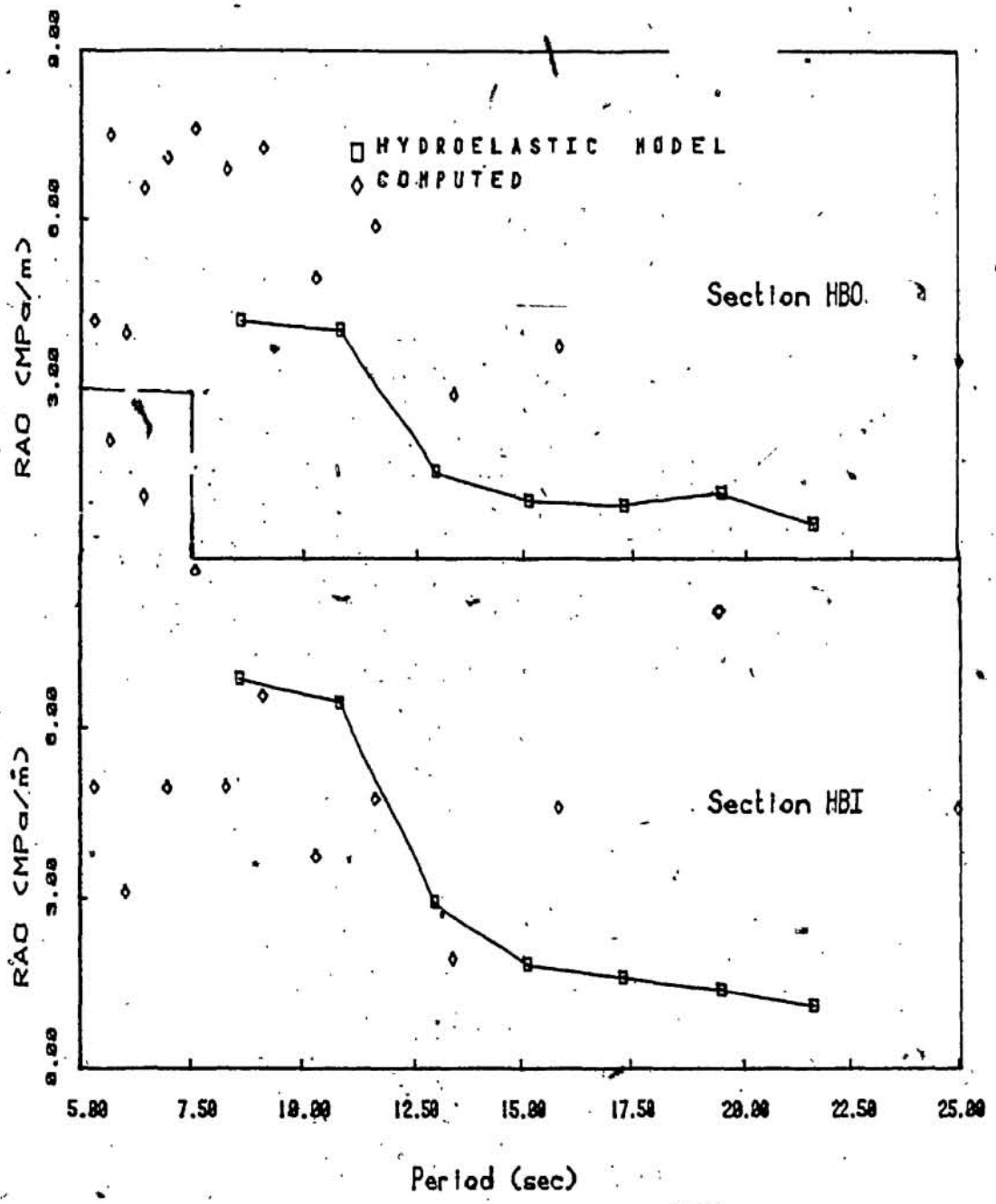

FIG. 5.21 COMPUTED AND MEASURED COMBINED STRESSES IN HORIZONTAL BRACINGS - BEAM SEA AT SURVIVAL DRAFT.

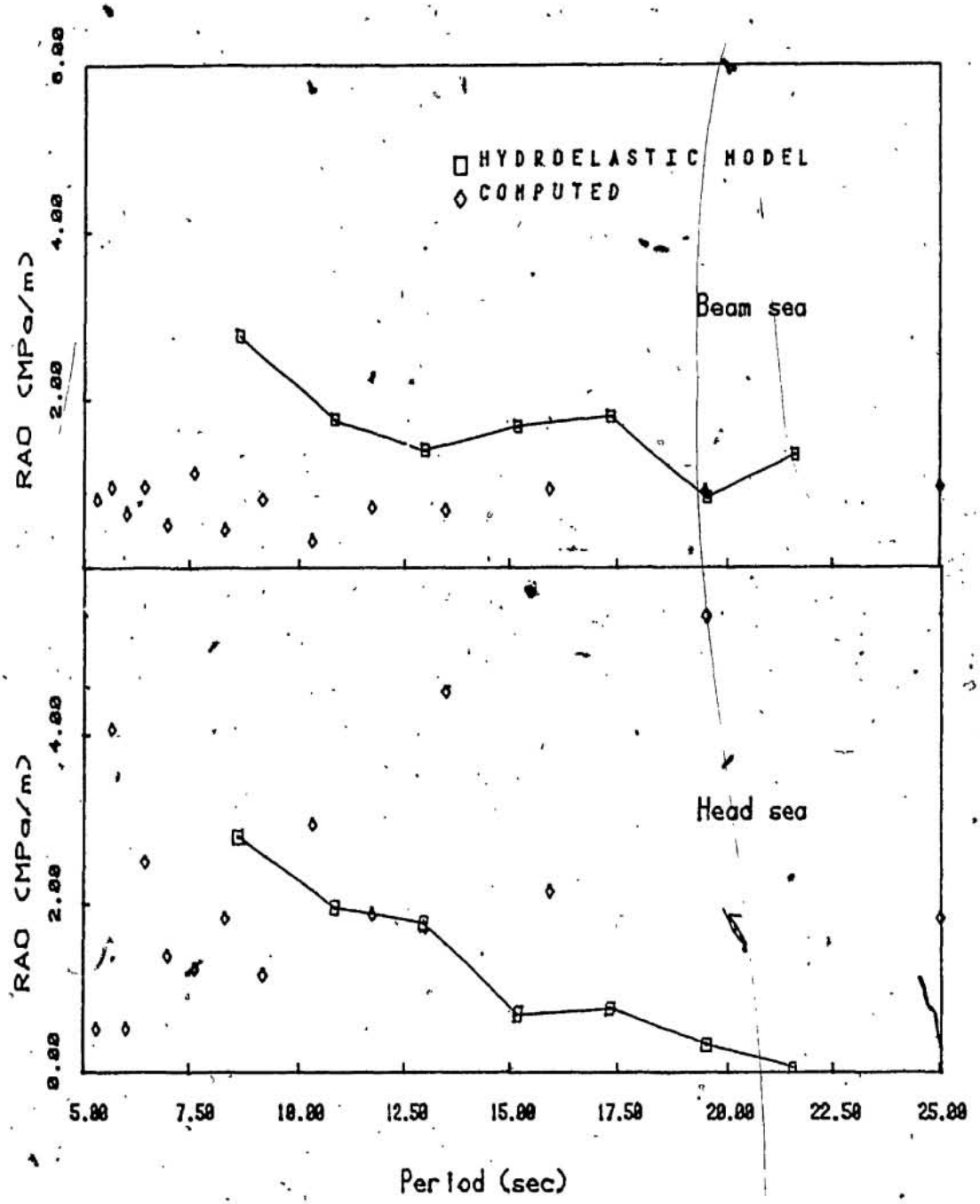

FIG. 5.22 COMPUTED AND MEASURED COMBINED STRESSES AT PONTOON SECTION PM - SUVIVAL DRAFT.

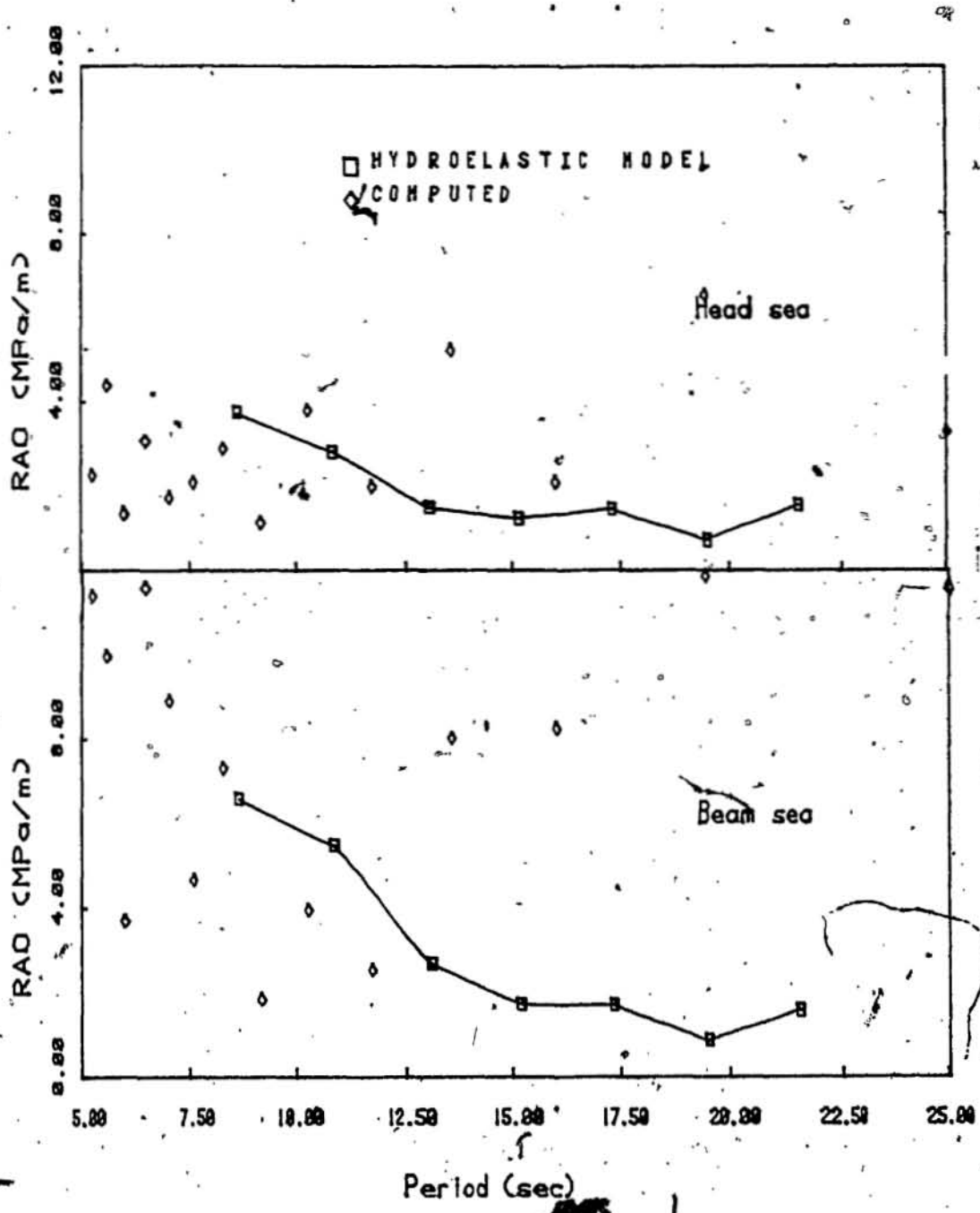

FIG. 5.23 COMPUTED AND MEASURED COMBINED STRESSES AT MAIN COLUMN SECTION MB - SURVIVAL DRAFT.

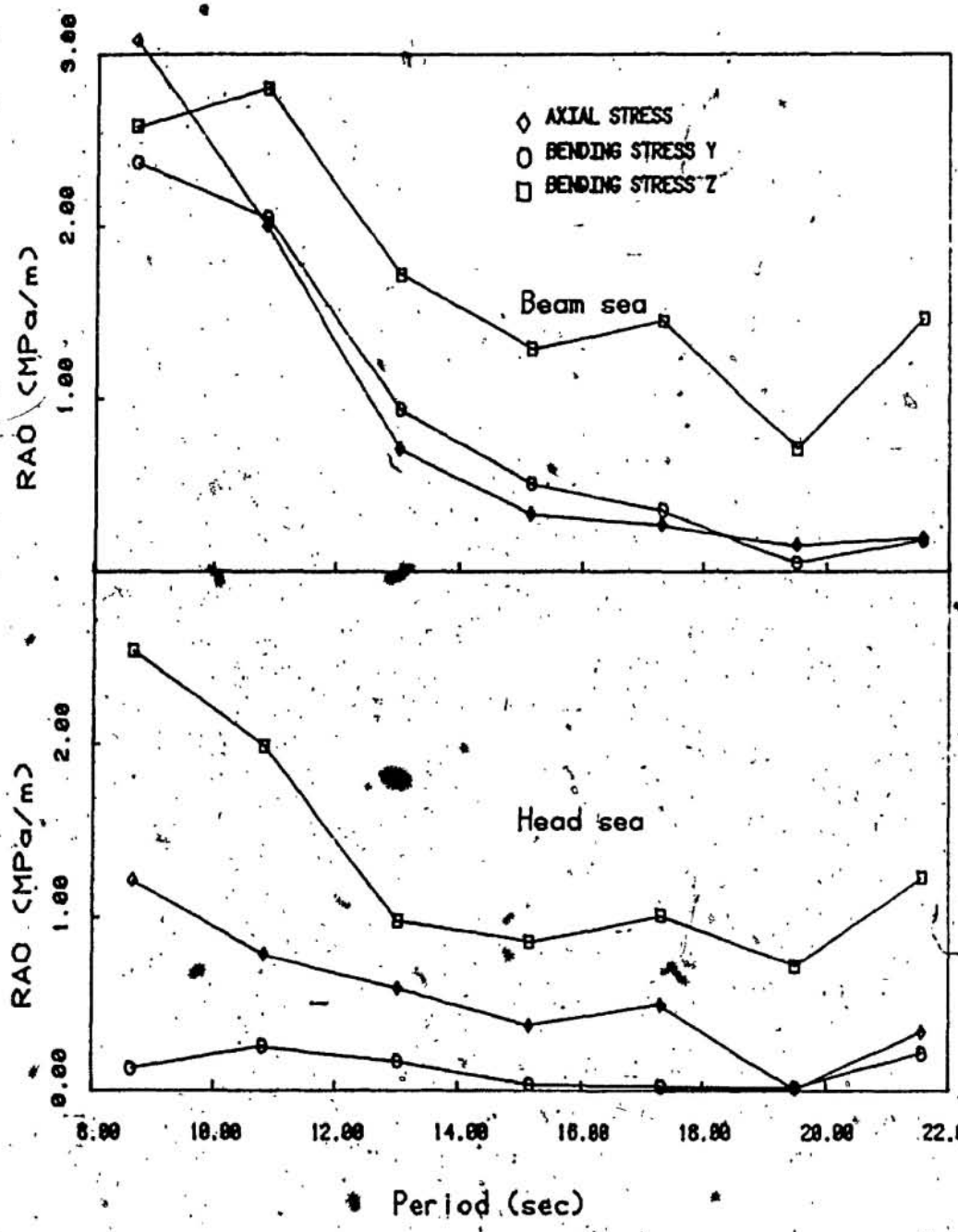

FIG. 5.24 STRESS RAO PLOTS FOR MAIN COLUMN SECTION MB - SURVIVAL DRAFT.

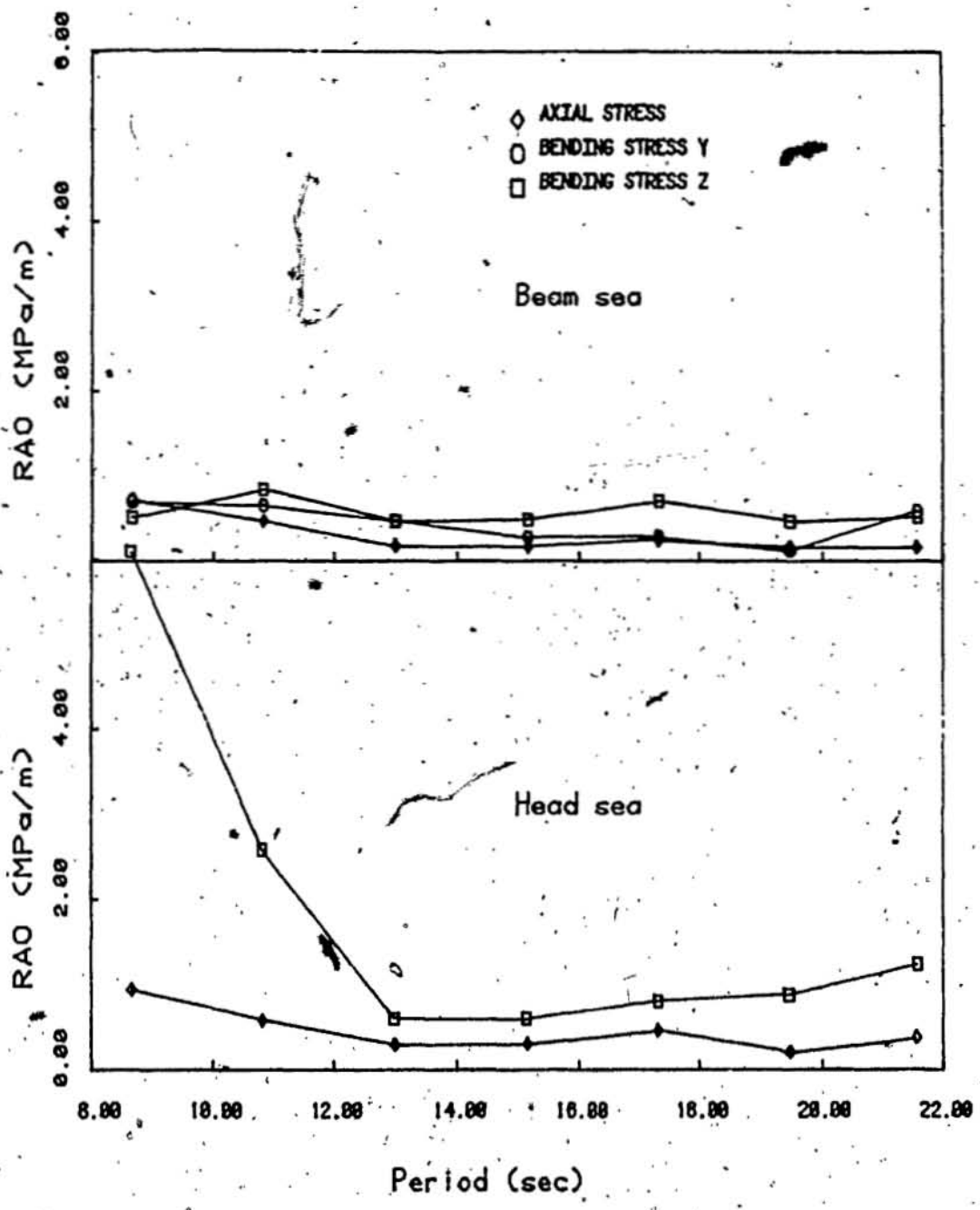

FIG. 5.25 STRESS RAO PLOTS FOR SECONDARY COLUMN SECTION ST - SURVIVAL DRAFT.

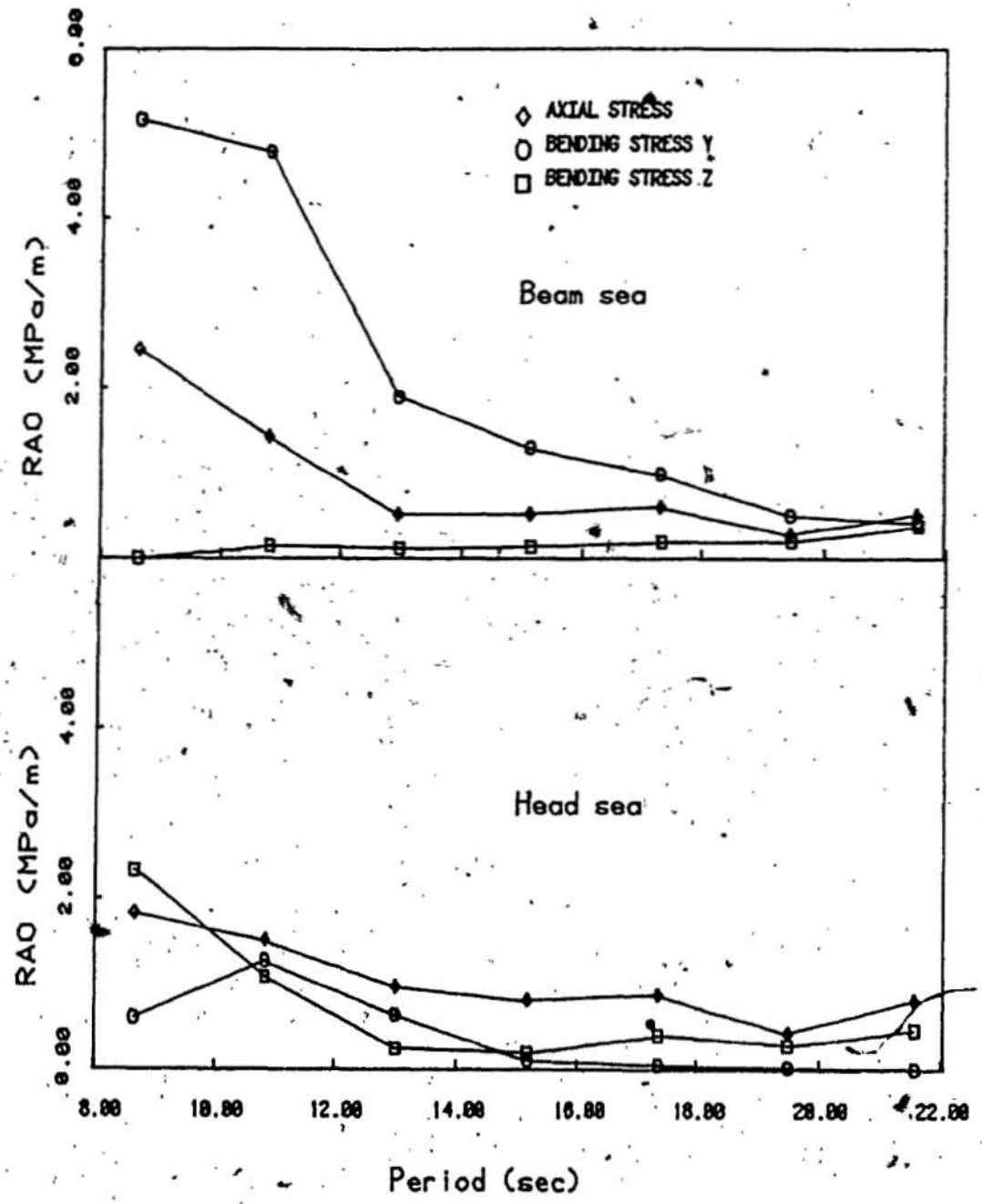

FIG. 5.26 STRESS RAO PLOTS FOR SECONDARY COLUMN SECTION SB - SURVIVAL DRAFT.

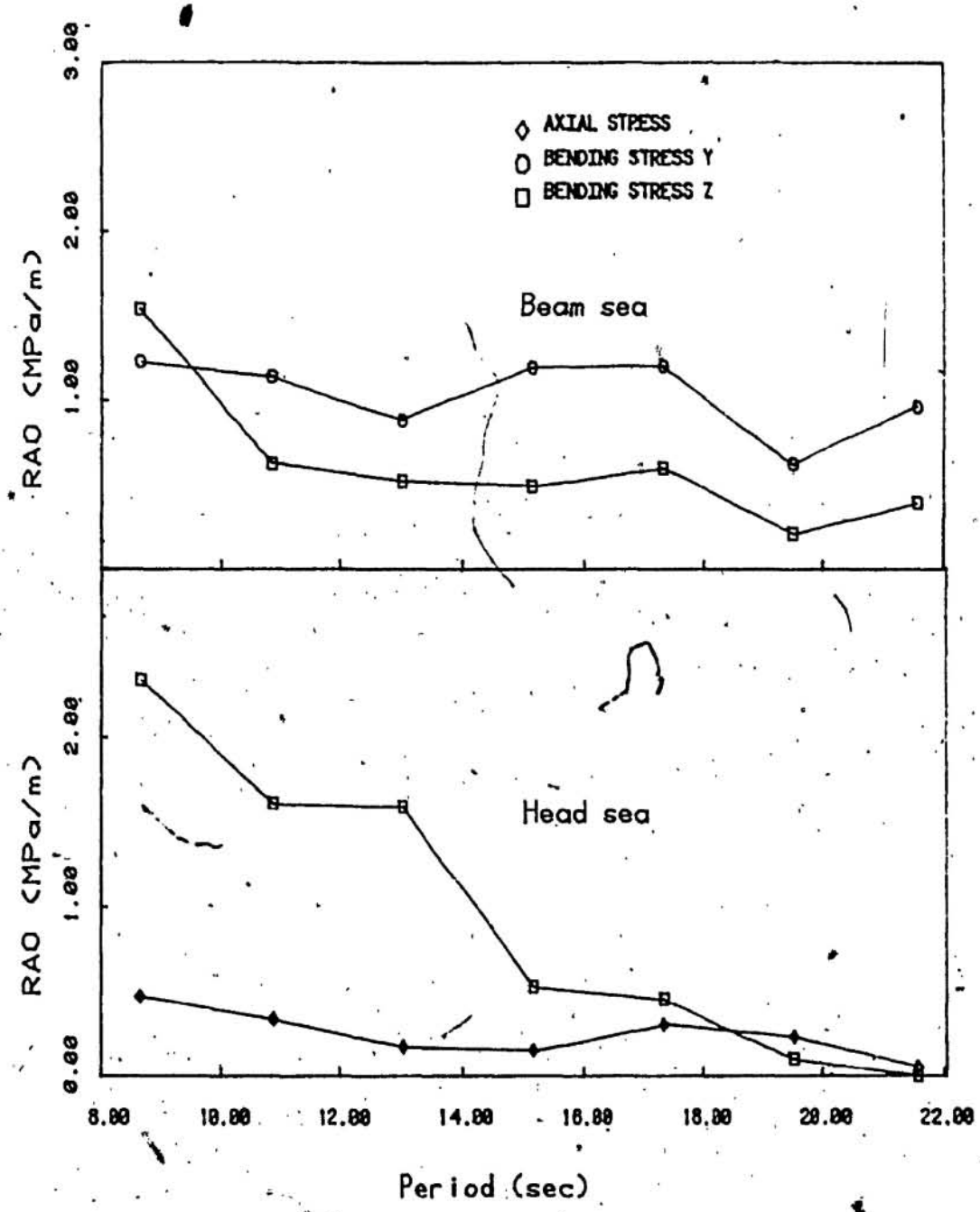

FIG. 5.27 STRESS RAO PLOTS FOR PONTOON MIDDLE SECTION PM - SURVIVAL DRAFT.

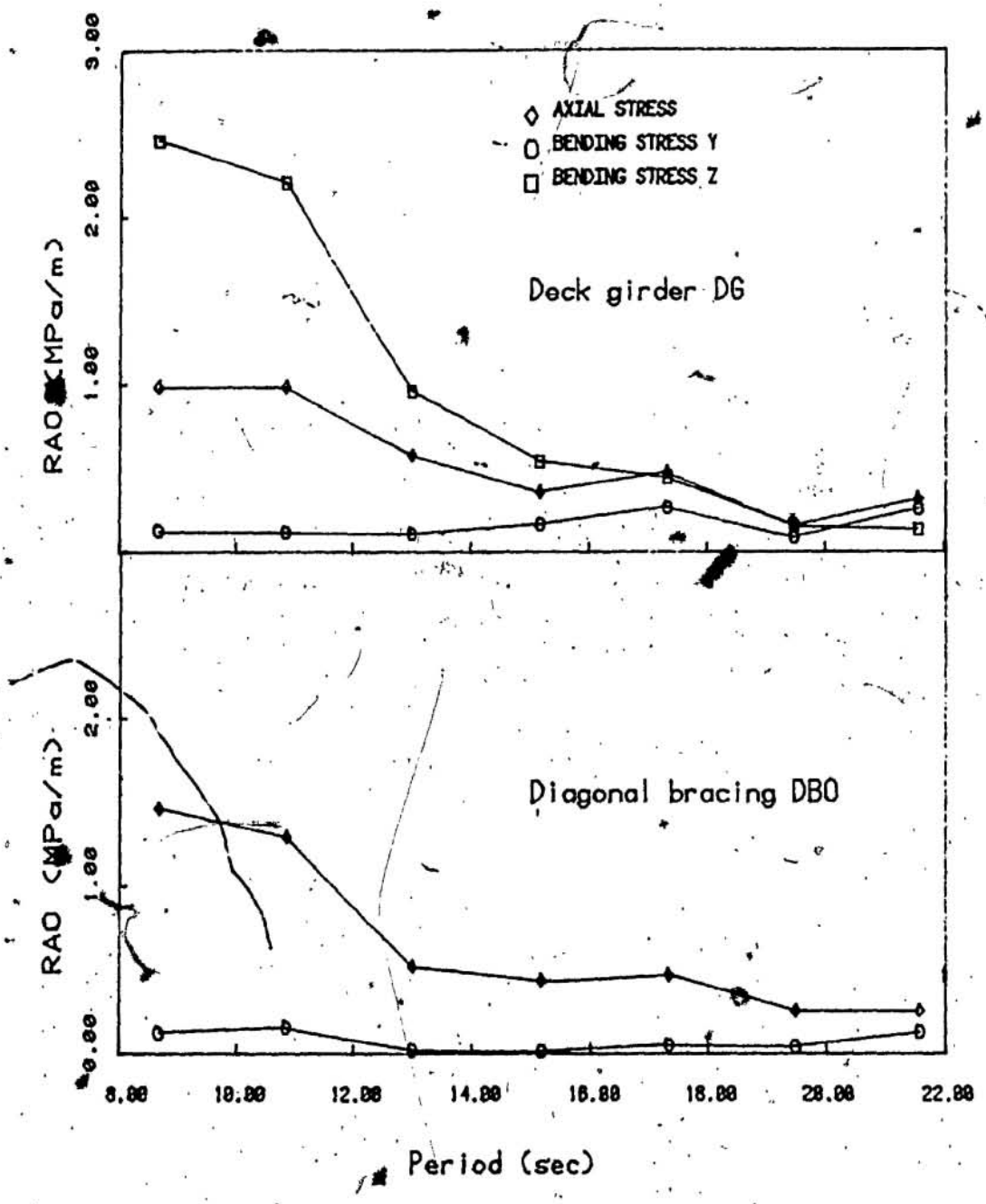

FIG. 5.28 STRESS RAO PLOTS - BEAM SEA AT SURVIVAL DRAFT.

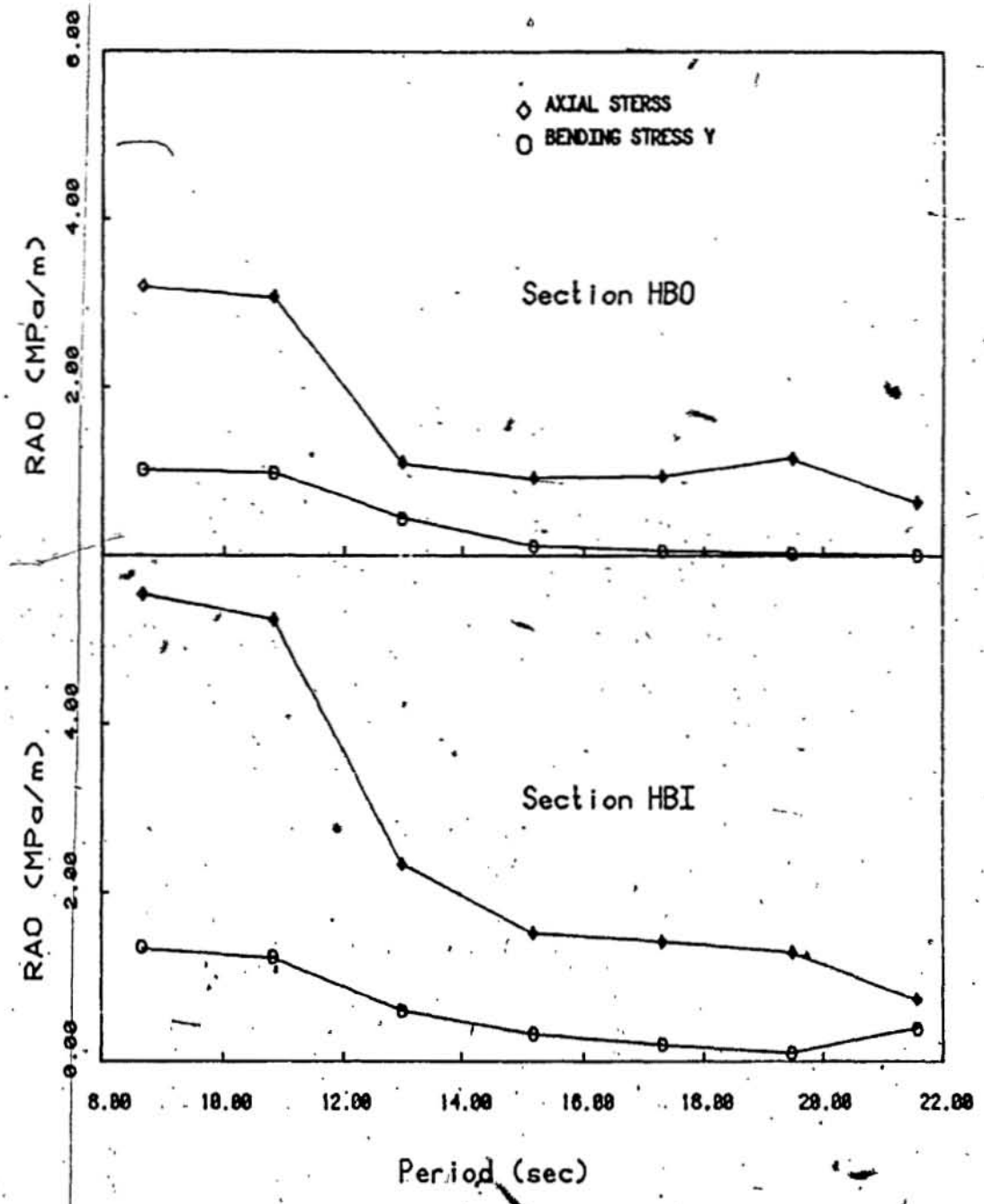

FIG. 5.29 STRESS RAO PLOTS FOR HORIZONTAL BRACINGS - BEAM SEA AT SURVIVAL DRAFT.

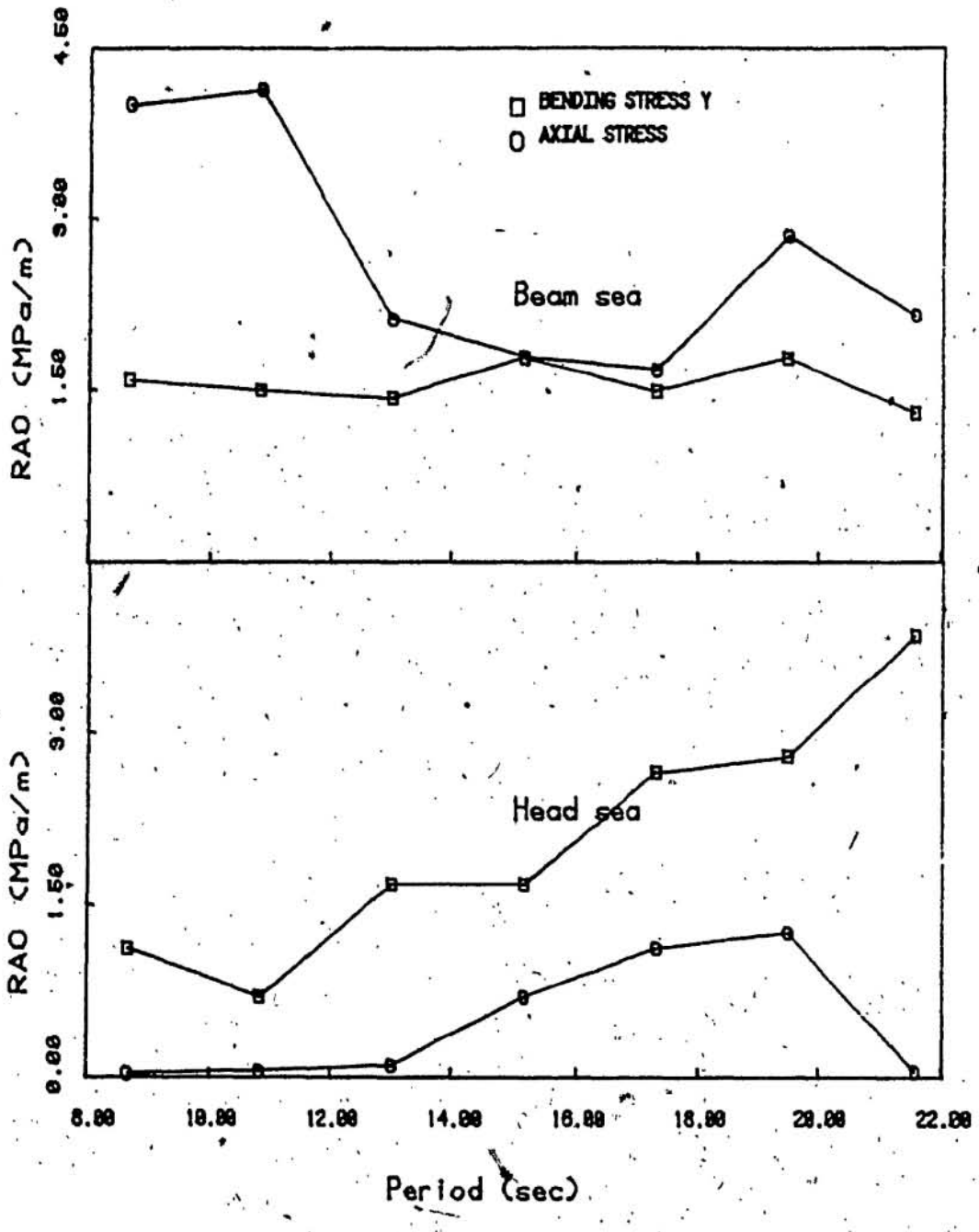

FIG. 5.30 RAO PLOTS FOR HORIZONTAL BRACING STRESS AT SECTION HBO - OPERATING DRAFT.

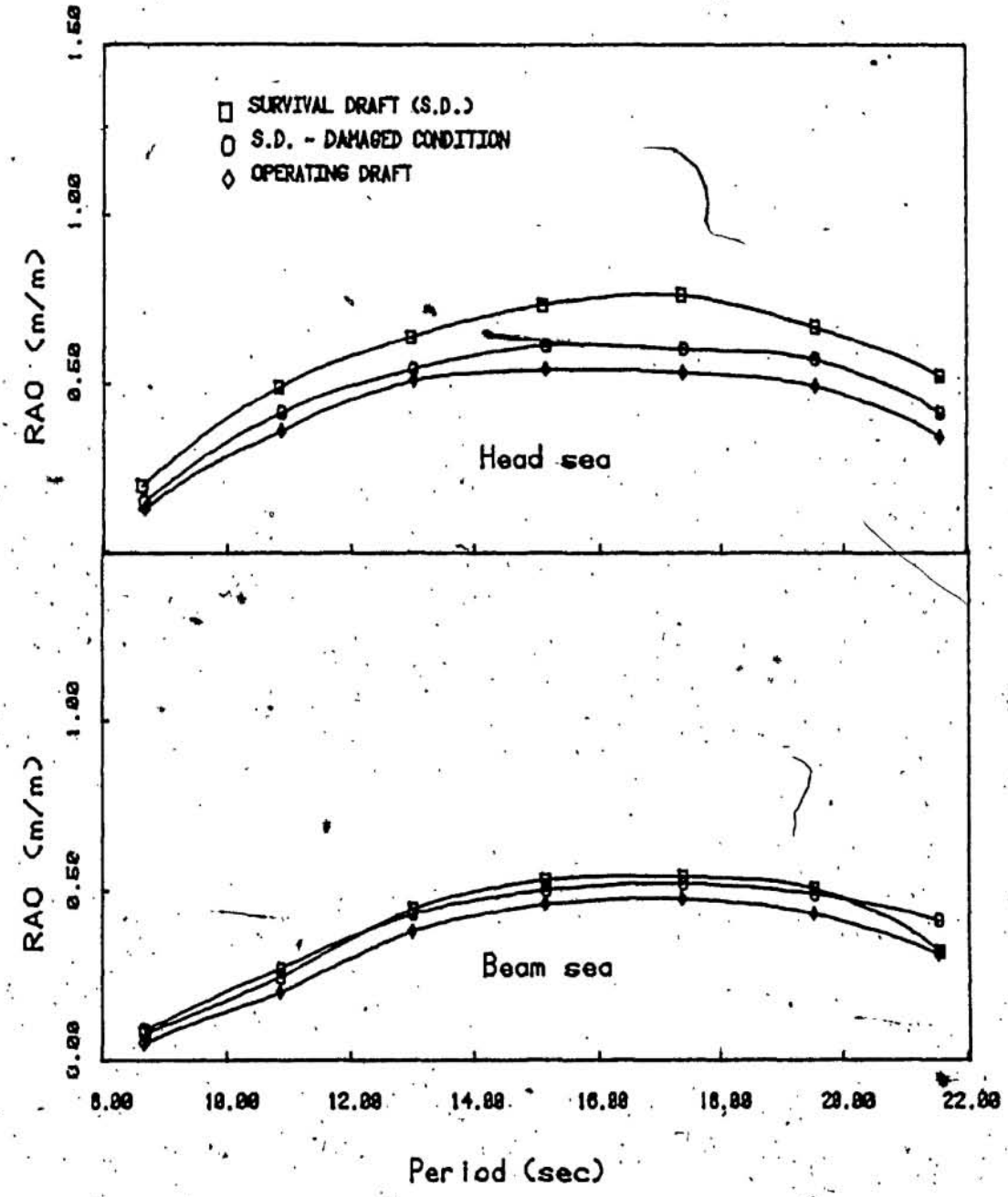

FIG. 5.31 HEAVE RESPONSE IN REGULAR WAVES.

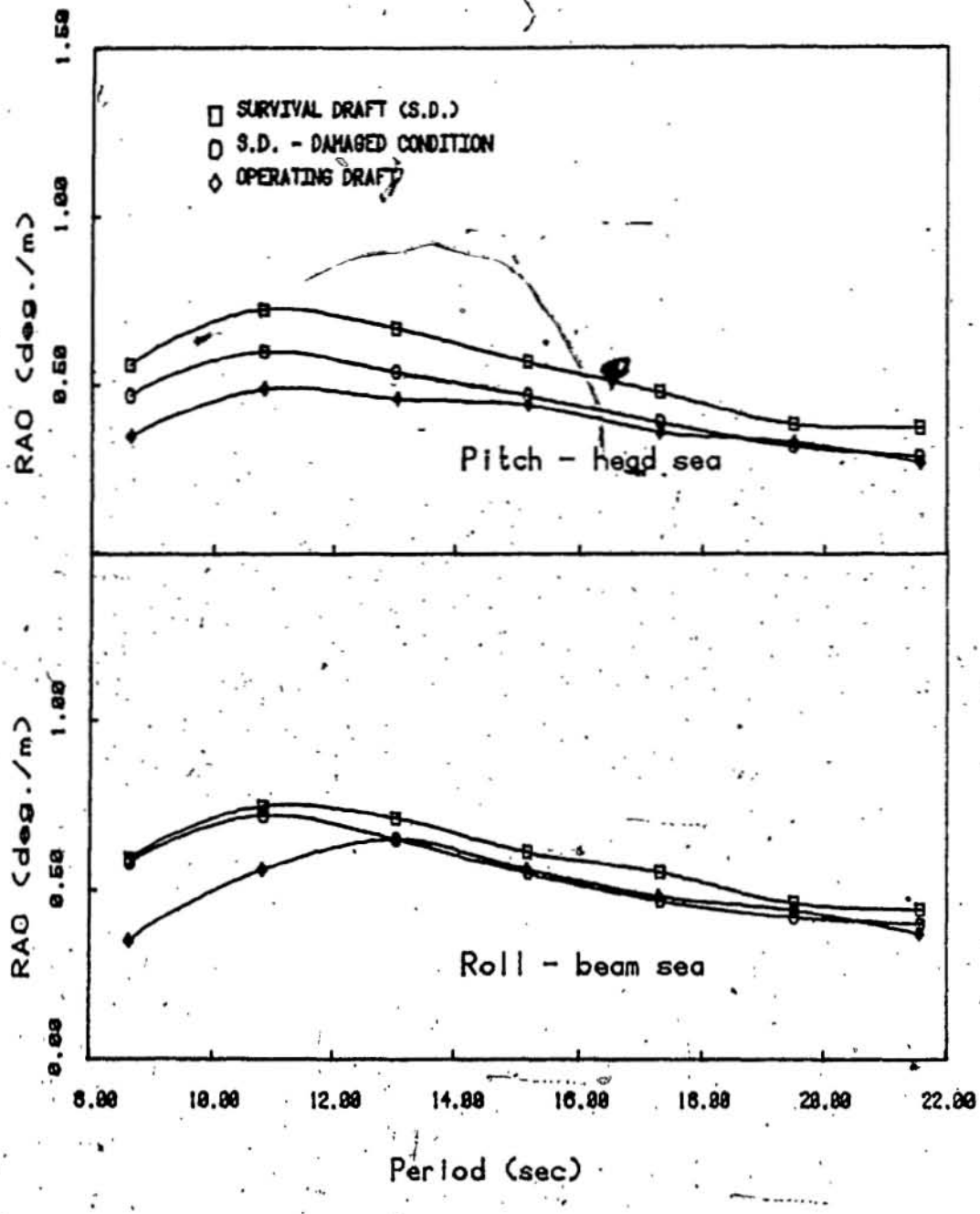

FIG. 5.32 PITCH AND ROLL RESPONSES IN REGULAR WAVES.

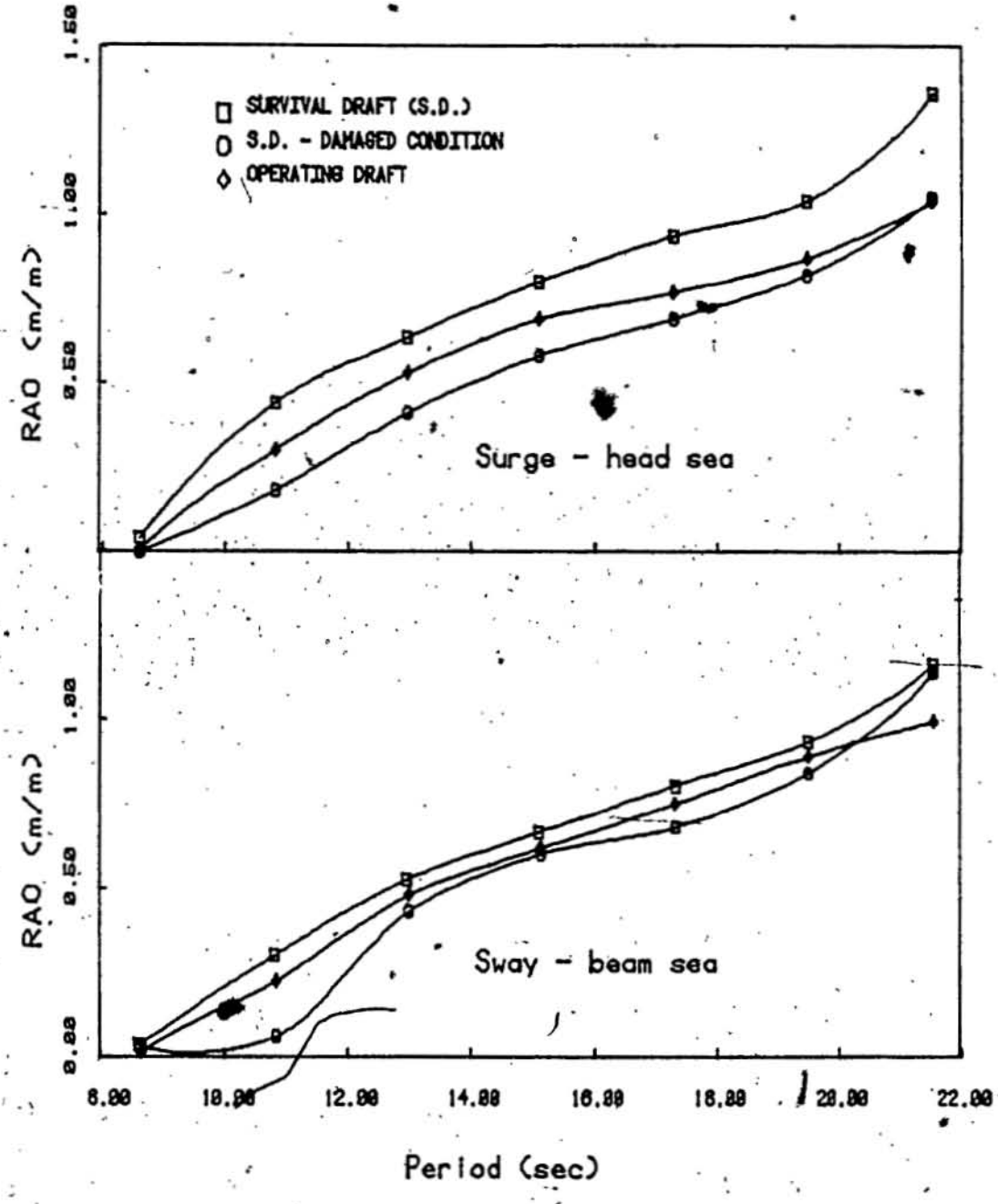

FIG. 5.33 SURGE AND SWAY RESPONSES IN REGULAR WAVES.

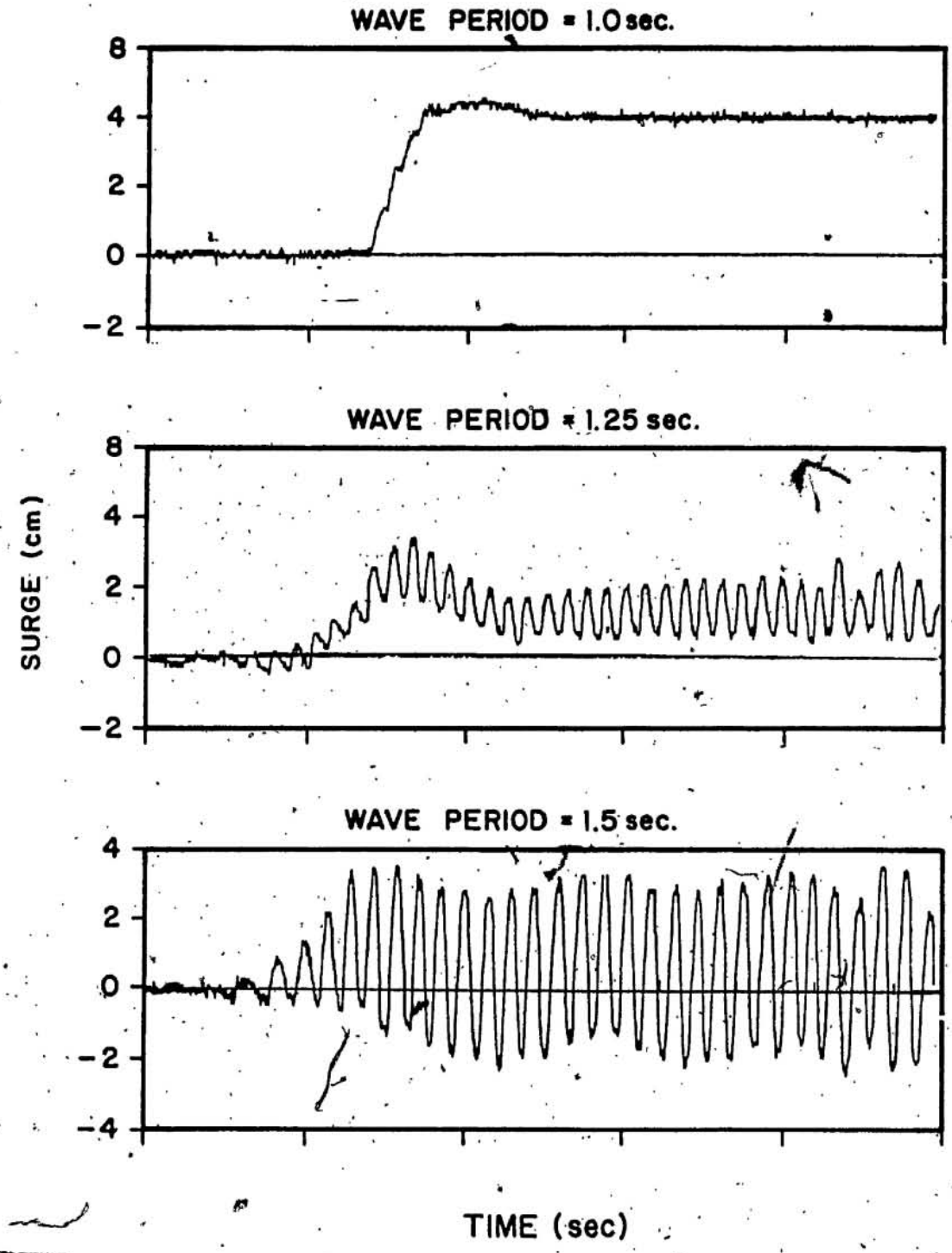

FIG. 5.34 SURGE MOTION UNDER DAMAGED CONDITION.

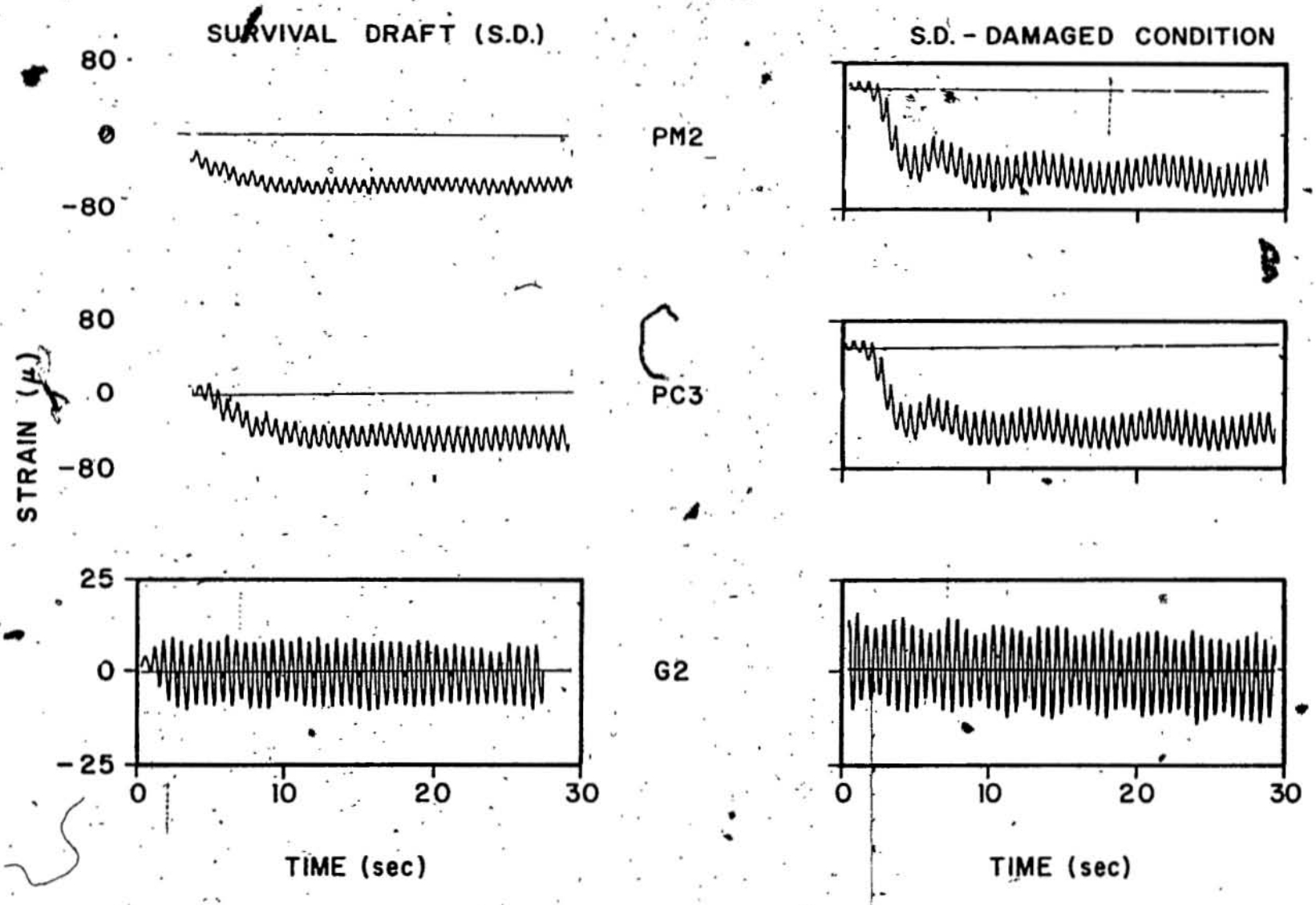

FIG. 5.35 MODEL STRAIN AS MEASURED BY INDICATED STRAIN GAUGES FOR LEVEL AND LISTING CONDITIONS WAVE PERIOD = 1 SEC.

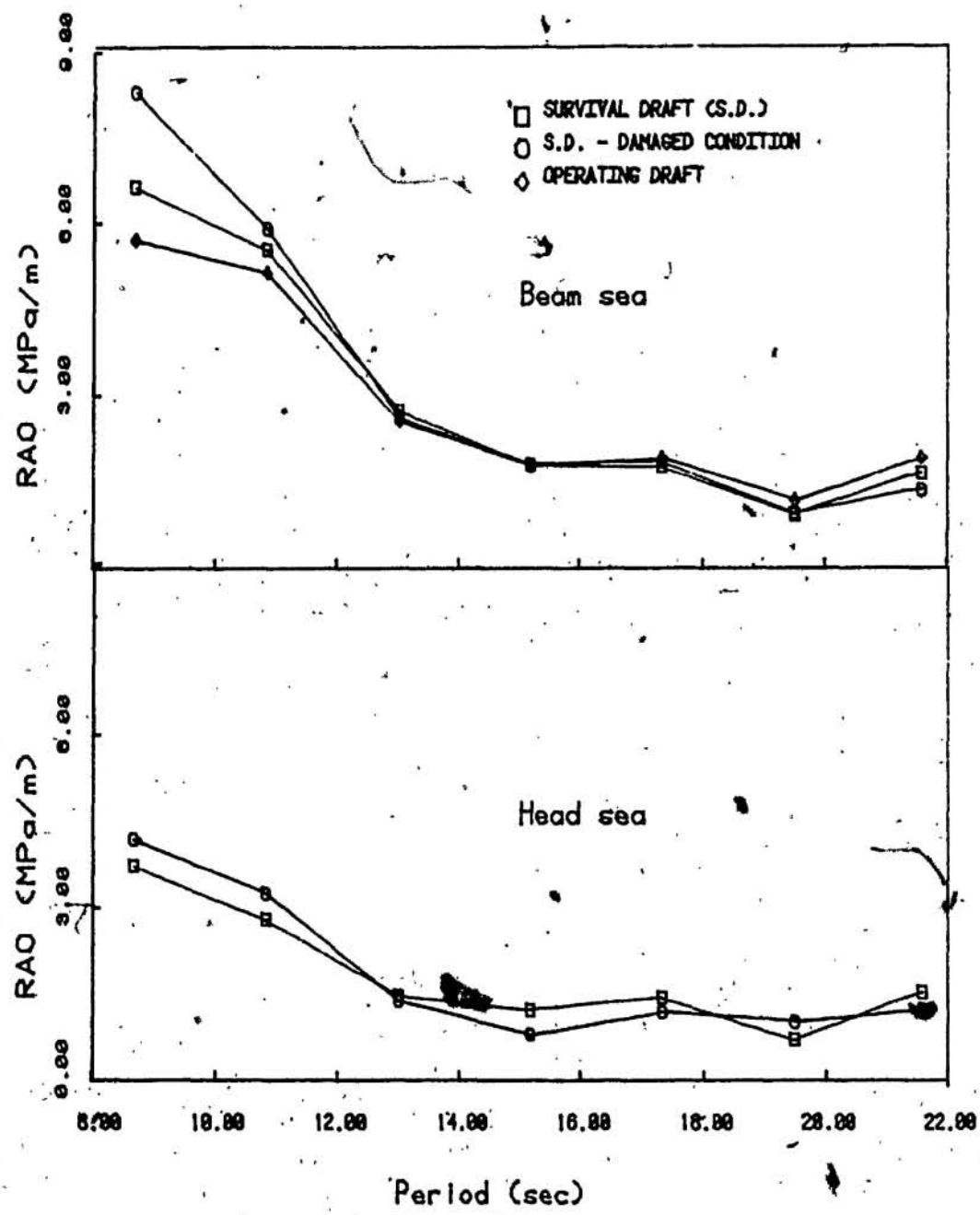

FIG. 5.36 RAO PLOTS FOR COMBINED STRESSES AT BASE OF MAIN COLUMN - SECTION MB.

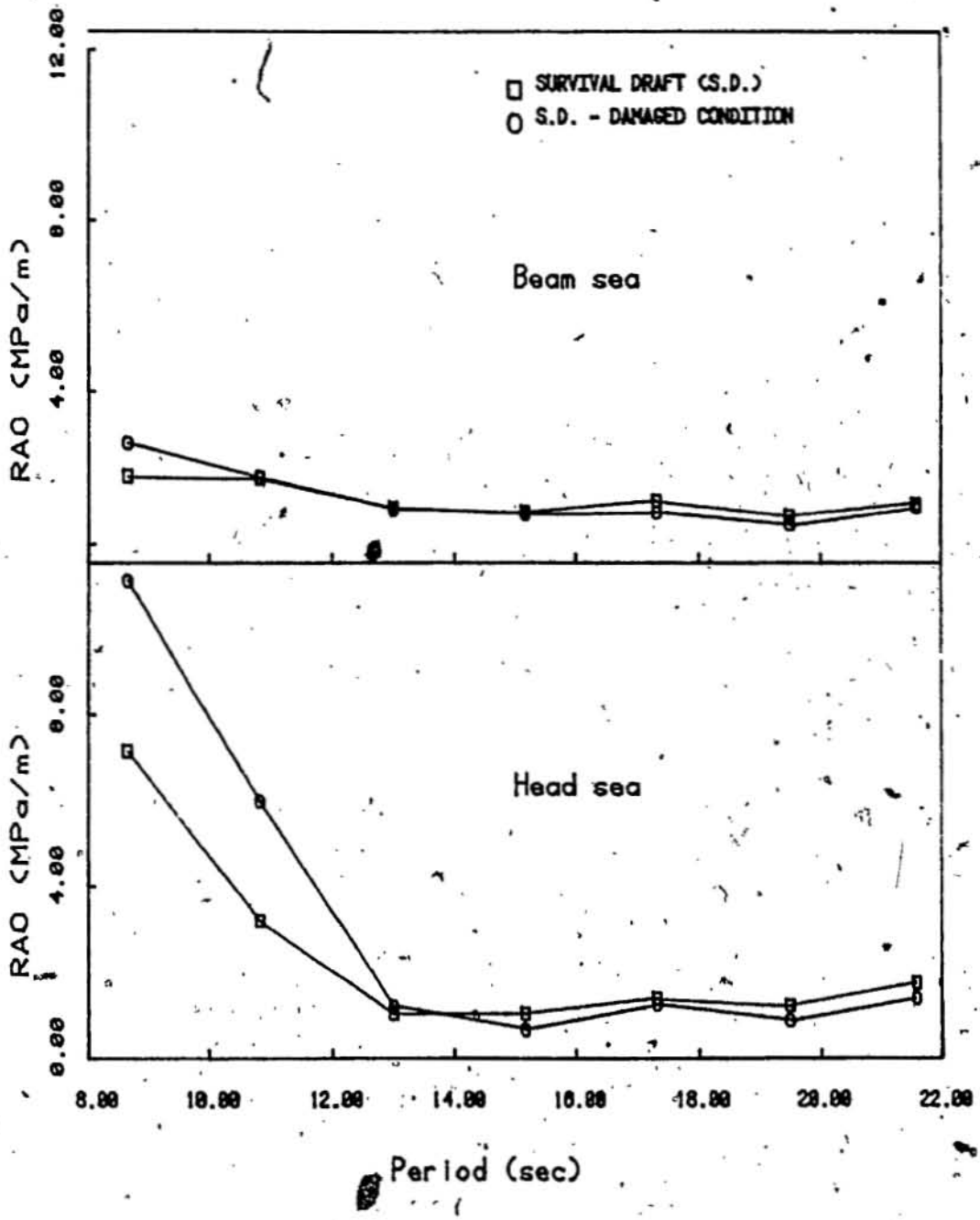

FIG. 5.37 RAO PLOTS FOR COMBINED STRESSES AT TOP OF SECONDARY COLUMN - SECTION ST.

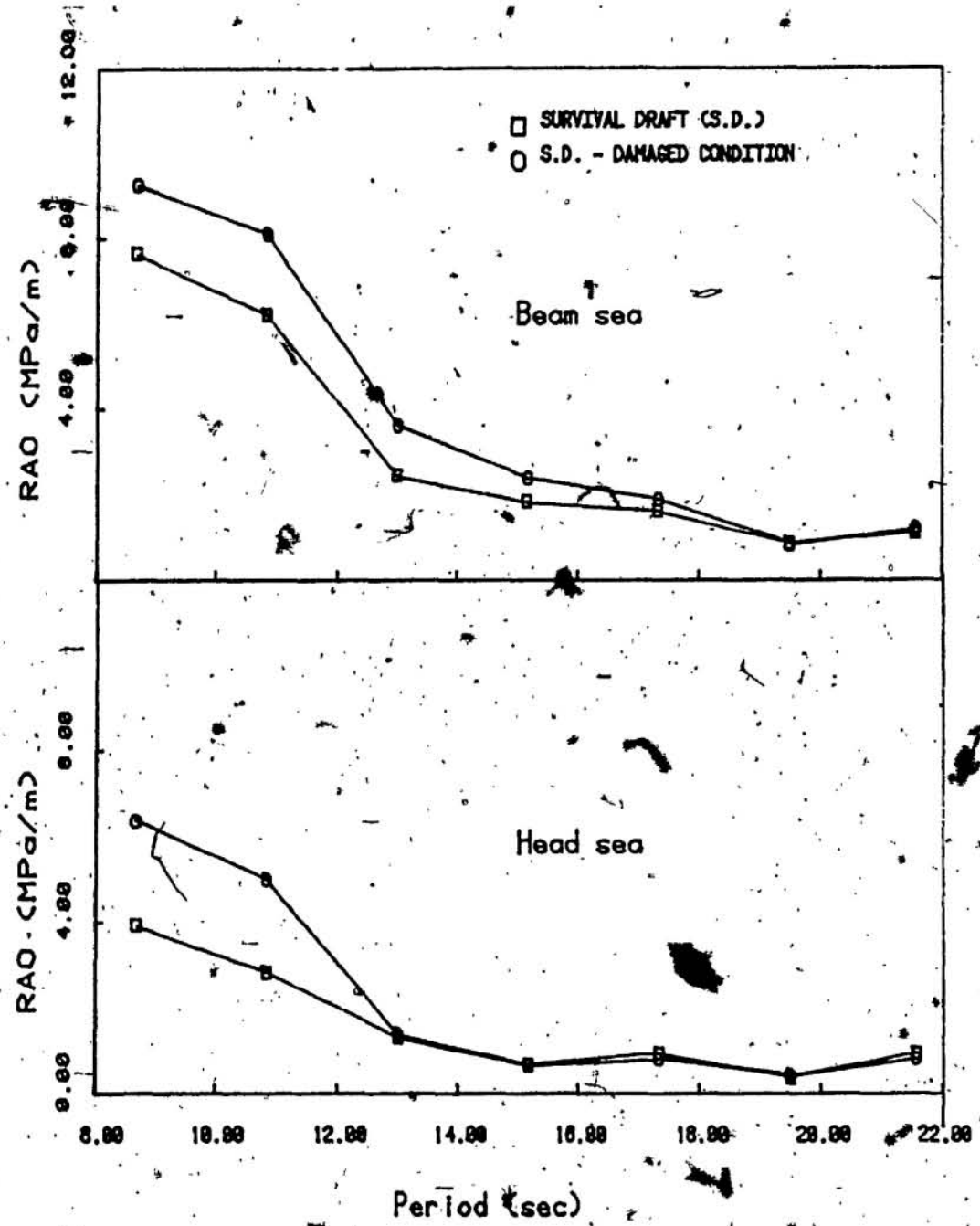

FIG. 5.38 RAO PLOTS FOR COMBINED STRESSES AT BASE OF SECONDARY COLUMN - SECTION SB.

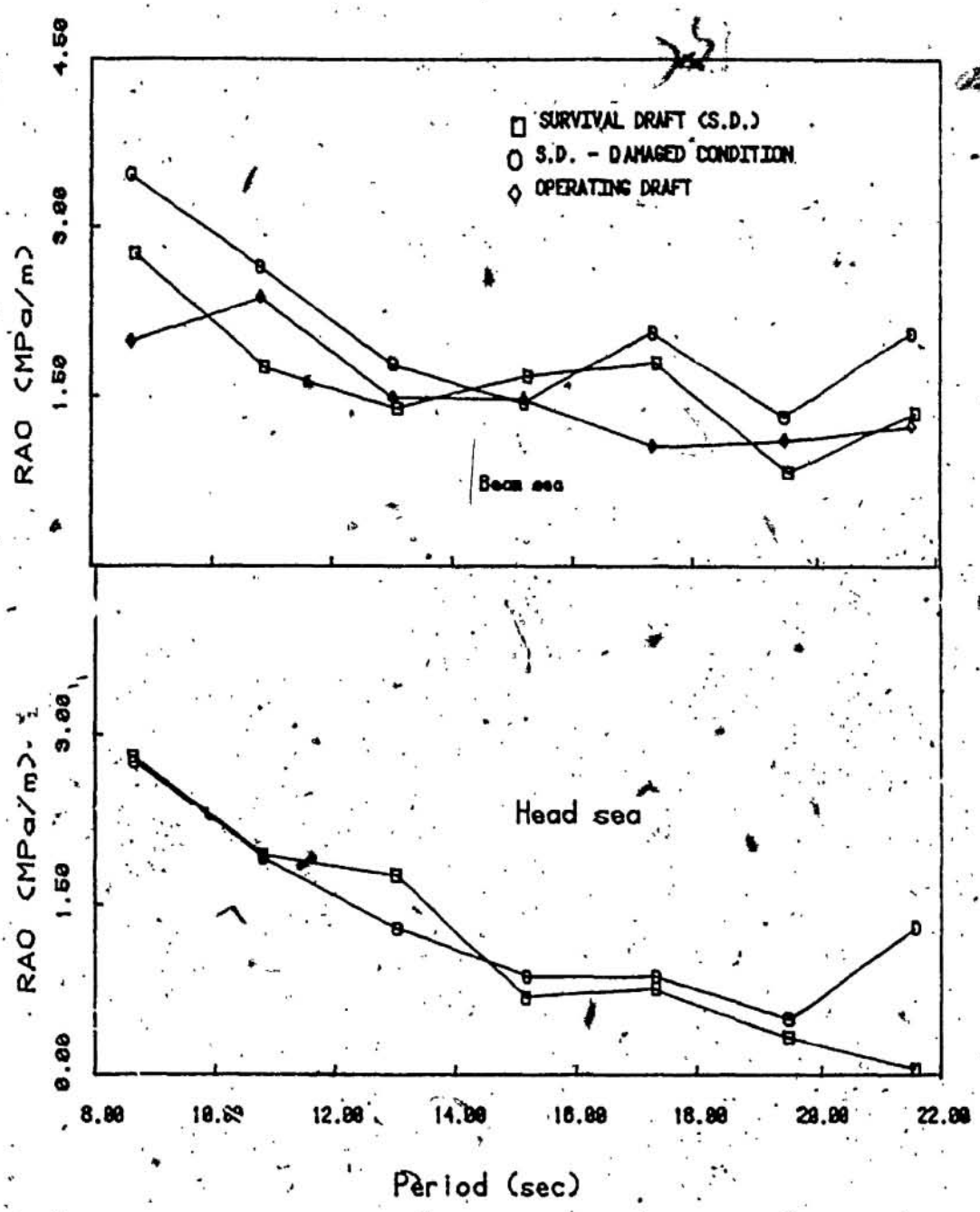

FIG. 5.39 RAO PLOTS FOR COMBINED STRESSES AT PONTOON MIDDLE SECTION PM.

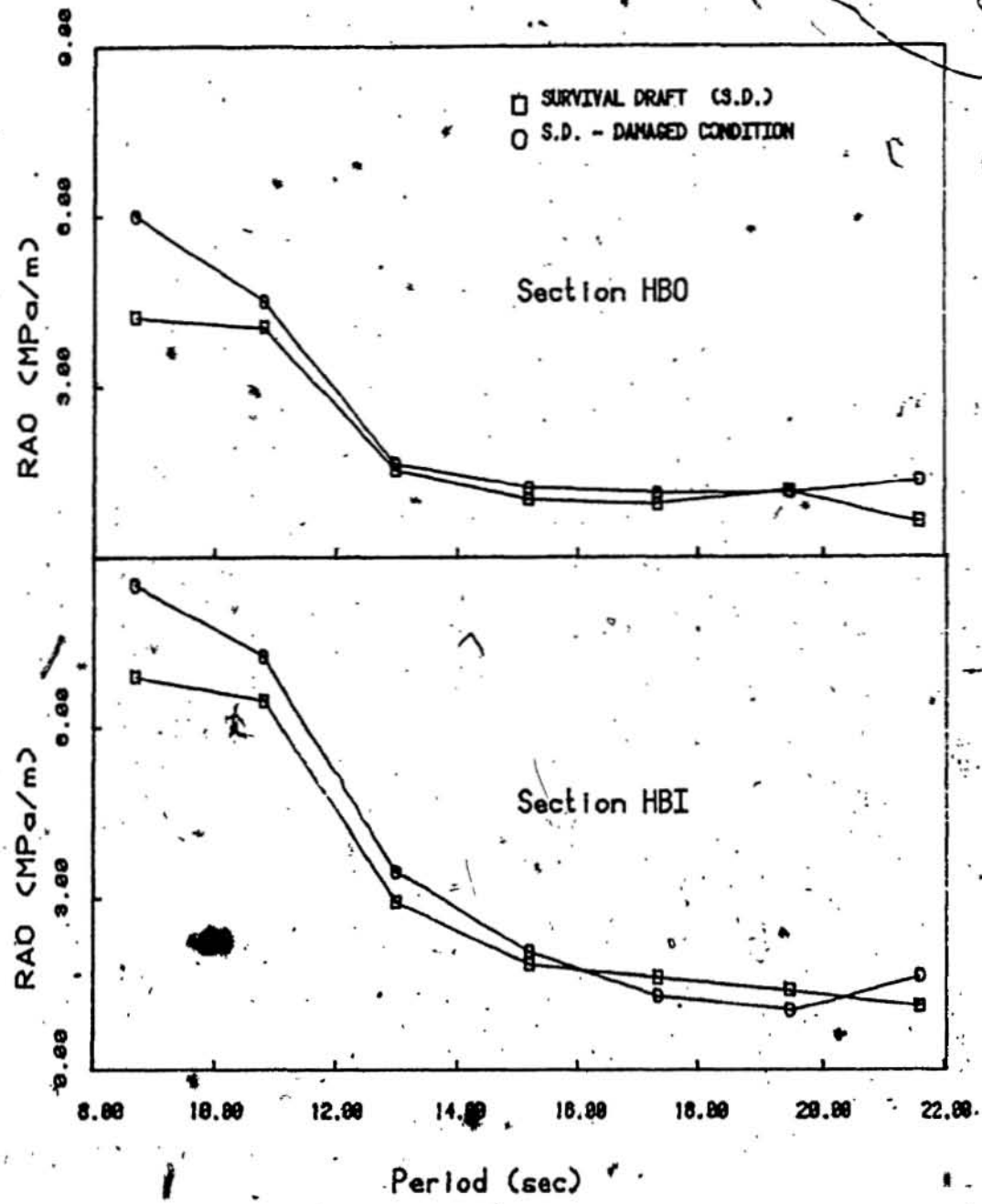

FIG. 5.40 RAO PLOTS FOR COMBINED STRESSES IN HORIZONTAL BRACINGS - BEAM SEA.

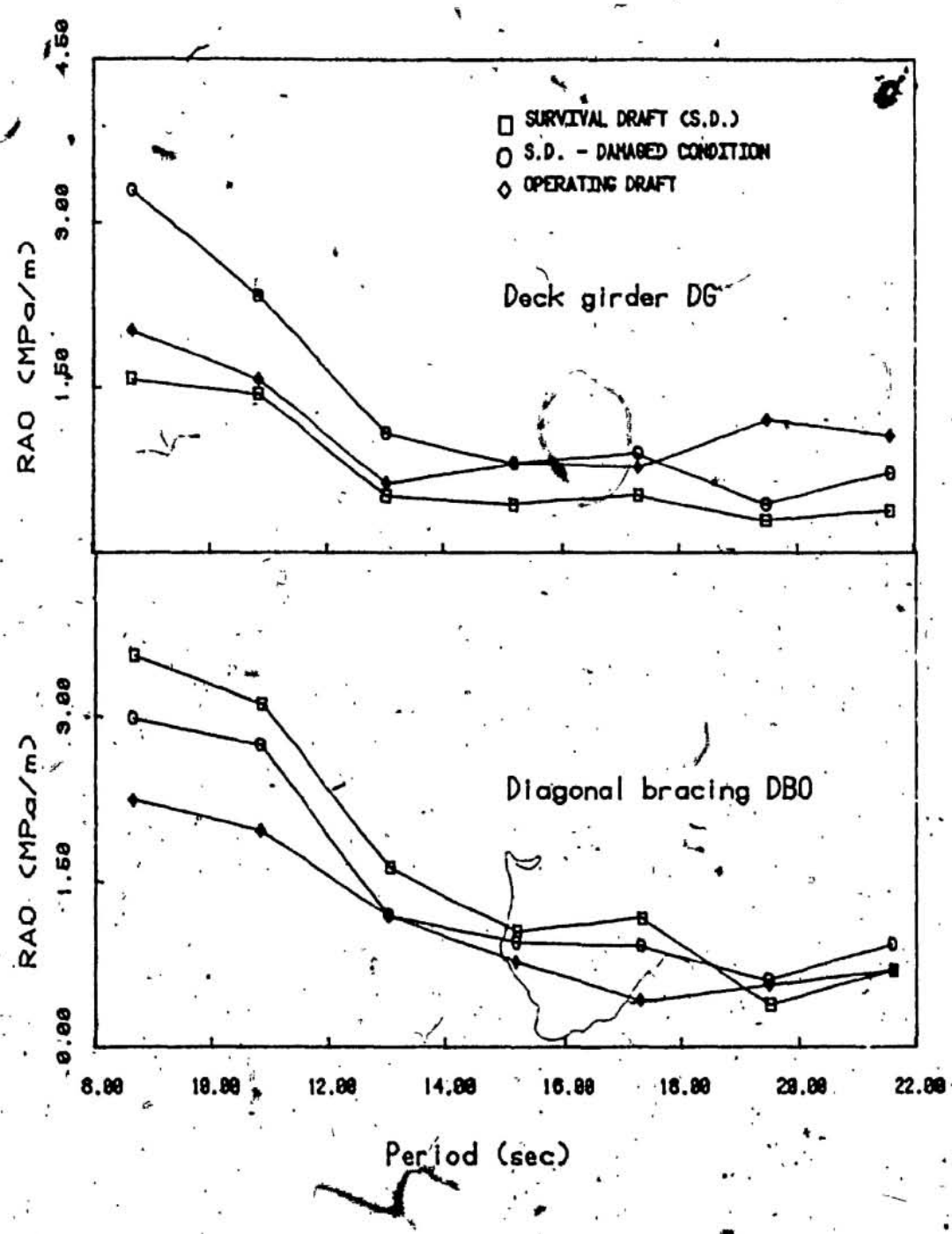

FIG. 5.41 RAO PLOTS FOR COMBINED STRESSES - BEAM SEA.

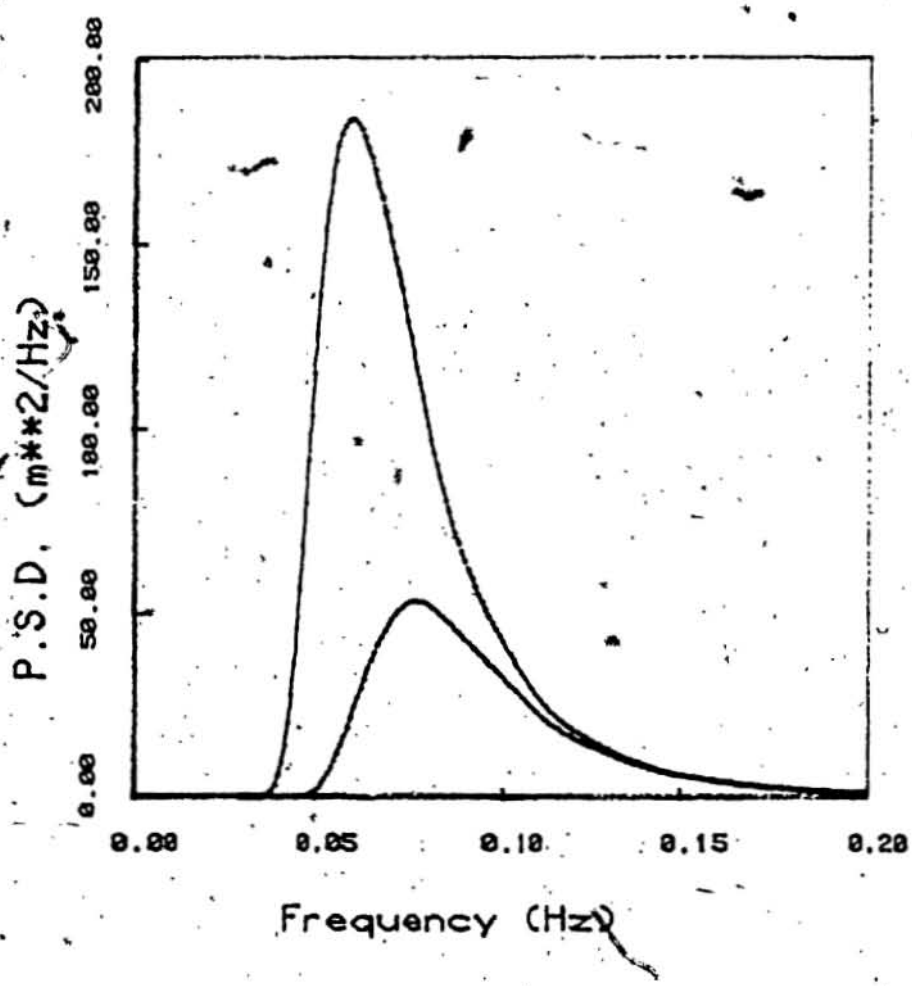

FIG. 5.42 TARGET P-M SPECTRA

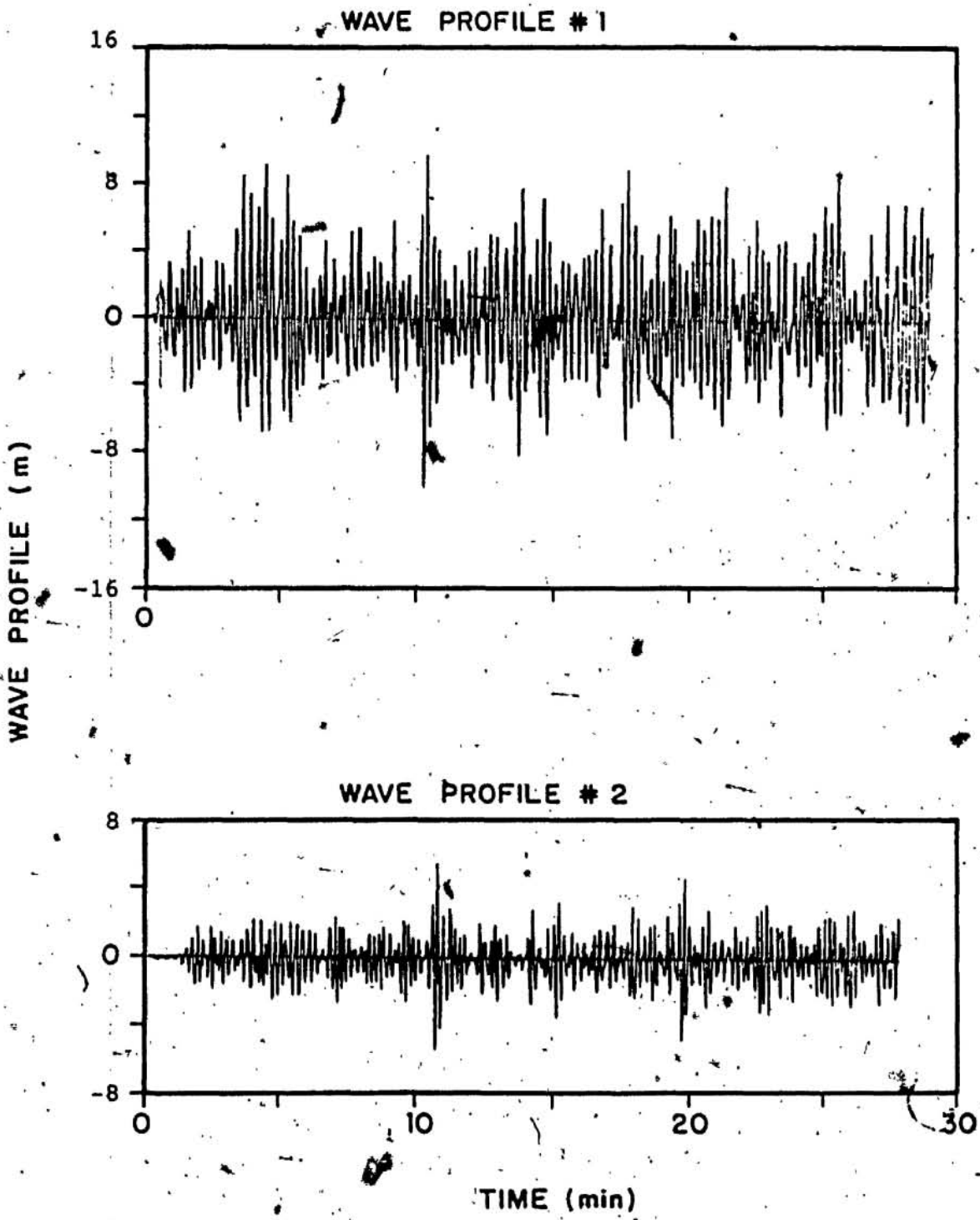

FIG. 5.43 IRREGULAR WAVE PROFILES.

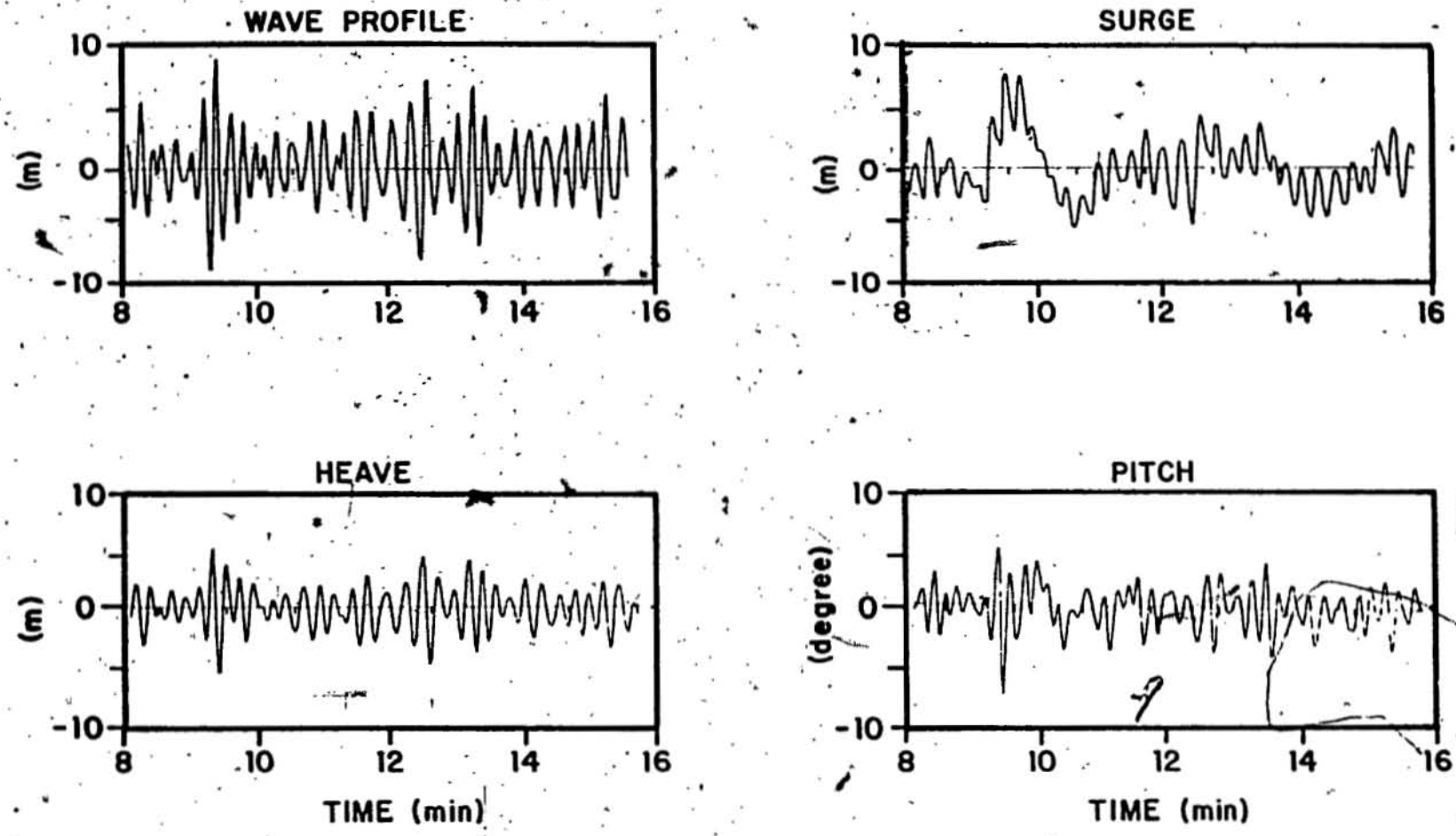

FIG. 5.44 PORTION OF WAVE PROFILE #1 AND MOTION HISTORY IN HEAD SEA

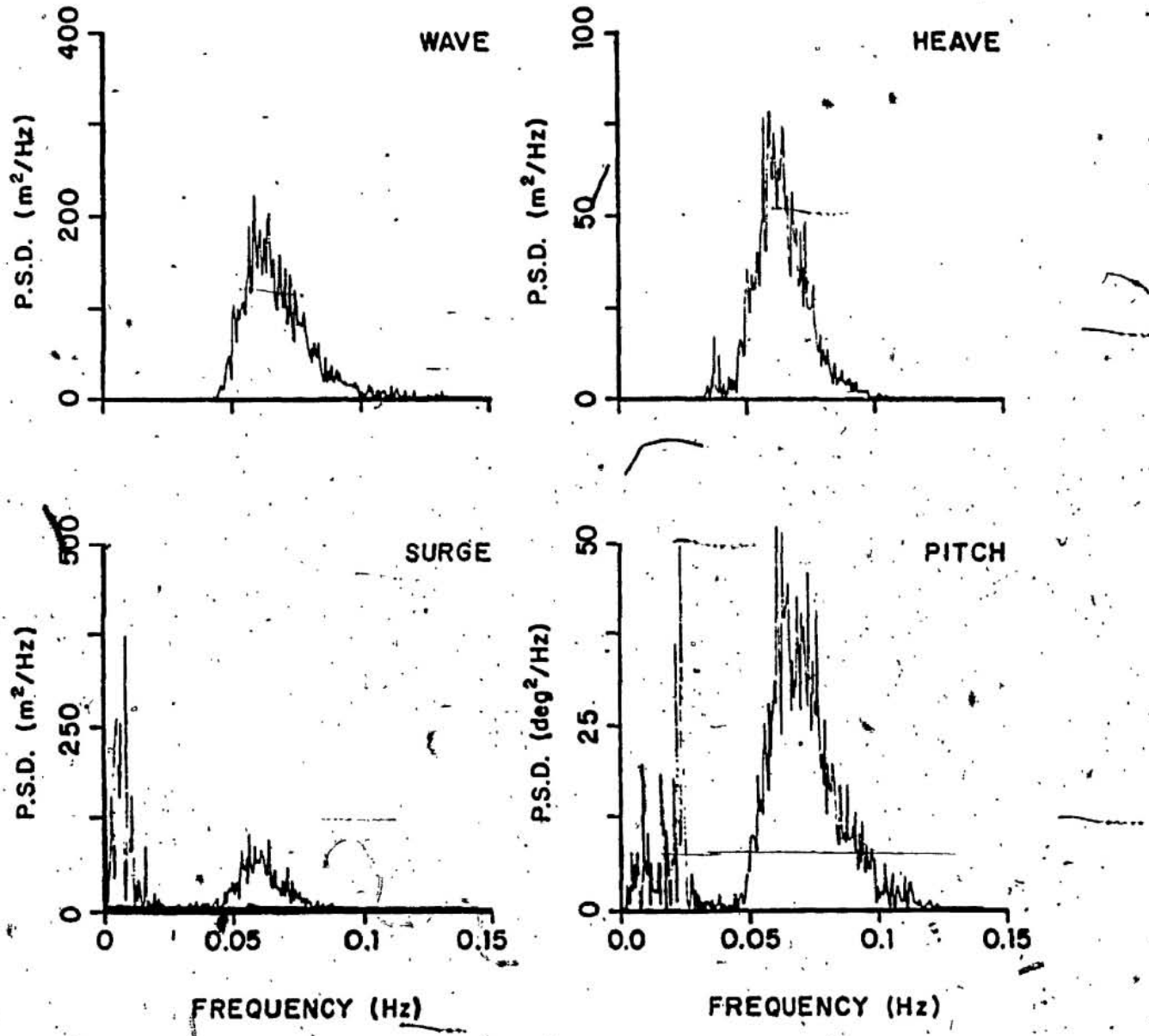

FIG. 5.45 POWER SPECTRAL DENSITY PLOTS FOR WAVE AND MOTION IN HEAD SEA - WAVE SPECTRUM # 1.

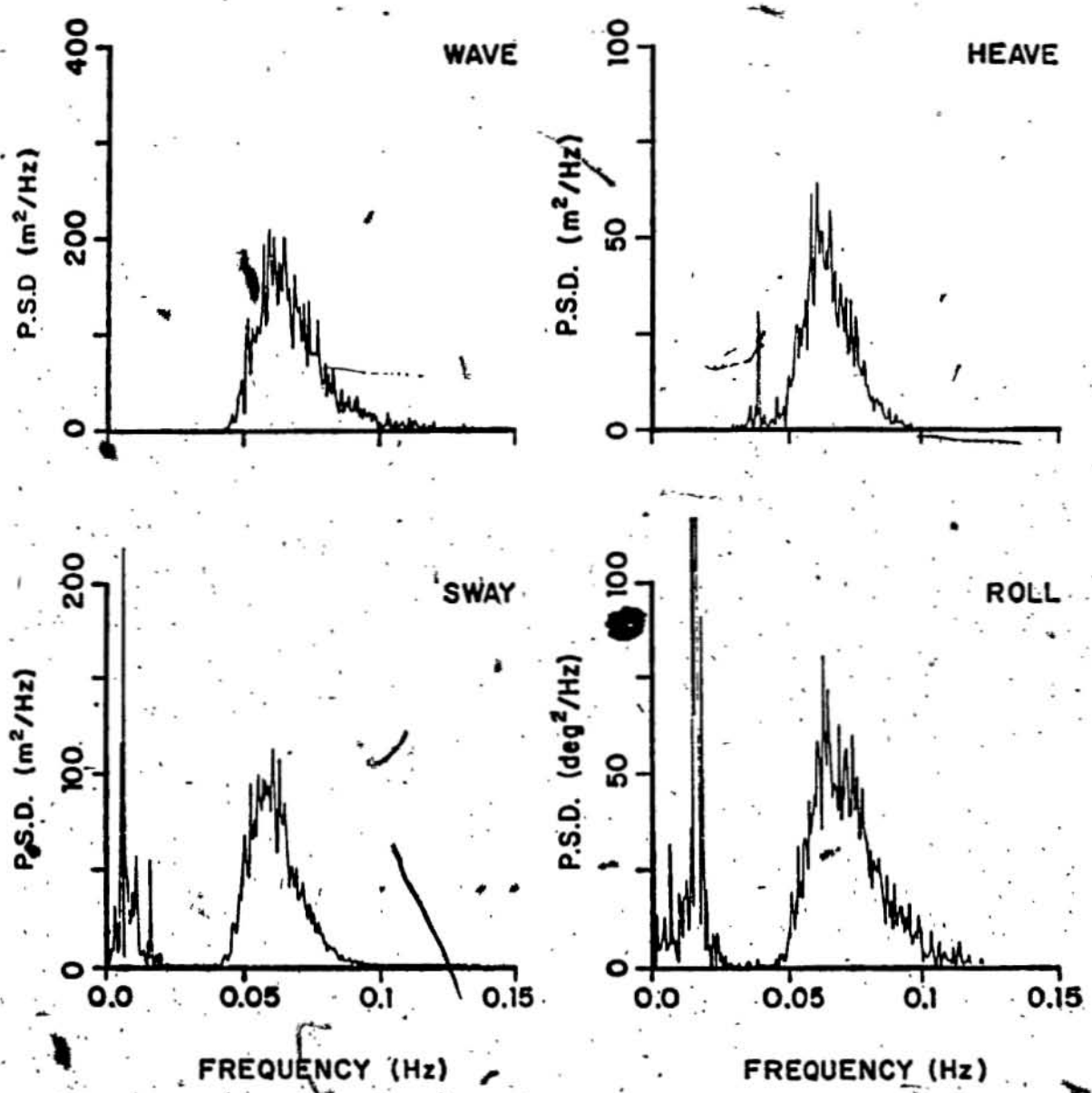

FIG. 5.46 POWER SPECTRAL DENSITY PLOTS FOR WAVE AND MOTION IN BEAM SEA - WAVE SPECTRUM # 1.

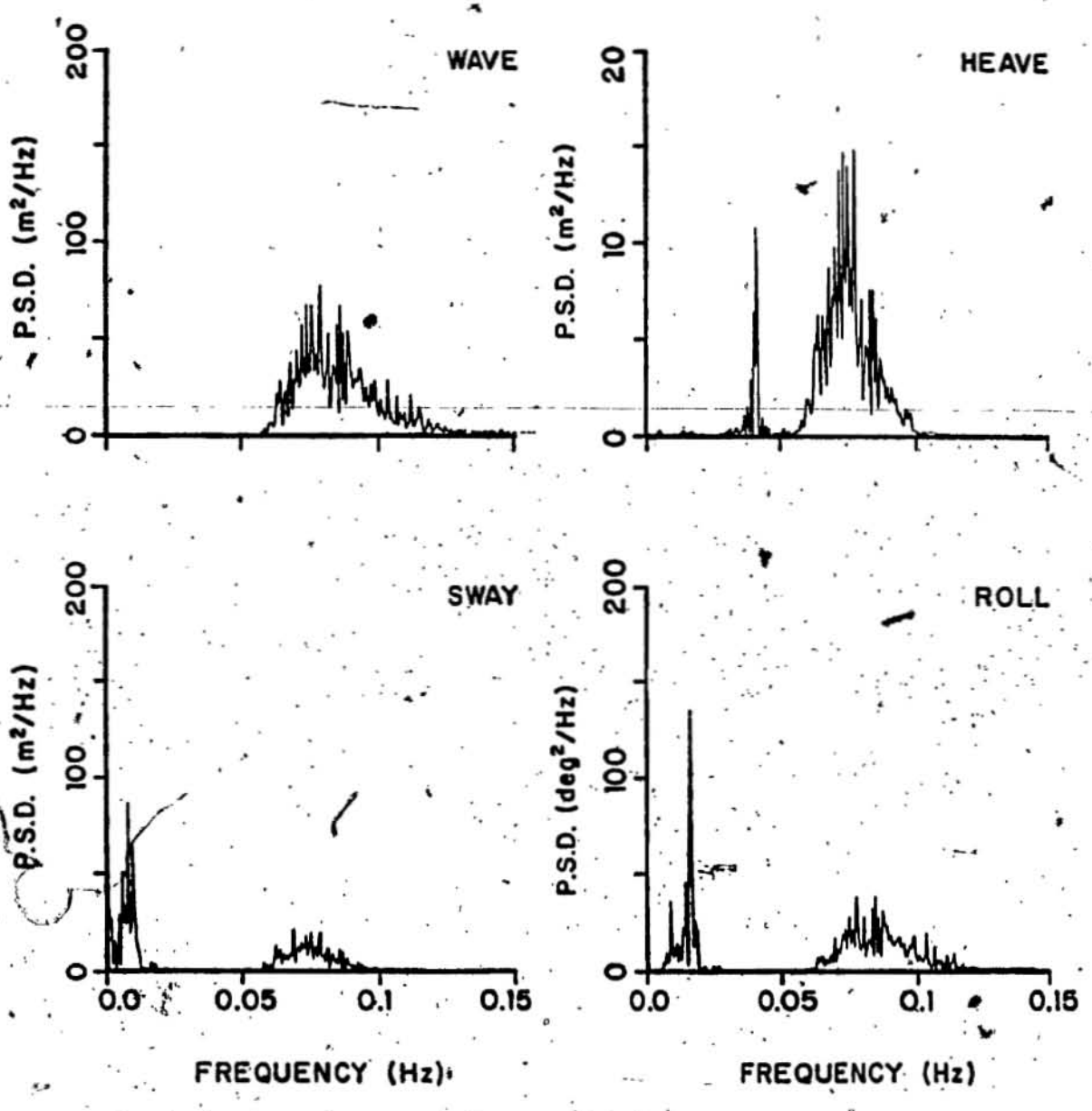

FIG. 5.47 POWER SPECTRAL DENSITY PLOTS FOR WAVE AND MOTION IN BEAM SEA - WAVE SPECTRUM #2.

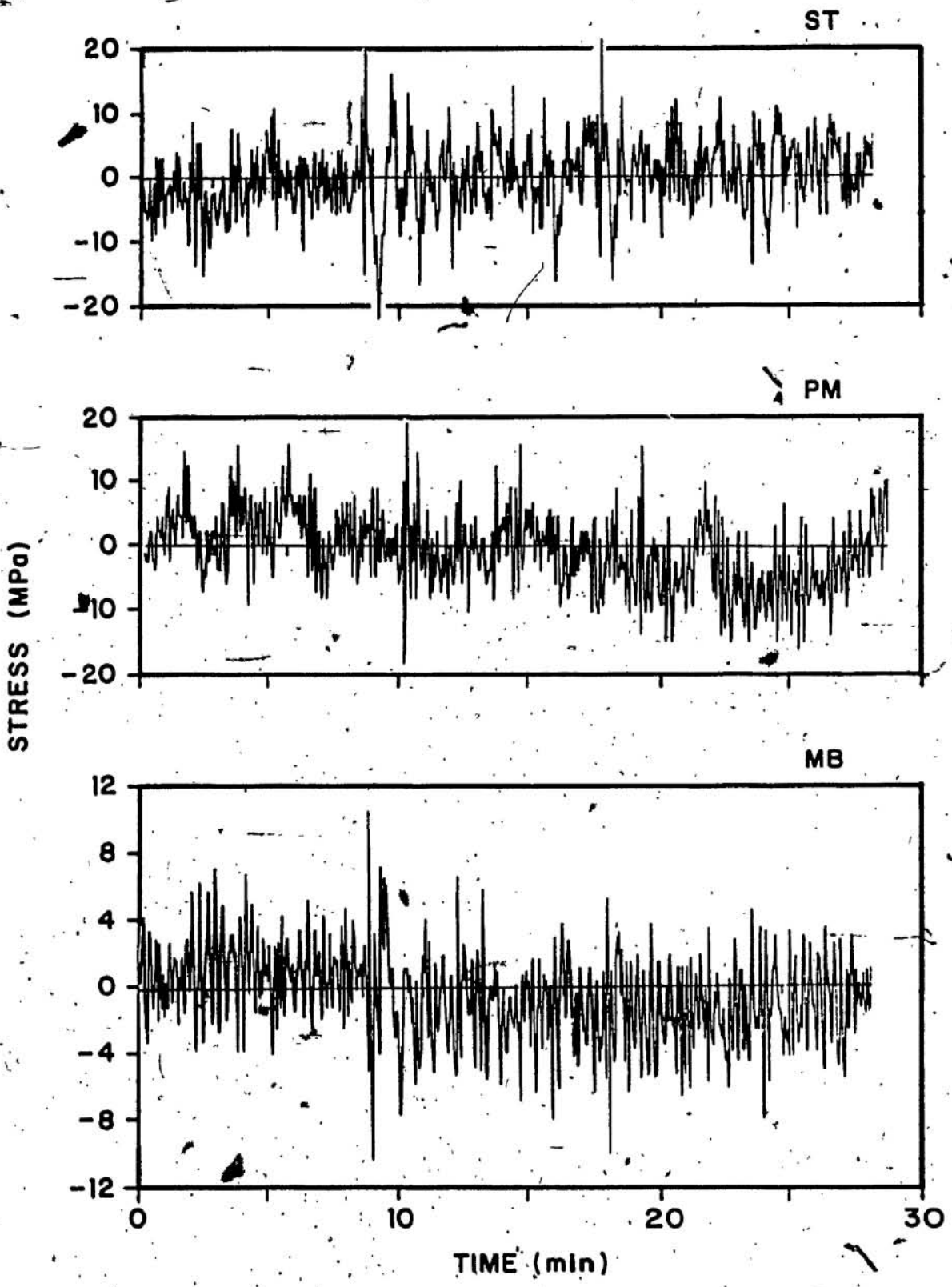

FIG. 5.48 MEASURED BENDING STRESS Z IN INDICATED SECTIONS – HEAD SEA.

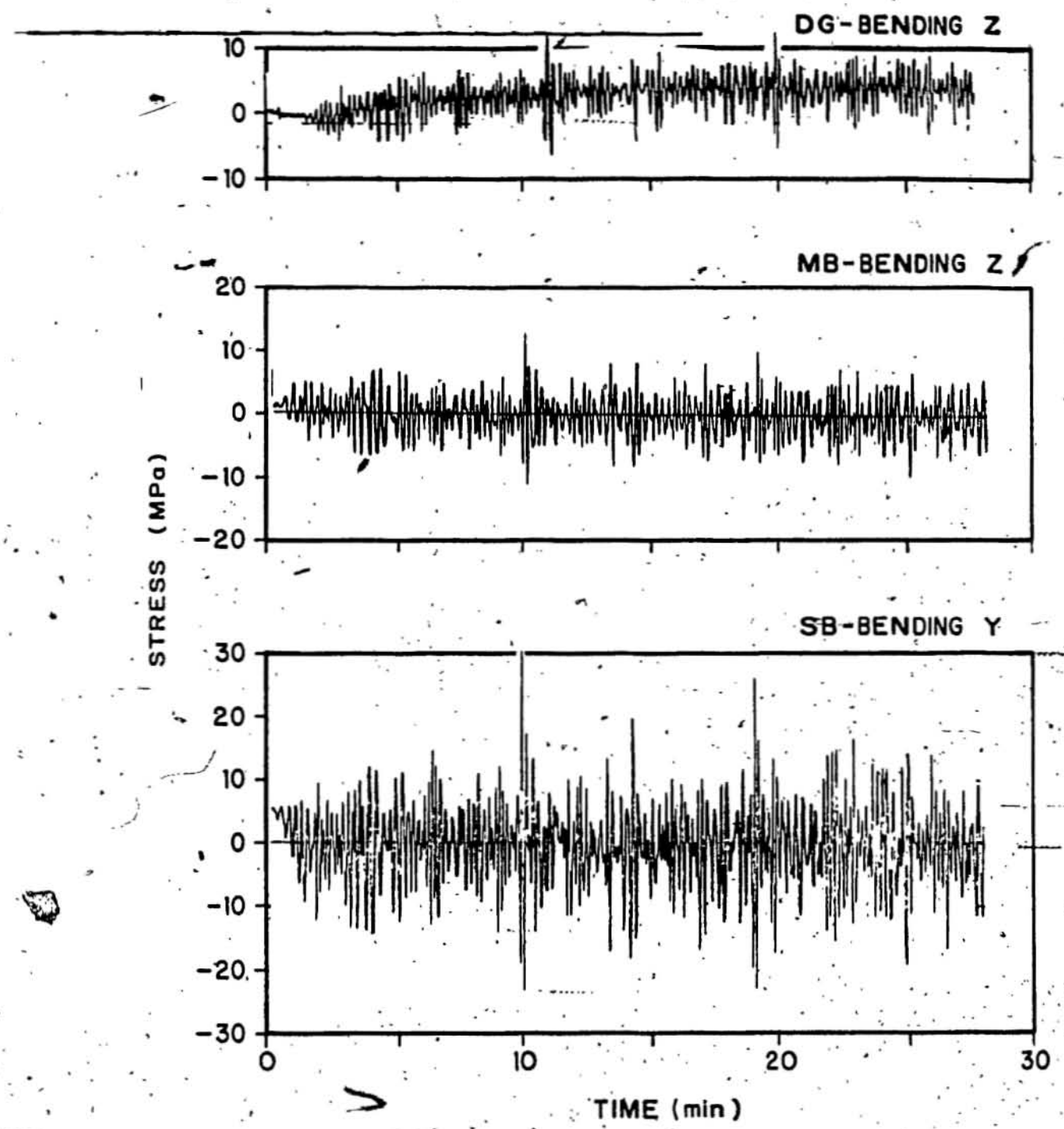

FIG. 5.49 MEASURED BENDING STRESS IN INDICATED SECTIONS BEAM SEA.

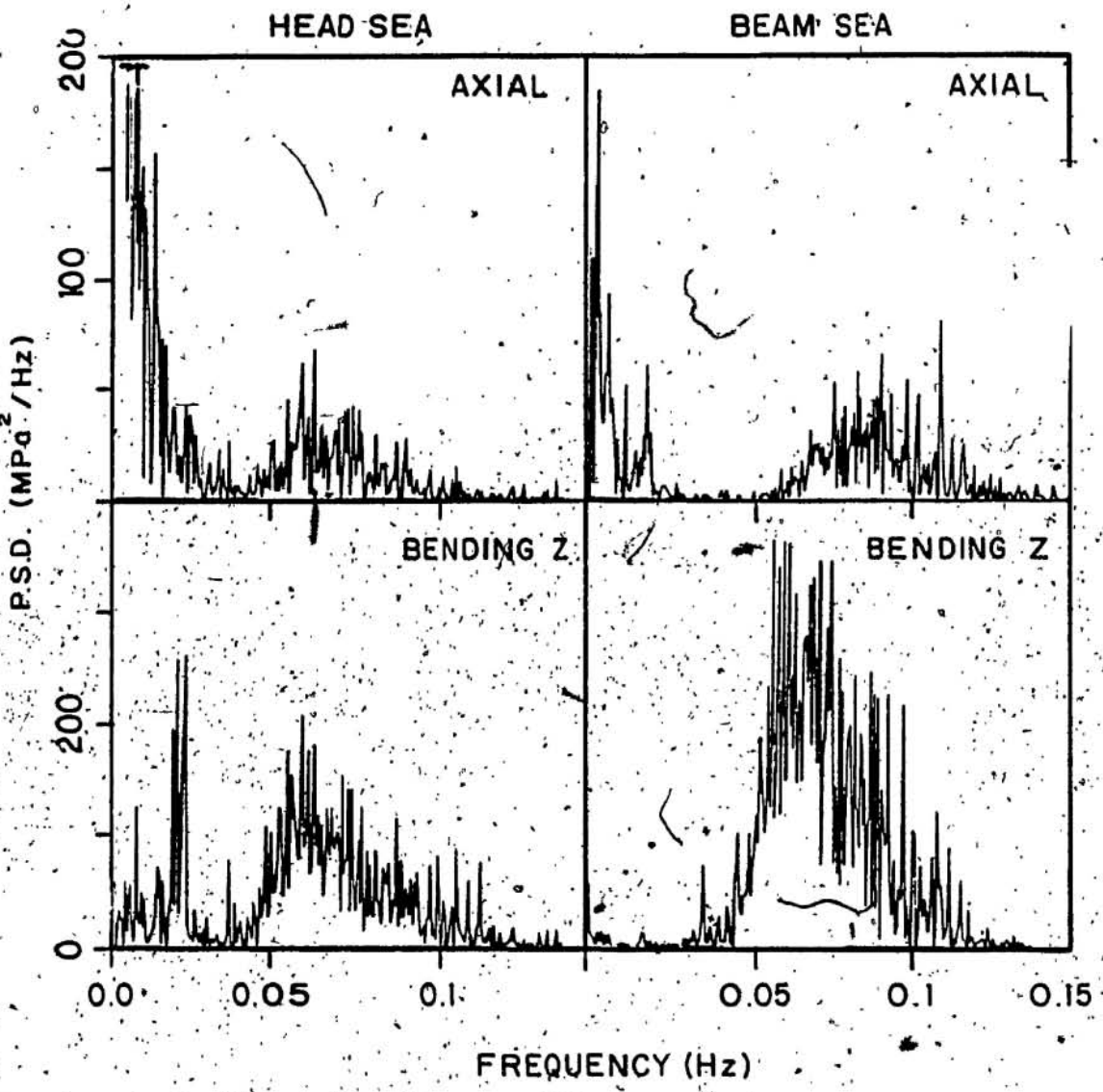

FIG. 5.50 P.S.D. PLOTS FOR STRESSES IN COLUMN SECTION MB.

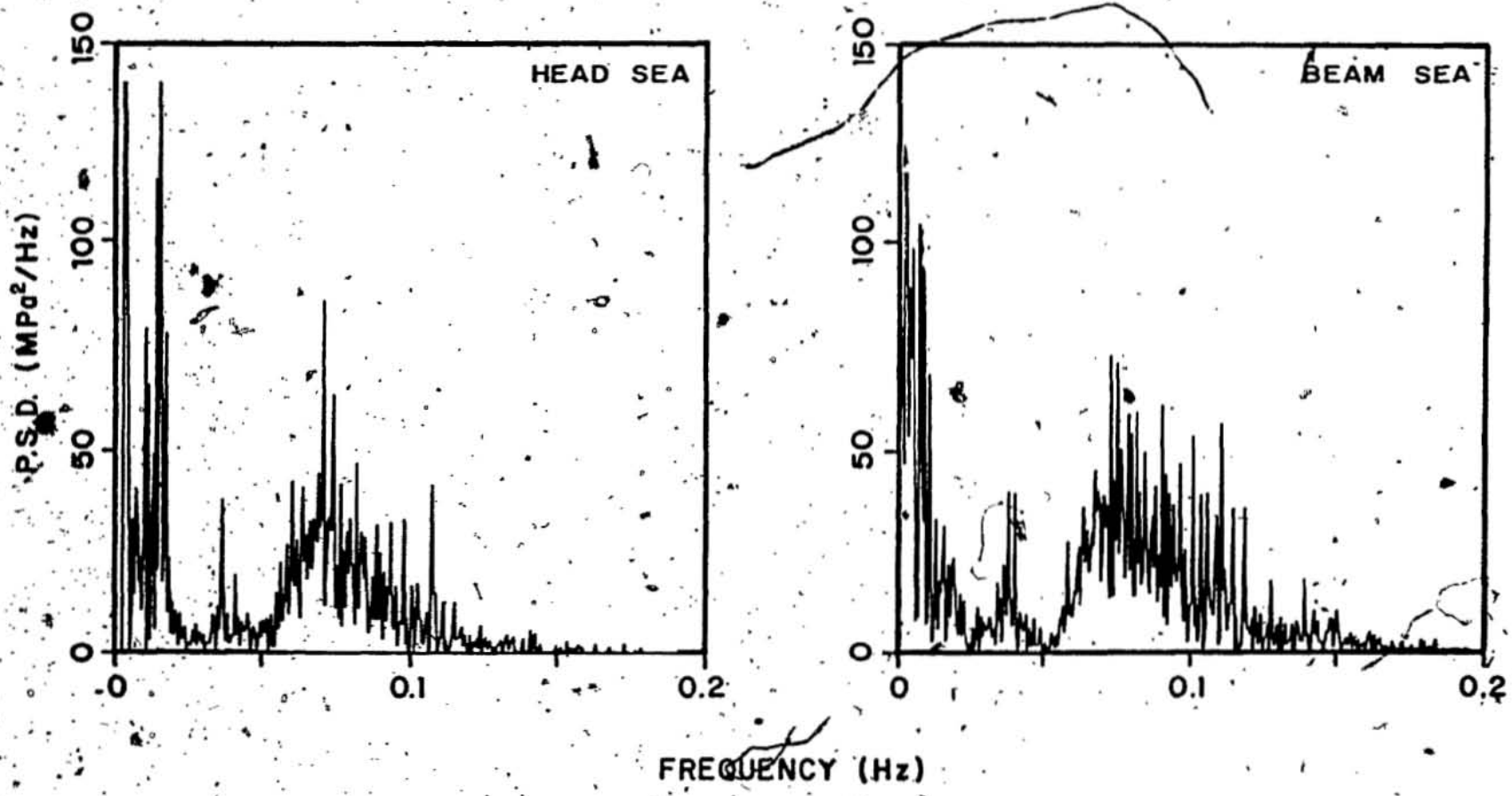

FIG. 5.51 P.S.D. PLOTS FOR BENDING STRESSES Z IN PONTOON SECTION PM.

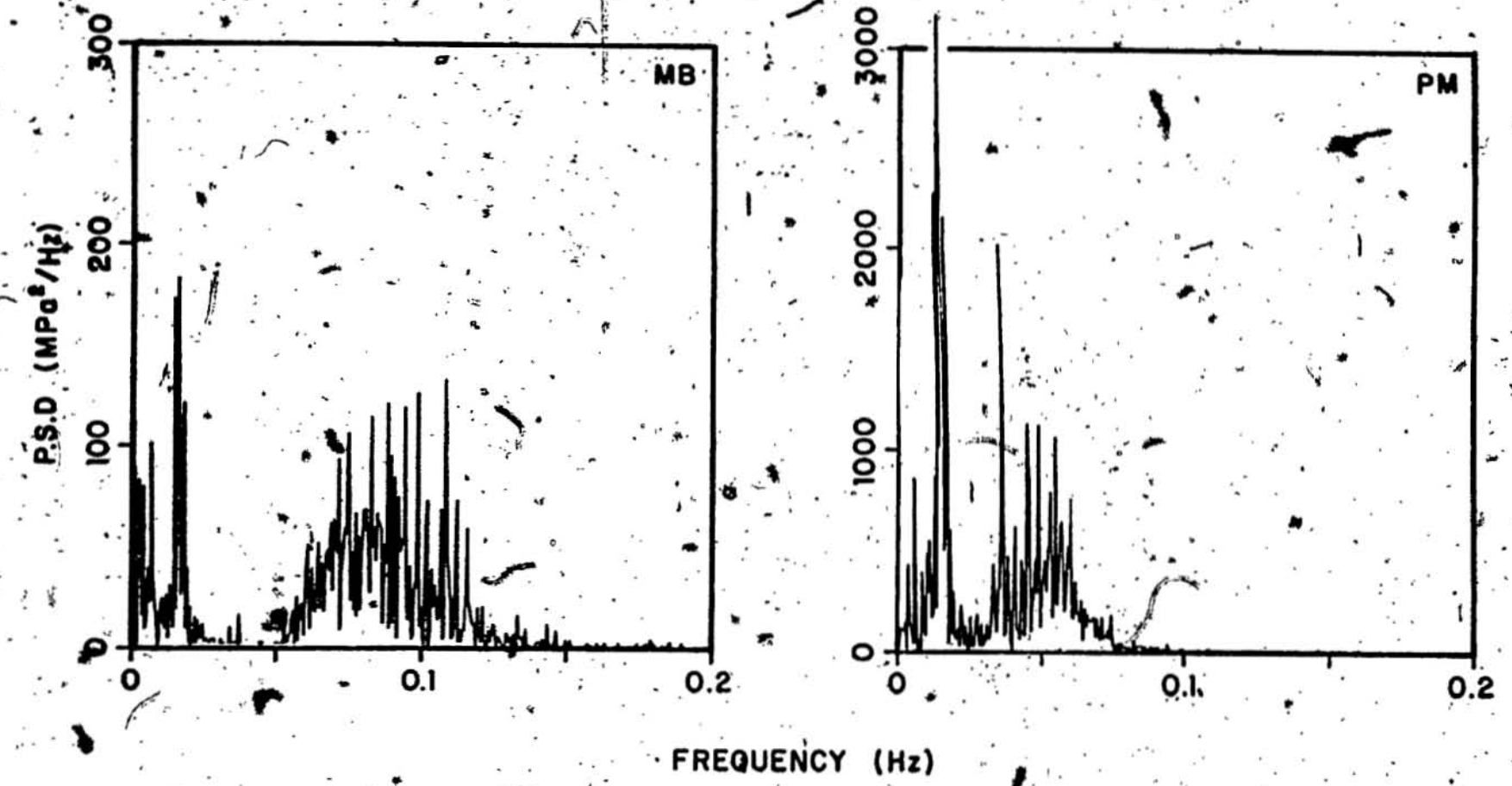

FIG. 5.52 P.S.D. PLOTS FOR BENDING STRESSES Y IN SECTIONS OF MAIN COLUMN AND PONTOON – BEAM SEA.

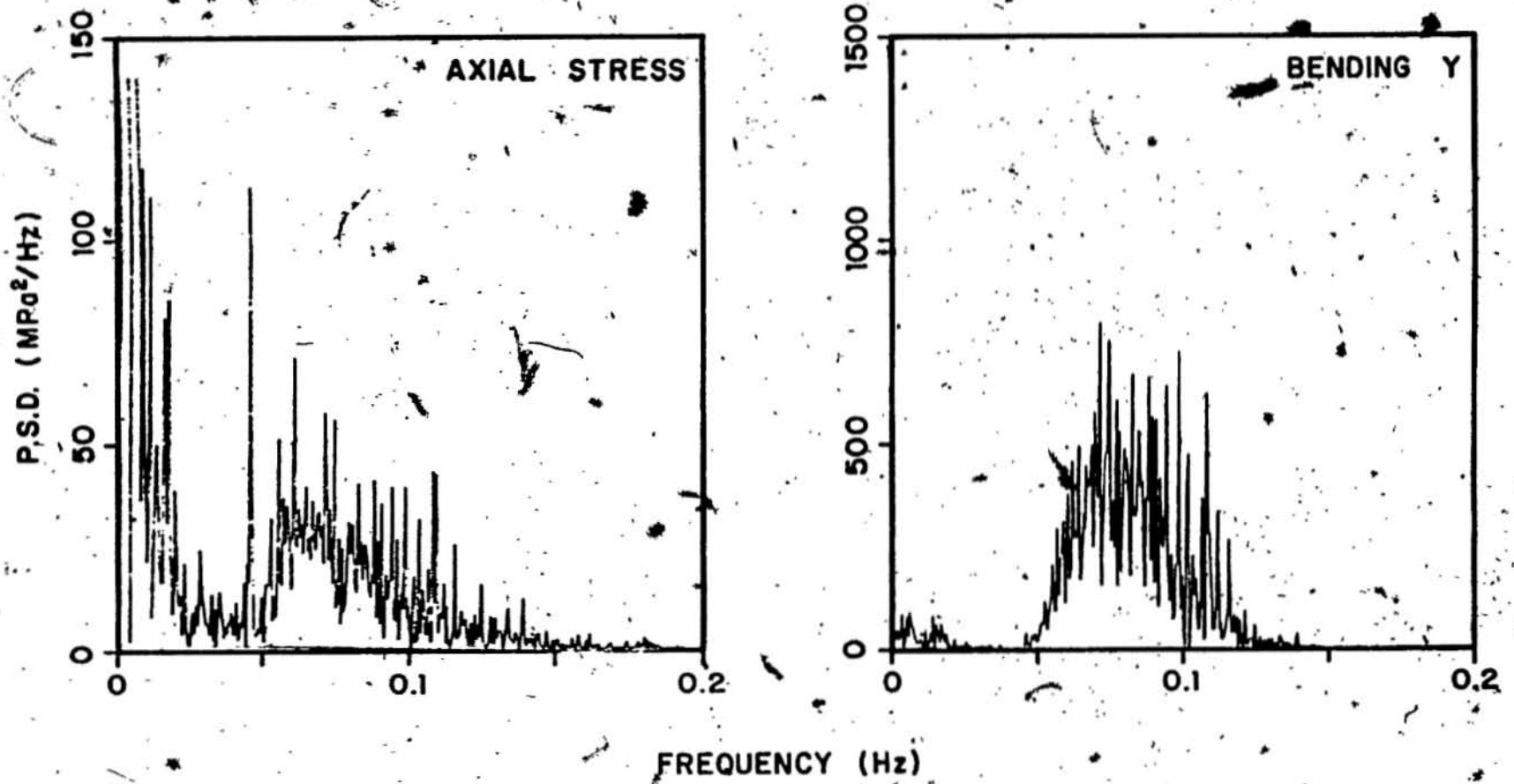

FIG. 5.53 P.S.D. PLOTS FOR STRESSES IN COLUMN SECTION SB – BEAM SEA.

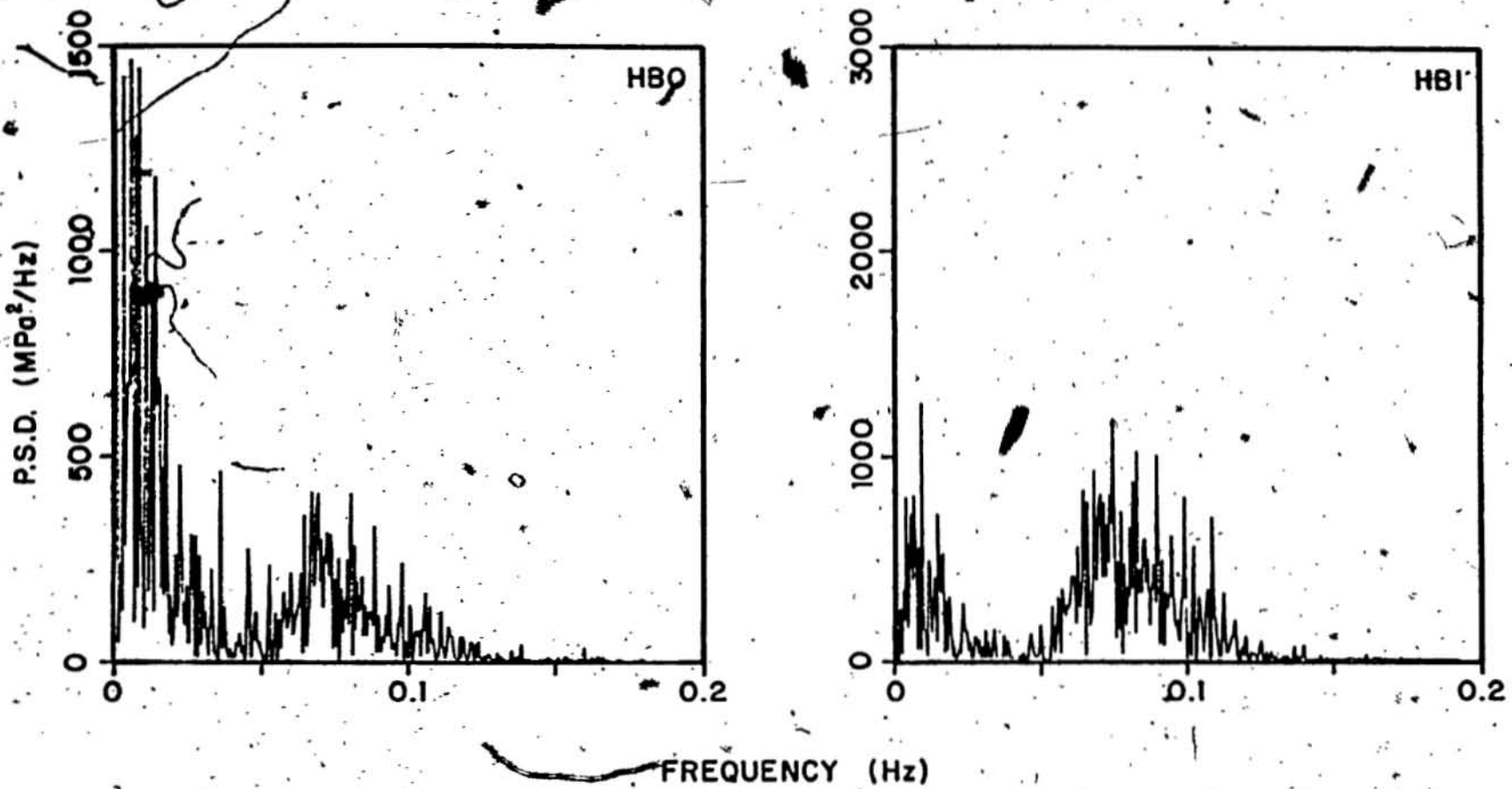

FIG. 5.54 P.S.D. PLOTS FOR AXIAL STRESSES IN HORIZONTAL BRACES – BEAM SEA.

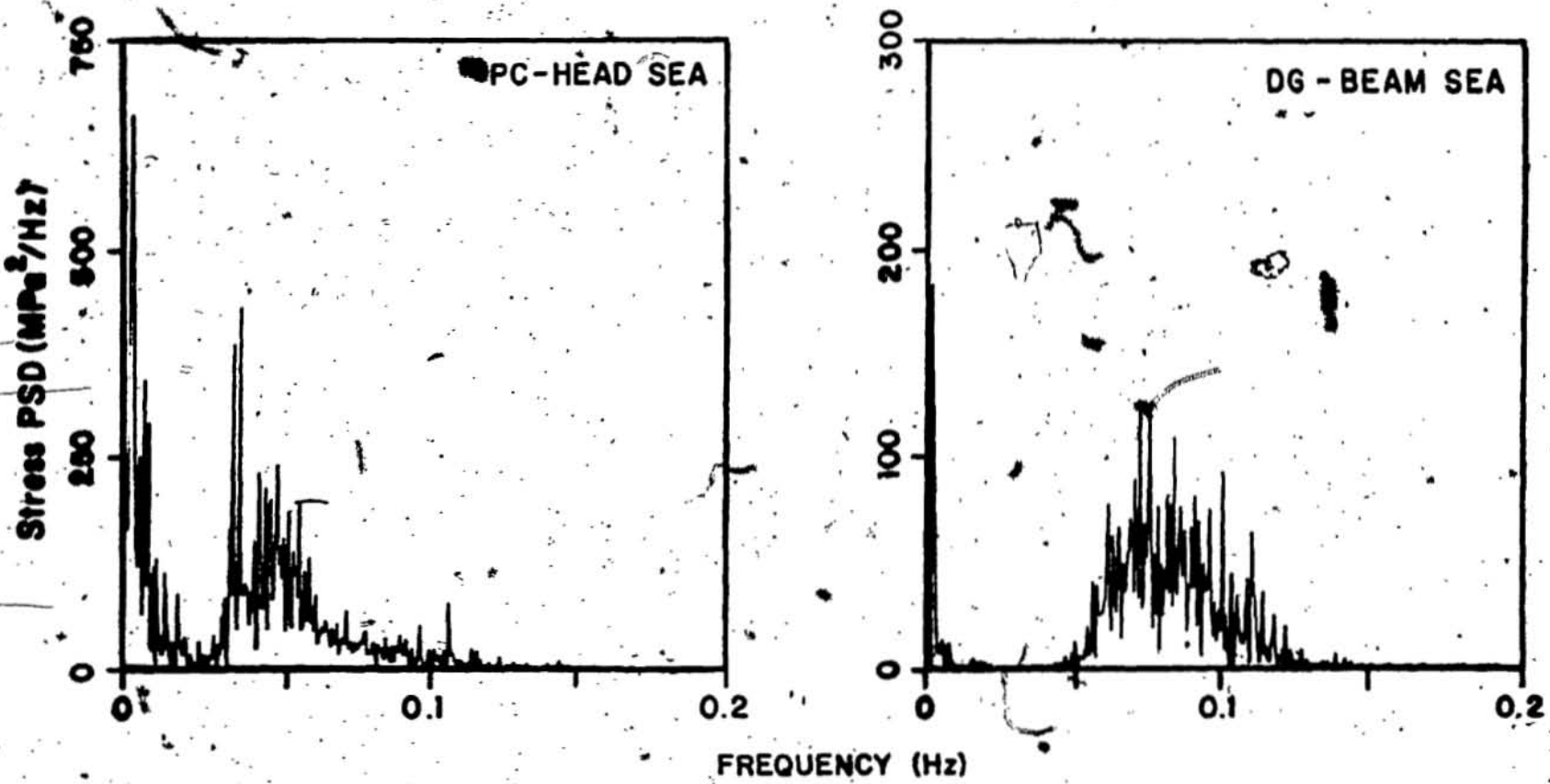

FIG. 5.55 P.S.D. PLOTS FOR BENDING STRESSES IN INDICATED PONTOON AND DECK GIRDER SECTIONS

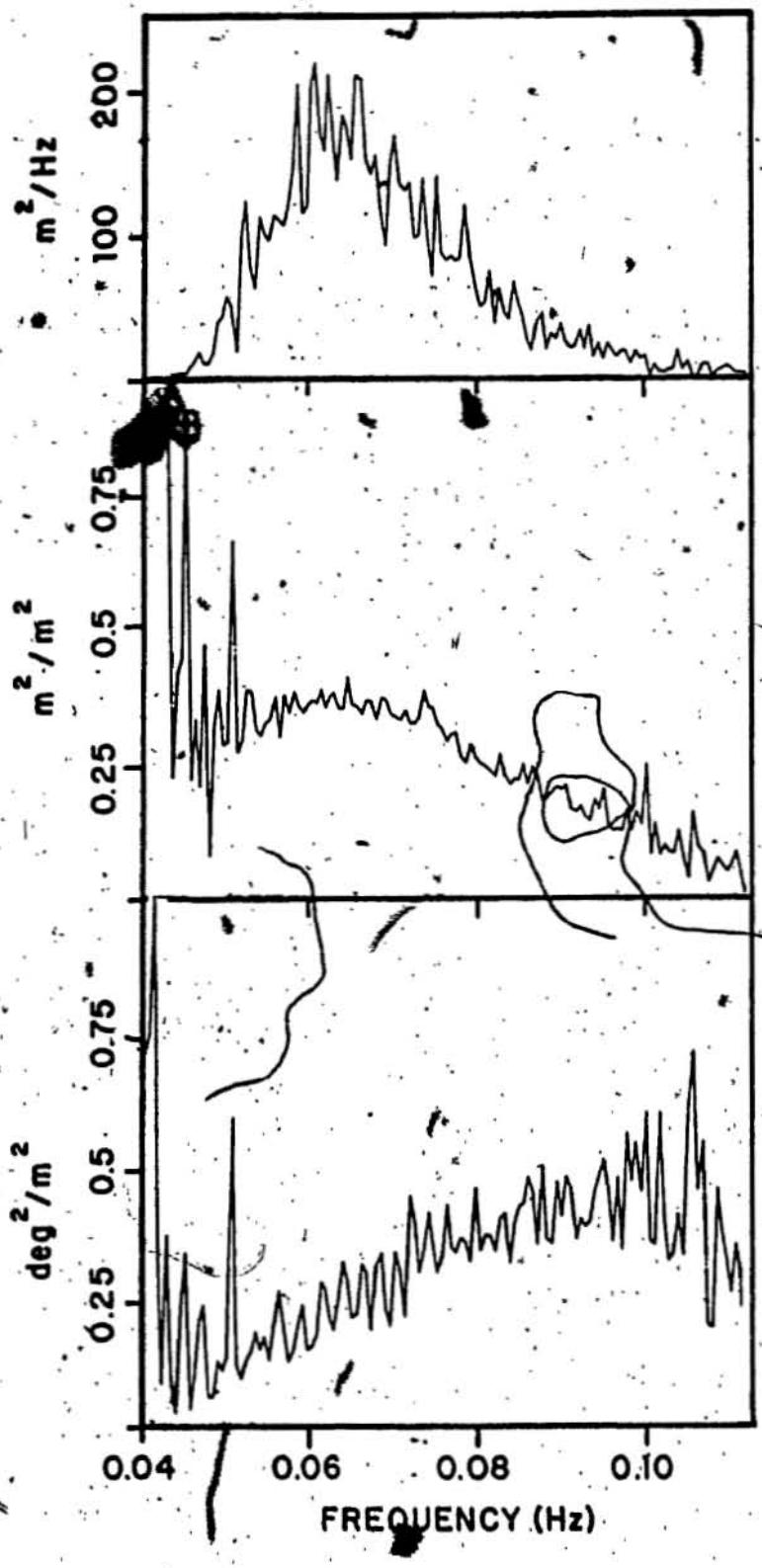

FIG. 5.56 SAMPLE TRANSFER FUNCTION PLOTS (AMPLITUDE SQUARED)

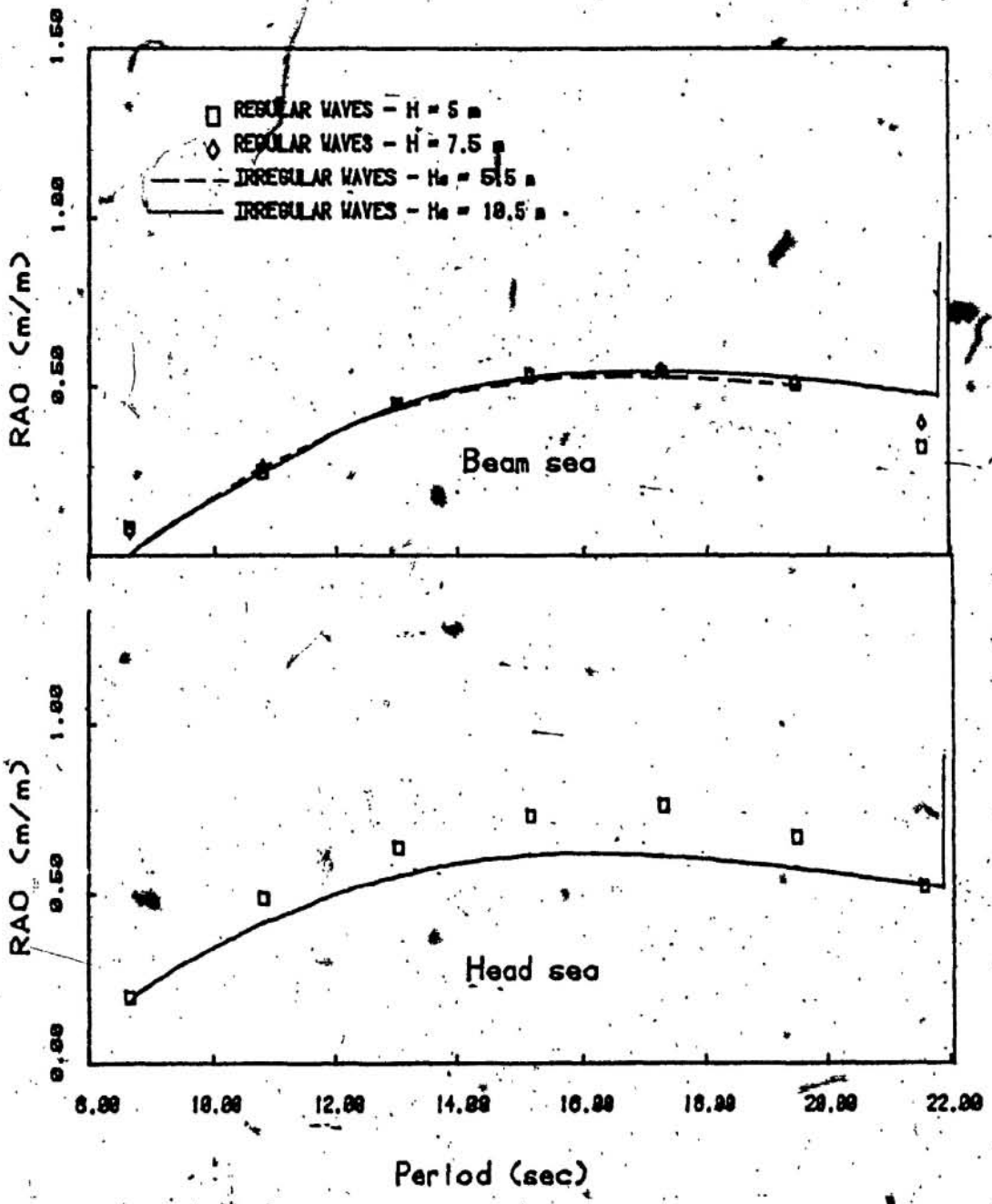

FIG. 5.57 HEAVE RESPONSE IN REGULAR AND IRREGULAR WAVES.

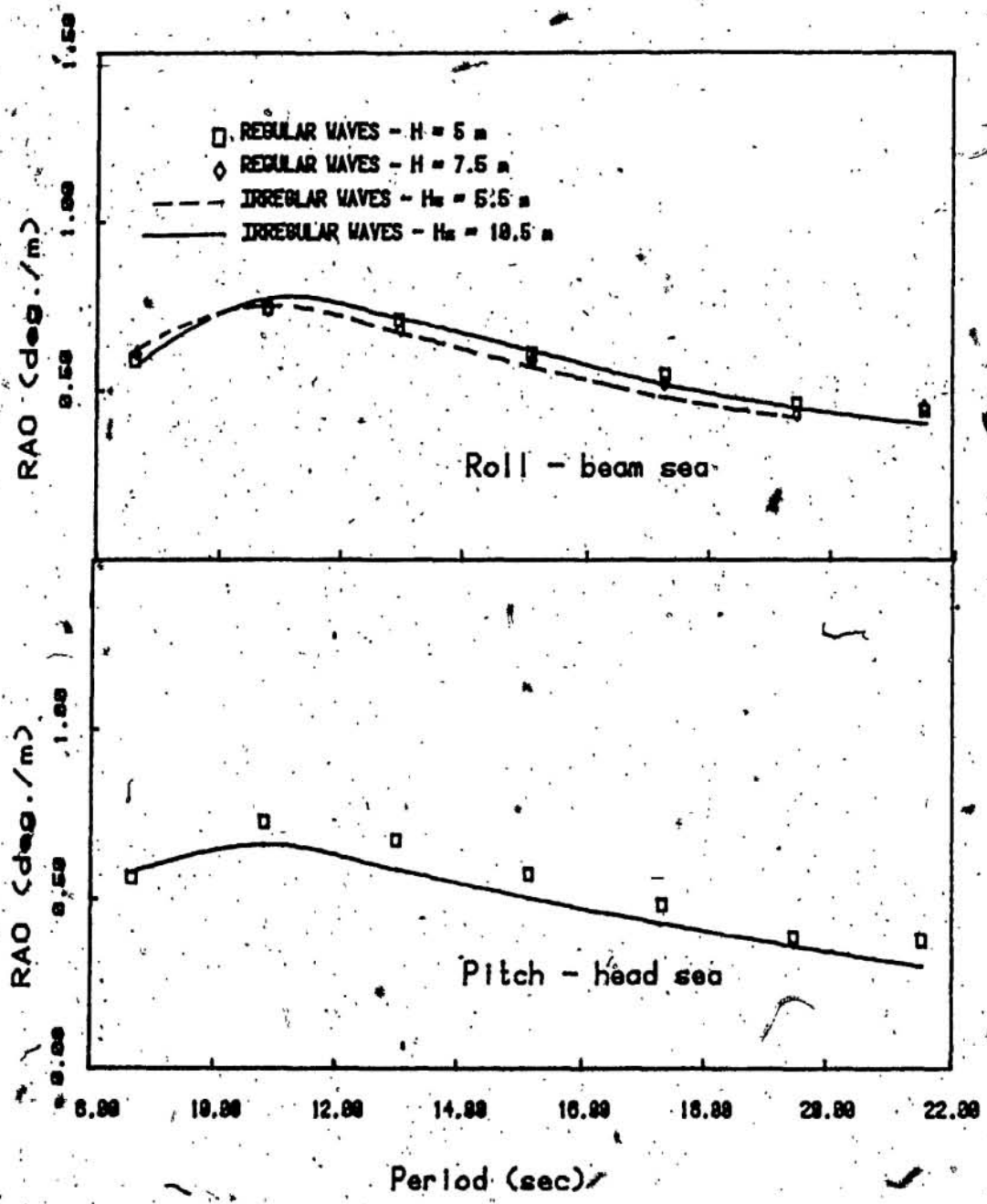

FIG. 5.58 PITCH AND ROLL RESPONSES IN REGULAR AND IRREGULAR WAVES.

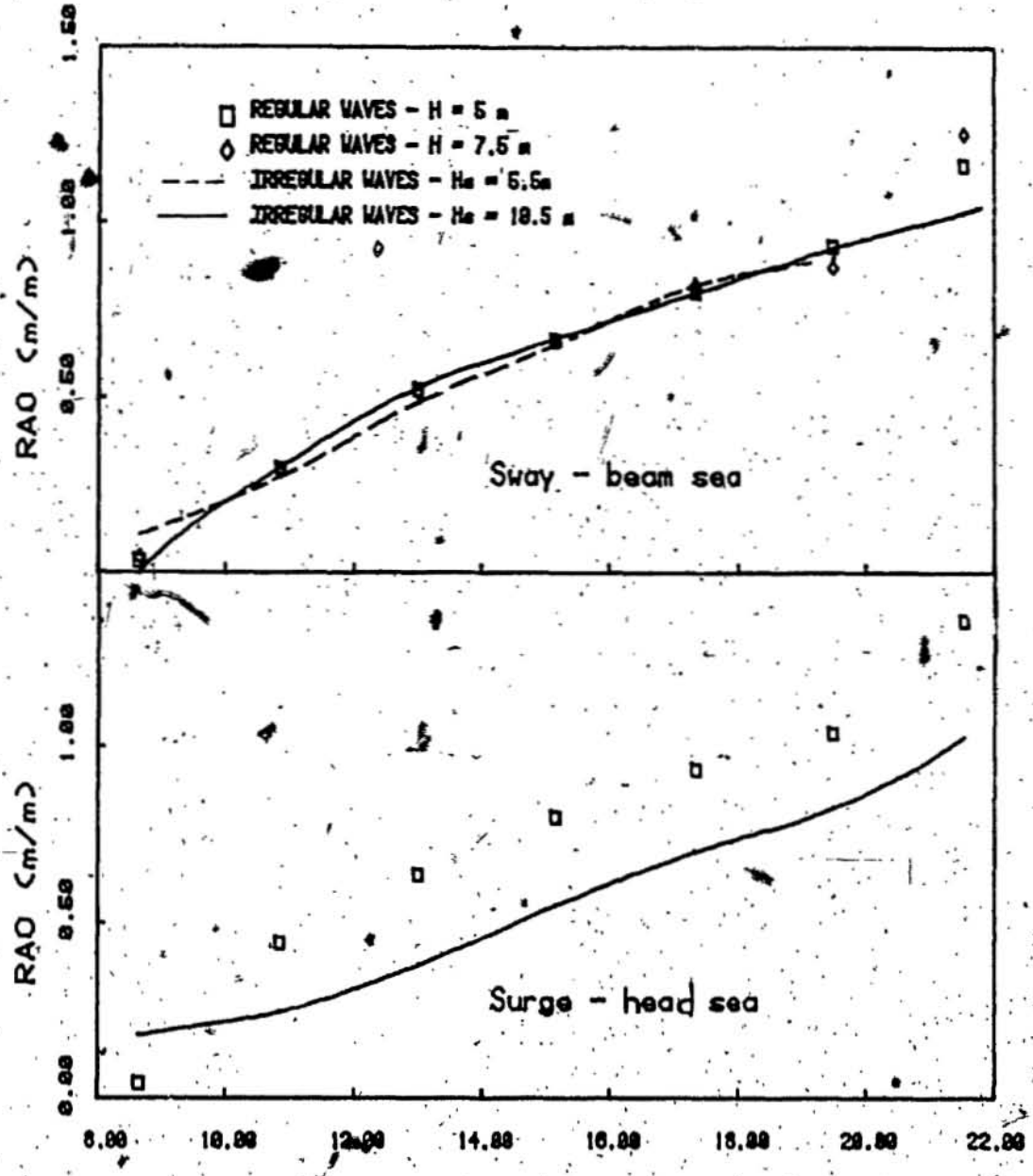

FIG. 5.59 SURGE AND SWAY RESPONSES IN REGULAR AND IRREGULAR WAVES.

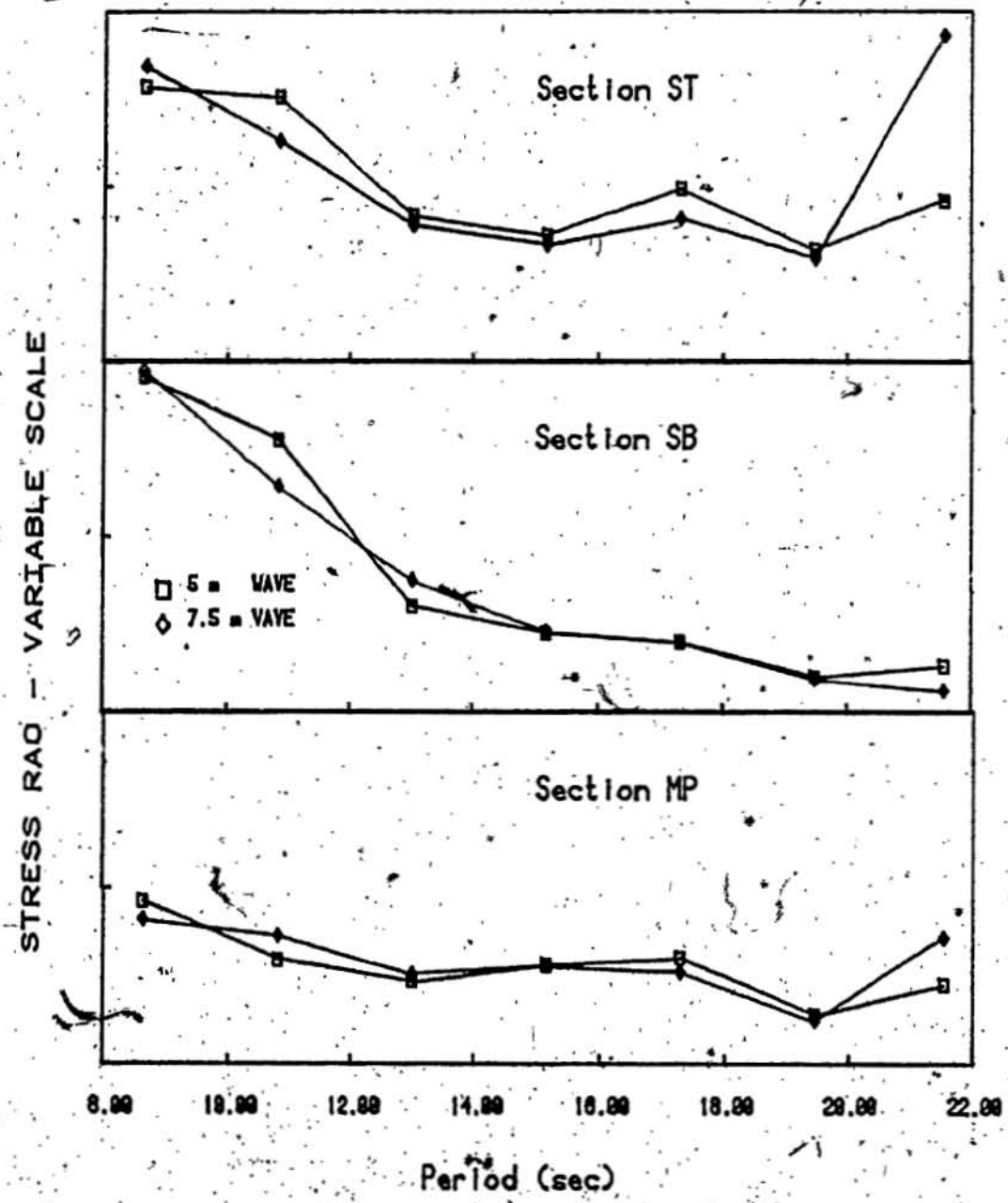

FIG. 5.60 EFFECT OF WAVE HEIGHT ON STRESS RAO PLOTS - BEAM SEA AT SURVIVAL DRAFT.

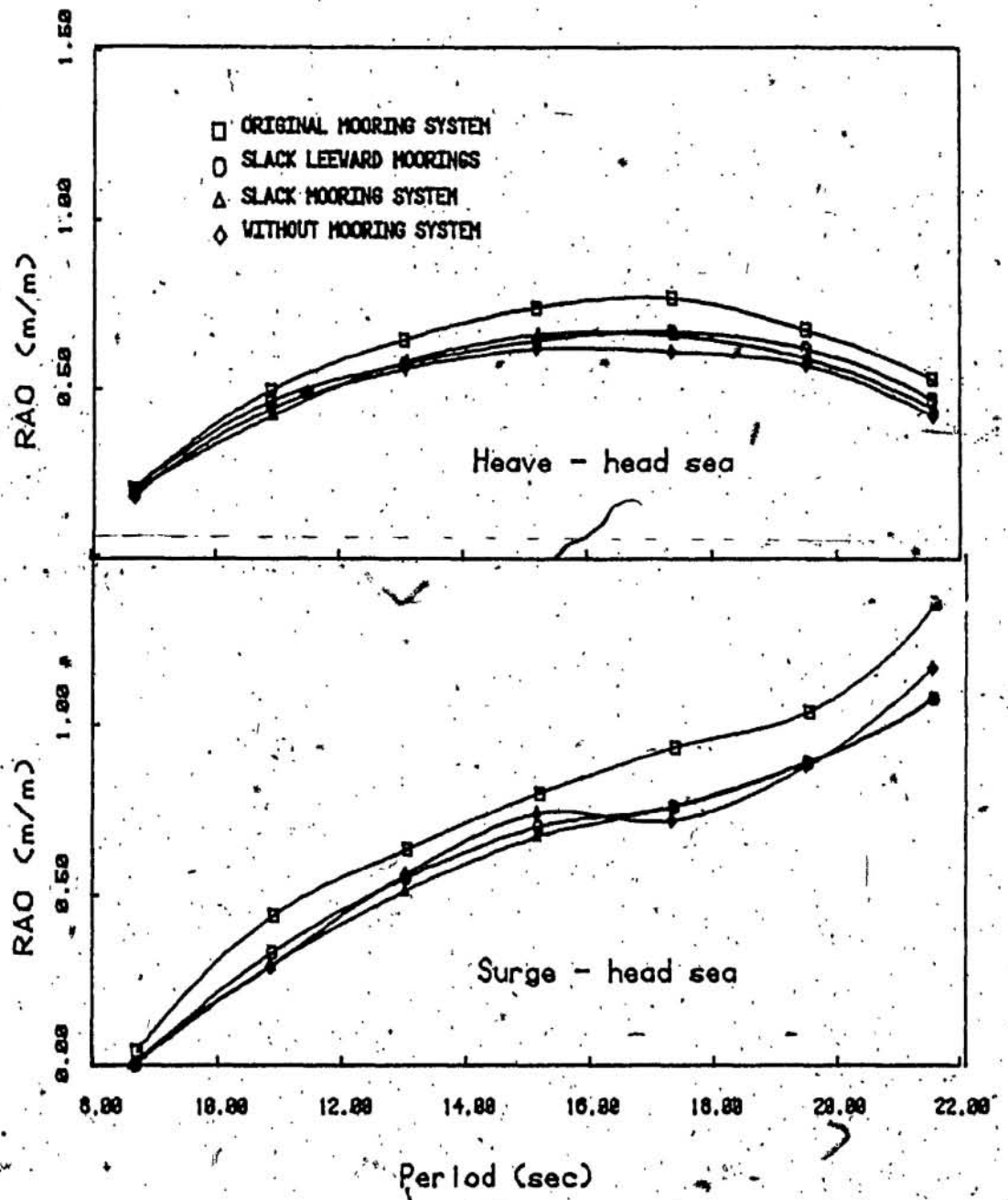

FIG. 5.61 EFFECT OF MOORING SYSTEM STIFFNESS ON HEAVE AND SURGE.

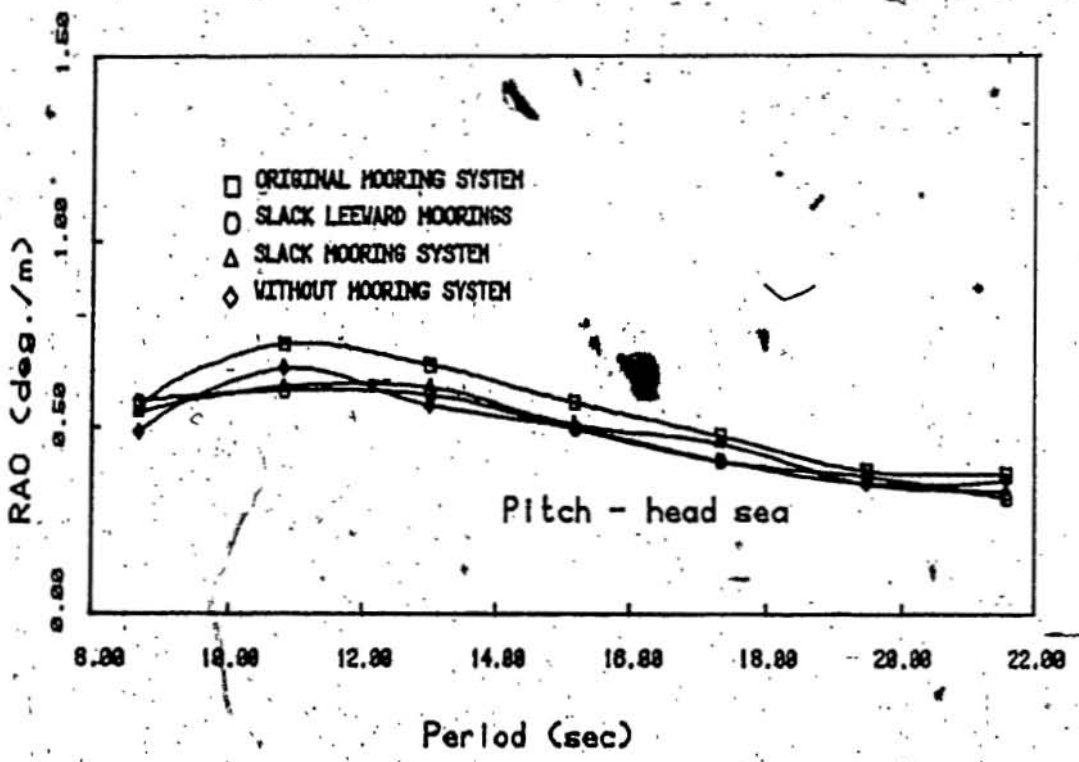

FIG. 5.62 EFFECT OF MOORING SYSTEM STIFFNESS ON PITCH RESPONSE .

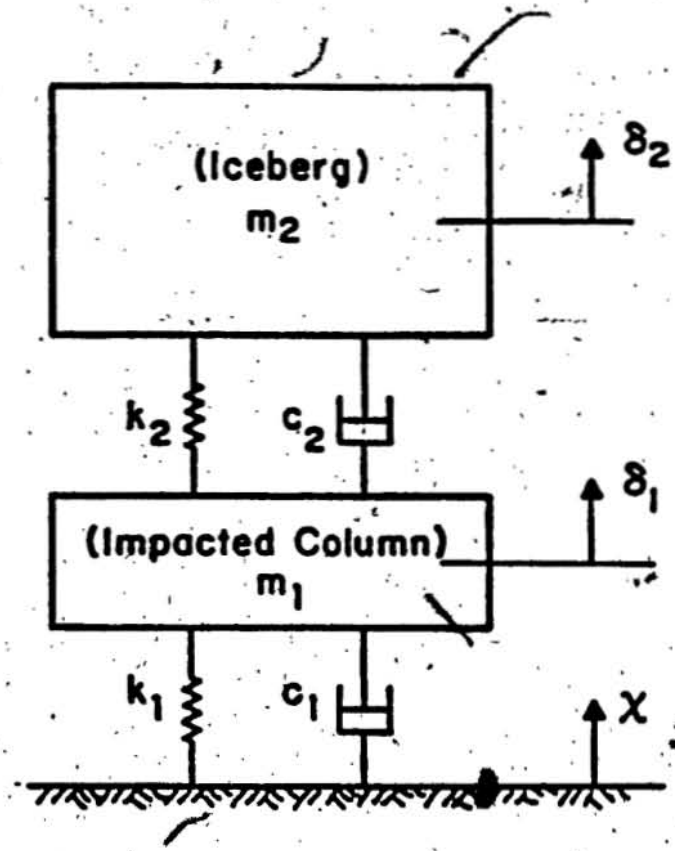

FIG. 6.1 LUMPED MASS MODEL FOR IMPACT INTERFACE

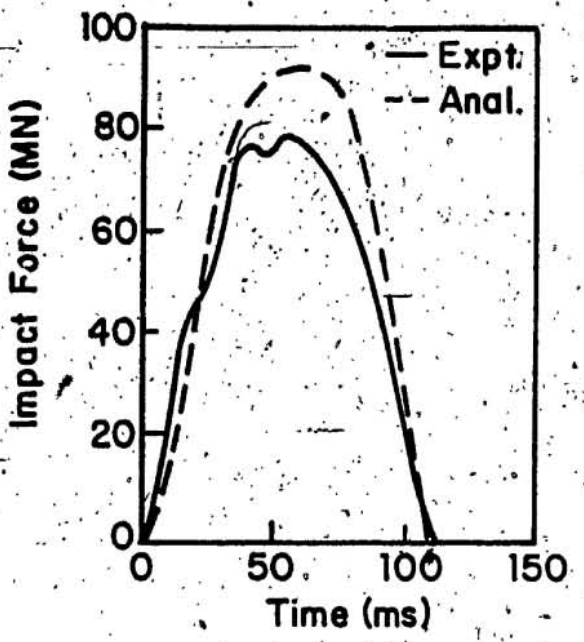

1000 tonne, 4 m/sec

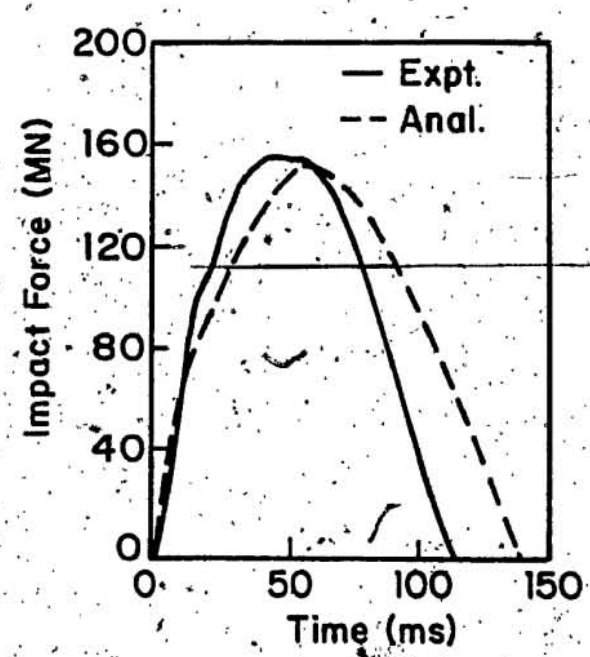

2000 tonne, 4 m/sec

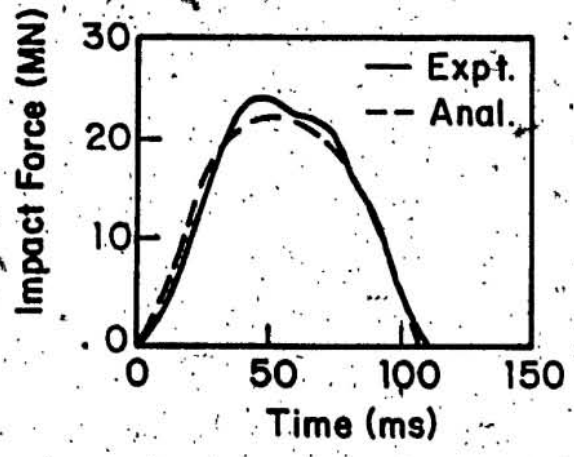

1000 tonne, 1 m/sec.

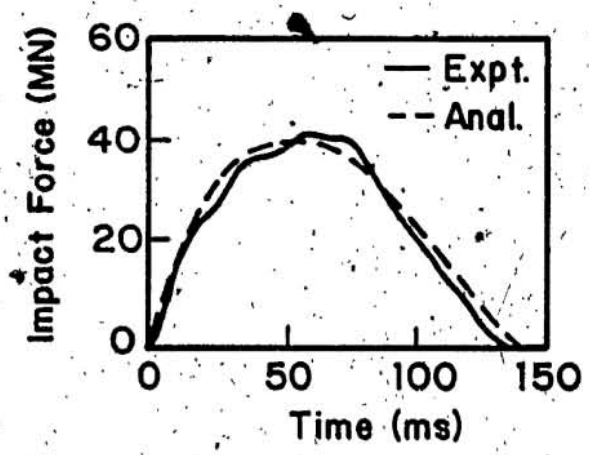

2000 tonne, 1 m/sec

FIG. 6.2 IMPACT FORCE OF 1000 AND 2000 TONNE BERGYBITS COLLIDING WITH THE CORNER COLUMN OF THE SEMI-SUBMERSIBLE - HEAD SEA IMPACT

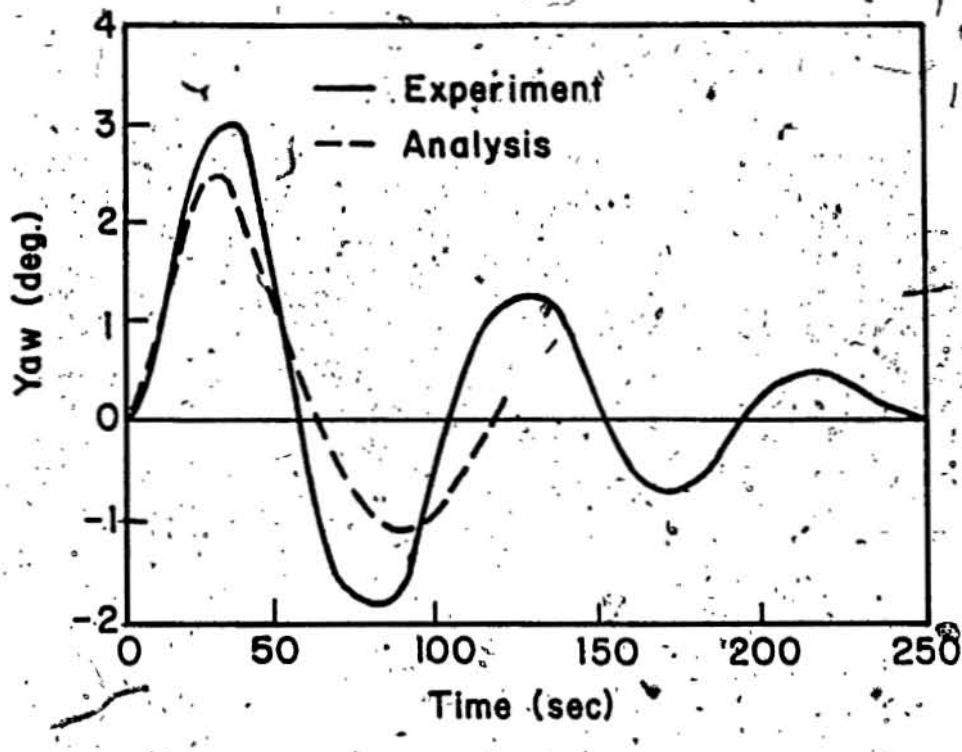

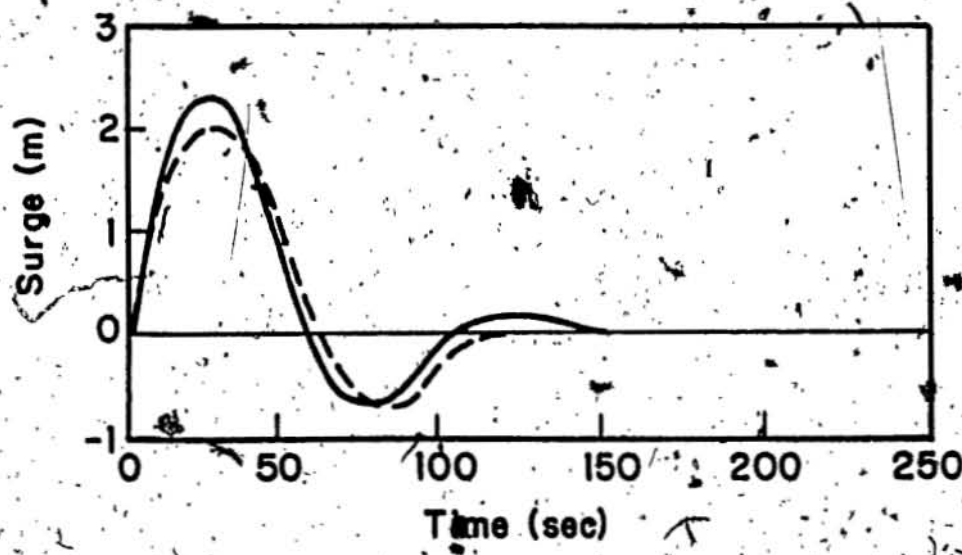

FIG.16.3 YAW AND SURGE MOTIONS OF THE SEMI-SUBMERSIBLE AFTER IMPACT OF A 1000 TONNE BERGY BIT MOVING AT 4m/sec.

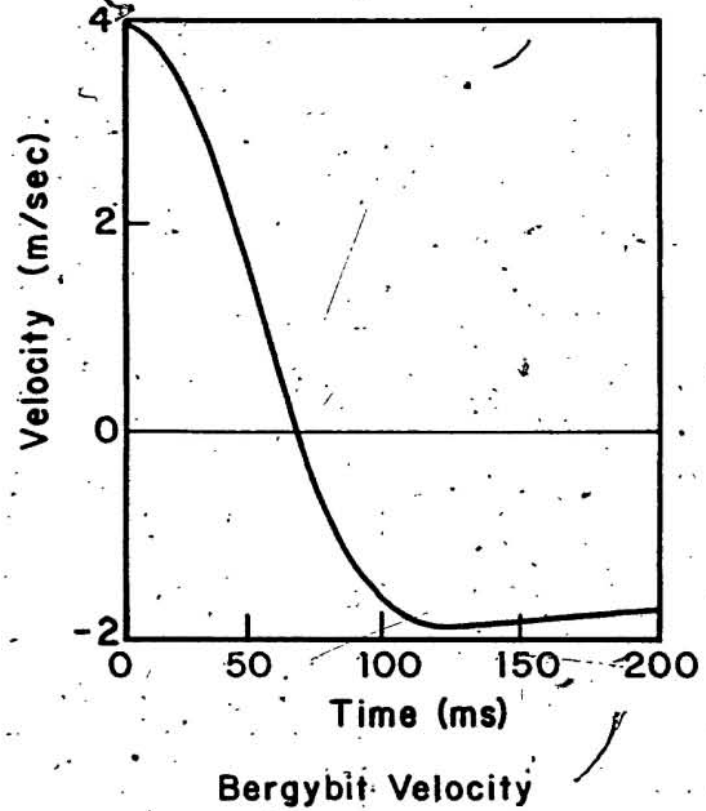

Bergybit Velocity

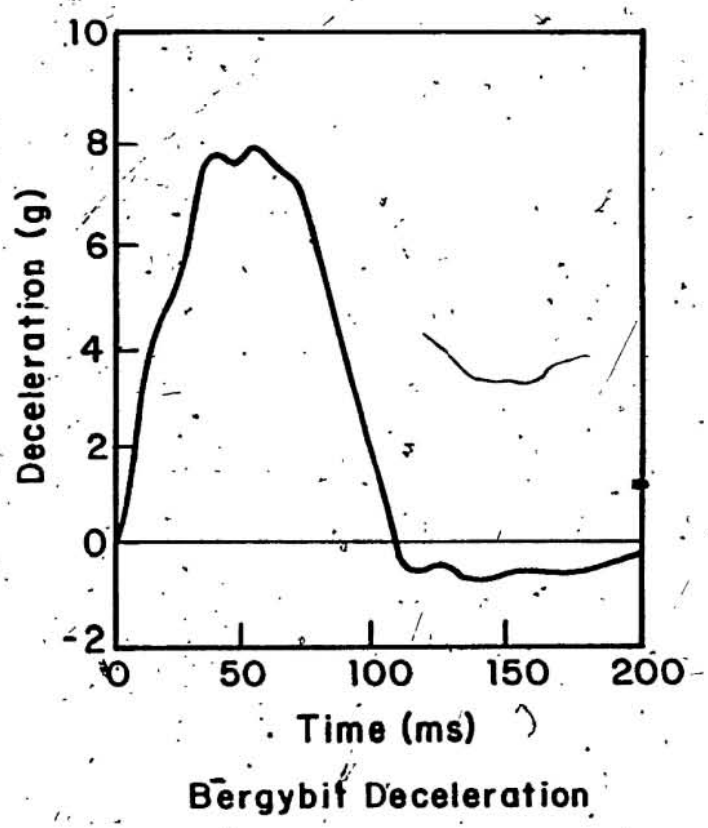

Bergybit Deceleration

FIG. 6.4 VELOCITY AND ACCELERATION TIME HISTORIES OF A 1000 TONNE BERGYBIT DURING IMPACT WITH THE SEMI-SUBMERSIBLE CORNER COLUMN - IMPACT VELOCITY = 4 m/sec - HEAD SEA IMPACT.

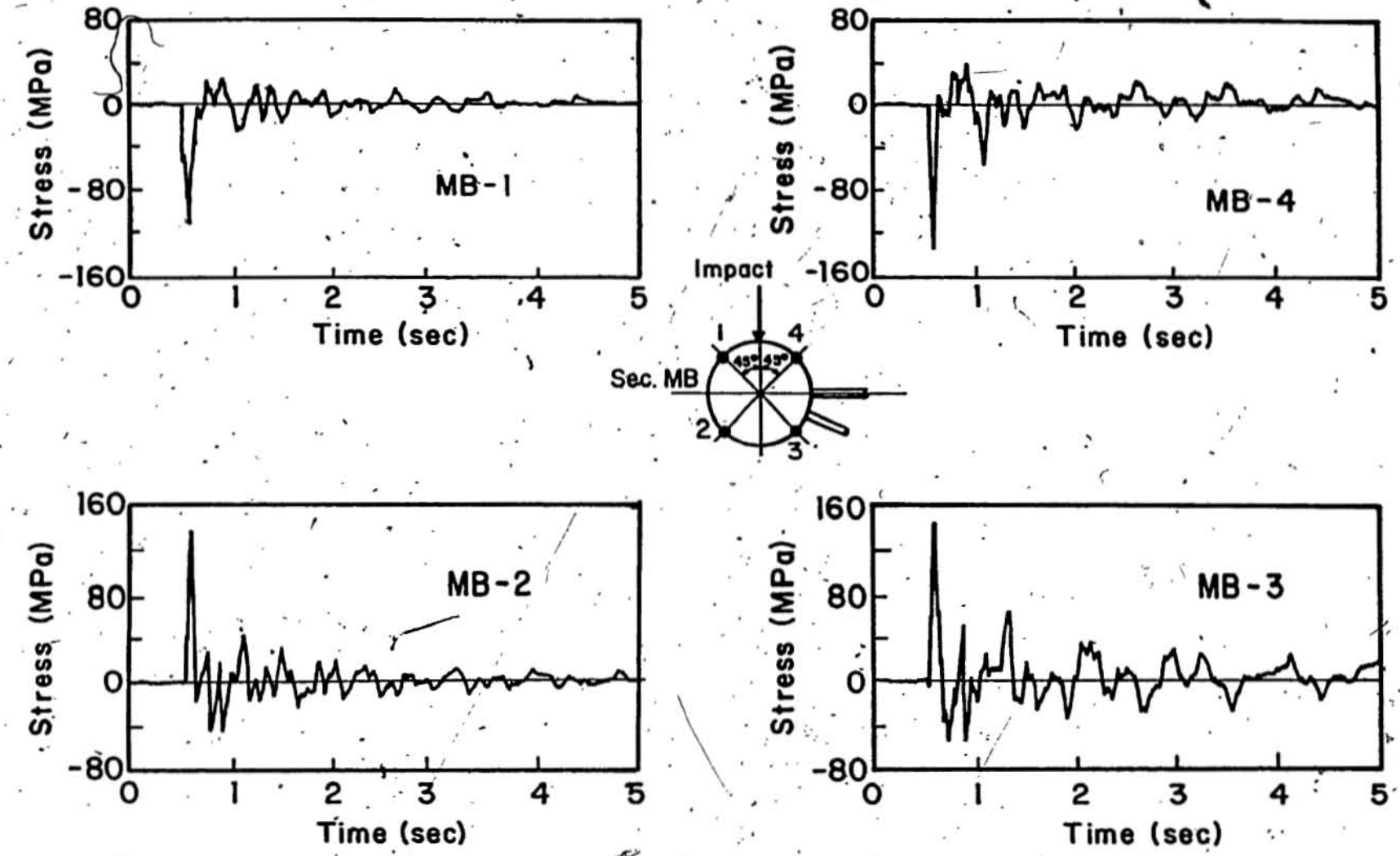

FIG.6.5 IMPACT STRESSES AT SECTION MB IN THE MAIN COLUMN - 1000 TONNE BERGYBIT MOVING AT 4 m/sec.

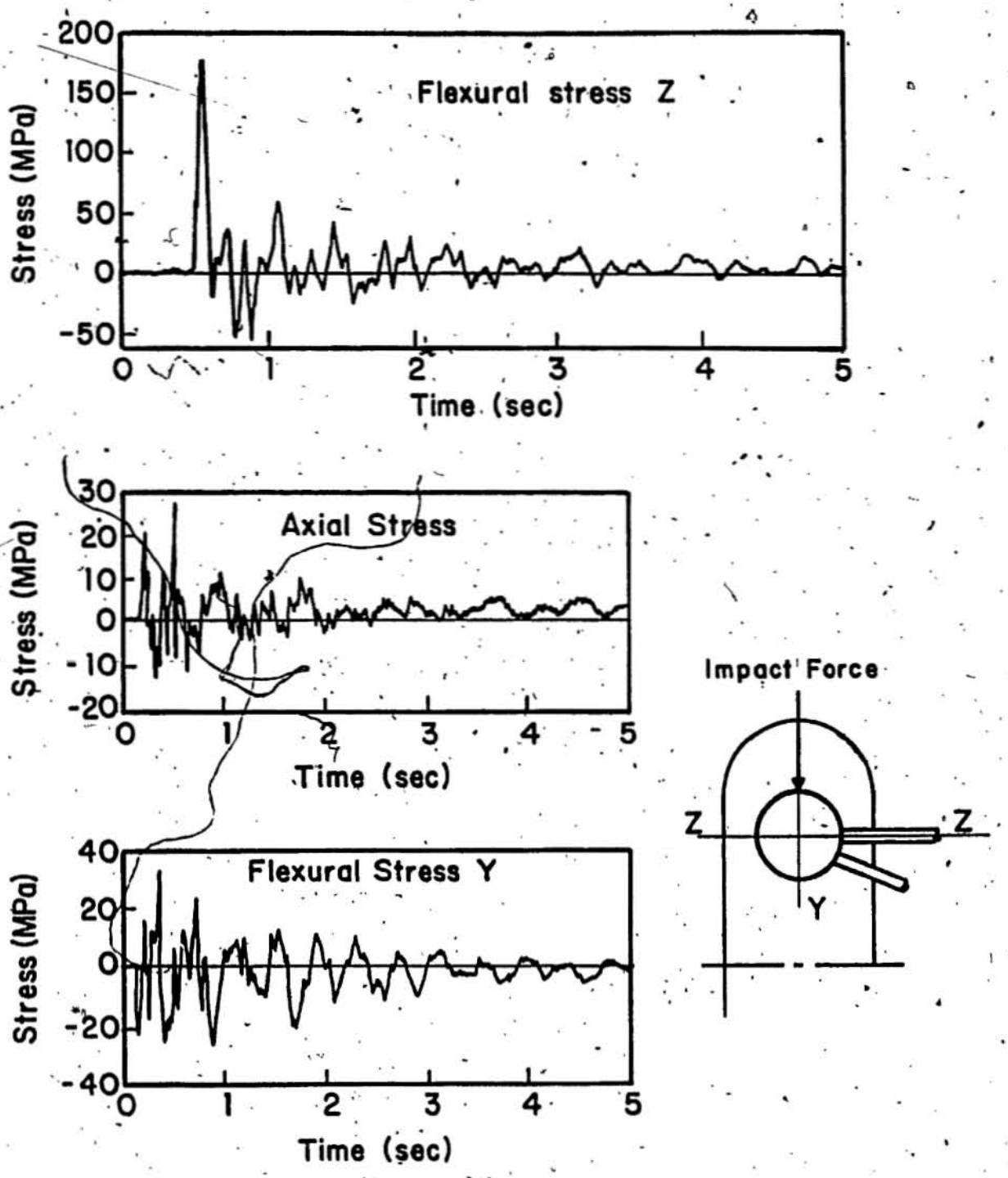

FIG. 6.6 STRESS TIME HISTORIES AT THE BASE OF THE CORNER COLUMN (SECTION MB) DUE TO IMPACT OF A 1000 TONNE BERGYBIT WITH A VELOCITY OF 4 m/sec.

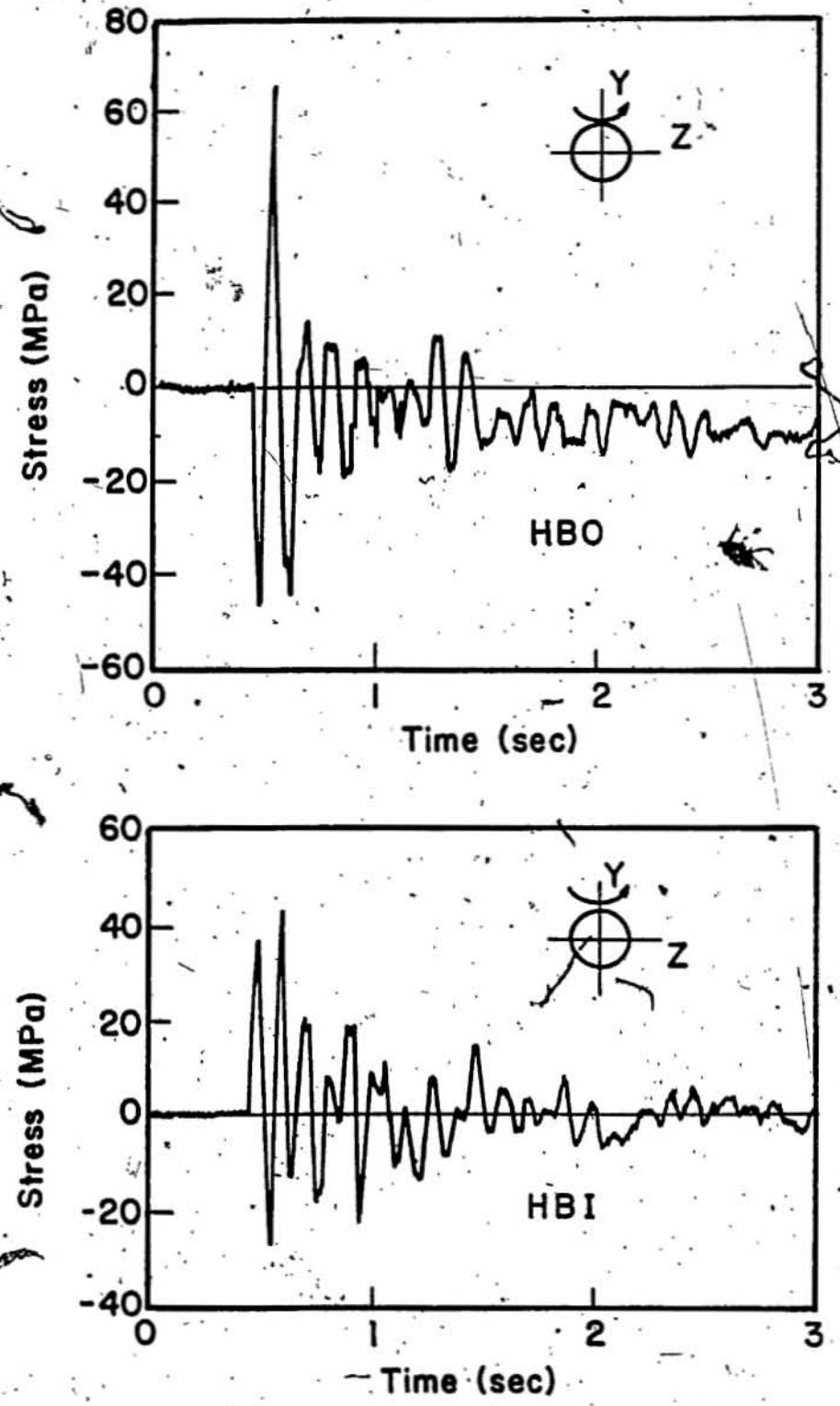

FIG. 6.7 FLEXURAL STRESS (Y) IN HORIZONTAL BRACING SECTIONS HBO AND HBI DUE TO IMPACT OF A 1000 TONNE BERGYBIT AGAINST THE CORNER COLUMN - IMPACT SPEED 4 m/sec.

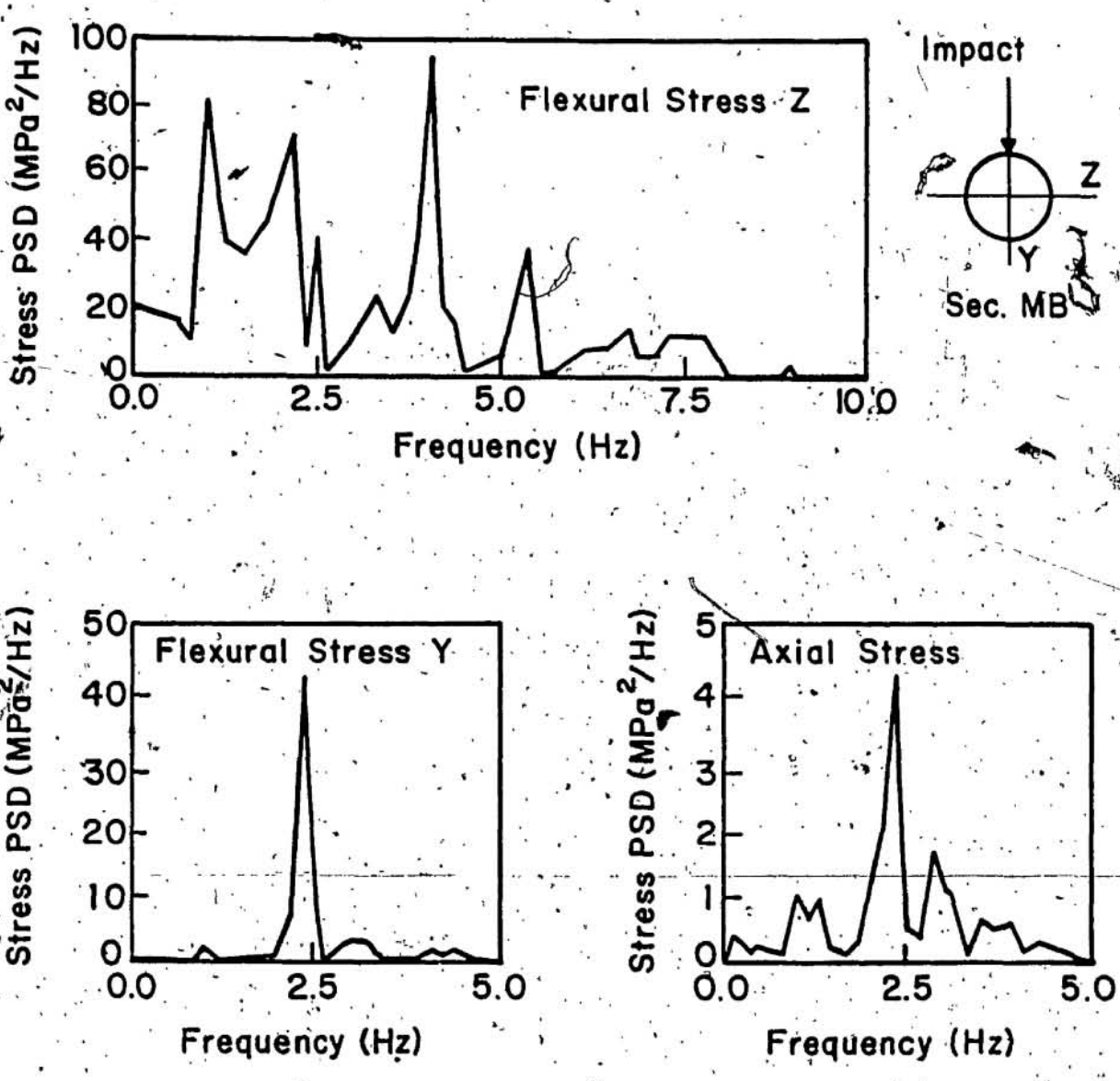

FIG. 6.8 POWER SPECTRAL DENSITY FOR AXIAL AND FLEXURAL STRESS AT SECTION MB DUE TO THE CORNER COLUMN IMPACT OF A 1000 TONNE BERGYBIT - IMPACT VELOCITY = 4 m/sec

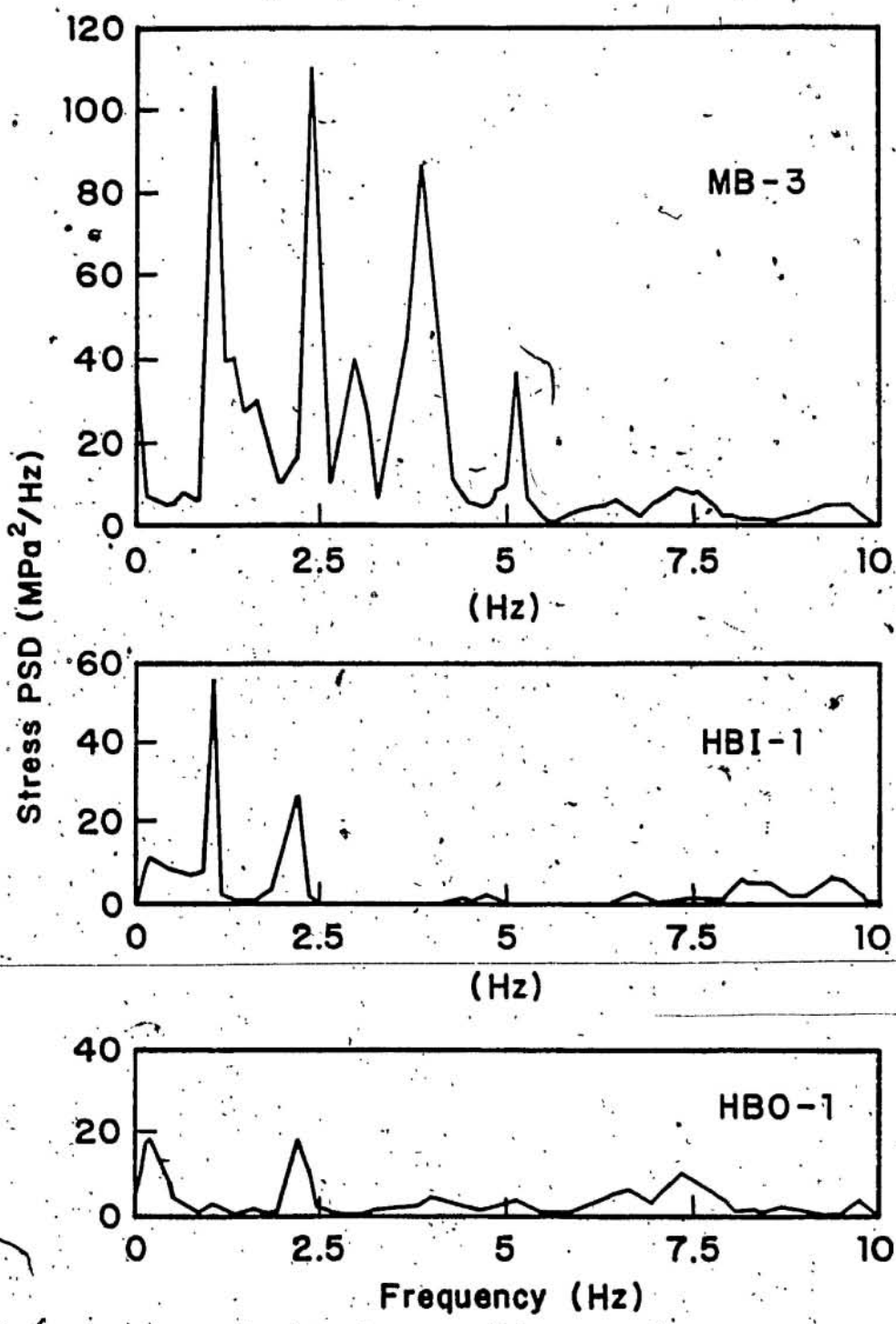

FIG. 6.9 POWER SPECTRAL DENSITY FOR NORMAL STRESSES MEASURED AT THE INDICATED STRAIN GAGES DUE TO CORNER COLUMN IMPACT OF A 1000 TONNE BERGY BIT - IMPACT VELOCITY = 4 m / sec.

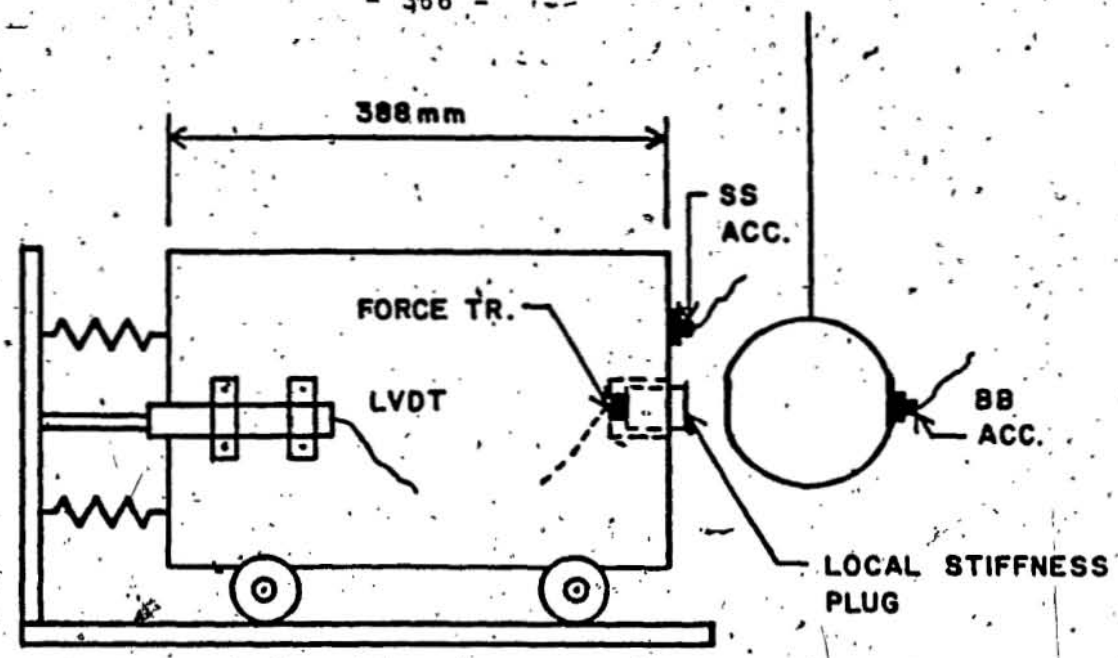

FIG. 6.10 OUTLINE OF THE TWO-DEGREES-OF-FREEDOM MODEL AND THE INSTRUMENTATION.

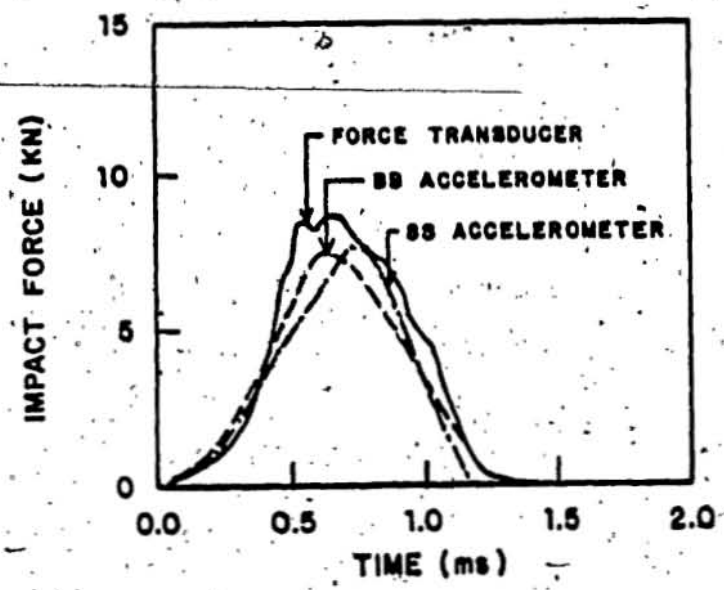

FIG. 6.11 IMPACT FORCE AS OBTAINED FROM DIFFERENT INSTRUMENTATIONS. (OAK ELEMENT)

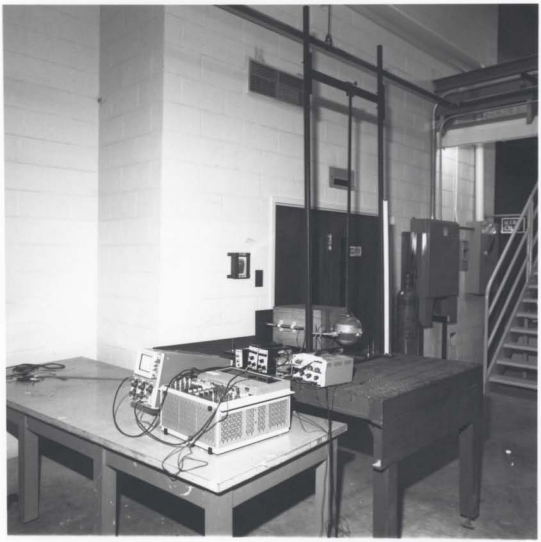

FIG. 6.12 TEST SET-UP FOR THE
TWO-DEGREES-OF-FREEDOM MODEL.

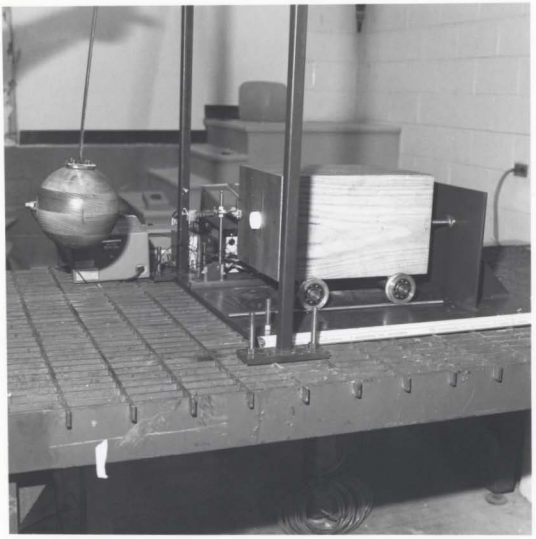

FIG. 6.13 THE TWO-DEGREES-OF-FREEDOM MODEL.

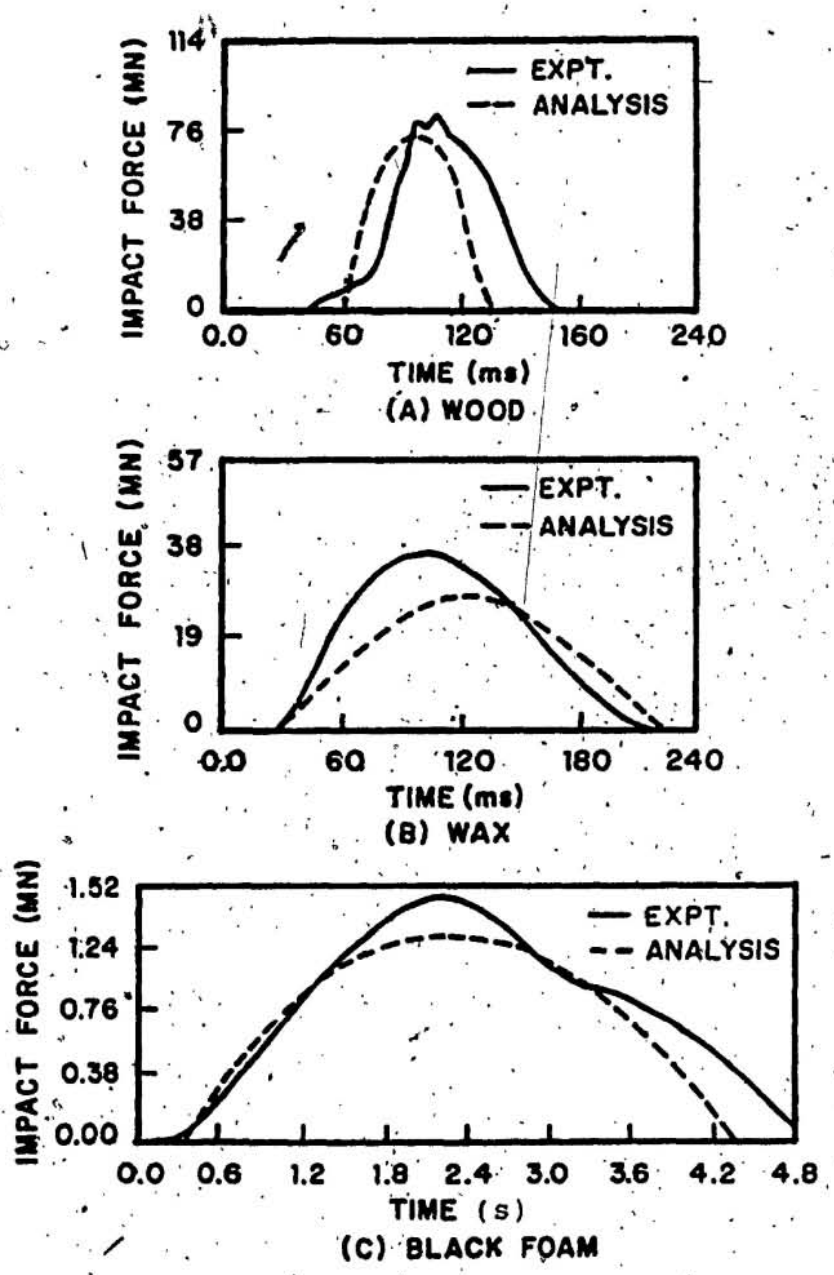

FIG. 6.14 IMPACT FORCE TIME HISTORY FOR THREE LOCAL STIFFNESS ELEMENTS.

APPENDIX A

DATA PROCESSING AND ANALYSES

A.1 Data Processing

Time histories of test parameters (motion, strains, acceleration, etc.) were recorded on eight-channel HP tape recorders. These recorders are capable of recording frequency components of up to 60 kHz, which is about two orders of magnitude higher than the maximum frequency of the impact test data. Time histories of the measured parameters were displayed on an oscilloscope, pictured and compared with the corresponding recorded signal to make sure that filtering of the data did not take place during recording.

All recorded time histories were plotted using a chart recorder for preliminary ahalysis. The plots were compared with the corresponding signal obtained from the oscilloscope. The recorded signals were digitized and analysed using a four-channel HP Fourier analyser. The maximum digitization frequency was at least one order of magnitude higher than the maximum frequency contained in the signal. The amplitude of each regular wave data record (wave, motion and strain) was obtained using polar Fourier transform. The Response Amplitude Operator (RAO) for any parameter was computed as the amplitude of the parameter (motion or stress) divided by the wave amplitude. The model values were converted to full-scale values using the scaling factors provided in Table 4.4.

A.2 Analysis of Stresses

Strains were measured at four points in the pontoon, column and girder sections while those in the bracing members were measured at 2 points (Figures 4.14 and 4.16).

Strains were converted to stresses using the modulus of elasticity values presented in Table 4.5.

Time histories of the measured stresses were decoupled to obtain axial and bending stresses as outlined below. Axial stresses are produced by axial forces and bending stresses are the maximum fibre stresses produced by bending moments. Using basic principles of structural mechanics, the measured stresses are related to axial stresses (σ_a) and bending stresses σ_y and σ_z as follows (see Figure 4.16):

a) Pontoon Sections

$$\sigma_1 = \sigma_a + \sigma_z$$

$$\sigma_2 = \sigma_a + \sigma_y$$

$$\sigma_3 = \sigma_a - \sigma_z$$

$$\sigma_4 = \sigma_a - \sigma_y \qquad \ldots\ldots(1)$$

Solving these equations we get

$$\sigma_a = (\sigma_1 + \sigma_2 + \sigma_3 + \sigma_4)/4$$

$$\sigma_y = (\sigma_2 - \sigma_4)/2$$

$$\sigma_z = (\sigma_1 - \sigma_3)/2$$

b) Column Sections

$$\sigma_1 = \sigma_a + (\sigma_y + \sigma_z) \cos(\pi/4)$$

$$\sigma_2 = \sigma_a + (\sigma_y - \sigma_z) \cos(\pi/4)$$

$$\sigma_3 = \sigma_a - (\sigma_y + \sigma_z) \cos(\pi/4)$$

$$\sigma_4 = \sigma_a - (\sigma_y - \sigma_z) \cos(\pi/4) \quad \ldots.(3)$$

Solving the above equations we get:

$$\sigma_a = (\sigma_1 + \sigma_2 + \sigma_3 + \sigma_4)/4$$

$$\sigma_y = (\sigma_1 + \sigma_2 - \sigma_3 - \sigma_4)/4 \cos(\pi/4)$$

$$\sigma_z = (\sigma_1 - \sigma_2 - \sigma_3 + \sigma_4)/4 \cos(\pi/4) \quad \ldots.(4)$$

c) Bracing Sections.

Following the same procedure it can be easily seen that

$$\sigma_a = (\sigma_1 + \sigma_2)/2$$

$$\sigma_y = (\sigma_1 - \sigma_2)/2 \qquad \ldots.(5)$$

Time histories of axial and bending stresses due to waves or impact loads were obtained using Equations 2, 4, and 5 and the four-channel Fourier analyser. Model values were scaled up to full scale values using scale factors presented in Table 4.5.